takece.com
Continuing Education Simplified!

Course Title: Use of Ultrasound in Abdomen and Superficial Structures

Topic List:-

Chapter

Introductory Chapter: Common Pitfalls and How to Overcome

Samia Ali Abdo Gamie

1. Introduction

Medical ultrasound is an imaging modality using high-frequency sound waves to recognize unique tissue characteristics. The normal human range of audible sound is from 20 Hz to 20 KHz; in contrast the frequency used in medical ultrasound is >20,000 Hz. The frequency range that is used for medical imaging is generally between 2 and 18 MHz [1].

Piezoelectric effect discovered by Pierre and Jacques Curie in 1880 is the basic principle of ultrasound transducer. They discovered that when pressure is applied to quartz or some certain crystals, it creates an electrical charge in that material. Curie's brothers soon discovered the inverse piezoelectric effect; when an electric field was enforced onto crystal leads, it led to a disorder in the crystal lead—now called the inverse piezoelectric effect [2].

Piezoelectric transducer generates the ultrasound beam as a pulse travels through the tissue; the echo signals return to the transducer after undergoing absorption, reflection, and refraction depending on the tissue structure, leading to a real grayscale image formation. The basic rules in image formation can be summarized as follows. First, ultrasound pulse travels in a straight line, so echo signals travel in a narrow beam, giving a real-time scanning. Second, as the velocity of the ultrasound is constant, the distance is directly proportional to how far the structure is from the transducer. Third, the echo strength is related to the tissue reaction with the ultrasound waves; the reflected waves give the echo brightness on the screen that is referred to as tissue echogenicity [3].

Physics of the ultrasound is essential for all physicians to understand and interpret ultrasound images. Frequency is the number of the sound waves per second. It usually remains constant maintaining the frequency of the original source, but the velocity of the ultrasound wave changes depending on the physical properties of the medium. These variations in velocity introduce artifacts into the image, mainly attributed to bone and fat. The frequency of transducer determines the resolution of the ultrasound image. The resolution of the ultrasound machine is its ability to detect and display two close structures as distinct. Higher-frequency transducers have higher resolution, but its ability to penetrate to deep structures is low; therefore it is used for superficial structures. On the other hand, low-frequency transducers can penetrate to deep structures with lesser resolution; therefore it is suitable for deeper structures. Using high transducers of high frequency to screen deep structures results in more attenuation to the image of the deep tissue [4]. Choosing the proper transducer for a proper image of different organs is based on this rule of thumb regarding the transducer's frequency. Therefore, always use a sector transducer from 3.5 to 5 MHz to screen deep abdominal structures but higher frequency for superficial structures [5].

Practical image orientation is performed in two planes sagittal plane and transverse plane. Using the transducer in the sagittal plane, the left side of the image represents the cranial plane. Meanwhile putting the transducer in a transverse plane, the left side of the image represents the right side of the patient. Abdominal examination is usually started while the patient is lying comfortably in supine position, and then they must be examined on both sides. Systematic scanning is important; scanning of all organs and all areas is essential to complete your mental checklist in an ultrasound report.

Preparation for abdominal ultrasound generally requires fasting for 8 h, decreasing the gas in the intestine. Also, for the gall bladder and biliary tree exploration, fasting is essential for screening. Other conditions such as emergency ultrasound require no special preparations. In each chapter of this book, if any special preparation for screening the organ is required, it will be mentioned.

In practice, ultrasound artifacts are common; thus understanding these artifacts' physics is vital to help correct it to improve the images, leading to good interpretation for a correct diagnosis. The artifacts arise either from improper operator technique or from the physics of ultrasound transmission and traveling. Identification of the artifact from improper technique is the first step, so it can be avoided. The second step is to know how the physics' artifacts can be corrected, keeping in mind that some of these artifacts may be good clues for proper diagnosis of structures with special characteristics. In this book, in each chapter, we try to explain some of these artifacts and how to avoid them. Potential US artifact correction is important for image quality improvement, optimal interpretation, and diagnosis.

Artifacts can be classified into two: One, related to the beam and the resolution, and the other, related to the location and the attenuation. Here are some common examples of these artifacts, their clinical relevance, their physical mechanism, and how to make alteration.

Beam- and resolution-related artifacts

Beamwidth artifact: Lateral resolution is the ability to detect two close points in the transverse plane as two distinct points. It leads to lateral blurring of the image and aberrant echoes from adjacent highly echogenic objects. It can be reduced by focusing the sound selection. Focusing improves the beamwidth, so it becomes narrower at the target focal zone [6].

Section thickness artifact: It is the ability to distinguish two vertical beams as two distinct points. It is called elevation resolution as the point planes are perpendicular to the transducer plane. It appears like debris in anechoic structure as cyst or ascites. It can be overcome by putting it in a focal zone with a standoff pad [7].

Secondary lobe artifacts: It mimics debris in anechoic structures. It is from the reflected echo that comes back from ultrasound waves that are transmitted outside the beam. It can be corrected by reducing the gain [8].

Location characteristics ultrasound artifact

Reverberation artifact: It appears as multiple bright parallel lines at regular intervals that decrease in intensity as the depth increase. It is due to reflections between highly reflective interfaces in parallel (reverberates). It may be useful in the detection of air in abnormal locations, as in pneumatosis, pneumoperitoneum, and pneumobilia. It can be reduced by decreasing gain, changing the angle of insonation, or using multiple windows [9].

Comet tail artifact: Adenomyomatosis, based on the same principle of reverberation artifact. It is caused by highly reflective interfaces that are closely spaced, so the individual echoes cannot be distinguishable. This artifact is useful as it considered a fingerprint for identification and diagnosis of cholesterol crystals in adenomyomatosis of the gallbladder (**Figure 1**) [10].

Ring-down artifacts: It arises from resonant vibrations within trapped air bubbles. These vibrations produce a continuous sound wave transmitted back to the transducer; it appears as a streak or series of parallel bands deep to a focus of gas. It can be useful in identifying abnormal foci of air, e.g., pneumoperitoneum and portal venous gas. Also, it can be indicative of appendicitis if it is detected in the appendix [11].

Mirror image artifact: It mimics disease, such as pseudo-thickened bowel wall and lesions in the lung. It is due to reflections of a highly reflective structure, e.g., the diaphragm, producing a mirror-like image of an object. The second image is generated along that path, deeper than the true site of the structure due to increased time of the return echo. A common example is in the case of a liver lesion near the diaphragm; the transmitted beam is reflected off the diaphragm and will be faced with a liver lesion that reflects it to the diaphragm again as well as the transducer. The image on the screen contains two lesions similar on both sides of the diaphragm and the same distance from it (**Figure 2**). This type of artifact may be corrected by decreasing gain or changing the angle of insonation [11].

Accentuation and attenuation characteristics of ultrasound artifacts

Increased transmission (accentuation): It is due to increased intensity of echoes distal to a low-attenuating structure. It is useful in practice to differentiate between cystic and solid structures. Distal to cystic structure there is an increased echo intensity, as the ultrasound waves pass through the cystic structure without any disturbance or loss. This accentuation is important to confirm the diagnosis of the anechoic cystic lesion (**Figure 3**). It can be increased by using tissue harmonic imaging [12].

Attenuation artifacts: Attenuation is a loss of ultrasound energy and amplitude as it goes deeper through the tissue. Therefore, echo from deeper structure comes weaker than the echo from the superficial structure; the ultrasound machine is computerized to amplify the return echo from the deeper structures. If the tissue is reflective, as in the case of a fat tissue, less echo reaches the deeper structure, and screening will be difficult. This attenuation is adequately compensated by first-order correction schemes such as time gain compensation.

Acoustic shadowing: It is due to a reduction in echo strength distal to a highly reflective object. Three types of acoustic shadowing, clean, partial, and dirty,

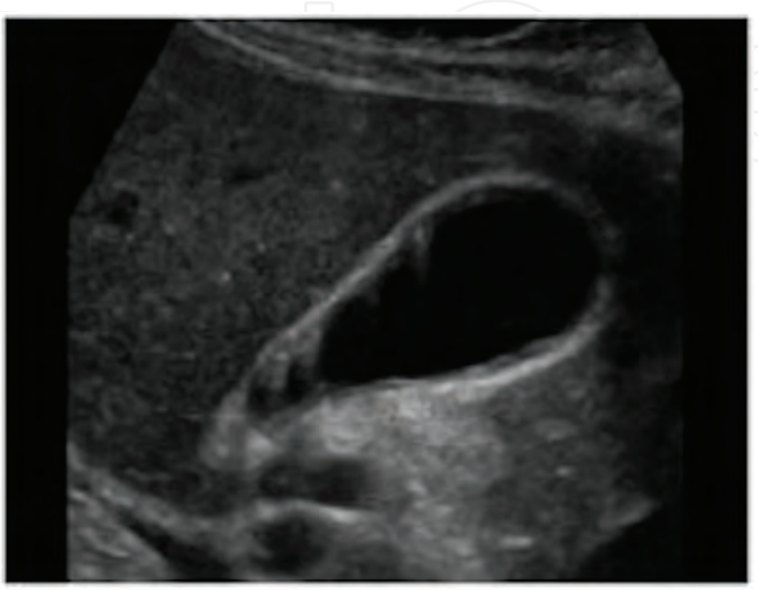

Figure 1.
Longitudinal US image of the gallbladder shows comet tail artifact caused by cholesterol crystals in Rokitansky-Aschoff sinuses. This finding is diagnostic of adenomyomatosis.

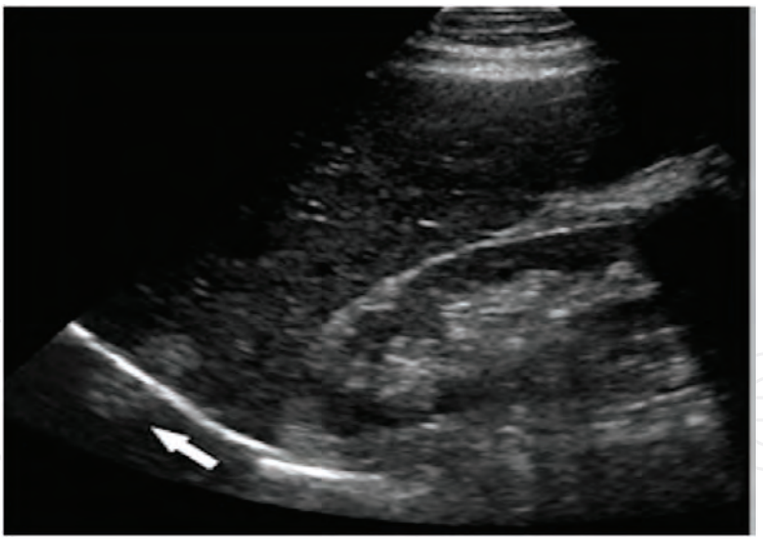

Figure 2.
Longitudinal US image shows an echogenic lesion in the right hepatic lobe (hepatic hemangioma), and a duplicated echogenic lesion (arrow) on the other side equidistant from the diaphragm mimics lesion in lung parenchyma.

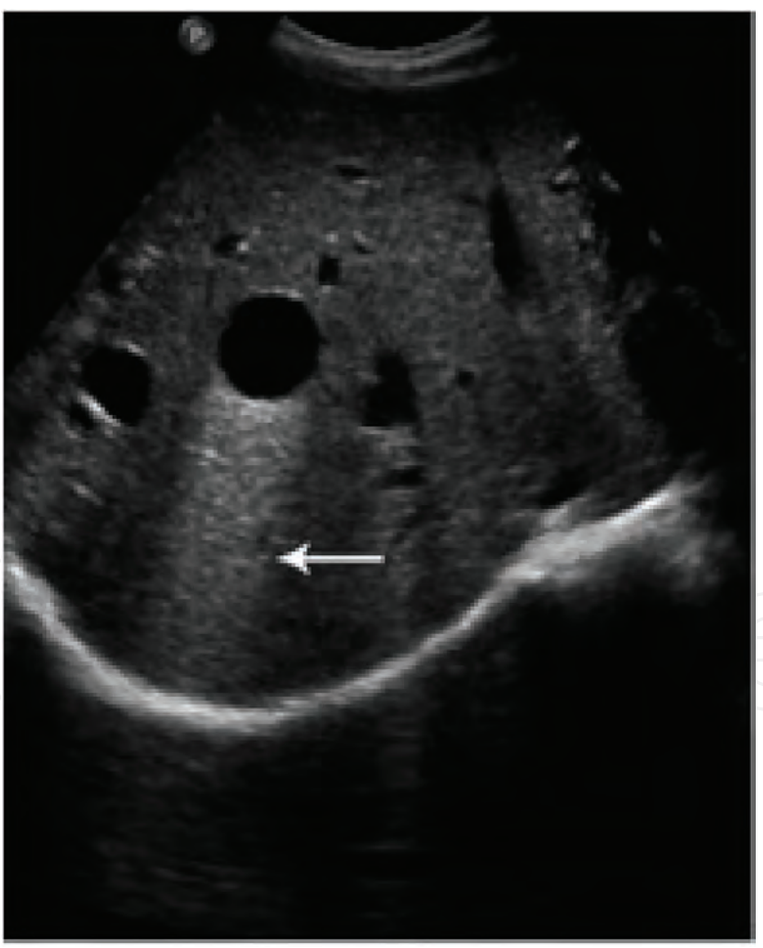

Figure 3.
Transverse US image of the liver shows anechoic hepatic cysts. The hepatic parenchyma distal to the cysts is falsely displayed as increased intensity (arrow) secondary to increased through-transmission artifact.

are used to describe the shadow of stones, calcification, and air, respectively. It is very helpful in practice to identify the clear shadow as a dark band due to all the ultrasound waves being absorbed. Its presence can help detect stones in echogenic structures such as kidney stones. Also, a shadow is important to differentiate a

gall bladder (GB) stone (**Figure 4**), with its clear shadow, from a non-shadowing polyp or a sludge ball in GB. Dirty shadowing is seen in the case of highly refracting structure like gas. In clinical practice, it is important to increase the shadowing to help with the diagnosis of important pathology, so the focal zone and beam width are important to be adjusted in these cases [11].

The edge (refraction) artifact: It occurs in rounded structures like a cyst or urinary bladder as the ultrasound refracted at its edges results in shadows at both edges (**Figure 5**). These artifact shadows are corrected, and the shadows disappear by changing the angle of the ultrasound beam after identification of the artifact.

Anisotropy: It commonly occurs in tendons and, to a lesser extent, muscles, ligaments, and nerves. It appears as a hypoechoic area in a structure that has anisotropy. This phenomenon can be misinterpreted as a discontinuation of the course's structure. As the ultrasound beam is perpendicular to the tendon throughout its course, the tendon is uniformly hyperechoic. If the tendon is curved, the ultrasound beam is not perpendicular to the tendon; the tendon becomes hypoechoic and disappears. These phenomena can be overcome by changing the transducer position (heel-to-toe movement to make the transducer perpendicular on the tendon along its course) [13].

Understanding of these artifacts will minimize any misinterpretation in the report, and in certain situations it helps in the diagnosis. In this book, we used some of these artifact expressions for diagnosis or for explaining how to avoid any mistakes during scanning.

Standardized evaluation of abdominal ultrasound should optimally take place after overnight fasting in most of the ultrasound techniques; however, this is not a condition in urgent situations. In an emergency ultrasound, no special preparation is required. In routine clinical practice, fasting is important to avoid interfering bowel gas; also, it is recommended to assess the abdomen from a more lateral aspect through both flanks. Keeping in mind the need to take precautions, and being systematic in scanning, will provide clues to reach the correct diagnosis and avoid misinterpretation.

Starting ultrasound examination of the abdomen, it is usually done in a systematic manner. Your guide for scanning must be based on your mental checklist in the examination. Start by the right side considering the liver the acoustic window of the right upper quadrant of the abdomen. Go through the anatomical four areas of the abdomen, namely, the right upper quadrant, the left upper quadrant, the right lower quadrant, and the left lower quadrant. Intestinal loops can be screened in the

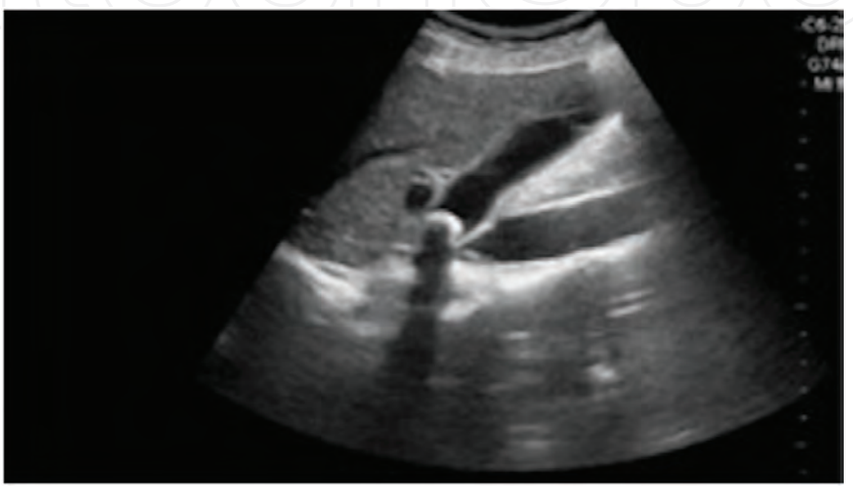

Figure 4.
Longitudinal US image of the gallbladder shows echogenic gallstones with clear shadow.

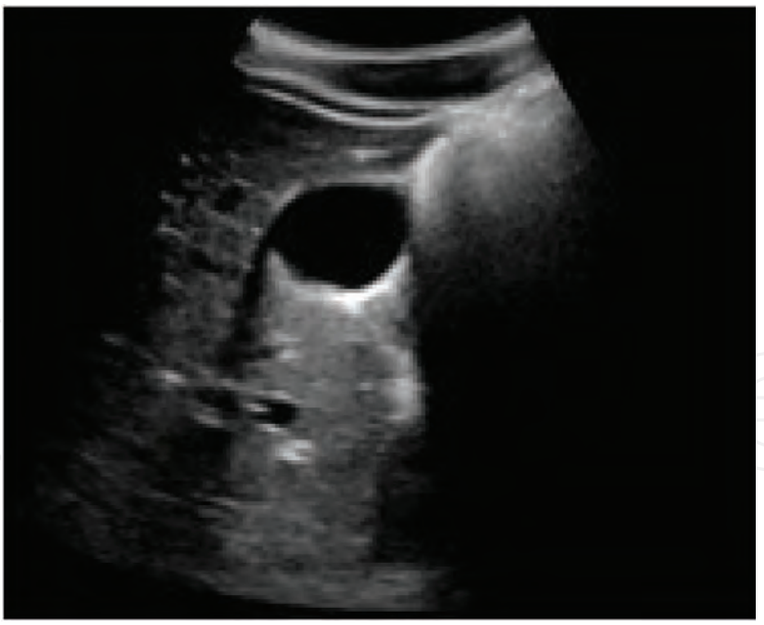

Figure 5.
Transverse US image of the liver shows transverse image of gallbladder with false shadow edge artifact.

"grid"-type pattern starting from the right side passing through the areas to the left side in a slow screening movement allowing to explore any intestinal pathology.

Ultrasound reports must fulfill all abdominal organs, with a full description of each in a systemic manner. A general outline of the sonographic description includes the architectures, the echogenicity of the parenchyma, and blood vessel distribution with a special comment on its variation from normal. The full screen of the organ is usually done with a complete orientation about the organ pathology. Any pathology is described as diffuse or localized, followed by detail descriptions of its site, size, echogenicity, regularity, and any special artifacts as mentioned above.

At the end of the report, there is a summary of the findings with your brainstorm conclusion. Ultrasound report is your mind checklist representing your systematic work and screening for the complete abdominal examination. Keep in mind that ultrasound findings are not histological but rather pathological. If from your clinical knowledge any additional investigation is required to confirm the diagnosis, it must be mentioned as a recommendation. Also, according to the ultrasound findings, a simple interventional process as ultrasound-guided biopsy procedures may be required. Also, good technical skills are needed for better interpretation of any valuable knowledge in the screening while avoiding the pitfalls and artifacts that can result in more confusion to the sonographers. In this text, many valuable technical skills are available from experts each in his field.

DOI: http://dx.doi.org/10.5772/intechopen.87964

Author details

Samia Ali Abdo Gamie
Helwan University, Cairo, Egypt

References

[1] Hangiandreou NJ. AAPM/RSNA physics tutorial for residents. Topics in US: B-mode US: Basic concepts and new technology. RadioGraphics. 2003;**23**:1019-1033

[2] Genovese M. Journal of Diagnostic Medical Sonography Ultrasound Transducers. 2016;**32**(1):48-53

[3] Manbachi A, Cobbold RSC. Development and application of piezoelectric materials for ultrasound generation and detection. Ultrasound. 2011;**19**(4):187-196

[4] Abu-Zidan FM, Hefny AF, Corr P. Clinical ultrasound physics. Journal of Emergencies, Trauma, and Shock. 2011;**4**(4):501-503

[5] Szabo TL, Lewin PA. Ultrasound transducer selection in clinical imaging practice. Journal of Ultrasound in Medicine. 2013;**32**:573-582

[6] Bertrand PB, Levine RA, Isselbacher EM, Vandervoort PM. Fact or artifact in two-dimensional echocardiography: Avoiding misdiagnosis and missed diagnosis. Journal of the American Society of Echocardiography. 2016;**29**(5):381-391

[7] Hoskins PR, Martin K, Thrush A. Diagnostic Ultrasound: Physics and Equipment. 2nd ed. Cambridge: Cambridge, England; 2010

[8] Middleton WD, Siegel MJ, Dahiya N. Ultrasound artifacts. In: Siegel MJ, editor. Pediatric Sonography. 4th ed. Philadelphia, PA: Lippincott Williams & Wilkins; 2011. pp. 21-42

[9] Baad M, Lu ZF, Reiser I, Paushter D. Clinical significance of US artifacts. RadioGraphics. 2017;**37**:1408-1423

[10] Bonatti M, Vezzali N, Lombardo F, Ferro F, Zamboni G, Tauber M, et al. Gallbladder adenomyomatosis: Imaging findings, tricks and pitfalls. Insights into Imaging. 2017;**8**(2):243-253

[11] Feldman MK, Katyal S, Blackwood MS. US artifacts. RadioGraphics. 2009;**29**:1179-1189

[12] Rose JS, Bair AE. Fundamentals of ultrasound. In: Cosby KS, Kendall JL, editors. Practical Guide to Emergency Ultrasound. PA: Lippincott Williams and Wilkins; 2006. pp. 27-41

[13] Serafin-Król M, Maliborski A. Diagnostic errors in musculoskeletal ultrasound imaging and how to avoid them. Journal of Ultrasonography. 2017;**17**(70):188-196

Chapter

The Influence of Ultrasound Equipment Knobology in Abdominal Sonography

Yaw Amo Wiafe and Augustina Badu-Peprah

Abstract

Ultrasonography is a highly operator dependent imaging modality with a number of knobology variables that are under the control of the operator. Knobology is a terminology that describes the manipulation of ultrasound knobs and system controls in order to obtain the best image possible from diagnostic ultrasound. The inadequate use of knobology variables may impair image quality and can result in misdiagnosis. In abdominal sonography, selecting the appropriate application preset for abdominal examination is first step towards achieving an optimum image. The next step is to select an appropriate transducer frequency which must take the size of the patient into account. Transducer frequency is typically in the range of 3–5 MHz, but a lower frequency may achieve better depth penetration in larger patients. While the output power may improve image quality by increasing the intensity of transmitted sound energy, the impact is usually insignificant. The practice of using high output power should therefore be limited because of the risk of biologic effect. Other essential knobs for better image optimization include controlling the overall gain, time gain compensation, focal zone, dynamic range and tissue harmonic imaging. In the assessment of blood flow in abdominal vessels the regulation of the pulse repetition frequency, Doppler gain, imaging angle, and wall filter improves the sensitivity of color and spectral Doppler.

Keywords: knobology, resolution, greyscale imaging, Doppler imaging, ALARA principle

1. Introduction

Ultrasonography is a highly operator dependent imaging modality with a number of knobology variables that are under the control of the operator. Knobology is a terminology that describes the manipulation of ultrasound knobs and system controls in order to obtain the best image possible from diagnostic ultrasound. The inadequate use of knobology variables may impair image quality and can result in misdiagnosis.

This chapter explains the functions of the various ultrasound system controls and knobs and the impact they have on greyscale ultrasound imaging. It demonstrates the effect of transducer selection on image quality, and the role of knobology variables in image optimization. This includes a description of the Application Preset, Output Power, Overall Gain, Time Gain Compensation (TGC), Focus, Depth, Zoom, Dynamic Range and Tissue Harmonics. The influence of these

essential knobs and system controls on spatial resolution (including lateral and axial resolution) and Contrast resolution are explained. In addition, the utility of Doppler knobs for imaging abdominal blood vessels are also explained and demonstrated.

The need to adhere to the principle of As Low As Reasonably Achievable (ALARA) is also explained with emphasis on the imaging of neonates and children. Lastly, the chapter also emphasizes the potential detrimental effect of underutilizing ultrasound knobs and system controls in abdominal sonography.

2. Switching-on the ultrasound machine

Switching on the ultrasound machine is the first knob to press if the machine is switched off. By switching on the machine, the ultrasound system is given access to a source of electricity, which excites the tiny piezoelectric crystals within the connected transducer. These piezoelectric crystals emit sound waves as a result of their exposure to electricity. The sound waves produced by the piezoelectric crystals can then be transmitted into the human body, normally aided by a coupling gel which serves as an acoustic medium for eliminating the air between the surface of the transducer and the skin.

3. Application preset

Modern machines allow the operator to preset an application setting for a certain examination type. Ultrasound imaging is used for a wide range of medical applications. Aside its use in assessing the abdomen, it is also used in obstetrics and gynecology, cardiac and vascular examinations, and other small-part examinations such as breast, thyroid, and musculoskeletal imaging. Different sonographic settings are needed for the various examinations, due to their differences in terms of the depth of region of interest, tissue-type, and the size of organs and structures in that region. Because of the uniqueness of these examinations, adjusting the settings between patients for a different examination can be time consuming, and may compromise the adherence to ALARA principles. In addressing this limitation, the manufacturer makes it easier by allowing the operator to select the type of examination which will activate the pre-defined factory settings for the specific type of examination. By selecting the appropriate 'Application Preset' for abdominal examination, the pre-defined factory settings are activated for abdominal sonography. This automatically adjusts the basic settings for the selected examination, which include an adjustment of the transducer frequency, acoustic Output Power, Overall Gain, Dynamic Range, Depth and other related settings.

Performing an abdominal ultrasound with a different application preset may impair the image quality which could mislead image interpretation. For example, a user performing an obstetric examination may identify a need for including abdominal examination without switching to the abdomen preset. This may impair the image quality of the abdominal examination if careful adjustments of relevant knobology variables are not made. In **Figure 1a**, obstetric preset was used in imaging the kidneys of an obstetric patient who complained of flank pain during an obstetric ultrasound examination. Upon using the basic obstetric preset without further manipulation of essential knobs, there was the tendency of suspecting a focal lesion in the right kidney (see arrow in **Figure 1a**). However, a switch to the basic abdomen preset without further manipulation resulted in an improved image quality which shows a normal kidney (see arrow of **Figure 1b** in the same person).

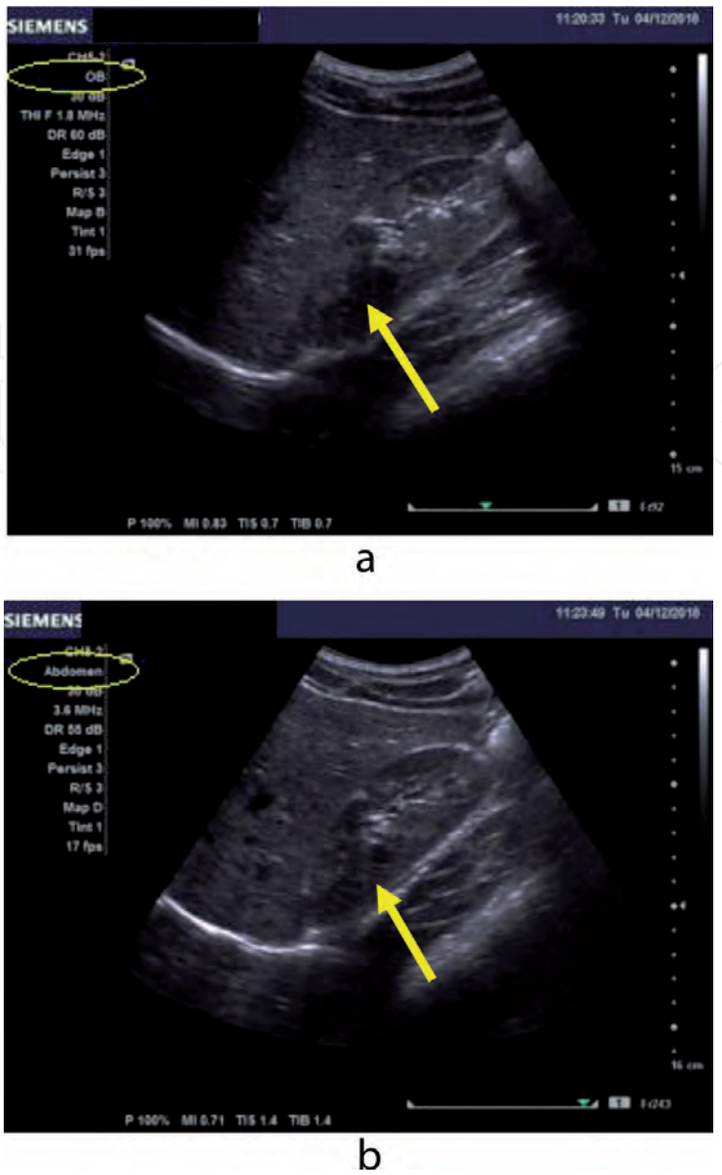

Figure 1.
(a) Image of the right kidney with OB preset suggests a focal change within kidney (see arrow). (b) Image of the right kidney with abdomen preset suggests normal appearance (see arrow).

It therefore suggests that much more manipulation of knobs will be required for selecting the 'wrong' application preset which may unduly extend the duration of the examination as a compromise on ALARA principles.

4. The transducer

Ultrasound images are produced from high frequency sound waves that are emitted by the transducer, typically in the range of 1–15 MHz [1, 2]. The frequency of the transducer is determined by the thickness of the piezoelectric crystals and the damping material behind them [3]. In producing a higher frequency, the manufacturer places a damping material behind very thin piezoelectric crystals in order to shorten the pulses of sound waves that are emitted [3]. However, shorter pulses of sound waves are unable to penetrate deeper because of shorter wavelength [3]. Due to this penetration limitation, different types of transducers are designed with different ranges of frequency. Higher frequency transducers offer better resolution at the expense of depth penetration, whilst lower frequency transducers offer better depth penetration for poorer image resolution [2, 3].

Since most abdominal organs such as the liver, spleen, kidneys, pancreas and aorta are relatively deeper, lower frequency transducers are used for this type of examination. Unlike the transducers designed for other examinations, the transducers for abdominal examination (i.e. sector or curvilinear) have a divergent and wider far field. Aside the lower frequency of curvilinear and sector transducers which makes image resolution relatively poorer, there is also an increase in attenuation as the sound beam travels deeper. This may adversely affect the image resolution of abdominal sonography. It is therefore incumbent on the operator to make a careful choice between better image resolution and depth penetration.

The typical frequency range for curvilinear transducers is in the range of 2-5 MHz. In selecting a frequency for an abdominal examination, the operator should consider the size of the patient. If the patient is smaller in size, a higher frequency should be used for better spatial resolution. Particularly in neonates and children, a higher frequency is highly useful, as this is likely to produce better image resolution to shorten the duration of the examination in fulfillment of ALARA principles. Secondly, children are less likely to cooperate during the examination, therefore using a lower frequency such as 3 MHz for abdominal examination may unduly delay the examination because of the lack of patient cooperation and a poorer image resolution. **Figure 2a** and **b** demonstrates two images of the right and left kidneys

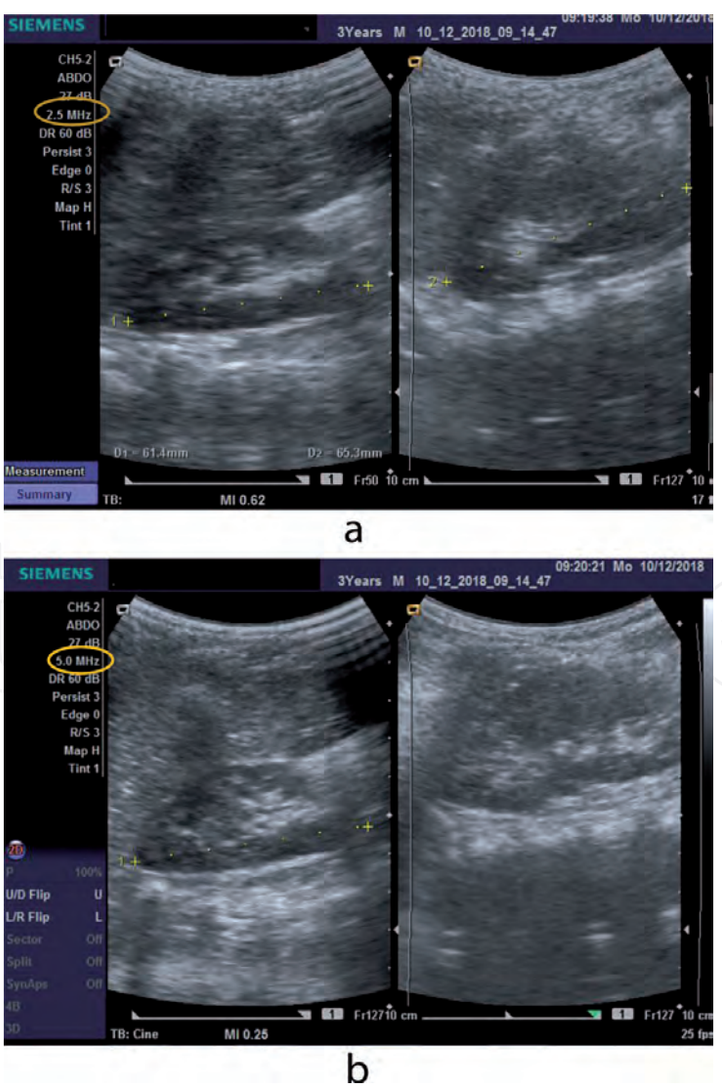

Figure 2.
(a) Image of the right kidney of right and left kidney in a 3-year-old non-cooperating patient showing poorer image resolution because of lower transducer frequency of 2.5 MHz. (b) Image of the right kidney of right and left kidney in the 3-year-old non-cooperating patient showing better visualization of renal margins because of lower transducer frequency of 2.5 MHz.

obtained from a 3-year-old infant with the higher frequency obviously showing more details than the lower frequency. However, a low frequency of 3-4 MHz is often ideal for imaging the average-sized adult, whilst larger or much more obese adults may require as low as 2 MHz of frequency for adequate depth penetration.

In addition, a linear transducer may also be used during abdominal ultrasound. Linear transducers use higher frequencies for imaging structures that are more superficial, such as the anterior abdominal wall and the surface of the liver. They are also used in assessing the appendix.

5. Output power

The acoustic output power of the machine must be considered at all times by the operator. As indicated above, selecting the appropriate preset for abdomen ultrasound will automatically adjust the output power to the recommended level. However, while it is important to observe the ALARA principle by using the minimum output power possible, the operator must not compromise image quality for output power reduction which may lead to misdiagnosis. In essence, there should be a balance between maximizing image quality with the minimum output power possible as a measure for reducing the risk of biological effect. Usually, the ultrasound

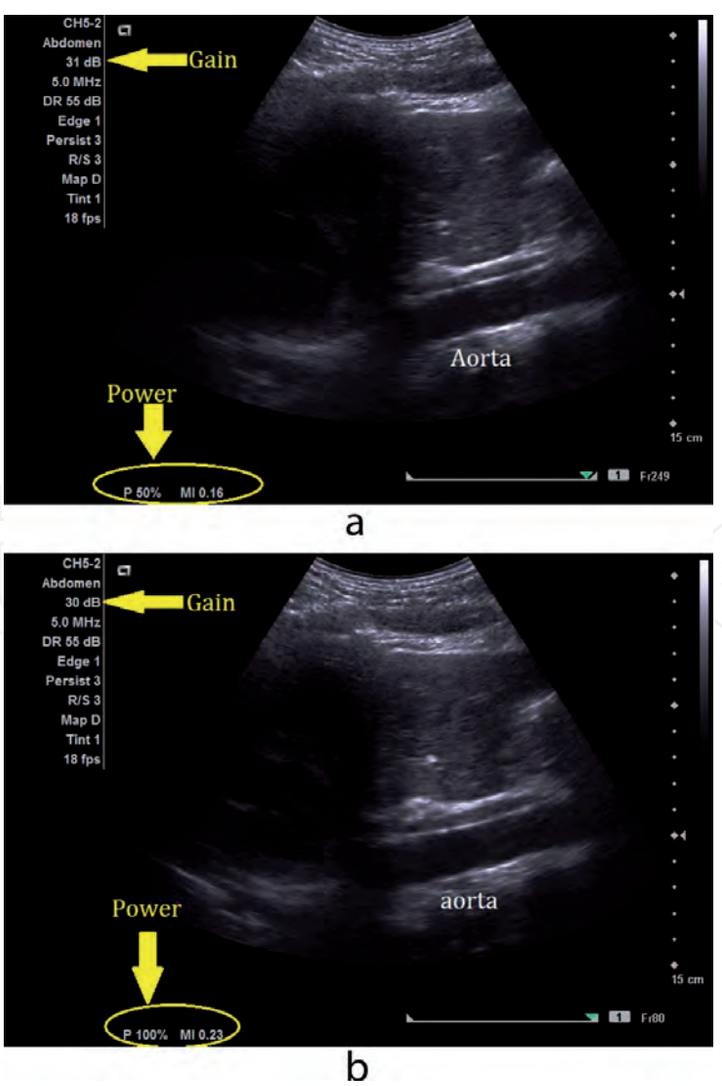

Figure 3.
(a) The appearance of the abdominal aorta at a reduced output power by 50%. (b) The appearance of the abdominal aorta when the output power increased was increased to 100 showed no significant difference %.

machine will display the output power on the screen at all times, allowing the operator to be constantly informed (**Figure 3a** and **b**). However, while increasing the power output may be useful, it may also be needless in many cases. The over-all Gain can play a better and safer role in image quality optimization than the output power. **Figure 3a** and **b** demonstrate that there is no significant difference between the appearance the abdominal aorta if the output power is reduced by 50% and the overall gain is about 30 decibels.

6. Overall gain

The overall gain is the recommended option to consider in place of increasing the output power. With the overall gain, image quality can be improved by adjusting the brightness of the entire field of view without increasing the intensity of transmitted sound energy. It achieves this by amplifying the echo-signals returning from the body after transmitting the sound waves. The overall gain can be considered as the 'microphone' in ultrasound imaging. The technology is similar to using a microphone to amplify someone's voice for the listener. Increasing or decreasing

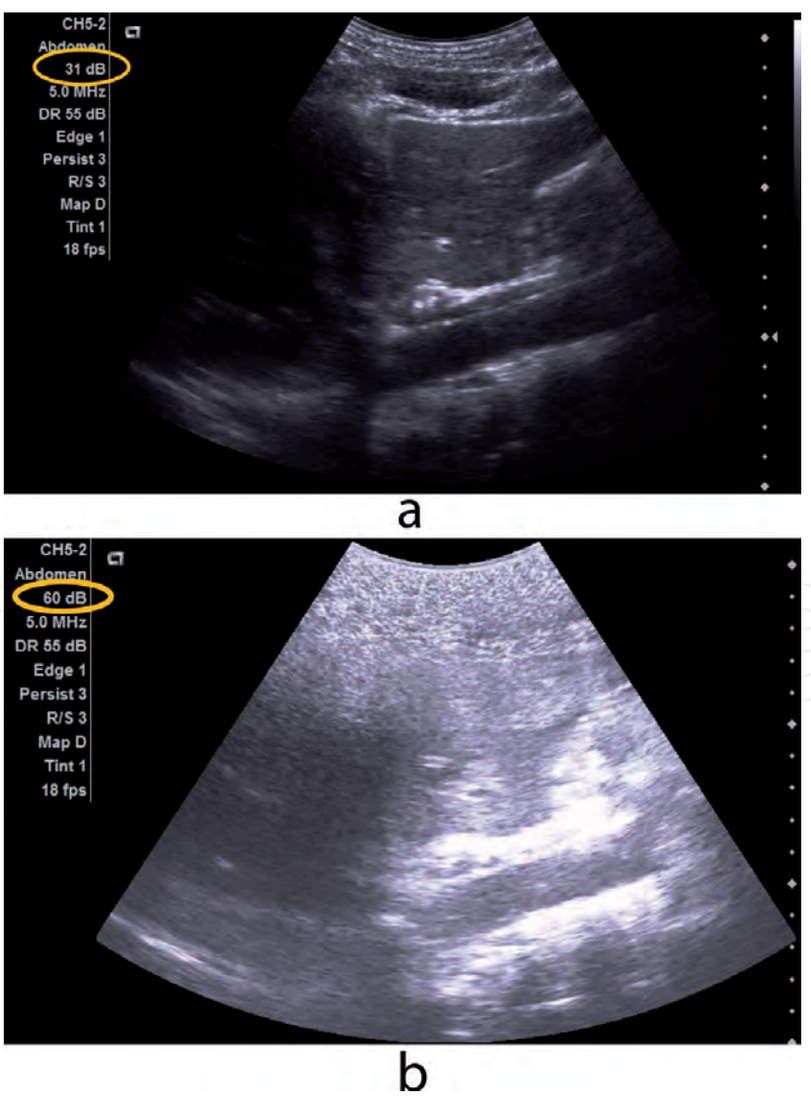

Figure 4.
(a) Adequate overall gain of 31 decibels with liver surface showing. (b) Too high overall gain of 60 decibels with liver surface missing.

the overall gain may improve contrast resolution for adequate visualization of the image. However, just as a microphone can sometimes produce noise and become a nuisance, increasing the overall gain beyond a certain point will affect contrast and spatial resolution by making the image appear too bright. Nonetheless, it is a knob you cannot do without in image optimization. Most modern machines integrate the overall gain in the Bmode or 2D knob, but it is still a separate knob in some machines. Manipulate the overall gain by adjusting it 'up and down' and carefully observe the changes that occur as you control the knob. **Figure 4a** and **b** shows images of adequate versus high overall gain and the effect it has on assessing the surface of the liver.

7. Time gain compensation

While the overall gain would adjust the brightness of the entire field of view, it may not address attenuation occurring at specific depths. Some structures in the body are much more affected by attenuation than others and would therefore need additional compensation for the loss of sound energy. For example, an optimum visualization of the left lobe of the liver requires a depth specific gain adjustment that is different from the gain compensation needed for optimum visualization of the right lobe. Hence the Time Gain Compensation (also known as Depth Gain Compensation), is a set of depth-specific slide controls that can be used for echo-signal amplification at different depths (see **Figure 5**). It allows the adjustment of echo-signals in the near-field, mid-field and far field to improve axial resolution. The TGC creates uniformity in the brightness of the echoes when used in conjunction with the overall gain. The best approach is to center all the TGC settings before adjusting the overall gain. After adjusting the overall gain, the TGC can then be adjusted to compensate for attenuation at specific depth.

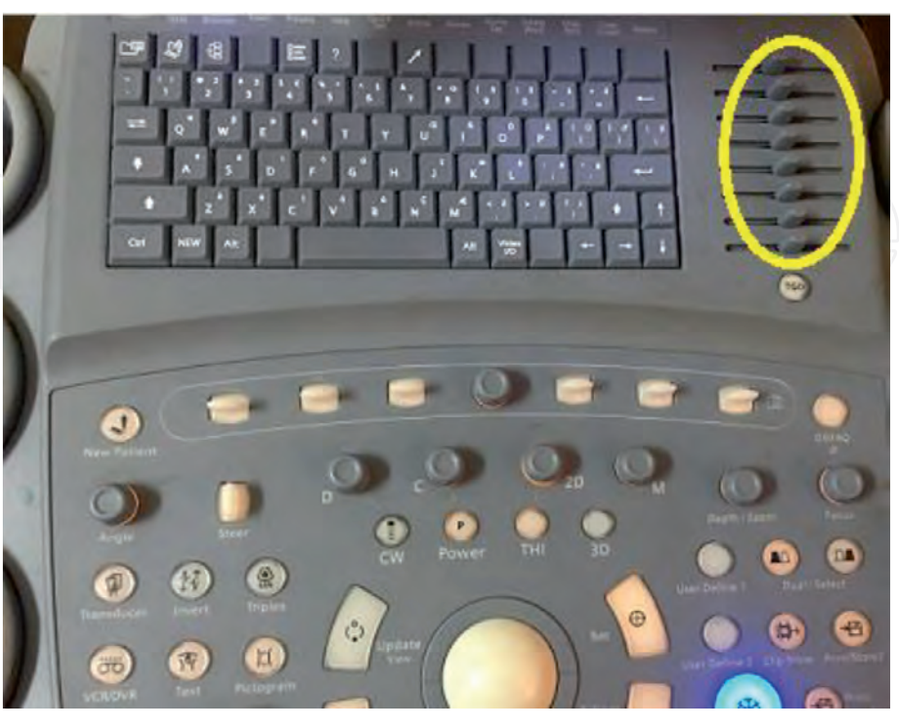

Figure 5.
TGC slide in the yellow circle.

8. Focal zone(s)

During scanning, the system allows the operator to improve lateral resolution in a region of interest by adjusting the focal zone. This is an additional measure to minimize the effect of attenuation. However, while other controls such as the overall gain and TGC are effective for improving axial resolution, adjusting the focal zone is much more effective for improving lateral resolution. Lateral resolution refers to the ability to identify structures lying side-by-side as separate structures, while axial resolution refers to the ability to identify a structure lying on another structure as separate structures.

The focal zone normally appears at the lateral side of Bmode as a triangular-shaped structure or a dot. It can be moved up or down by the operator and should be placed at the region of interest or posterior to that region. If a single focal zone is set too superficially a poorer image resolution will be observed in the far field (**Figure 6**). However if the focal zone placed below or at the level of region of interest, the resolution improves in the entire field of view (**Figure 6**). To improve lateral resolution in a wider region, more than one focal zones may be selected by the operator. However, increasing the number of focal zones also decreases the frame rate which has the tendency of slowing down the image production time to the detriment of temporal resolution. Thus using more focal zones slows down the scanning time which may not support the principles of ALARA in terms of keeping to a reasonable scanning time.

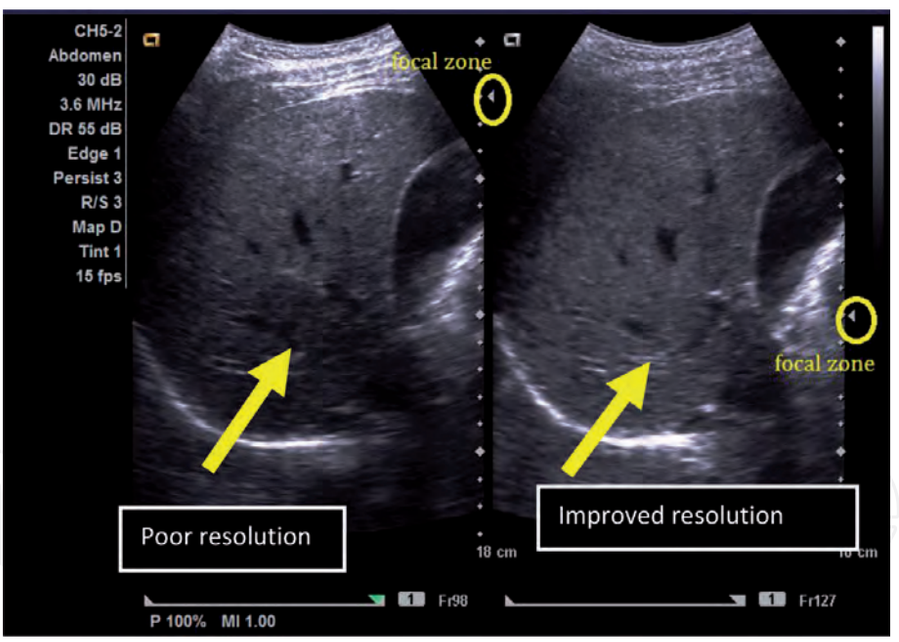

Figure 6.
Poorer resolution when focal zone is positioned in the near is compared to focal zone positioned at the level of interest.

9. Depth

The Depth is special a knob for adjusting the distance of the field of view. Structures within the field of view can be moved far or closer by adjusting the Depth. This is to ensure that the region of interest is closer enough for optimum visualization. It is also to avoid showing regions that are not relevant to the area of interest. **Figure 7a** is an example of a far depth image of the pancreas, with a wide irrelevant space showing behind the spine. This irrelevant space can be avoided by adjusting the

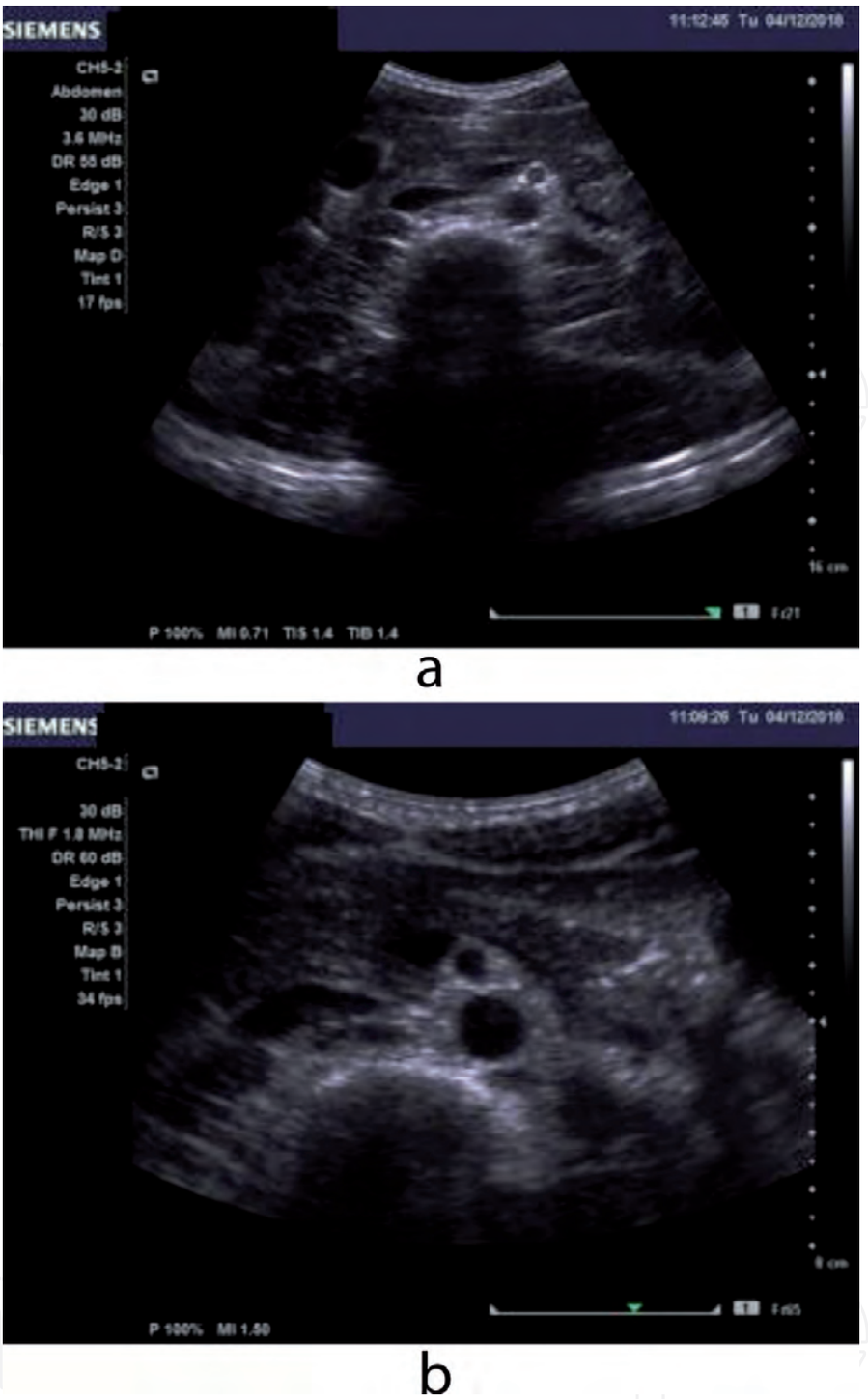

Figure 7.
(a) Far depth. (b) Closer depth.

Depth closer for adequate visualization (**Figure 7b**). The structure of interest should always take the center stage by occupying about two-thirds of the field view. In order to avoid missing a pathology beyond the field of view, the best practice is to adjust the Depth for a far field of view before adjusting for a closer field of view. **Figure 8** is an example of how one can miss a pathology, if the Depth is not adjusted for adequate visualization beyond the field view. It demonstrates how a closer Depth would have missed the pleural effusion if a far depth image was not assessed.

However, while moving the depth closer and far is necessary for evaluating various conditions and ruling out pathologies, moving the Depth closer has the tendency of generating noise which can worsen contrast resolution and may even mimic a pathology.

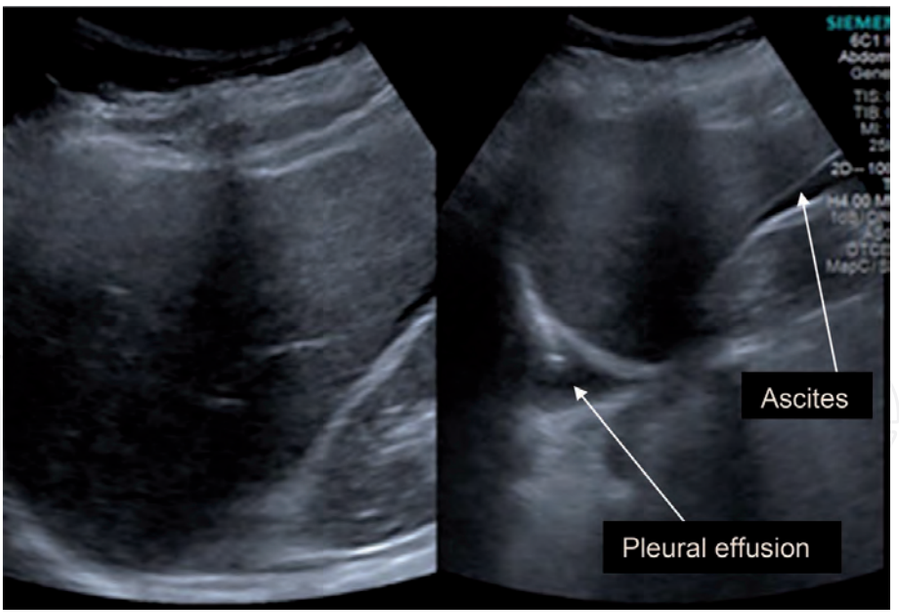

Figure 8.
Missing information on the right-side because of depth adjustment.

10. Zoom

The zoom is used for magnifying the area of interest. Unlike the depth which magnifies by moving the area of interest closer, the zoom actually magnifies by making the region of interest appear bigger. Another limitation of the depth that is

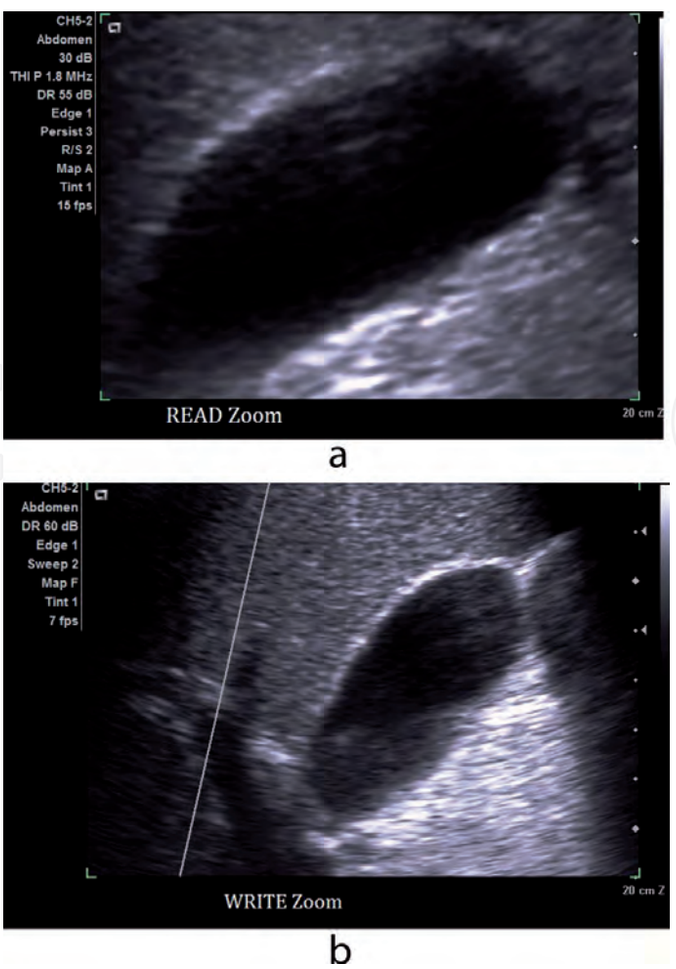

Figure 9.
(a) Read zoom. (b) Write zoom.

addressed by the zoom is the ability to enlarge a specific region of interest. Without using the zoom, measuring some tiny structures may difficult because of poor spatial resolution. For instance, in measuring the thickness of the gallbladder wall, using the zoom improves the visualization of the wall for an accurate measurement (**Figure 9a** and **b**).

Some manufacturers use READ zoom for their magnification, while others use WRITE zoom. Both read zoom and write zoom can produce poorer image depending on the size of the area magnified. However, READ zoom produces the worse kind of images because it relies on stored images which enlarges the pixel density in that region (**Figure 9a**). On the other hand, WRITE zoom tries to maintain the pixel density by zooming the image live which produces a better spatial resolution. Operators should check the type of zoom in their machine in order to appreciate how much zooming can be done without compromising the image quality.

11. Dynamic range

The Dynamic Range is a control on the ultrasound system that allows the operator to determine the range of shades of gray to be displayed on the monitor. Broad shades of gray displays a wider range of echo-intensity between bright and

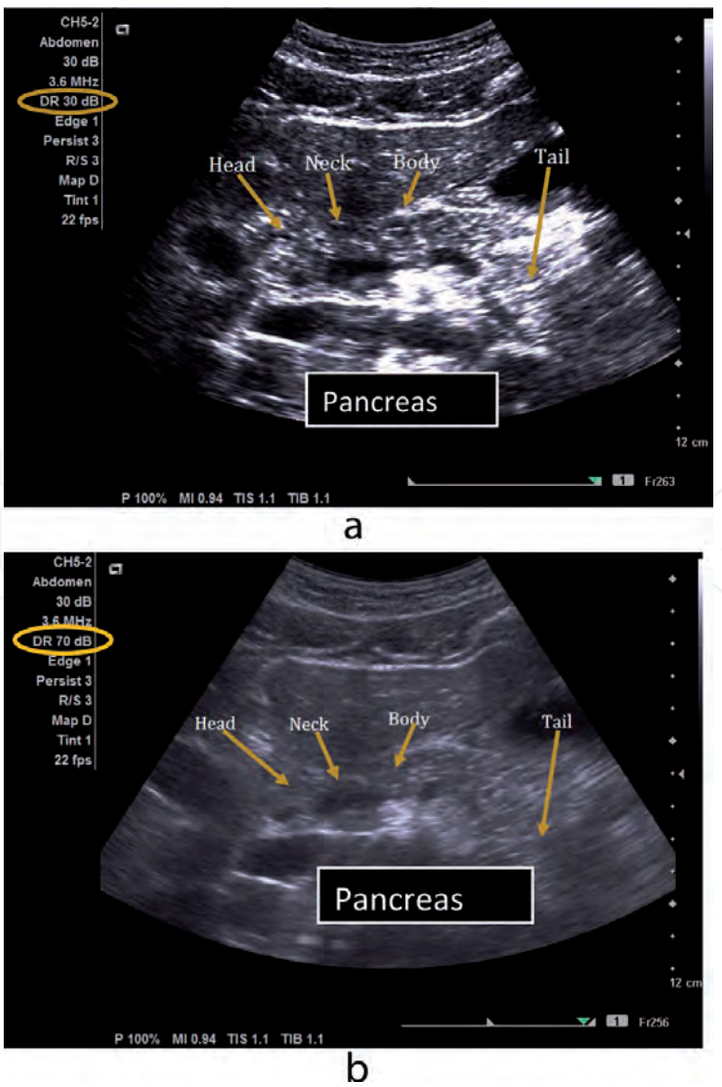

Figure 10.
(a) Narrow dynamic range. (b) Broad dynamic range.

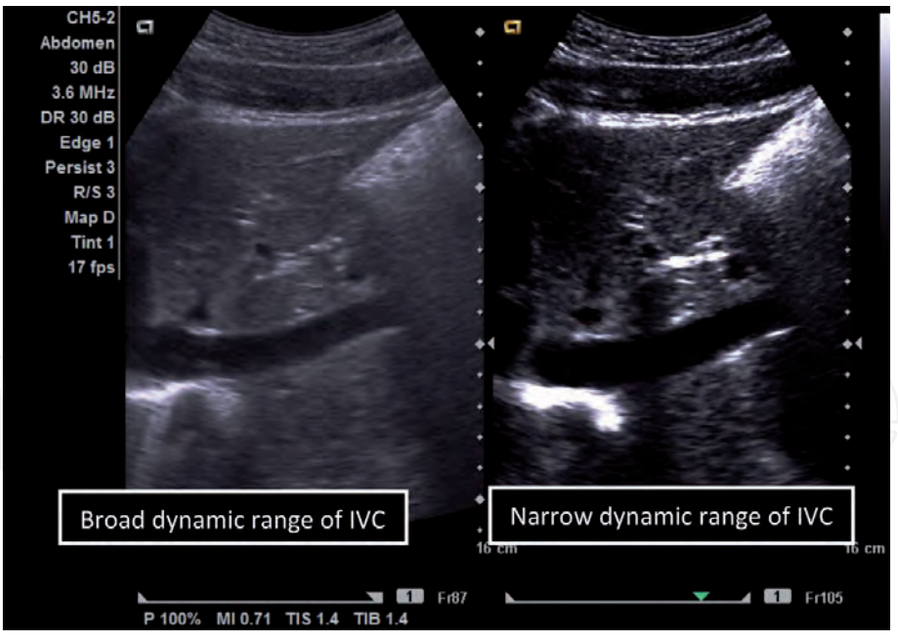

Figure 11.
Broad versus narrow dynamic range of IVC.

dark and produces a smoother image overall, whilst narrow shades of gray displays a narrower range of echo-intensity between bright and dark and produces a higher contrast between two regions of different echogenicity. In abdominal sonography, a broad dynamic range is the most appropriate option for assessing the echotexture of homogeneous soft-tissue structures like the liver, pancreas and spleen. Narrow dynamic range is most appropriate for assessing anechoic structures such as the aorta and IVC. **Figure 10a** shows the effect of narrow dynamic range of the pancreas in comparison to the liver, and **Figure 10b** shows the effect of broad dynamic range on the pancreas which shows poor differentiation in echotexture in comparison to the liver. In **Figure 11** also shows the effect of long and short dynamic range on the appearance of the IVC.

12. Tissue harmonic imaging

Tissue harmonic Imaging (THI) is an additional control for image optimization in most ultrasound machines. It improves image quality by eliminating weak echoes that cloud the image when the fundamental frequency of the transducer is used. It replaces the returning echoes from the fundamental frequency with echoes in the harmonic frequency which improves spatial resolution. This eliminates side lobe artifacts and noticeable noise in the area of interest. It can therefore be used in conjunction with the utilization of other knobs that may generate noise. For example, noise generated by increasing the Depth can be instantly eliminated by activating THI. **Figure 12** also shows an increase in noise as a result of increasing the overall gain and Depth, and how it is instantly eliminated by the activation of THI. The activation of the THI in **Figure 12** instantly changed the settings from the fundamental frequency to the harmonic frequency. In **Figure 13**, you also appreciate the importance of THI, in terms of how it improves visualization of the margins of liver surface in comparison with the adjacent image which did not use THI.

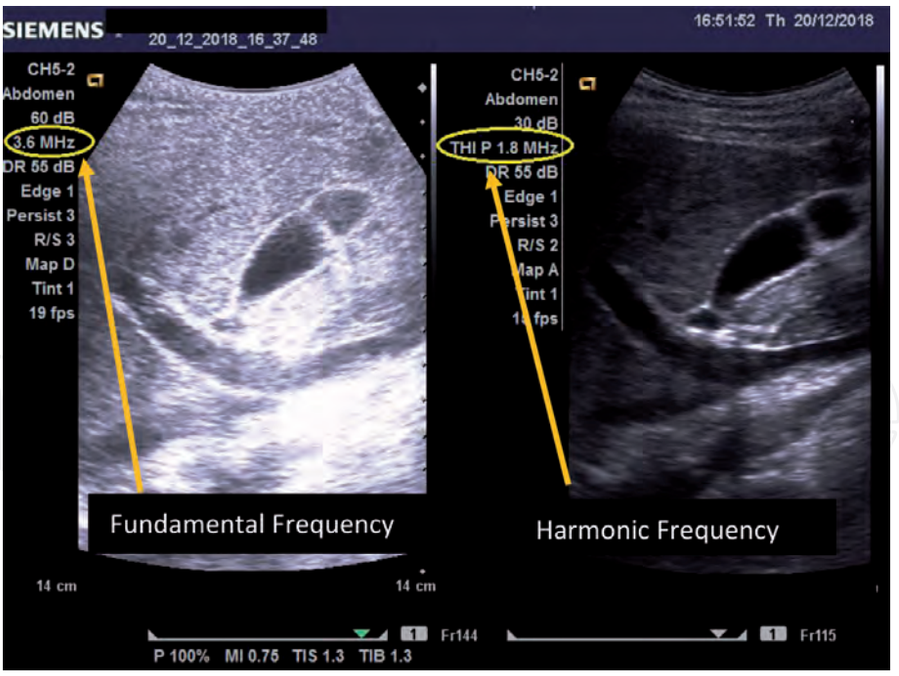

Figure 12.
Noise from increased overall gain and depth is instantly eliminated THI activation.

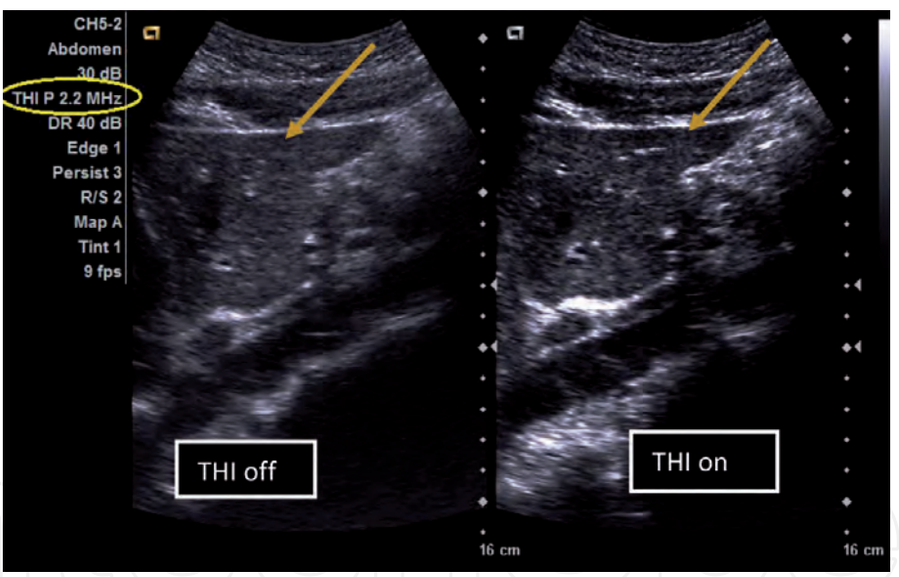

Figure 13.
Improved liver margins with activated THI.

13. Freezing and cineloop

The ultrasound machine also has a freeze button which enables the operator to stop and evaluate the image quality before storage. Saving an image without freezing implies that the image was not evaluated for quality. Freezing the image before storage is therefore recommended.

The cineloop is additional control that helps with selecting the best of the image frozen image. It displays image frames acquired in the last few seconds prior to freezing. The cineloop can be highly useful when scanning children.

14. Additional controls for imaging abdominal blood vessels

An abdominal ultrasound examination may also require the assessment of blood vessels and Doppler evaluation of blood flow. The fundamental knobs that influence both color and spectral Doppler imaging include the Doppler gain, pulse repetition period (PRF), and the wall filter. In assessing the presence of flow in smaller blood vessel, the minimum standard is to adjust the system for a higher Doppler gain, a lower PRF and a lower wall filter [4]. Careful manipulation is used in balancing these knobs, as a slight overlap between them can generate noise artifacts.

Figure 14a shows the poorer flow in the hepatic vein in comparison to the portal vein as a result of higher PRF. This is much improved in **Figure 14b** with decreased PRF.

In larger abdominal blood vessels such as the aorta, additional knob controls that are highly relevant include the imaging angle which must not be parallel to the surface of

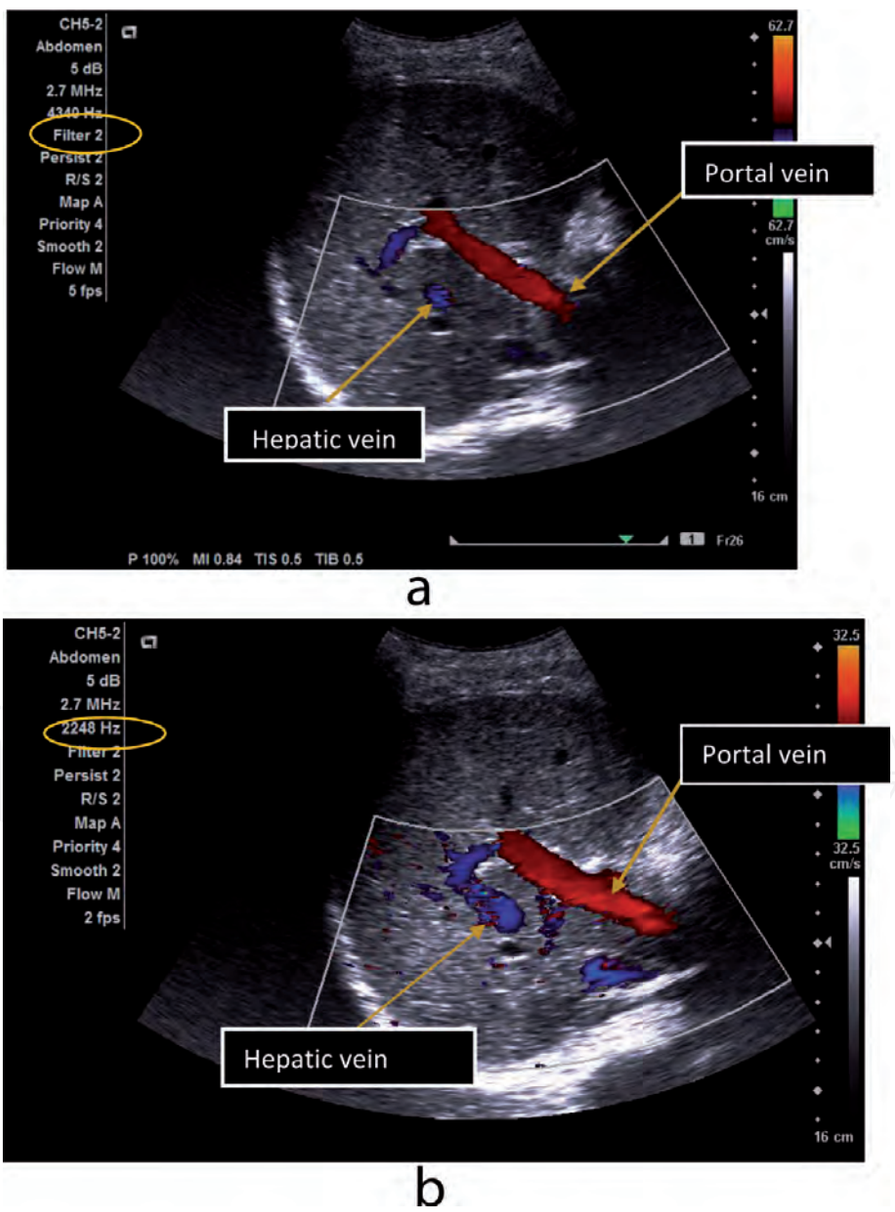

Figure 14.
(a) High PRF with low flow sensitivity in hepatic vein. (b) Low PRF with high flow sensitivity in hepatic vein.

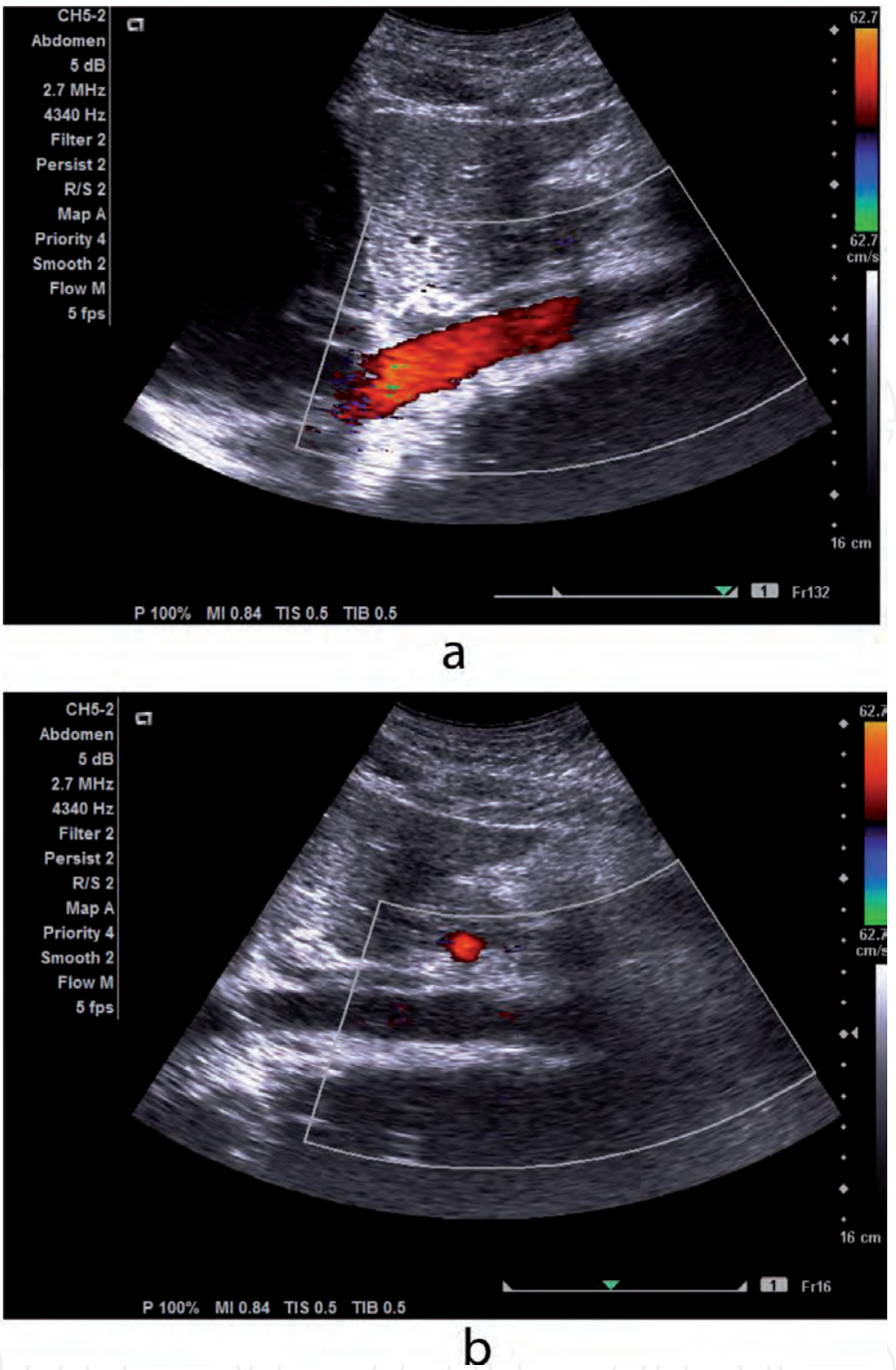

Figure 15.
(a) Color flow showing in angled vessel. (b) Color flow absent in parallel vessel.

the transducer. **Figure 15a** and **b** shows the effect of imaging angle on color flow in the aorta which is absent when the vessel is parallel to the surface of the transducer.

In spectral Doppler Imaging, however, lower PRF may cause aliasing artifact, especially when the baseline is high [5]. This can be corrected by increasing the PRF of the spectral waveform and lowering the baseline. **Figure 16a** shows aliasing artifact of the Superior Mesenteric Artery (SMA) which was as a result of a lower PRF and a higher baseline. By increasing the PRF and lowering the baseline, a normal waveform of the SMA was obtained in **Figure 16b**. Other essential knobology settings which improves spectral waveform in the assessment of peak systolic velocity include using a smaller sample gate and ensuring an angle correct setting that aligns with the vessel wall as demonstrated in **Figure 16a** and **b**.

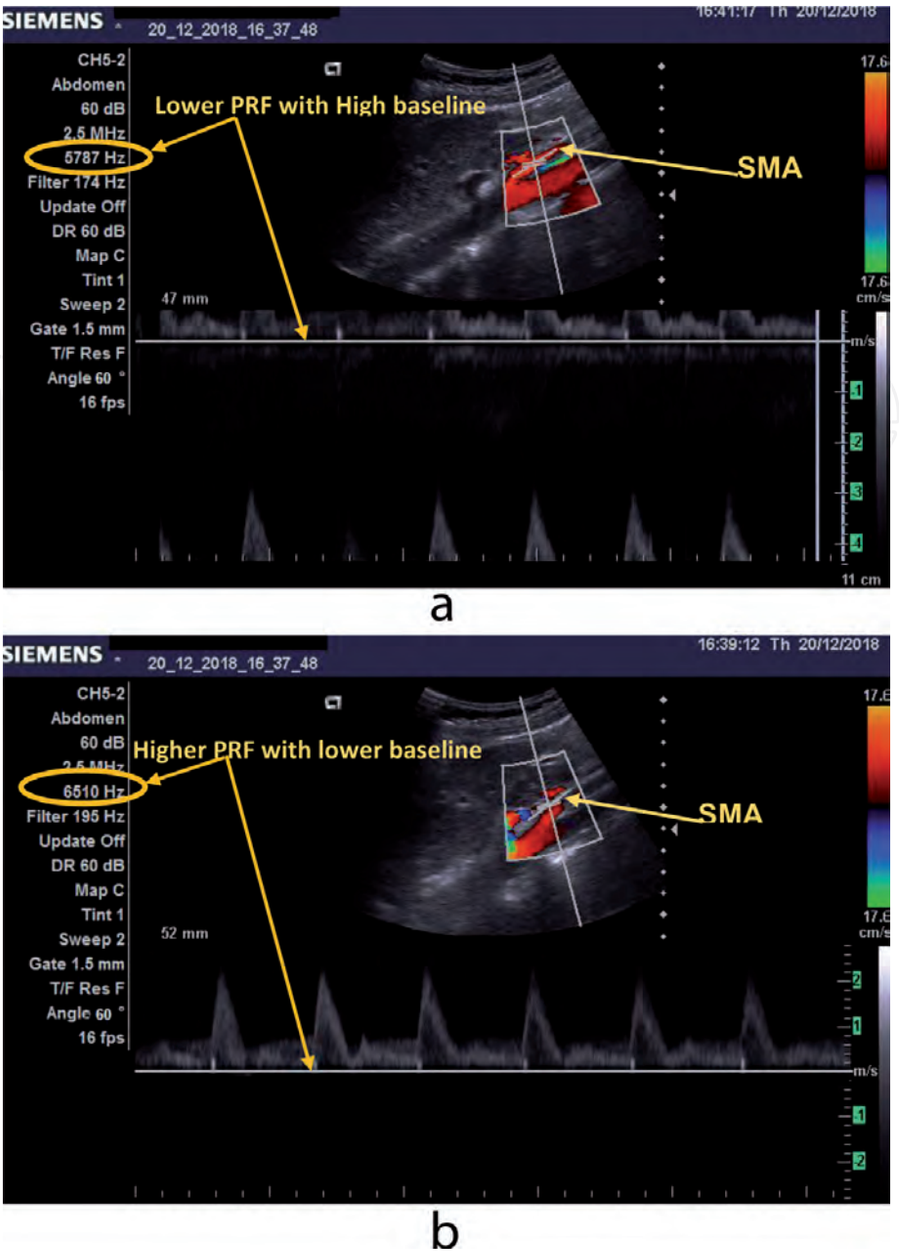

Figure 16.
(a) Aliasing artifact in the superior mesenteric artery as a result of lower PRF and higher baseline. (b) Adequate waveform for assessing peak systolic velocity in the superior mesenteric artery, after increasing the PRF and lowering the baseline.

15. Conclusion

Understanding the influence of knobology in ultrasound imaging is essential in abdominal sonography. The image quality can be optimized by selecting the appropriate application preset and transducer frequency. While using the highest output power may be useful, it is not necessary in many instances. The various knobology variables with direct influence on greyscale and color Doppler should be regularly manipulated by the operator for the best image possible in abdominal sonography.

Author details

Yaw Amo Wiafe[1*] and Augustina Badu-Peprah[2]

1 Medical Imaging Section, Department of Medical Diagnostics, Kwame Nkrumah University of Science and Technology, Kumasi, Ghana

2 Department of Radiology, Komfo Anokye Teaching Hospital, Kumasi, Ghana

References

[1] Merritt C. In: Rumack CM, Wilson SR, Charboeau JW, Levine D, editors. Diagnostic Ultrasound. 4th ed. Mosby: Elsevier; 2011. p. 3. Ch. 1

[2] Venables H. How does ultrasound work? Ultrasound. 2011;**19**(1):44-49. DOI: 10.1258/ult.2010.010051

[3] Kremkau FW. Diagnostic Ultrasound: Principles and Instruments. Philadelphia, USA: WB Saunders Company; 2005

[4] Kim MJ, Kim KW, Kim SY, Kim JK, Won HJ, Shin YM, Kim PN, Lee MG. Technical essentials of hepatic doppler sonography. Current Problems in Diagnostic Radiology. 1 Mar 2009;**38**(2):53-60. Available from: https://doi.org/10.1067/j.cpradiol.2007.08.008

[5] Kruskal JB, Newman PA, Sammons LG, Kane RA. Optimizing doppler and color flow US: Application to hepatic sonography. Radiographics. May 2004;**24**(3):657-675. Available from: https://doi.org/10.1148/rg.243035139

Chapter

Liver Ultrasound Abnormalities in Alcohol Use Disorder

Daniel Fuster, Xavier Garcia-Calvo, Paola Zuluaga, Inmaculada Rivas, Arantza Sanvisens, Jordi Tor and Robert Muga

Abstract

Alcohol-related liver disease is the most common alcohol-related medical illness, and it is the major driver of liver-related deaths worldwide. However, no screening guidelines currently exist for the early detection of liver disease in patients with risky drinking or those with alcohol use disorder. Moreover, most patients with alcohol-related liver fibrosis, which is the main prognostic factor of progression to end-stage liver disease, have normal blood tests. Abdominal ultrasound is a cheap and readily available diagnostic procedure that is rarely used in patients with alcohol use disorder without overt liver disease. In addition, abdominal ultrasound can detect other forms of liver disease, which are not uncommon in patients with unhealthy alcohol use, and can have a negative impact on the natural history of alcohol-related liver disease. In this chapter we will review the current knowledge about the use of liver ultrasound in patients with alcohol use disorder for the early detection of alcohol-related liver disease, as well as the potential use to detect other forms of liver disease. We will also briefly discuss other methods for the noninvasive detection of liver steatosis and/or liver fibrosis in patients with alcohol use disorder.

Keywords: abdominal ultrasound, alcohol-related liver disease, alcohol use disorder, liver steatosis; cirrhosis

1. Introduction

According to the last update of the Global Burden of Disease Study, alcohol consumption is the seventh leading risk factor for both death and the burden of disease and injury [1]. Besides tobacco, alcohol accounts for a higher burden of disease than any other drug, and alcohol-related liver disease is the most common alcohol-related chronic medical illness [2]. In recent years, there has been a worldwide increase in liver-related mortality due to end-stage liver disease [3], mostly because of the impact of alcohol consumption [4, 5]. With the recent advances in hepatitis B and C treatment, alcohol-related liver disease has become the main cause of liver-related mortality [6].

It is important to note that, compared with other forms of liver disease, alcohol-related liver disease has received little attention in the literature, as it is often stigmatized as a self-inflicted disease [7]. This is also true in clinical practice, as

alcohol use is often not properly screened or accounted for in medical charts, both in primary care and hospital settings [8], and treatment for alcohol use is offered to a minority of patients [2].

In this chapter, after a brief introduction about generalities of alcohol-related liver disease and about the assessment of alcohol use in patients with liver disease, we will discuss the current evidence for the use of abdominal ultrasounds in patients with alcohol use disorder (AUD). The current evidence includes a recently published Cochrane review and our own experience with the systematic performance of abdominal ultrasounds in otherwise healthy adults with AUD admitted for hospital detoxification.

In addition, we will also discuss other potential benefits of the use of abdominal ultrasound to detect other forms of liver disease, which are not uncommon in patients with unhealthy alcohol use. We will address the use of liver ultrasound for hepatocellular carcinoma surveillance in patients with alcohol-related liver cirrhosis. Finally, we will include a brief mention of other available methods to screen for alcohol-related liver steatosis and alcohol-related liver fibrosis.

2. General overview of alcohol-related liver disease

Liver disease in patients with AUD encompasses a spectrum of histological abnormalities that includes steatosis, steatohepatitis, fibrosis, cirrhosis of the liver, and hepatocellular carcinoma [9, 10]. Those abnormalities, rather than being different stages of the disease, can coexist in the same patient. Acute alcoholic hepatitis is a severe complication that can occur at any point in the course of alcohol-related liver disease and is associated with liver failure and with high short-term mortality [2].

Alcohol-related liver steatosis in the absence of alcoholic hepatitis is potentially reversible with the cessation of alcohol consumption, but continued alcohol use is associated with progressive liver damage and an increased risk of alcoholic hepatitis [11]. Therefore, abstinence is advisable for patients with AUD and any form of alcohol-related liver disease, as it tends to diminish portal hypertension even in the more advanced forms of the disease [2]. Active alcohol consumption is a formal contraindication for liver transplantation, which is of concern as alcohol-related liver disease is the leading cause of liver transplantation in Europe [12].

A timely diagnosis of liver disease in apparently asymptomatic patients with AUD contributes to a better prognosis and facilitates treatment [13, 14]. In patients with unhealthy alcohol use, liver damage is a major driver of disease burden, and it is often diagnosed in advanced stages, including decompensated liver cirrhosis [14]. In fact, nearly 75% of patients with liver disease present for the first time with a nonelective hospital admission due to end-stage liver disease [5].

The use of liver ultrasound is recommended by the current European guidelines to promote an early detection of nonalcoholic steatohepatitis [15]. However, no guidelines exist for the screening and early detection of liver damage in unhealthy drinkers, and screening approaches in this population are currently a matter of debate [16, 17].

Therefore, there is a need for screening and early detection of alcohol-related liver disease in patients who drink alcohol in excess, as it is well established that sharing abnormal findings suggestive of liver disease with patients can trigger behavioral change and decrease the use of alcohol [18].

Moreover, surveillance aimed to detect hepatocellular carcinoma in patients with alcohol-related liver disease is suboptimal, and liver cancer is often diagnosed at a later stage when potential curative treatments are futile [10].

3. Assessment of alcohol use in patients with suspected liver disease

The Alcohol Use Disorders Identification Test (AUDIT) is a validated tool for identifying AUD in patients [19]. AUD encompasses both alcohol dependence and alcohol abuse [20], and represents the more extreme form of unhealthy alcohol use [21]. The use of AUDIT is recommended by both the American Association for the Study of Liver Diseases (AASLD) and the European Association for the Study of the Liver (EASL) guidelines [22, 23]. Other options are AUDIT-C (a shorter version of the AUDIT) [24], and the single-question screening tool that has been validated for the screening in primary care of unhealthy alcohol use, that is, the spectrum of alcohol use that goes from risky alcohol use to AUD [25].

Patients who screen positive for unhealthy alcohol use merit further assessment to rule out health consequences of alcohol with an emphasis on alcohol-related liver disease [2]. Besides laboratory testing, we believe that the performance of an abdominal ultrasound can be useful in this setting [17].

In addition, referral of patients to physicians who are specialists in addiction medicine is an option to increase the chances of successfully remaining abstinent [2].

4. General overview of abdominal ultrasound for the study of liver diseases

Abdominal ultrasound is a cheap and widely available technique that is not usually performed to detect subjacent liver abnormalities in patients with AUD without overt liver disease.

4.1 Normal ultrasound findings of the liver

Abdominal ultrasound is an accurate method for estimating liver size, which should be determined at the midclavicular line and in normal conditions is less than 16 cm [26]. The liver parenchyma should be evaluated for focal and/or diffuse abnormalities. The normal liver appears as homogeneous with an echogenic texture. In normal conditions, liver echogenicity equals or slightly exceeds that of the renal cortex. This comparison heavily relies on the visual perception of the observer and on the presence (or absence) of disease processes in the renal cortex [27].

The right and left lobes, as well as the caudate lobe can be identified with the use of an ultrasound [28]. Other structures that should be identified are the main lobal fissure, which separates the left and right lobes and appears as an echogenic line that extends to the gallbladder fossa; the falciform ligament, which divides the left lobe into the medial and the lateral segments and appears as an echogenic area in the left lobe; and the ligamentum venosum, which separates the caudate from the left lobe and appears as an echogenic line anterior to the caudate lobe [28].

An abdominal ultrasound can also identify the major hepatic and perihepatic vessels, including the inferior vena cava (IVC), the hepatic veins, the main portal vein, and the right and left branches of the portal vein [28]. The main portal vein is characterized by thick and echogenic walls and enters the liver at the hilum. It divides into the right and left portal branches, and the left branch then divides into medial and lateral branches. The hepatic veins, which drain in the inferior vena cava, have thinner walls in comparison to the portal vein [28]. In addition, abdominal ultrasound is a reliable method for a first-line evaluation of portal vein abnormalities suggestive of portal hypertension [29]. It is also very useful to evaluate the biliary tree and to detect ascitic fluid, and it can also be used to guide the performance of a paracentesis [28].

Doppler evaluation should be used to document blood flow characteristics and blood flow direction, which is crucial in the diagnosis of portal hypertension [30]. In addition, Doppler evaluation can distinguish nodular lesions that are suggestive of hemangiomas, of hepatocellular carcinoma, or of liver metastases [31].

Figure 1 shows how a normal liver appears in an abdominal ultrasound.

4.2 Liver ultrasound in alcohol-related liver disease

In abdominal ultrasounds, liver steatosis appears as hyper-echogenicity due to the increased parenchymal reflectivity that intracellular fat accumulation produces [32]. The sensitivity of abdominal ultrasound to detect liver steatosis is impacted by the amount of fat content and severely decreases if fat content is lower than 10–20% [14].

The results about the ability of liver ultrasound to differentiate between liver steatosis and liver fibrosis have been mixed [33–35], and it is easier to differentiate when the degree of liver fibrosis is higher, as there is an increase in coarse echoes without posterior beam attenuation [32, 33, 36].

How to quantify liver steatosis with abdominal ultrasound is also a matter of debate. Liver steatosis is often classified as "mild," "moderate," or "severe" based on hyper-echogenicity, the discrepancy between echo amplitude in the liver and the kidney, impaired visualization of hepatic vessels, and loss of echoes from the walls of the portal system [36, 37].

Many authors consider steatosis to be *mild* if there is presence of hyper-echogenic liver tissue with fine and tightly packed echo targets and of normal beam penetration with normal visualization of the diaphragm and portal vein borders [38].

If there is decreased beam penetration with slightly decreased visualization of the diaphragm and the portal vein borders as well as moderate or diffuse increase of echo intensity, liver steatosis would then be considered to be *moderate* [38].

If there is a marked increase in echogenicity with no visualization of the portal vein border, an obscured diaphragm and posterior portion of the right lobe, and reduced visibility of the kidney, liver steatosis would be considered *severe* [38].

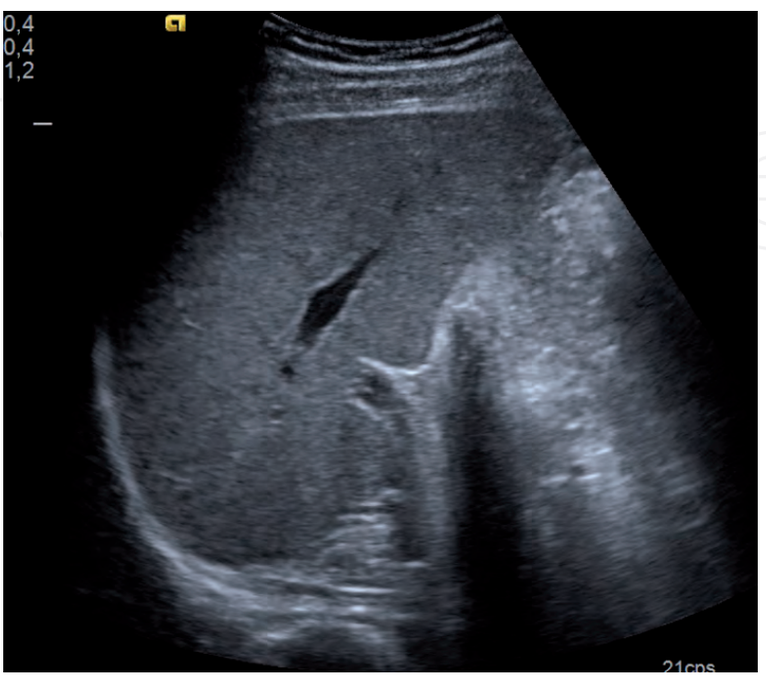

Figure 1.
Normal liver.

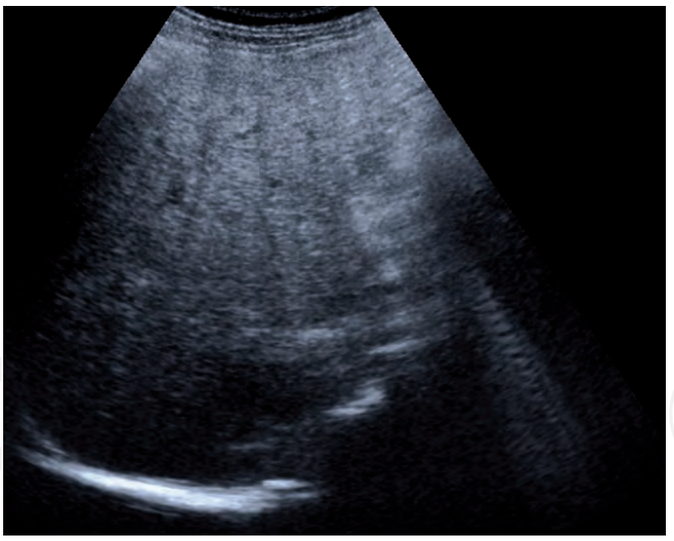

Figure 2.
Severe steatosis in an heterogeneous liver.

As mentioned in the introduction, different alcohol-related liver disease abnormalities can coexist in the same patient. **Figure 2** shows an abdominal ultrasound consistent with severe steatosis in a patient with AUD admitted for hospital treatment that also harbors a heterogeneous liver.

A potential weakness of liver ultrasound is operator dependency in assessing liver steatosis [27]. In a retrospective study that used static images of liver ultrasounds and included 168 patients from routine clinical practice and three independent radiologists, the mean inter-observer agreement rates for the presence of liver steatosis were 72%, while the mean intra-observer agreement 1 month later was 76% [27]. In that study, intra-observer agreement for the severity of liver steatosis ranged from 55 to 68% [27].

In general, there is agreement that abdominal ultrasound is a cheap and reliable method to identify moderate or severe liver steatosis [38], but its accuracy for mild forms of steatosis is lower and may increase with the use of a computer-aided method [38]. Besides liver steatosis, ultrasound findings that contribute to the detection of alcohol-related liver disease include (among others) liver size,

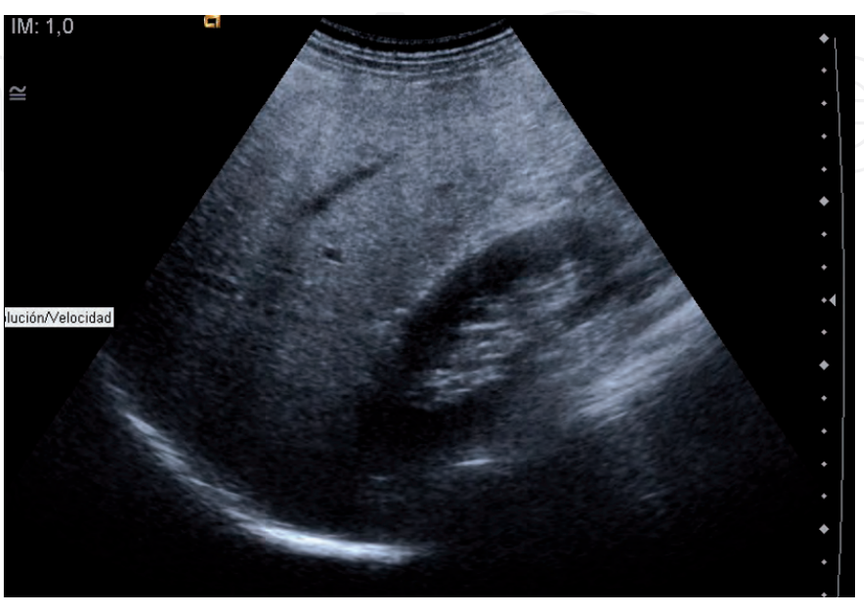

Figure 3.
Heterogeneous liver in a patient with AUD admitted for hospital detoxification.

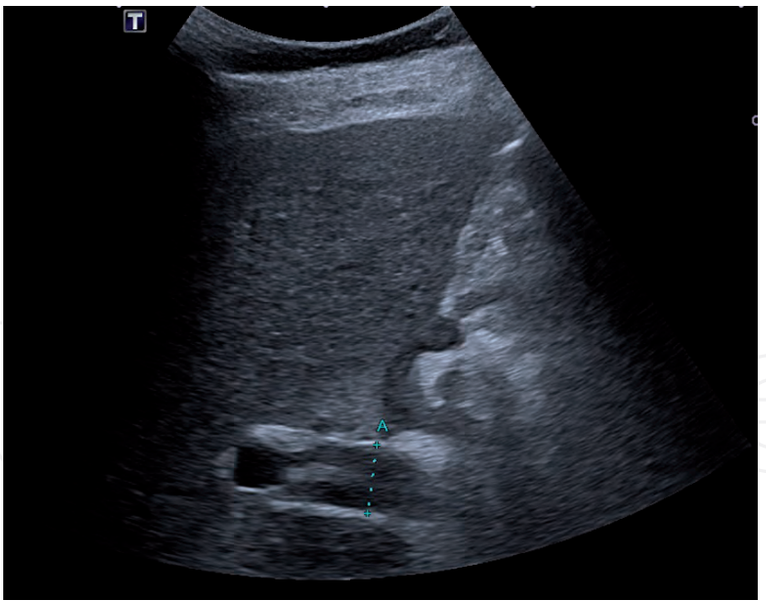

Figure 4.
Cirrhosis of the liver with an enlarged portal vein, consistent with portal hypertension.

bluntness of the edge, coarseness of parenchyma, nodularity of the surface, size of the lymph nodes around the hepatic artery, irregularity and narrowness of the inferior vena cava, portal vein velocity and caliber, and spleen size [28].

Figure 3 shows a heterogeneous liver in a 45-year-old patient with alcohol-related liver disease, and **Figure 4** shows an ultrasound of a 50-year-old patient with AUD and alcohol-related cirrhosis of the liver, as well as an enlarged portal vein, consistent with portal hypertension.

5. Use of liver ultrasound in patients with AUD: current evidence

Evidence about the use of liver ultrasounds to detect underlying liver disease in patients with AUD is scarce and includes a Cochrane systematic review and a recently published study by our group.

5.1 Cochrane systematic review

A Cochrane review published in 2016 stated that there was a need for studies of adequate sample size to study the efficacy of liver ultrasound in alcohol-related liver disease [39], as the review could only include two studies that aimed to assess alcohol-related liver cirrhosis with liver ultrasound [39].

The first study was published by French researchers in 1985 and included 126 alcoholic patients who underwent liver ultrasound [40]. Of those, a hundred patients also underwent liver biopsy. The mean age of participants was 55.6 years. In that study, the main ultrasound findings were as follows: 100 patients (78%) presented hepatomegaly, 59 (46%) presented heterogeneous liver, 44 (34%) presented portal hypertension, and 82 (64%) presented liver cirrhosis. In those who underwent liver biopsy, liver cirrhosis was confirmed in 72 participants, so ultrasound had a 81% sensitivity and 79% specificity for the detection of liver cirrhosis [40].

The second study was performed in Korea and published in 2013. It included 230 patients (81% male) who underwent abdominal ultrasound and liver elastography prior to liver biopsy [41]. The mean age of the study population was 50.4 years; 199 patients (86.5%) and 170 (74%) presented an ultrasound that was suggestive of

heterogeneous liver and liver cirrhosis, respectively. Liver cirrhosis was confirmed in 111 participants; therefore, ultrasound had a 94% sensitivity and 49% specificity for the detection of liver cirrhosis [41].

Due to differences in the selection criteria and the small number of patients included in both studies, the systematic review could reach no conclusion around the usefulness of liver ultrasound to detect underlying liver cirrhosis in patients with alcohol use [39].

5.2 Ultrasound findings of liver damage in a series of AUD patients consecutively admitted for hospital detoxification

We recently published a cross-sectional study of the use of abdominal ultrasound in 301 patients with AUD without overt liver disease that were admitted for hospital detoxification [17].

In that study, clinical and laboratory parameters were obtained at admission, and an abdominal ultrasound was performed on the third day of admission. Abdominal ultrasound was used to identify steatosis, hepatomegaly, heterogeneous liver, and portal hypertension. Portal hypertension was defined as having any of the following abnormalities: splenomegaly, enlarged portal vein, ascites, and/or abnormal portal vein flow.

For the purpose of the analysis, we defined analytical liver injury (ALI) as at least two of the following abnormalities: aspartate aminotransferase (AST) levels ≥74 < 300 U/L, AST/alanine aminotransferase (ALT) ratio >2, and total bilirubin>1.2 mg/dL. Advanced liver fibrosis (ALF) was measured with the FIB-4 (a noninvasive index for the detection of liver fibrosis) [42], and was defined as a FIB-4 score ≥ 3.25.

We wanted to study bivariate associations of ultrasound abnormalities with three commonly observed conditions, hepatitis C virus infection (HCV), ALI, and ALF. We also used logistic regression to see if any of those three conditions predicted the presence of two or more ultrasound abnormalities.

In brief, 80% of the participants were male, with a median age of 46 years (Interquartile range [IQR]: 39–51 years) and had an alcohol consumption of 180 g/day upon admission (IQR: 120–201 g). The prevalence of HCV was 21.2%; AST and ALT serum levels were 42 U/L (IQR: 23–78 U/L) and 35 U/L (IQR: 19–60 U/L), respectively; 16% of patients had ALI and 24% ALF. Ultrasound findings in the study population were as follows: 57.2% steatosis, 49.5% hepatomegaly, 17% heterogeneous liver, and 16% portal hypertension. Of note, 77% had at least one ultrasound abnormality, and 45% had ≥2.

In logistic regression analyses, ALI and ALF were associated with having ≥2 ultrasound abnormalities [Odds Ratio (OR) (95% Confidence Interval [CI]): 5.2 (2.1–12.8), $p < 0.01$ and 4.7 (2.2–9.7), $p < 0.01$, respectively], while HCV infection was not (we performed a multivariate regression model for each of the three potential predictors) [17].

Most patients with only one ultrasound abnormality had hepatomegaly or mild to moderate steatosis, both of which represent morphologic changes that are potentially reversible with alcohol cessation. Therefore, we believe that implementation of abdominal ultrasound in the regular care of patients seeking AUD treatment might be helpful for making clinical decisions and determining therapeutic interventions.

In fact, ultrasound abnormalities were very common in this series of patients, even in patients without HCV, ALI, and ALF, as only 31% of patients in that group had a totally normal abdominal ultrasound. In this regard, we believe that the use of ultrasound to detect early stages of liver disease may promote alcohol cessation, what might have a tremendous impact on the natural history of alcohol-related liver

cirrhosis, especially in patients that present earlier stages of the disease [17]. As previously described by other researchers, sharing findings that might impact negatively the prognosis with patients may also be associated with a decrease in unhealthy drinking [18]. Upon publication of this study, a literature search did not identify any large ultrasound study of AUD patients with compensated liver disease [17].

5.3 Hepatocellular carcinoma surveillance

As mentioned before, hepatocellular carcinoma is the last stage of alcohol-related liver disease, with an annual incidence of 2.9% in patients that already harbor liver cirrhosis [10]. It entails a very poor prognosis if not detected at the earliest possible stage [43]. This is the reason why all patients with alcohol-related cirrhosis should be included in hepatocellular carcinoma surveillance programs that typically consist of an abdominal ultrasound every 6 months [10].

However, periodical surveillance is not optimal in clinical practice, as surveillance is missed by one-third of patients and the interval between screening ultrasounds is often greater than 6 months [10]. In fact, less than 30% of hepatocellular carcinomas diagnosed in Europe and the USA are detected by surveillance [10, 44]. In addition, patients with alcohol-related liver cirrhosis are more likely to have deficient surveillance than those with HCV infection [43, 45].

In our series of 301 patients with AUD that underwent liver ultrasound, 15 (4.9%) had space occupying lesions; most of those lesions were hepatic hemangiomas, but hepatocellular carcinoma was diagnosed in 2 patients [17].

Figure 5 shows a liver nodule, suggestive of hepatocellular carcinoma over a cirrhotic liver in a 52-year-old woman with AUD and untreated chronic HCV.

5.4 Other potential uses of abdominal ultrasound in patients with AUD

Beyond the early detection of liver steatosis or liver cirrhosis, abdominal ultrasound might be useful for the detection of other forms of liver disease that may coexist with alcohol-related liver disease.

Alcohol use is common in patients with other forms of liver disease, and even alcohol use that would be considered moderate can be detrimental in these

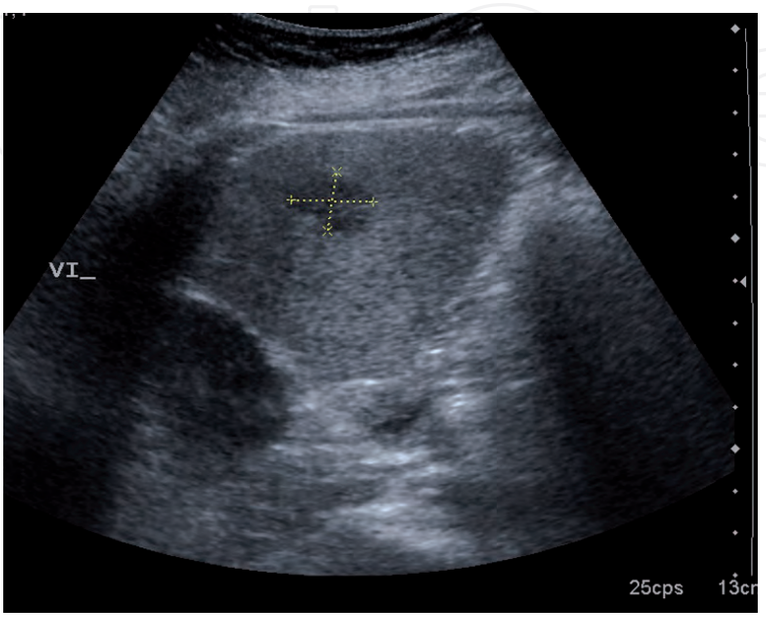

Figure 5.
A liver nodule, suggestive of hepatocellular carcinoma over a cirrhotic liver in a 52-year-old woman with AUD and untreated chronic hepatitis C virus infection.

situations [46, 47]. In fact, alcohol use is a cofactor for the progression of liver disease in patients with HCV, hepatitis B virus infection (HBV), nonalcoholic fatty liver disease, and hemochromatosis, among others. It is important to note that an arbitrary threshold of a daily alcohol intake of 30 grams for men and 20 grams for women is used to differentiate between alcohol-related liver damage and damage due to other etiologies [2]. However, with the current epidemic of overweight and obesity in Western societies, alcohol-related liver disease and nonalcoholic liver steatosis often coexist in the same patient [48]. In fact, in our cohort of patients with AUD that underwent abdominal ultrasound, the median body mass index was 24.7 kg/m^2, that is, a significant amount of patients were overweight [17].

In addition, the performance of abdominal ultrasound can detect less prevalent forms of liver disease, like vascular diseases (Budd-Chiari syndrome, hepatic vein congestion, and noncirrhotic portal hypertension) as well as other parenchymatous diseases.

6. Other noninvasive procedures used to detect liver steatosis in patients with AUD

Controlled attenuation parameter (CAP) is a noninvasive tool to detect liver steatosis that measures ultrasound attenuation when trespassing fatty liver tissue [49]. CAP software is incorporated into the transient elastography equipment, thus facilitating the bedside estimation of both liver steatosis and liver fibrosis [14].

In a recent individual patient data meta-analysis that included 2, 735 cases with both liver biopsy and CAP, cutoffs for moderate and severe liver steatosis were defined, with a diagnostic accuracy between 0.65 and 0.90 [50]. Patients included in that meta-analysis had mainly HBV (37%) and HCV (36%), or nonalcoholic fatty liver disease (20%), while patients with alcohol-related liver disease were underrepresented [50]. Given that all patients included in the meta-analysis harbored liver diseases that are strongly associated with liver fibrosis, there is a need for further validation of those cutoffs in a healthier population [51].

Another study by Thiele and colleagues published in 2018 that included 562 patients with alcohol-related liver steatosis found that CAP above 290 dB/m ruled in any steatosis with 88% specificity and 92% positive predictive value, while CAP below 220 dB/m ruled out steatosis with 90% sensitivity, but 62% negative predictive value [52]. Researchers concluded that CAP had a good diagnostic accuracy for diagnosing severe alcoholic liver steatosis and could be used to rule in any steatosis. The study also included a cohort of patients who were admitted for alcohol detoxification and found that CAP rapidly declined in nonobese patients [52]. This finding speaks to the double-hit model of alcohol use and obesity in a significant proportion of patients commonly seen in clinical practice [53].

7. Alternative noninvasive methods to detect liver fibrosis in patients with AUD

7.1 Transient elastography

Transient elastography has also been used for analyzing liver injury in patients with AUD. A study found elastography provided an assessment of fibrosis that was comparable to liver biopsy [16]. Other authors, however, have expressed concerns that alcohol-related steatohepatitis may distort results, leading to overestimation of

liver fibrosis in this population [54], especially in patients who maintain abstinence from alcohol, as liver stiffness seems to dramatically decrease with cessation of alcohol use [55].

A systematic review and meta-analysis published in 2016 that included 14 different studies suggested that transient elastography was a good method to exclude the presence of liver cirrhosis or advanced liver cirrhosis but advised that caution should be needed when using the same cutoffs described for viral hepatitis in other forms of liver disease [56].

A recently published individual patient data meta-analysis that included 1026 patients suggested that cutoffs for transient elastography should be higher, especially in patients with elevated AST and/or bilirubin, suggestive of active alcoholic hepatitis [57].

Therefore, transient elastography is a promising tool, but it is mainly used in European countries in specialty clinics or teaching institutions [14]. In other countries its use is limited because of budget constraints or because it is only approved for research purposes.

7.2 Noninvasive laboratory-driven indices

There are several noninvasive indices to estimate liver fibrosis that are derived from laboratory parameters routinely used in clinical practice, including AST, ALT, and platelet count.

Among those, the most widely used are the FIB-4 [42], and the AST/platelet ratio index (APRI) [58], which have been validated against the gold standard of liver biopsy in HCV-monoinfected patients as well as HCV- and HIV-coinfected patients [59–61]. These indices perform better for detecting either the absence of liver fibrosis or the presence of advanced liver fibrosis [42, 58]. However, clinical experience using these markers in patients with AUD is somewhat limited [62]. In fact, some researchers have expressed concerns because of potential overestimation of liver fibrosis when using these noninvasive indices in alcohol-related liver disease [62, 63].

In a series of patients with HIV and/or HCV infection, results around the ability of noninvasive indices to capture the impact of alcohol and liver fibrosis have been mixed, probably because of the different methods used to describe alcohol intake and other characteristics of the study population. A cross-sectional study in an urban cohort of HIV-infected individuals in Baltimore (USA) revealed that heavy alcohol use was associated with advanced liver fibrosis measured using the APRI score [64]. In that same study, when patients were stratified by HCV infection, high APRI score was associated with hazardous alcohol use only among patients without HCV infection [64]. In a cohort of HIV-infected women, Blackard and colleagues demonstrated that alcohol use was not associated with FIB-4 values among those with HCV-/HIV-coinfected women [65].

In a cohort of Boston HIV-infected patients with alcohol problems, lifetime alcohol consumption was not associated with the presence of advanced liver fibrosis (FIB-4 $\geq$ 3.25) [66, 67]. Another study performed in the Veterans Aging Cohort Study (VACS) reported greater risks of advanced liver fibrosis (measured with FIB-4) among HCV-/HIV-coinfected patients who exhibited any level of alcohol consumption or who had alcohol-related diagnoses [68].

Despite these somewhat discordant results, noninvasive markers of liver fibrosis have been widely used in populations with alcohol or other substance use disorders that are unlikely to undergo a liver biopsy [67, 69]. Besides, those noninvasive indices have been able to predict midterm mortality in epidemiological studies [69, 70]. A rather innovative approach is the combination of noninvasive indices and transient

elastography, so as to better characterize patients in the intermediate range of FIB-4 values (1.45–3.25) [71].

8. Conclusions

Abdominal ultrasound is a cheap and easily available noninvasive method that could be useful as a first-line screening to assess underlying liver disease in patients with excessive alcohol intake. For patients that need further assessment, transient elastography and CAP, if available, might be helpful in defining the extent and magnitude of alcohol-related liver disease.

Acknowledgements

The research was partially funded by the Ministry of Economy and Competitiveness; Institute of Health Carlos III (RETICS RD16/0017/0003, grant PI17/00174, and Rio Hortega Program CM17/022), Spain; and European Fund for Regional Development (FEDER); Ministry of Health, Social Services and Equality, and National Plan on Drugs (grants 2015/027 and 2018/020), Spain; Gilead Fellowship Program, Gilead Sciences (grant GLD17/00187); Health Department Intensification Program (grant SLT006/17/00107) and Consolidated Research Group (grant 2017-SGR-316), Autonomous of Catalonia, Spain.

Conflict of interest

The authors report no conflict of interest.

Author details

Daniel Fuster[1*], Xavier Garcia-Calvo[1], Paola Zuluaga[1], Inmaculada Rivas[2], Arantza Sanvisens[1], Jordi Tor[1] and Robert Muga[1]

1 Internal Medicine Service, Hospital Universitari Germans Trias i Pujol, Universitat Autònoma de Barcelona, Badalona, Spain

2 Municipal Centre for Substance Abuse Treatment (Centro Delta), Badalona Serveis Assistencials, Badalona, Spain

References

[1] Griswold MG, Fullman N, Hawley C, et al. Alcohol use and burden for 195 countries and territories, 1990-2016: A systematic analysis for the global burden of disease study 2016. Lancet. 2018;**392**(10152):1015-1035. DOI: 10.1016/S0140-6736(18)31310-2

[2] Fuster D, Samet JH. Alcohol use in patients with chronic liver disease. The New England Journal of Medicine. 2018;**379**(26):2577-2579. DOI: 10.1056/NEJMc1814129

[3] Rehm J, Samokhvalov AV, Shield KD. Global burden of alcoholic liver diseases. Journal of Hepatology. 2013;**59**(1):160-168. DOI: 10.1016/j.jhep.2013.03.007

[4] Jinjuvadia R, Liangpunsakul S. Translational research and evolving alcoholic hepatitis treatment consortium. Trends in alcoholic hepatitis-related hospitalizations, financial burden, and mortality in the United States. Journal of Clinical Gastroenterology. 2015;**49**(6):506-511. DOI: 10.1097/MCG.0000000000000161

[5] Williams R, Aspinall R, Bellis M, et al. Addressing liver disease in the UK: A blueprint for attaining excellence in health care and reducing premature mortality from lifestyle issues of excess consumption of alcohol, obesity, and viral hepatitis. Lancet. 2014;**384**(9958):1953-1997. DOI: 10.1016/S0140-6736(14)61838-9

[6] Stein E, Cruz-Lemini M, Altamirano J, et al. Heavy daily alcohol intake at the population level predicts the weight of alcohol in cirrhosis burden worldwide. Journal of Hepatology. 2016;**65**(5):998-1005. DOI: 10.1016/j.jhep.2016.06.018

[7] Bataller R, Arteel GE, Moreno C, Shah V. Alcohol-related liver disease: Time for action. Journal of Hepatology. 2019;**70**(2):221-222. DOI: 10.1016/j.jhep.2018.12.007

[8] Roson B, Monte R, Gamallo R, et al. Prevalence and routine assessment of unhealthy alcohol use in hospitalized patients. European Journal of Internal Medicine. 2010;**21**(5):458-464. DOI: 10.1016/j.ejim.2010.04.006; 1

[9] Seitz HK, Bataller R, Cortez-Pinto H, et al. Alcoholic liver disease. Nature Reviews. Disease Primers. 2018;**4**(1):16. DOI: 10.1038/s41572-018-0014-7

[10] Ganne-Carrié N, Nahon P. Hepatocellular carcinoma in the setting of alcohol-related liver disease. Journal of Hepatology. 2019;**70**(2):284-293. DOI: 10.1016/j.jhep.2018.10.008

[11] Lackner C, Tiniakos D. Fibrosis and alcohol-related liver disease. Journal of Hepatology. 2019;**70**(2):294-304. DOI: 10.1016/j.jhep.2018.12.003

[12] Mathurin P, Moreno C, Samuel D, et al. Early liver transplantation for severe alcoholic hepatitis. The New England Journal of Medicine. 2011;**365**(19):1790-1800. DOI: 10.1056/NEJMoa1105703

[13] Ratib S, Fleming KM, Crooks CJ, Walker AJ, West J. Causes of death in people with liver cirrhosis in England compared with the general population: A population-based cohort study. The American Journal of Gastroenterology. 2015;**110**(8):1149-1158. DOI: 10.1038/ajg.2015.191

[14] Moreno C, Mueller S, Szabo G. Non-invasive diagnosis and biomarkers in alcohol-related liver disease. Journal of Hepatology. 2019;**70**(2):273-283. DOI: 10.1016/j.jhep.2018.11.025

[15] Ratziu V, Bellentani S, Cortez-Pinto H, Day C, Marchesini G. A position statement on NAFLD/NASH based

on the EASL 2009 special conference. Journal of Hepatology. 2010;**53**(2): 372-384. DOI: 10.1016/j.jhep.2010.04.008

[16] Thiele M, Detlefsen S, Sevelsted Møller L, et al. Transient and 2-dimensional shear-wave elastography provide comparable assessment of alcoholic liver fibrosis and cirrhosis. Gastroenterology. 2016;**150**(1):123-133. DOI: 10.1053/j.gastro.2015.09.040

[17] Fuster D, Garcia-Calvo X, Zuluaga P, et al. Ultrasound findings of liver damage in a series of patients consecutively admitted for treatment of alcohol use disorder. Drug and Alcohol Dependence. 2018;**190**:195-199. DOI: 10.1016/j.drugalcdep.2018.06.012

[18] Tsui JI, Saitz R, Cheng DM, et al. Awareness of hepatitis C diagnosis is associated with less alcohol use among persons co-infected with HIV. Journal of General Internal Medicine. 2007;**22**(6):822-825. DOI: 10.1007/s11606-007-0147-y

[19] Saunders JB, Aasland OG, Babor TF, de la Fuente JR, Grant M. Development of the alcohol use disorders identification test (AUDIT): WHO collaborative project on early detection of persons with harmful alcohol consumption--II. Addiction. 1993;**88**(6):791-804

[20] American Psychiatric Association. Diagnostic and Statistical Manual of Mental Disorders. 4th ed. (DSM IV-TR) ed. Washington DC: Government Printing Office; 2000

[21] Diagnostic and Statistical Manual of Mental Disorders, DSM-5. Washington DC: American Psychiatric Association, Government Printing Office; 2013

[22] O'Shea RS, Dasarathy S, McCullough AJ. Practice guideline Committee of the American Association for the study of liver, practice parameters Committee of the American College of gastroenterology. Alcoholic liver disease. Hepatology. 2010;**51**(1):307-328. DOI: 10.1002/hep.23258

[23] Thursz M, Gual A, Lackner C, et al. EASL clinical practice guidelines: Management of alcohol-related liver disease. Journal of Hepatology. 2018;**69**(1):154-181. DOI: 10.1016/j.jhep.2018.03.018

[24] Bush K, Kivlahan DR, McDonell MB, Fihn SD, Bradley KA. The AUDIT alcohol consumption questions (AUDIT-C): An effective brief screening test for problem drinking. Ambulatory care quality improvement project (ACQUIP). Alcohol Use Disorders Identification Test. Archives of Internal Medicine. 1998;**158**(16):1789-1795

[25] Smith PC, Schmidt SM, Allensworth-Davies D, Saitz R. A single-question screening test for drug use in primary care. Archives of Internal Medicine. 2010;**170**(13):1155-1160. DOI: 10.1001/archinternmed.2010.140

[26] Kratzer W, Fritz V, Mason RA, Haenle MM, Kaechele V, Roemerstein Study Group. Factors affecting liver size: A sonographic survey of 2080 subjects. Journal of Ultrasound in Medicine. 2003;**22**(11):1155-1161

[27] Strauss S, Gavish E, Gottlieb P, Katsnelson L. Interobserver and intraobserver variability in the sonographic assessment of fatty liver. AJR. American Journal of Roentgenology. 2007;**189**(6):W320-W323. DOI: 10.2214/AJR.07.2123

[28] American College of Radiology. Practice Parameter for the Performance of an Ultrasound Examination of the Abdomen and/or Retroperitoneum. 2018. Available at: https://www.acr.org/Quality-Safety/Standards-uidelines/media/ACR/Documents/PGTS/

guidelines/US_Abdomen_Retro.pdf [Accessed: December 12, 2019]

[29] Kim MY, Jeong WK, Baik SK. Invasive and non-invasive diagnosis of cirrhosis and portal hypertension. World Journal of Gastroenterology. 2014;**20**(15):4300. DOI: 10.3748/wjg.v20.i15.4300

[30] Kruskal JB, Newman PA, Sammons LG, Kane RA. Optimizing Doppler and color flow US: Application to hepatic sonography. Radiographics. 2004;**24**(3):657-675. DOI: 10.1148/rg.243035139

[31] Reinhold C, Hammers L, Taylor CR, Quedens-Case CL, Holland CK, Taylor KJ. Characterization of focal hepatic lesions with duplex sonography: Findings in 198 patients. AJR. American Journal of Roentgenology. 1995;**164**(5):1131-1135. DOI: 10.2214/ajr.164.5.7717219

[32] Schwenzer NF, Springer F, Schraml C, Stefan N, Machann J, Schick F. Non-invasive assessment and quantification of liver steatosis by ultrasound, computed tomography and magnetic resonance. Journal of Hepatology. 2009;**51**(3):433-445. DOI: 10.1016/j.jhep.2009.05.023

[33] Palmentieri B, de Sio I, La Mura V, et al. The role of bright liver echo pattern on ultrasound B-mode examination in the diagnosis of liver steatosis. Digestive and Liver Disease. 2006;**38**(7):485-489. DOI: 10.1016/j.dld.2006.03.021

[34] Taylor KJ, Gorelick FS, Rosenfield AT, Riely CA. Ultrasonography of alcoholic liver disease with histological correlation. Radiology. 1981;**141**(1):157-161. DOI: 10.1148/radiology.141.1.6270725

[35] Meek DR, Mills PR, Gray HW, Duncan JG, Russell RI, McKillop JH. A comparison of computed tomography, ultrasound and scintigraphy in the diagnosis of alcoholic liver disease. The British Journal of Radiology. 1984;**57**(673):23-27. DOI: 10.1259/0007-1285-57-673-23

[36] Hamaguchi M, Kojima T, Itoh Y, et al. The severity of ultrasonographic findings in nonalcoholic fatty liver disease reflects the metabolic syndrome and visceral fat accumulation. The American Journal of Gastroenterology. 2007;**102**(12):2708-2715. DOI: 10.1111/j.1572-0241.2007.01526.x

[37] Saverymuttu SH, Joseph AE, Maxwell JD. Ultrasound scanning in the detection of hepatic fibrosis and steatosis. British Medical Journal (Clinical Research Ed.). 1986;**292**(6512):13-15

[38] Mancini M, Prinster A, Annuzzi G, et al. Sonographic hepatic-renal ratio as indicator of hepatic steatosis: Comparison with 1H magnetic resonance spectroscopy. Metabolism. 2009;**58**(12):1724-1730. DOI: 10.1016/J.METABOL.2009.05.032

[39] Pavlov CS, Casazza G, Semenistaia M, et al. Ultrasonography for diagnosis of alcoholic cirrhosis in people with alcoholic liver disease. Cochrane Database of Systematic Reviews. 2016;**3**:CD011602. DOI: 10.1002/14651858.CD011602.pub2

[40] Richard P, Bonniaud P, Barthélémy C, et al. Value of ultrasonography in the diagnosis of cirrhoses. Prospective study of 128 patients. Journal de Radiologie;**66**(8-9):503-506. Available from: http://www.ncbi.nlm.nih.gov/pubmed/3912496 [Accessed: August 31, 2016]

[41] Moon KM, Kim G, Baik SK, et al. Ultrasonographic scoring system score versus liver stiffness measurement in prediction of cirrhosis. Clinical and Molecular Hepatology. 2013;**19**(4):389-398. DOI: 10.3350/cmh.2013.19.4.389

[42] Sterling RK, Lissen E, Clumeck N, et al. Development of a simple noninvasive index to predict significant fibrosis in patients with HIV/HCV coinfection. Hepatology. 2006;**43**(6):1317-1325. DOI: 10.1002/hep.21178

[43] Schütte K, Bornschein J, Kahl S, et al. Delayed diagnosis of HCC with chronic alcoholic liver disease. Liver Cancer. 2012;**1**(3-4):257-266. DOI: 10.1159/000343840

[44] Davila JA, Morgan RO, Richardson PA, Du XL, McGlynn KA, El-Serag HB. Use of surveillance for hepatocellular carcinoma among patients with cirrhosis in the United States. Hepatology. 2010;**52**(1):132-141. DOI: 10.1002/hep.23615

[45] Bucci L, Garuti F, Camelli V, et al. Comparison between alcohol- and hepatitis C virus-related hepatocellular carcinoma: Clinical presentation, treatment and outcome. Alimentary Pharmacology & Therapeutics. 2016;**43**(3):385-399. DOI: 10.1111/apt.13485

[46] Hutchinson SJ, Bird SM, Goldberg DJ. Influence of alcohol on the progression of hepatitis C virus infection: A meta-analysis. Clinical Gastroenterology and Hepatology. 2005;**3**(11):1150-1159

[47] Hagström H. Alcohol consumption in concomitant liver disease: How much is too much? Current Hepatology Reports. 2017;**16**(2):152-157. DOI: 10.1007/s11901-017-0343-0

[48] Ajmera VH, Terrault NA, Harrison SA. Is moderate alcohol use in nonalcoholic fatty liver disease good or bad? A critical review. Hepatology. 2017;**65**(6):2090-2099. DOI: 10.1002/hep.29055

[49] Sasso M, Beaugrand M, de Ledinghen V, et al. Controlled attenuation parameter (CAP): A novel VCTE™ guided ultrasonic attenuation measurement for the evaluation of hepatic steatosis: Preliminary study and validation in a cohort of patients with chronic liver disease from various causes. Ultrasound in Medicine & Biology. 2010;**36**(11):1825-1835. DOI: 10.1016/j.ultrasmedbio.2010.07.005

[50] Karlas T, Petroff D, Sasso M, et al. Individual patient data meta-analysis of controlled attenuation parameter (CAP) technology for assessing steatosis. Journal of Hepatology. 2017;**66**(5):1022-1030. DOI: 10.1016/j.jhep.2016.12.022

[51] Romero-Gómez M, Cortez-Pinto H. Detecting liver fat from viscoelasticity: How good is CAP in clinical practice? The need for universal cut-offs. Journal of Hepatology. 2017;**66**(5):886-887. DOI: 10.1016/J.JHEP.2017.01.029

[52] Thiele M, Rausch V, Fluhr G, et al. Controlled attenuation parameter and alcoholic hepatic steatosis: Diagnostic accuracy and role of alcohol detoxification. Journal of Hepatology. 2018;**68**(5):1025-1032. DOI: 10.1016/j.jhep.2017.12.029

[53] Bellentani S, Saccoccio G, Masutti F, et al. Prevalence of and risk factors for hepatic steatosis in northern Italy. Annals of Internal Medicine. 2000;**132**(2):112-117

[54] Mueller S, Englert S, Seitz HK, et al. Inflammation-adapted liver stiffness values for improved fibrosis staging in patients with hepatitis C virus and alcoholic liver disease. Liver International. 2015;**35**(12):2514-2521. DOI: 10.1111/liv.12904

[55] Gianni E, Forte P, Galli V, Razzolini G, Bardazzi G, Annese V. Prospective evaluation of liver stiffness using transient elastography in alcoholic patients following abstinence. Alcohol

and Alcoholism. 2017;**52**(1):42-47. DOI: 10.1093/alcalc/agw053

[56] Pavlov CS, Casazza G, Nikolova D, Tsochatzis E, Gluud C. Systematic review with meta-analysis: Diagnostic accuracy of transient elastography for staging of fibrosis in people with alcoholic liver disease. Alimentary Pharmacology & Therapeutics. 2016;**43**(5):575-585. DOI: 10.1111/apt.13524

[57] Nguyen-Khac E, Thiele M, Voican C,et al. Non-invasive diagnosis of liver fibrosis in patients with alcohol-related liver disease by transient elastography: An individual patient data meta-analysis. The Lancet Gastroenterology & Hepatology. 2018;**3**(9):614-625. DOI: 10.1016/S2468-1253(18)30124-9

[58] Wai CT, Greenson JK, Fontana RJ, et al. A simple noninvasive index can predict both significant fibrosis and cirrhosis in patients with chronic hepatitis C. Hepatology. 2003;**38**(2):518-526. DOI: 10.1053/jhep.2003.50346

[59] Nunes D, Fleming C, Offner G, et al. HIV infection does not affect the performance of noninvasive markers of fibrosis for the diagnosis of hepatitis C virus-related liver disease. Journal of Acquired Immune Deficiency Syndromes. 2005;**40**(5):538-544

[60] Loko MA, Castera L, Dabis F, et al. Validation and comparison of simple noninvasive indexes for predicting liver fibrosis in HIV-HCV-coinfected patients: ANRS CO3 Aquitaine cohort. The American Journal of Gastroenterology. 2008;**103**(8):1973-1980. DOI: 10.1111/j.1572-0241.2008.01954.x

[61] Vallet-Pichard A, Mallet V, Nalpas B, et al. FIB-4: An inexpensive and accurate marker of fibrosis in HCV infection. Comparison with liver biopsy and fibrotest. Hepatology. 2007;**46**(1):32-36. DOI: 10.1002/hep.21669

[62] Lieber CS, Weiss DG, Morgan TR, Paronetto F. Aspartate aminotransferase to platelet ratio index in patients with alcoholic liver fibrosis. The American Journal of Gastroenterology. 2006;**101**(7):1500-1508. DOI: 10.1111/j.1572-0241.2006.00610.x

[63] Trabut J-B, Thépot V, Terris B, Sogni P, Nalpas B, Pol S. Prognosis assessment of alcoholic liver disease: How and why? Presse Médicale. 2014;**43**(2):124-134. DOI: 10.1016/j.lpm.2013.04.016

[64] Chaudhry AA, Sulkowski MS, Chander G, Moore RD. Hazardous drinking is associated with an elevated aspartate aminotransferase to platelet ratio index in an urban HIV-infected clinical cohort. HIV Medicine. 2009;**10**(3):133-142. DOI: 10.1111/j.1468-1293.2008.00662.x

[65] Blackard JT, Welge JA, Taylor LE, et al. HIV mono-infection is associated with FIB-4 - a noninvasive index of liver fibrosis - in women. Clinical Infectious Diseases. 2011;**52**(5):674-680. DOI: 10.1093/cid/ciq199

[66] Skinner HA, Sheu WJ. Reliability of alcohol use indices. The lifetime drinking history and the MAST. Journal of Studies on Alcohol. 1982;**43**(11):1157-1170

[67] Fuster D, Tsui JI, Cheng DM, et al. Impact of lifetime alcohol use on liver fibrosis in a population of HIV-infected patients with and without hepatitis C coinfection. Alcoholism, Clinical and Experimental Research. 2013;**37**(9):1527-1535. DOI: 10.1111/acer.12129

[68] Lim JK, Tate JP, Fultz SL, et al. Relationship between alcohol use categories and noninvasive markers of advanced hepatic fibrosis in HIV-infected, chronic hepatitis

C virus-infected, and uninfected patients. Clinical Infectious Diseases. 2014;**58**(10):1449-1458. DOI: 10.1093/cid/ciu097

[69] Nunes D, Fleming C, Offner G, et al. Noninvasive markers of liver fibrosis are highly predictive of liver-related death in a cohort of HCV-infected individuals with and without HIV infection. The American Journal of Gastroenterology. 2010;**105**(6):1346-1353. DOI: 10.1038/ajg.2009.746

[70] Sanvisens A, Fuster D, Serra I, et al. Estimated liver fibrosis and its impact on all-cause mortality of HCV-monoinfected and HCV/HIV-coinfected drug users. Current HIV Research. 2011;**9**(4):256-262

[71] Gnatienko N, Freiberg MS, Blokhina E, et al. Design of a randomized controlled trial of zinc supplementation to improve markers of mortality and HIV disease progression in HIV-positive drinkers in St. Petersburg, Russia. HIV Clinical Trials. 2018;**19**(3):101-111. DOI: 10.1080/15284336.2018.1459344

Chapter

The Kidney

Ercan Ayaz

Abstract

Ultrasound and conventional radiographs still remain the first-line radiological tools for most of the kidney disorders. Ultrasonographic image quality has been astonishingly improved in recent years with the development of technology and software algorithms. In line with these developments, ultrasound is not only the primary imaging modality for kidney anatomy and lesions, but also sufficient for definitive diagnosis and follow up for some lesions. The aim of this chapter is to focus on the areas that ultrasound is used primarily about the kidney. These topics include kidney anatomy, anatomic variants that mimic lesions, congenital diseases, kidney stones, nephrocalcinosis, most of the cystic diseases, and some solid lesions, infection, and trauma.

Keywords: kidney, ultrasound, renal cyst, kidney stone, nephrocalcinosis

1. Introduction

Major functions of the kidney are excreting metabolic waste products and maintaining homeostasis by regulating water, salt, and acid-base balance. The kidney is also an endocrine organ that secretes many hormones, including erythropoietin, renin, and prostaglandins. Ultrasound (US) represents the first-line radiologic imaging technique in the assessment of the kidney anatomy and various disorders. Imaging quality of US has greatly developed in recent years with the advances in the transducer, beam-former technology, and image processing software. Grayscale B-mode US, with the addition of tissue harmonic imaging and compound modes, and color Doppler US definitely provide a diagnostic clue in most renal abnormalities. US artifacts are extremely important in the US evaluation of the kidney because they must be differentiated by true images and may add valuable information in some lesions such as stone and cyst. US presents several advantages over the other imaging modalities including low financial cost, portability, availability, lack of restrictions in performing frequent serial examinations at short intervals, and absence of exposure to radiation or nuclear tracers.

In this chapter, grayscale US findings of normal kidney anatomy, anatomic variants, congenital anomalies, kidney stones, cystic and solid lesions, infections, and traumatic lesions have been discussed. Moreover, embryology and anatomy of the kidney have been explained along with the sonography technique briefly.

2. Embryology and anatomy

During the third week of the development of the human embryo, the urogenital apparatus derives from the intermediate mesoderm. The intermediate mesoderm

initially divides into a set of small cell groups called nephrotomes in the cervical and thoracolumbar regions. These cell masses represent three different excretory sets: the pronephros, the mesonephros, and the metanephros. The pronephros is formed at the beginning of the fourth week and remains rudimentary. It is analogous to the kidney in primitive fishes. The mesonephros appears at the end of the fourth week and it is the first functioning unit until the development of metanephros at the ninth week [1]. It is analogous to the kidney of amphibians. Metanephros begins to be active in the 9–10th week [45]. After that time, it becomes a permanent kidney. Metanephros divided into two parts, which originate from different sources, called the metanephric mass and the metanpehric diverticulum. The metanephric mass derived from intermediate mesoderm and their cells give rise to nephrons which are the morphological functional units of the kidney. The metanephric diverticulum or ureteric bud develops from mesonephric duct, which constitutes collecting tubules, calices, renal pelvis, and ureter.

Initially, the permanent kidneys are located close to each other in the pelvis at the caudal end of the mesonephros and ventrally to the sacrum. With fetal growth, the kidneys progressively come to the retroperitoneum and move farther apart, while the abdomen and pelvis grow. At the end of the eighth week, the kidneys set themselves at the first four lumbar vertebral levels, just below the adrenal glands. This migration occurs not only by the caudal migration of the kidneys, but also the growth of the caudal part of the body away from the kidneys. The hilum of the kidney, which includes renal pelvis, vessels, and nerves, faces ventrally before migration; it rotates medially almost 90° during the ascent of kidney. In the ninth week, the renal pelvis is directed anteromedially [1].

During fetal life, the human kidney surface is lobulated which decreases gradually at the end of pregnancy but is still present in the kidneys of neonates. Lobulation disappears during infancy. The reason of the lobulation is the caliceal structure of the collecting system [45]. The buds of minor calices penetrate into the metanephric blastema and give rise to 13 trees of excretory ductules. Every minor calyx brings on a big glandular unit that consists of a medullar unit called Malpighi pyramid and a cortical unit which is separated from the others by interlobular sulci that causes lobulated surface of the kidney. Metanephric tissue penetrates between the pyramids, goes toward renal pelvis, and constitutes the Bertin column [1].

Primarily, fetal kidney derives blood supply, branches from the iliac artery. As the kidney ascends, it receives new branches from the abdominal aorta. Meanwhile, the branches from iliac artery undergo involution and disappear. Migration of the kidney ends at the ninth week, when the kidney takes tight contact with the suprarenal gland. Finally, the kidney receives the permanent renal arteries originating from the abdominal aorta. About 70% of people exhibit single renal artery to each kidney. On the other hand, two to four renal arteries are seen in 25% of adults [2]. The supernumerary arteries usually originate from the abdominal aorta above or below the main renal artery and follow it through the renal hilum. However, they may also enter the kidney from the superior and/or the inferior pole which is called polar artery. Inferior polar artery may cross anterior the ureter and occlude it, leading to hydronephrosis. It is important to recognize supernumerary arteries, since if an accessory artery is damaged or ligated, the region of the kidney supplied by it may undergo ischemia.

In the adult, each kidney is located in the retroperitoneum and measures approximately 10–12 cm long, 2–3 cm thick, and 3–5 cm wide and weighs 250–270 g [3]. The right kidney is located posterior to the inferior surface of the liver with peritoneal interposition, and lateral to the second portion of the duodenum without any peritoneal interposition since the second portion of the duodenum is retroperitoneal. The left kidney lies posterior to the pancreatic tail, the stomach, the ligament of Treitz, and posterior medial to the spleen.

The volume of the right kidney is smaller than that of the left kidney, possibly due to limited potential space for the right kidney (large volume of liver in the right upper quadrant) or relatively increased left renal flow (left kidney is closer to aorta and left renal artery is shorter than right renal artery) [4].

The kidney is a bean shaped organ with a smooth, regular border. Renal hilum is located at the medial surface of the kidney and continues with a central cavity called renal sinus. Renal sinus contains the major branches of the renal artery, major tributaries of the renal vein, and the collecting system [5]. The background of renal pelvis is composed of fat tissue. Renal pelvis is generally located posterior to the vessels. The kidney is covered by a renal capsule which is composed of an inner fibrous layer and an outer perinephric adipose layer. Renal cortex is the outer part of the kidney between fibrous renal capsule and the renal medulla. It has a smooth outer contour with a number of projections (columns of Bertin) extending between the Malpighi pyramids. Renal medulla is the inner part of the kidney consisting of a number of 8–18 cone shaped sections, known as renal pyramids. The inner tip of each renal pyramid is called renal papilla where the urine drains into the renal pelvis. The renal pelvis extrudes from the kidney anteromedially and continues as the ureter. The left kidney is usually located 1–2 cm higher than the right kidney and in supine position; right renal pelvis is usually located at the level of the second lumbar vertebra [6].

Renal pyramids are hypoechoic relative to the cortex in the adult kidney which allows demonstrating both structures in ultrasound. The renal cortex should be hypo- or isoechoic relative to the adjacent liver or spleen in most of the normal adults. Hyperechoic renal cortex showed a specificity of 96%and a positive predictive value of 67% for detecting abnormal renal function, but with a poor sensitivity (20%) [7]. However, in neonates, renal cortex is iso- or hyperechoic relative to liver and spleen parenchyma and pyramids are more prominent. Even in premature infants, cortical hyperechogenicity is more prominent [8]. However, an excessive increased renal echogenicity in newborns may also be due to infantile polycystic kidney disease, hemolytic-uremic syndrome, or renal vein thrombosis [8]. Within the range of 2–6 months, the kidneys become gradually less echogenic than the liver and assume the features of the adult kidney between 6 and 24 months of life [3].

There are some variations that affect the border and cortex of the kidney such as junctional parenchymal defect, fetal lobulations, dromedary hump, and hypertrophied column of Bertin (HCB) (**Figure 1**). HCB is an unresorbed polar parenchyma from one or both of the two subdivisions of kidneys that combine to form the normal kidney [9]. HCB is generally located at the junction of the upper and middle thirds of the kidney and contain renal cortex which extends to the renal sinus. HCB also contains adjacent renal pyramids and usually measures less than 3 cm [10]. Sometimes, echogenicity of the HCBs is different from the adjacent renal cortex due to alterations in tissue orientation, which result in different acoustic reflectivity [9]. It may be challenging to differentiate a small, avascular tumor from an HCB, and occasionally contrast enhanced computed tomography (CT) may be necessary to differentiate them.

Junctional parenchymal defects occur at the site of two parenchymal masses called ranunculi which constitute the normal kidney. It is a horizontally oriented linear echogenicity most often located anterior and superiorly and traced medially into the renal sinus.

Dromedary hump is a prominent bulging on the superolateral aspect of the left kidney. It is believed to arise secondary to compression of the upper pole of the left kidney by the spleen during development. The normal nature of this finding is appreciated by the constant thickness of the bulging renal cortex over the underlying renal calyces.

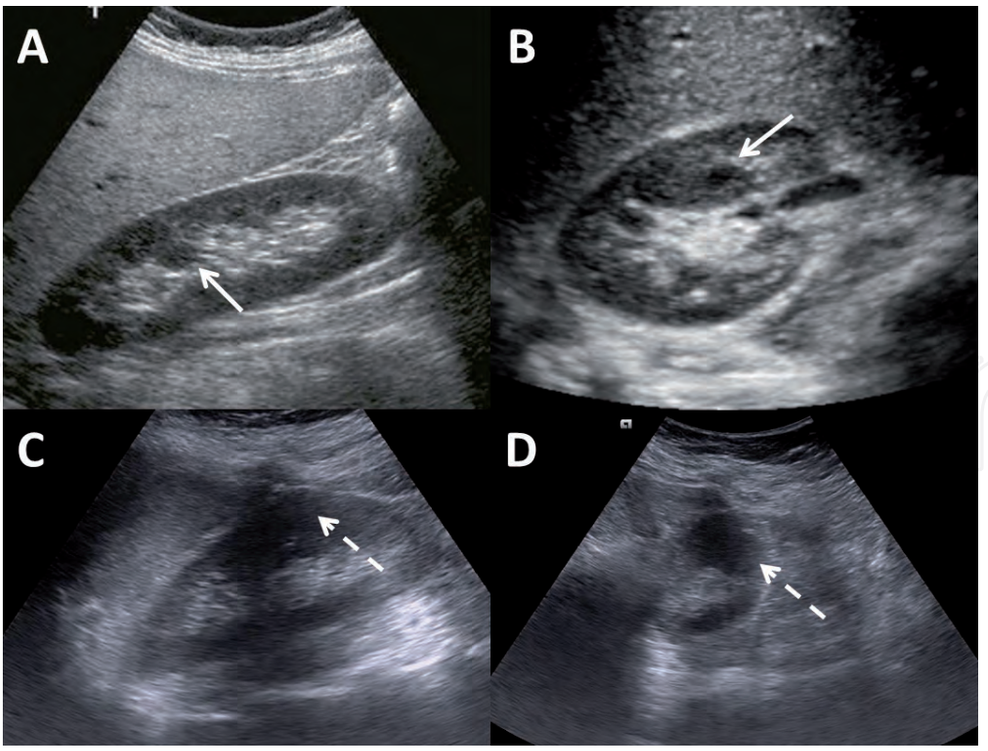

Figure 1.
Congenital variations of the kidney. On sagittal (A) and transverse (B) section of the kidney, hypertrophied column of Bertini (arrow) is seen as a hypoechoic cortical extension to the renal sinus. Sagittal (C) and transverse (D) section of another kidney reveals cortical bulging (dashed arrow) on the superolateral aspect, adjacent to the spleen termed as "dromedary hump".

3. Sonography technique

Before the examination, the adult patients should fast for a minimum of 6 hours before the examination to avoid extensive bowel gas. Convex-array US transducers (with a frequency of 2–5 MHz in adults and 5–8 MHz in pediatric patients) are usually preferred for the US scanning of the kidney. In newborns and infants, even in children, liner US transducers with higher frequency (8–12 MHz) should be additionally employed for better evaluation of cortex and medulla. Tissue harmonic imaging and compound imaging may often be useful for increasing lesion conspicuity and decreasing artifacts [11].

Optimal patient positioning depends on patient habitus, but supine and lateral decubitus positions are often sufficient; while the breath-hold technique is frequently necessary to obtain a complete examination of the renal parenchyma. If there is bowel gas superposition on subcostal view, intercostal window can be used to display kidneys on both sides. The kidneys should be evaluated in the transverse and coronal plane from the superior tip to the inferior [11].

4. Congenital anomalies

Ectopic kidneys are generally located at the pelvis (**Figure 2B**); however, it can be rarely located in the thorax. Crossed renal ectopia is defined as the presence of both kidneys in the same side of the body. The ectopic kidney is fused to the normal kidney in 85–90% of cases called crossed fused ectopy [12]. The upper pole of the ectopic kidney is commonly fused to the lower pole of the normal kidney. Fusion of the kidneys limits the ascent while developments, and thus, both kidneys are located caudally.

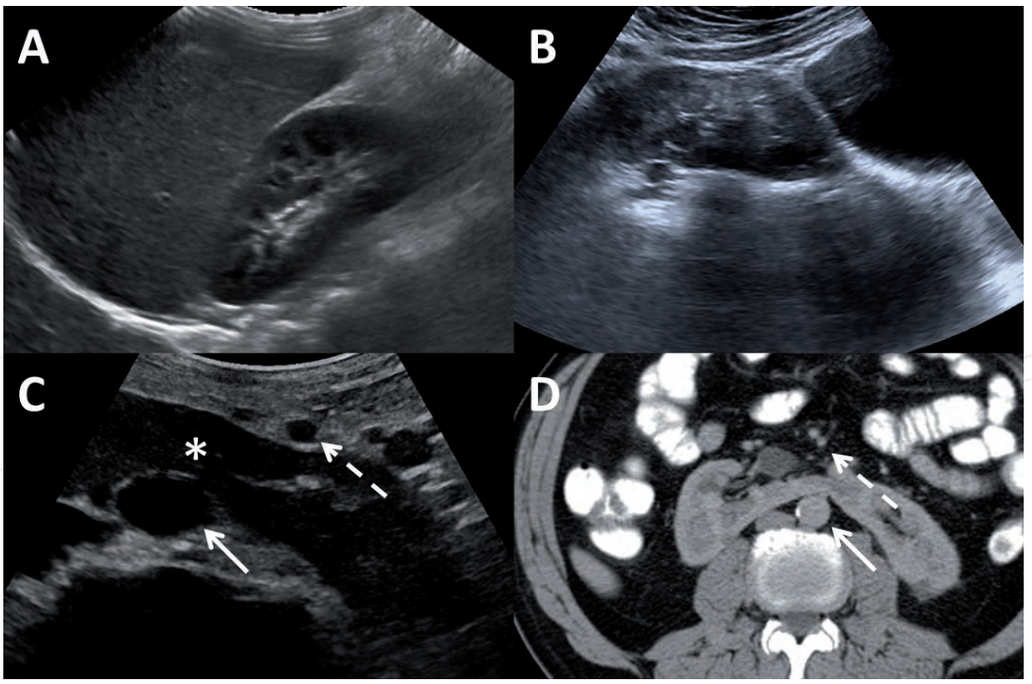

Figure 2.
Congenital anomalies of the kidney. Normal kidney is located inferomedially adjacent to the liver (A). An example of a right ectopic kidney located adjacent to the bladder (B). Ultrasound (C) and computed tomography (D) image of a horseshoe kidney reveals that right and left kidney fused from lower poles at the midline (asterix) from lower poles (asterix) and located between abdominal aorta (arrow) and inferior mesenteric artery (dashed arrow).

Horseshoe kidney is the fusion of the both metanephrogenic blastema from the lower poles prior to migration cranially. Isthmus may compose of either functioning renal cortex or fibrous tissue. The horseshoe kidney is more prone to infection and stone formation due to abnormal rotation of renal pelvis and ureteropelvic junction obstruction. On ultrasound, the horseshoe kidney is located more caudal than usual location and lower poles project inferomedially. Renal isthmus can be seen in the lower abdomen crossing the midline anterior to the aorta (**Figure 2C,D**).

Ureteropelvic junction (UPJ) obstruction is a common anomaly with a male preponderance and the left kidney suffers twice as frequently as the right kidney [13]. Patients with UPJ obstruction have an increased incidence of multicystic dysplastic kidney and renal agenesis of the other kidney. On ultrasound, marked hydronephrosis is present proximal to the level of UPJ obstruction along with normal caliber of the ureter. If long standing, renal parenchymal atrophy accompanies severe dilatation of the renal pelvis.

5. Nephrolithiasis and nephrocalcinosis

Nephrolithiasis is termed as calcification within the collecting system, bladder, ureter, and calyceal system, while nephrocalcinosis is defined as the deposition of calcium salts in the renal parenchyma.

Nephrolithiasis is a common disease with a prevalence of 2–3% in general population and 1.8/10,000 of hospital admissions [14, 15]. If we look at different regions of the world more closely, estimated prevalence is at 20.1% in Saudi Arabia, 1–5% in Asia, 5–9% in Europe, and 12–13% in Canada and North America [16]. White men who are in their fourth and fifth decade are affected most commonly [17]. A majority of the patients are present with acute, severe flank pain when a kidney

stone becomes impacted in the ureter due to obstruction, dysuria, strangury, and hematuria. Almost 70% of kidney stones are composed of calcium, and patients with calcium stones are more prone to further stone formation within 7 years [16].

Multiple predisposing factors have been identified for nephrolithiasis including metabolic diseases such as cystinuria (autosomal recessive) and hyperoxaluria, inherited conditions (polycystic kidney disease, renal tubular acidosis, hyperparathyroidism, and hypercalciuria), medications (triamterene, sulfonamides, carbonic anhydrase inhibitors, indinavir, acetazolamide, and corticosteroids), low urine volume, hypercalciuria (hyperparathyroidism and sarcoidosis), and hypocitraturia (distal renal tubular acidosis). Obesity is also associated with an increased risk of kidney stones, especially in women with a BMI over 40 [16].

Calcium oxalate stones constitute the majority (60%) of all renal stones, followed by calcium phosphate types (hydroxyapatite 20% and brushite 2%) and struvite stones (7–13%) usually composed of calcium-magnesium-ammonium phosphate. Struvite stones are formed secondary to urease positive bacterial infection and the most common composition of staghorn calculi. If struvite stones do not contain calcium like cystine stones, they become radiolucent and they are missed in radiographs.

Another radiolucent stone is uric acid stone with varying prevalence from 40% in Israel to 10% in the USA [16]. Hyperuricosuria, acidic urine, and low urinary volume are predisposing factors for urate stone. Radiolucent stones can be detected with ultrasound as well as calcium stones.

The main aims of imaging in patients with nephrolithiasis are to assess the size, number, and location of the stone(s), to reveal if there are complications, and to evaluate the contralateral kidney. Ultrasound can be applied to show dilatation of the collecting system, to identify stones, to assess the renal size and renal cortical thickness, and to detect complications. Hydration is very important before the examination, which increases the sensitivity from 24–73% to 85–100%, and increases the specificity from 74 to 83–100% [16, 18].

The composition of the stone does not affect the diagnostic sensitivity and specificity of ultrasound, while the calculus size and position and the body habitus may affect the detection rate along with the experience of the examiner.

The typical appearance of kidney stones is hyperechoic foci with acoustic shadowing (**Figure 3**). Kidney stones need to be at least 4–5 mm to be identified conspicuously on ultrasound [16]. For better visualization, the most appropriate transducer frequency tissue should be considered with a balance of tissue penetration and resolution. The focal zone should be adjusted at the level of stone for maximized shadowing. Furthermore, the detection of kidney stones and the visibility of posterior shadowing are significantly improved by tissue harmonic imaging [19]. Concomitant ultrasound findings in a patient with inflammation due to renal colic are increased echogenicity of renal parenchyma, dilatation of the collecting system, and subcapsular collections (urinomas). The application of color Doppler ultrasound which reveals twinkling artifact posteriorly in 83% of kidney stones improves the detection of small calculi [20].

Several mimickers for kidney stones at ultrasound may result in false-positive diagnosis, including intrarenal gas, renal artery calcification, calcified sloughed papilla, calcified transitional cell tumor, alkaline-encrusted pyelitis, and encrusted ureteral stents.

Nephrocalcinosis is a condition that is caused by hypercalcemia and hypercalciuria due to various diseases. Histologically, tissue calcification can be classified into two groups: calcification in normal and abnormal tissue. Dystrophic calcification arises in abnormal tissues such as vessels, haematoma, tumors, and inflammatory masses and when the solubility of the product of calcium and phosphate is exceeded due to pH changes or a reparative process. This is not considered to be

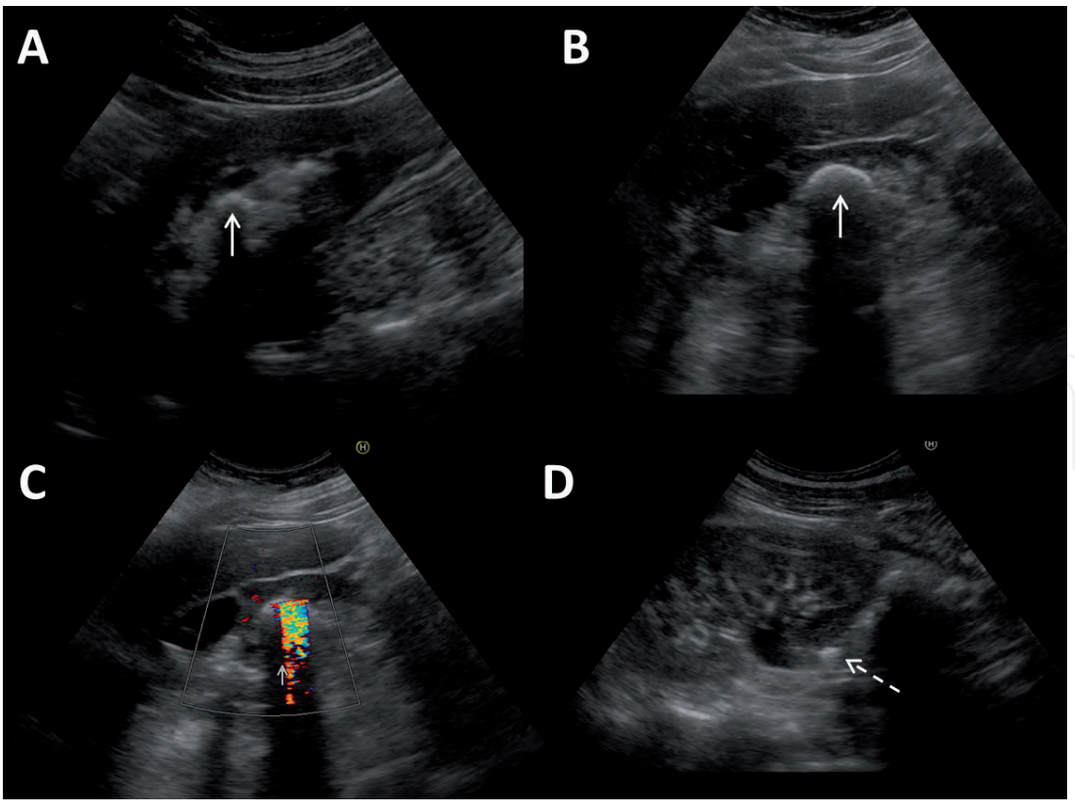

Figure 3.
Examples of kidney stone (arrow) in image (A–C) as a hyperechogenic lesion with acoustic shadowing. In image (D), proximal ureteric stone (dashed arrow) and collecting system dilatation due to obstruction are demonstrated.

nephrocalcinosis. On the other hand, metastatic calcification occurs in normal tissues such as kidneys. It is usually due to abnormal biochemistry, that is, elevated serum calcium. The metabolic imbalance results in metastatic calcification when the solubility of calcium and phosphate or oxalates in extracellular fluid is exceeded.

Metastatic calcification in kidney is further subdivided anatomically into medullary nephrocalcinosis or cortical nephrocalcinosis. Medullary nephrocalcinosis accounts for the 97.6% of nephrocalcinosis and common causes are hyperparathyroidism, renal tubular acidosis, medullary sponge kidney, bone metastases, chronic pyelonephritis, Cushing's syndrome, hyperthyroidism, malignancy, renal papillary necrosis, sarcoidosis, sickle cell disease, hypervitaminosis D, and Wilson's disease. Cortical nephrocalcinosis constitutes the remaining 2.4%, and the common etiologies are acute cortical necrosis, ethylene glycol poisoning, chronic glomerulonephritis, chronic hypercalcemic states, sickle cell disease, and rejected renal transplants [21].

Cortical nephrocalcinosis is seen outlining of the kidney and along the columns of Bertin. It is usually due to severe destructive cortical disease, often observed in patients with end-stage renal failure. Any form of chronic glomerulonephritis may result in cortical nephrocalcinosis. Acute cortical necrosis often related to course of hypovolemic shock and eclampsia may give rise to patchy calcification in the renal parenchyma [16]. Ultrasonographic features of cortical nephrocalcinosis are increased cortical echogenicity representing early cortical calcification. Further progressive calcification may result in hyperechoic rim with extensive shadowing.

Medullary nephrocalcinosis is characterized by diffuse calcium deposition within the renal pyramids. Normally, calcium is removed by lymphatics in renal medulla, and if the amount of calcium exceeds lymphatic capacity, calcium deposits in the fornical tip and margins of the medulla. The typical ultrasound features of early medullary nephrocalcinosis may be nonshadowing echogenic rims surrounding medullary pyramids (**Figure 4**). As the disease progresses, hyperechogenicity fills the entire

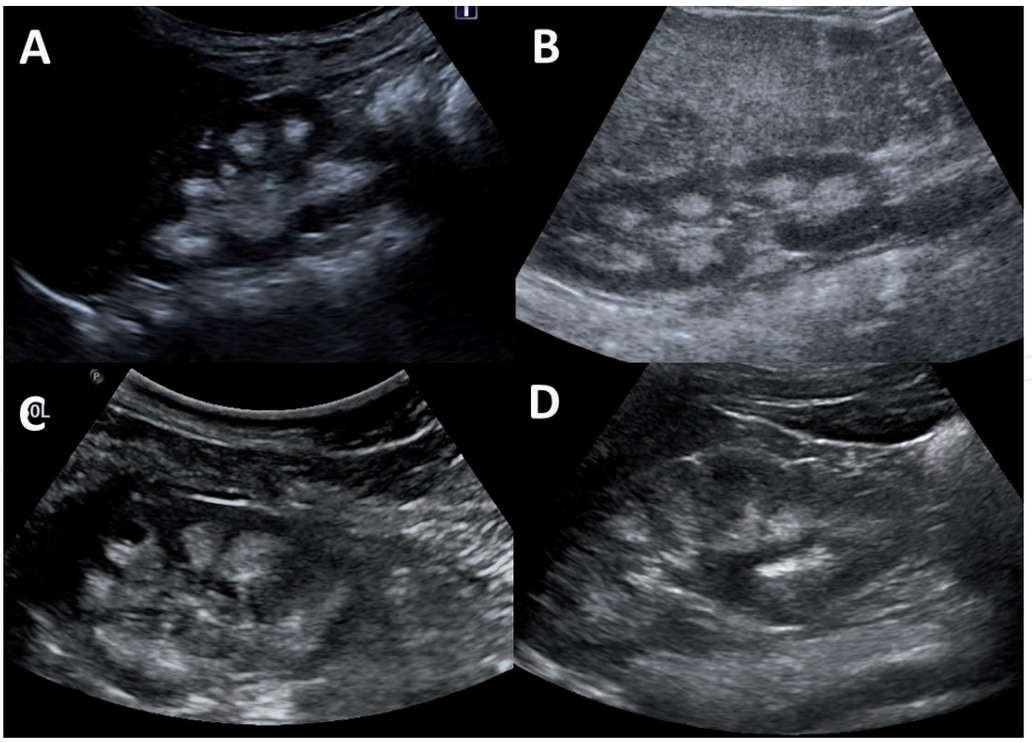

Figure 4.
Four patients with medullary nephrocalcinosis due to different etiology, such as hyperparathyroidism (A), Wilson's disease (B), and medullary sponge kidney (C and D). In all patients, the calyceal system is seen hyperechogenic.

pyramids. However, increased medullary echogenicity may also be seen in medullary sponge kidney; even it may be a physiologic transient finding in neonates [22]. In a similar way to cortical nephrocalcinosis, further calcium deposition induces acoustic shadowing at ultrasound in medullary nephrocalcinosis. These firm calcifications may perforate the caliceal wall and compose a nidus for further stone formation.

6. Cystic disease of kidney

Renal cystic disease is an entity that includes an enormous range of disorders including developmental (simple and complex cysts, localized cystic diseases, extraparenchymal sinus cysts, medullary sponge kidney, and multicystic dysplastic kidney), acquired (acquired cystic kidney disease), and hereditary (autosomal dominant polycystic kidney disease, autosomal recessive polycystic kidney disease, tuberous sclerosis complex, and von Hippel– Lindau disease) origin. Ultrasound is the primary and the most commonly used imaging modality for cystic renal disease but insufficient for the exact diagnosis in most of the cases. Key imaging features are the location, distribution, size, and composition of renal cysts as well as other coexisting noncystic renal lesions for the diagnosis [23].

Simple renal cysts are benign, fluid filled homogenous, and asymptomatic lesions, most of which are incidentally discovered on ultrasound. Prevalence of simple cysts increases with age in up to 27% of patients greater than 50 years of age [24]. They can be single or multiple, unilateral or bilateral, and commonly located in the renal cortex. Simple cysts are typically anechoic, round, or ovoid, with acoustic enhancement and no prominent wall thickness (**Figure 5**). If all these features are met with ultrasound, further evaluation or follow-up of the cyst is not required. All other sonographic findings, such as internal echo, septum, wall thickening, calcification, or acoustic shadowing, lead to the diagnosis of complex cyst.

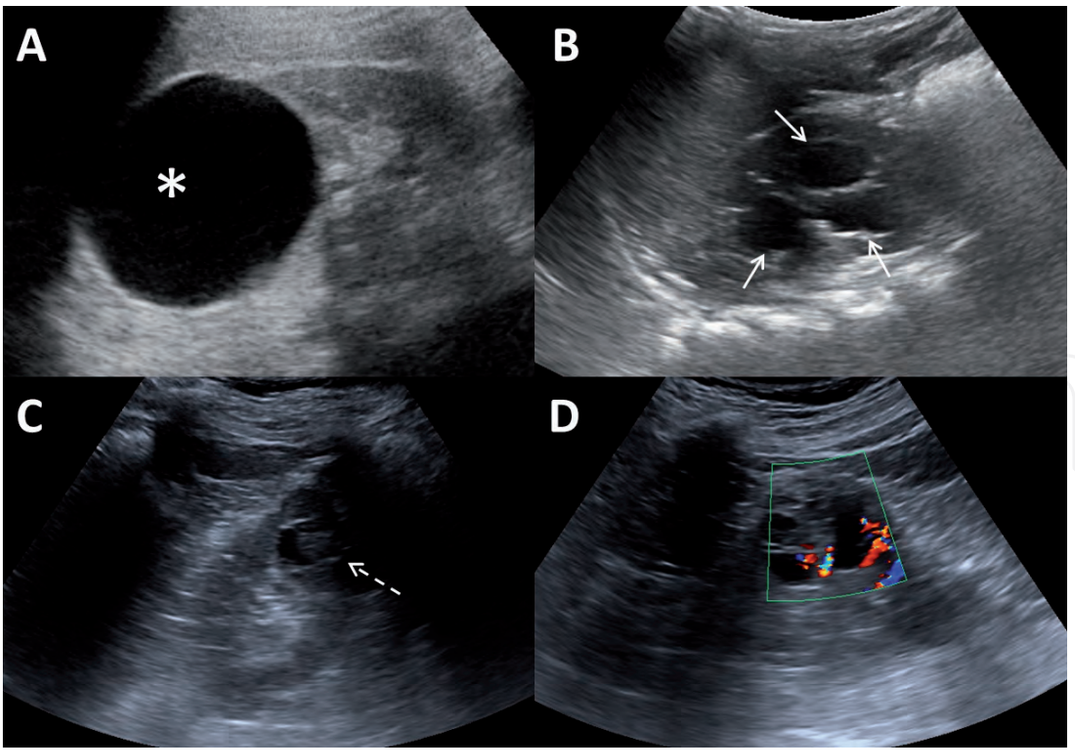

Figure 5.
Simple cyst of the kidney (asterix) should be purely anechoic with no septations and solid component (A). Also increased trough transmission can be seen posteriorly. Hydronephrosis (B) is seen as a multiple cystic structure (arrows) which is actually dilated calyx. In image (C), cystic lesion with multiple irregular septations is demonstrated (dashed arrow). On color Doppler ultrasound (D), vascularity in the septations is shown. Histopathologic evaluation confirmed the diagnosis of this cystic lesion as a clear cell type renal cell carcinoma.

Internal echoes within a cyst are generally due to hemorrhage or infection as in septations. Calcification can be seen in cyst wall or septa and may be fine and linear or amorphous and thick according to the shape. Thin wall or septal calcification suggests a complicated cyst rather than malignancy, while thick, irregular, amorphous calcification, perceptible, thickened walls, or mural nodularity should raise suspicion for malignancy, and further contrast enhanced imaging should be done (**Figure 5C,D**). Layering milk of calcium is seen as an echogenic focus with ring-down arifact in septa or cyst wall suggest that the cyst has a benign nature [25].

The most widely used classification system for complex renal cysts was introduced in 1991 by Bosniak [26], who grouped renal cysts into five categories based on imaging appearance in an attempt to predict the risk of malignancy and determine the outcome and management of complex cysts and cystic neoplasm (**Table 1**).

Extraparenchymal cysts are commonly seen in renal sinus and subdivided into parapelvic cyst and peripelvic cyst. Parapelvic cysts originate from the renal parenchyma and extend into the renal sinus, while peripelvic cysts arise directly in the renal sinus presumably due to lymphatic obstruction. Although these cysts differ in their origin, they are indistinguishable sonographically and benign nature, without a need for further imaging and follow up. However, these cysts may mimic hydronephrosis. Shape and extension of the cyst and concomitant caliceal dilatation of hydronephrosis are useful findings for differentiation [23].

Medullary cystic disease and juvenile nephronophthisis have similar imaging findings that are both composed of small multiple cysts at the corticomedullary junction and medulla. Juvenile nephronophthisis is an autosomal recessive condition usually present in childhood and generally progresses to end stage renal disease. On the other hand, medullary cystic disease is an autosomal dominant disorder present in the third or fourth decade of life with similar renal symptoms.

Autosomal dominant polycystic kidney disease (ADPKD) is the most common inherited renal disorder that is characterized by the progressive development of multiple asymmetrical and different sized cysts and marked renal enlargement [28]. ADPKD accounts for 10–15% of patients receiving dialysis and is the fourth leading cause of end stage renal disease in the world [23, 25]. Ultrasound is commonly used as a screening tool for the children of affected individuals (**Figure 6A**). According to Pei et al. [29], when evaluating patients with a positive family history of ADPKD, the number of renal cysts required for diagnosis is at least three (unilateral or bilateral) in subjects between 15 and 39 years old, at least two in each kidney in subjects between 40 and 59 years old, and at least four in each kidney in subjects more than 60 years old. Most of the cysts are simple cysts with varying size, which may be complicated by hemorrhage or infection and have thick walls, internal echoes, and/or fluid debris levels. Calcification in the cyst wall or stones may be seen as echogenic foci with acoustic shadowing. Most common associated extrarenal cysts of ADPKD are seen in liver, followed by pancreas, spleen, epididymis, seminal vesicle, uterus, ovary and thyroid [23]. Cerebral berry aneurysms, abdominal aortic aneurysm, cardiac valve diseases, and colonic diverticula may also accompany [25].

Autosomal recessive polycystic kidney disease (ARPKD) is characterized by renal tubular ectasia (manifesting as multiple bilateral renal cysts) and hepatic ductal plate malformation (leading to hepatic fibrosis and Caroli's disease) [23]. It is divided into four types depending on the age of onset: antenatal, neonatal, infantile, and juvenile forms. In the earlier age group, the more severe renal findings and the less pronounced hepatic involvement are encountered [30]. Ultrasound features of renal-dominant ARPKD include a lack of corticomedullary differentiation and massively enlarged, echogenic kidneys (**Figure 6B**). The increased echogenicity is due to the unresolved 1–2 mm cystic dilatation of the collecting tubules, which increases the number of acoustic interfaces. In neonates, small cysts may be revealed more clearly with high frequency linear-arrayed transducers.

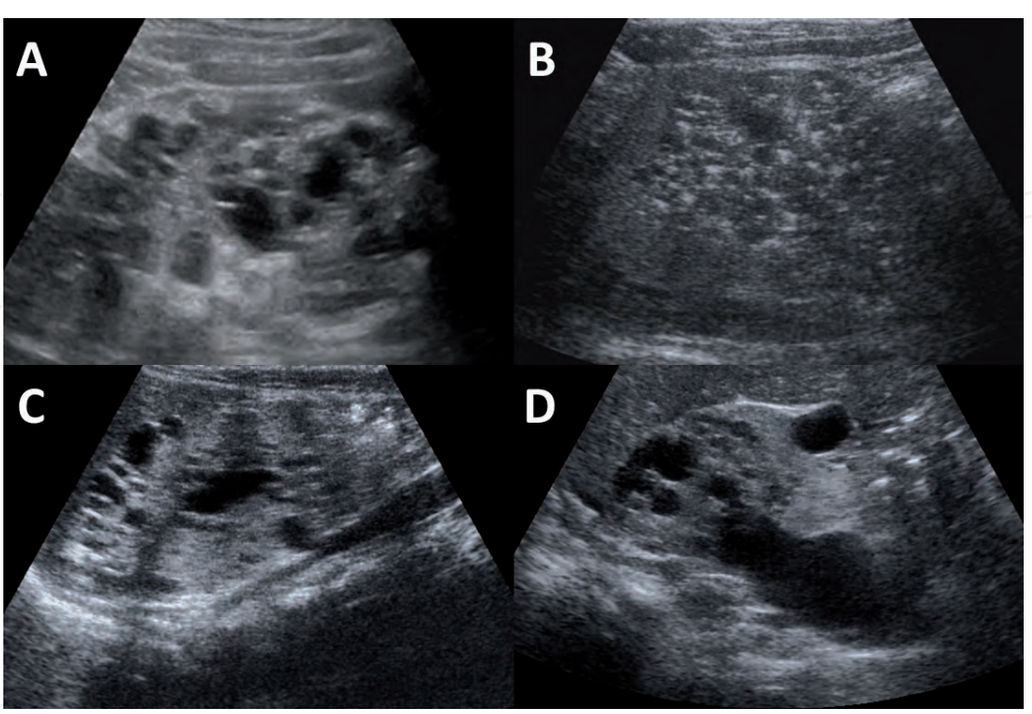

Figure 6.
Ultrasound images of different renal cystic diseases, autosomal dominant polycystic kidney disease (A), autosomal recessive polycystic kidney disease (B), acquired cysts after chronic dialysis with end stage renal disease (C), and cystic renal dysplasia of newborn (D).

Localized cystic disease is a rare, benign condition that may mimic ADPKD. It is characterized by a cluster of simple cysts localized in either a portion of kidney (segmental cystic disease of the kidney) or an entire kidney (unilateral cystic disease of the kidney) [31]. On ultrasound, it appears as a conglomerate mass of multiple cysts of varying size separated by normal or atrophic kidney parenchyma. Lack of cysts in the contralateral kidney and other organs differentiates the disease from ADPKD [25].

Acquired cystic kidney disease (ACKD) is a progressive disorder, which occurs in the native kidneys of patients with end stage renal disease undergoing either chronic hemodialysis or peritoneal dialysis (**Figure 6C**). The prevalence of ACKD depends on the duration of dialysis and accounts for 40–60% of patients by 5 years and over 90% by 10 years of dialysis. Although the affected kidneys are usually atrophic at the time of cyst development, they may have an enlarged appearance due to the formation of extensive renal cysts and thus resemble ADPKD in some cases [32]. Three to five cysts in each kidney at ultrasound and increase in number in follow-up in a patient with chronic dialysis are diagnostics for ACKD [25].

Multicystic dysplastic kidney (MCDK) is a nonhereditary, developmental disorder characterized by multiple renal cysts replacing functional kidney parenchyma in the affected entire or segmented kidney which is smaller and has a distorted appearance. It is the most common cystic disease in pediatric population with an incidence of 1:4000. The exact etiology is unclear but proposed underlying causes are genetic disturbances, teratogens, in utero infections, and more commonly urinary tract outflow obstruction [33]. Ipsilateral renal anomalies, such as vesicoureteral reflux, or contralateral renal anomalies such as ureteropelvic junction obstruction are usually associated with MCDK. Typical sonographic findings include multiple cysts without communication, absence of normal parenchyma, and renal sinus among the cysts. Focal hyperechoic areas representing primitive mesenchyma or tiny cysts can be seen between the cysts [25]. Since many of the MDCKs involute over time, follow-up with ultrasound is recommended and nephrectomy should be reserved for the cases with hypertension, malignant transformation, or exceptionally large cystic kidneys [34].

Cystic renal dysplasia is the consequence of a developmental anomaly composed of abnormal structural organization and development of metanephric elements (**Figure 6D**). Both kidneys are affected and may have multiple cysts. It is often associated with urinary tract obstruction and may be seen with posterior urethral valve, prune belly syndrome, and ureteropelvic junction obstruction. This suggests that obstruction and urinary retention may cause anomalous kidney development [35].

Multilocular cystic nephroma (MLCN) is a rare benign disorder, composed of multiple noncommunicating cysts contained within a well-defined capsule and occasionally affects both kidneys. It has a trimodal age distribution that is seen in male patients less than 4 years of age and in female patients aged 4–20 or 40–60 years. MLCN is generally asymptomatic or may present with abdominal pain, hematuria, and hypertension. If the cysts of MLCN are tiny, a more solid-appearing echogenic mass will be present that precludes to differentiate MLCN from cystic RCC with ultrasound [25].

Chronic lithium nephropathy (CLN) is caused by long-term treatment with lithium salts that result in chronic tubulointerstitial nephropathy. In up to 62% of cases with CLN, typical findings of multiple small cysts (<2 mm) localized in both the cortex and the medulla uniformly and symmetrically distributed are observed [36]. Due to small size, cysts may not be recognized with ultrasound in some patients and magnetic resonance imaging is required for delineation.

7. Solid kidney lesions

Angiomyolipoma (AML) is the most frequent mesenchymal benign neoplasms of the kidney with a prevalence of 0.3–3% and with a female preponderance [37]. It is composed of varying amounts of adipose tissue, smooth muscle cells, and blood vessels [25]. It is frequently associated with an autosomal dominant phakomatosis syndrome, and with lymphangioleiomyomatosis, a progressive disease which usually affects the lungs of young women and which is also related to tuberous sclerosis. In up to 80% children with tuberous sclerosis, AMLs are usually seen as bilateral, small, and multifocal. However, in sporadic patients, AMLs are typically unilateral and discovered in middle-aged women.

Small AMLs typically appear as homogenous hyperechoic lesion, sharply marginated with detectable shadowing (**Figure** 7). Since larger AMLs may be more heterogeneous, it may be difficult to differentiate them from RCC and retroperitoneal liposarcoma. Magnetic resonance imaging should be indicated for these lesions. AMLs may rarely behave locally aggressive, with infiltration to the adjacent lymph nodes or within the inferior vena cava. Small, asymptomatic AMLs may be followed but if they are larger than 3–4 cm, they may be complicated by hemorrhage, which can be spontaneous or associated with relatively minor or incidental trauma. Bleeding may occur either within the tumor, or in the adjacent renal parenchyma, subcapsular, or retroperitoneal area. Complicated AMLs are treated surgically or by selective embolization [38].

Due to the lack of lymphoid tissue in the normal kidney, lymphomatous involvement of the kidney occurs from either hematogenous dissemination or from infiltration of retroperitoneal disease [25]. The kidneys are the 6th most affected abdominal organ after spleen, liver, gastrointestinal tract, pancreas, and abdominal wall [39]. Renal involvement is usually bilateral and found in one third of lymphoma patients at autopsy series [25]. Five different ultrasound appearances are recognized for renal lymphoma, depending partially on the growth pattern of the tumor: (1) single mass, (2) multiple masses, (3) infiltrative disease, (4) perirenal disease, and (5) invasion from retroperitoneal disease [40]. Focal masses appear as hypoechoic or anechoic homogenous lesions. If they are anechoic, they can be differentiated from cysts with the absence of increased through-transmission behind the lesion [25]. Diffuse infiltration may usually enlarge the kidney and decrease echogenicity despite disruption of renal architecture. Isolated perirenal involvement is very rare (<10% of cases of perirenal lymphoma) and appears as a soft tissue mass involving the perirenal space partially or completely and compresses but does not infiltrate the kidney [40]. Perirenal disease is frequently a part of retroperitoneal extension. Perirenal or retroperitoneal tumor may be confused with hematoma or extramedullary hematopoiesis. The lack of renal venous invasion, despite extensive retroperitoneal and renal sinus invasion, may help in differentiating renal lymphoma from renal cell carcinoma (RCC). Contrast-enhanced CT and MRI are superior to ultrasound for diagnosis of renal lymphoma (higher sensitivity and specificity) and in evaluating the extent of disease [40].

Leukemia involves the kidney either diffusely or with focal masses. Leukemic infiltration of the kidney has been reported in 65% of patients at autopsy series [25]. Although the typical ultrasound appearance of renal leukemia is bilateral kidney enlargement, in 15% of the leukemia patients, the kidney may enlarge without leukemic infiltration [25]. Renal leukemia may also be manifested as single or multiple focal masses or a coarsened parenchymal echo pattern with a distorted central sinus echo complex. These patients are more prone to renal, subcapsular, perirenal, or retroperitoneal bleeding.

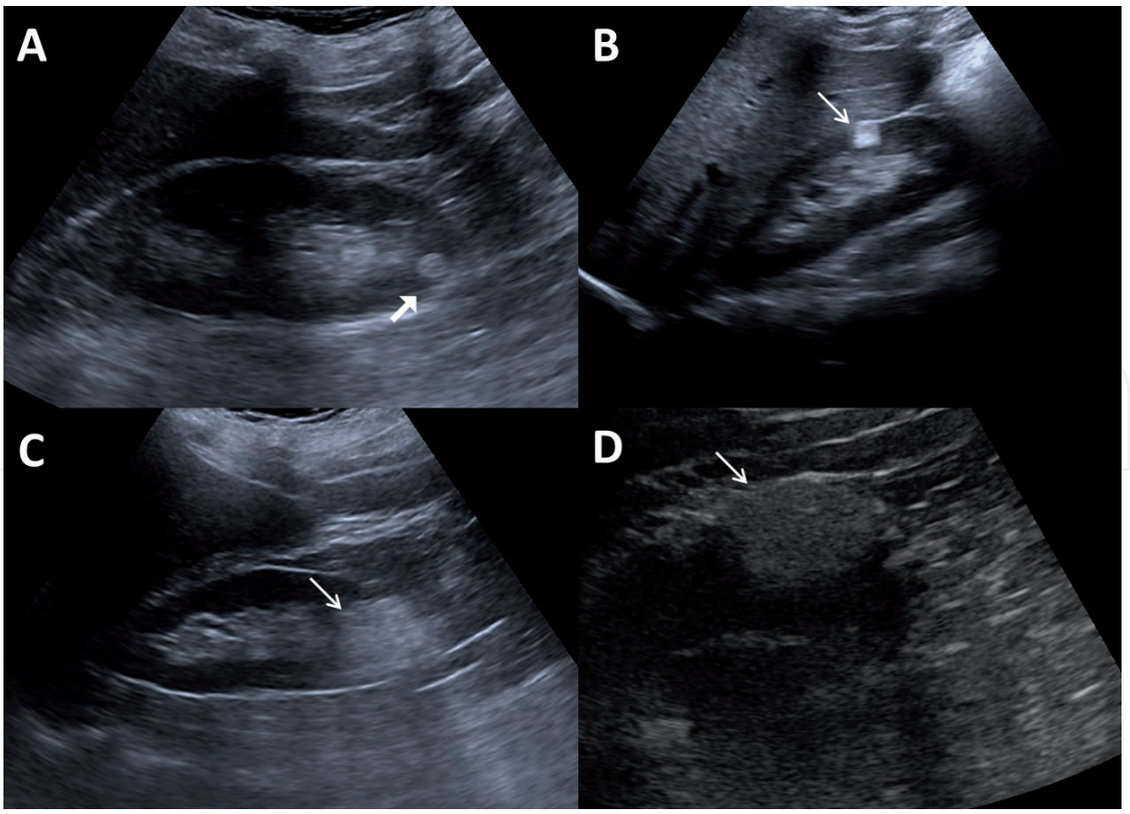

Figure 7.
Different patients with angiomyolipoma (arrows) with different sizes (A, B, C, D). Although appearances of the lesions are different, they are typically hyperechogenic.

Renal cell carcinoma (RCC) is the most common primary kidney malignancy in adults and constitutes 86% of all primary malignant renal tumors and 3% of all adult malignancies [25]. RCC most often occurs in patients aged 50–70 years with 2:1 male predominance [41]. Most of the RCCs appear solid on ultrasound without any specific echogenicity. Smaller RCCs are more hyperechoic and can be misdiagnosed as AML at ultrasound. Several distinguishing characteristics are hypoechoic rim or cystic spaces more common in RCCs, while weak posterior acoustic shadowing can be seen more often in AMLs [25].

The most common subtype of RCC is clear cell (70–75%), followed by papillary (15%), chromophobe (5%), and oncocytic (2–3%) subtypes [25]. The last three have much better prognosis than clear cell RCC. Although ultrasound is much less accurate than CT or MRI for characterization of tumor content, lack of cystic necrotic areas and the presence of calcification, which are more common in papillary and chromophobe subtypes, appear to be associated with a better prognosis. Ultrasound may also demonstrate additional findings related to RCCs, including hydronephrosis; vascular encasement with diminished Doppler flow to the area of involvement or deterioration of the normal central sinus echo complex may be seen [41].

Cystic RCCs account for 5–7% of all RCCs. Four subtypes have been described for cystic RCCs at ultrasound: (1) unilocular, (2) multilocular, (3) necrotic (cystic necrosis), and (4) tumors emerging in a simple cyst. Since the unilocular and multilocular subtypes behave less aggressive, recognition of subtypes may have clinical importance [25]. The typical sonographic features of a unilocular RCC are a debris-filled mass with thick, irregular capsule that may have calcifications. Multilocular RCC may manifest as a cystic mass with internal septations which are thick (>2 mm) and nodular and may contain calcification. Necrotic RCCs have varying appearance depending on the degree of tumor necrosis. RCCs originating

in a simple cyst are very rare and usually seen in Von Hippel Lindau disease patients. A solid mural nodule can be seen at the base of a simple cyst at ultrasound.

Transitional cell carcinoma (TCC) of the renal pelvis is the second most common primary kidney tumor with a prevalence of 7%, but it is 50 times less common than bladder TCCs. Renal TCCs are typically seen in elderly men who are admitted with gross or microscopic hematuria in 75% and flank pain in 25%. The variable appearance of renal sinus beclouds the evaluation of renal pelvis TCCs. Patients at increased risk for development of TCC (such as patients with Balkan nephritis, vesicoureteral reflux, analgesic abuse, heavy smoking habit, exposure to carcinogens, or cyclophosphamide therapy) may require close follow-up. Papillary TCCs appear as solid, central, hypoechoic masses in renal with or without associated proximal calyceal dilatation. The differential diagnosis of these masses includes fibrin clots, sloughed papillae, and mycetoma [25].

Kidney metastases are usually seen on imaging for staging without any symptoms and have an incidence of 2–20% at autopsy series. Renal involvement is generally due to hematogenous spread. The most common primary tumor that metastasizes to kidney is lung carcinoma followed by breast carcinoma and RCC of the contralateral kidney [25]. Colon adenocarcinoma usually has solitary metastasis as a solid lesion on ultrasound which is indistinguishable from RCC [25]. Involvement of perirenal and retroperitoneal space is particularly seen in malignant melanoma and lung cancer metastasis [25]. Infiltrating metastases with subtle margins may be misdiagnosed with ultrasound and contrast enhanced imaging is required for further delineation.

8. Infections

Acute pyelonephritis is defined as an inflammation of the kidney and renal pelvis and has typical symptoms consisting of an abrupt onset of chills, high-grade fever (>38.5°C), and unilateral or bilateral flank pain with costovertebral tenderness. Middle aged females are most commonly affected and *Escherichia coli* is by far the most common pathogen accounting for 80% of community-acquired and 50% of hospital-acquired infections most frequently due to ascending urinary tract infections [42]. In children, recurrent pyelonephritis commonly occurs as a result of vesicoureteral reflux.

The vast majority of acute pyelonephritis patients have normal findings on ultrasound. However, the following findings of pyelonephritis may be identified: kidney enlargement, abnormal echogenicity, loss of corticomedullary differentiation, ill-defined hyperechoic mass (es) (in focal pyelonephritis), compression of the renal sinus, and gas within kidney parenchyma (emphysematous pyelonephritis) (**Figure 8**). Untreated acute pyelonephritis may complicate with necrosis and abscess formation. Acute abscesses usually appear as a hypoechoic mass with increased through transmission posteriorly and indistinct margins. Over time, the abscess wall will be thickened and fluid levels will be developed within the abscess cavity [42]. Emphysematous pyelonephritis (EPN) is a rare, life-threatening infection seen in diabetic patients characterized by gas formation in the renal parenchyma. Dirty shadowing is revealed on ultrasound in EPN and contrast enhanced CT should be preferred for imaging to determine the location and extent of renal and perinephric gas [25].

Fungal infections of the kidney usually affect patients with diabetes mellitus, chronic indwelling catheters, malignancy, chronic antibiotic or steroid therapy, transplantation, and IV drug abusers [43]. *Candida albicans* is the most common fungal agent involved in genitourinary infections. Fungal infections usually manifest as unilateral small parenchymal abscesses which are tiny, hypoechoic, cortical

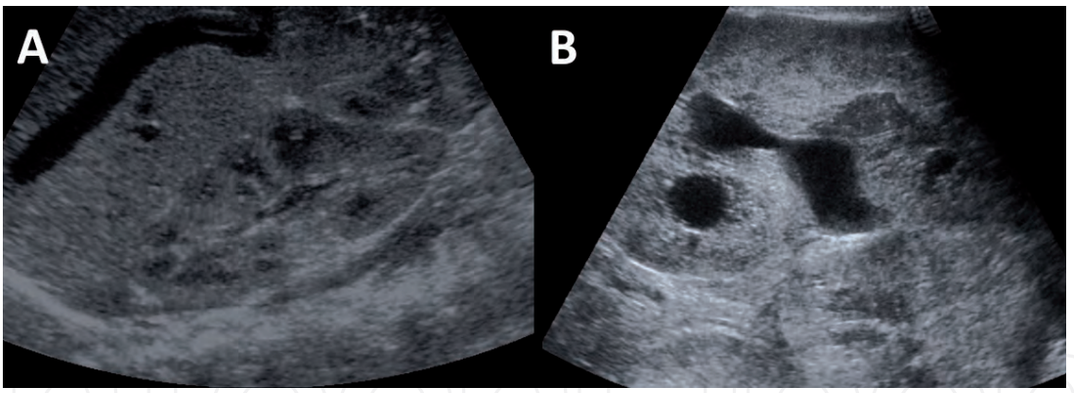

Figure 8.
Two patients with acute pyelonephritis (A and B). Although the majority of the acute pyelonephritis has normal ultrasound appearance, in severe form of the disease, kidney enlargement and increased echogenicity of the kidney can be seen. In image (B), collecting duct dilatation is also seen which might be due to obstructive stone in the ureter.

lesions that may calcify over time [25]. Invasion of the collecting system results in fungus balls which are seen as hyperechoic soft tissue masses without posterior acoustic shadowing within the collecting system [43]. Fungus balls are motile and cause obstruction that may be associated with varying degrees of hydronephrosis on ultrasound.

9. Trauma

Renal injury occurs in 8–10% of patients suffering from blunt or penetrating trauma [44]. Blunt injury is far more common than penetrating injury accounting for 66–90% of cases and the majority of blunt trauma patients have relatively minor injuries which heal without any treatment. While blunt injuries are most often caused by motor vehicle accidents, falls, and direct impact from assault or sports competition, penetrating injuries are usually the result of gunshot or stab wounds. Patients with renal lesions (such as cysts, tumor, or hydronephrosis) are more prone to severe injury. The broadly accepted renal injury grading system constituted by the American Association for the Surgery of Trauma (AAST) is shown in **Table 1** [27].

Most patients with grade I and II injury are managed conservatively, while grades IV and V often require surgical treatment [27]. Contrast enhanced computed

AAST injury grading	Description
Grade I	Renal contusion or subcapsular hematoma with intact capsule
Grade II	Superficial cortex laceration (≤1 cm) that does not extend to deep medulla or the collecting system or nonexpanding hematoma
Grade III	Deep laceration(s) (>1 cm) with or without urine Extravasation
Grade IV	Laceration(s) extending into the collecting system with contained urine leak
Grade V	Shattered kidney, renal vascular pedicle injury, or devitalized kidney

Table 1.
Renal injury grading scale of the American Association for the Surgery of Trauma [27].

tomography is the premier imaging modality for the evaluation of renal trauma. Technical limitations usually hinder an adequate examination with ultrasound in trauma patients. However, ultrasound may be used in the follow-up of patients with known kidney trauma [25]. Renal hematomas may be revealed as hypoechoic, hyperechoic, or heterogeneous depending on the stage of blood products. Lacerations are seen as linear hypoechoic defects that may extend through the kidney if a fracture is present and perinephric collections are associated with them. Subcapsular hemorrhage may appear as a perinephric heterogeneous fluid collection that flattens the underlying renal border. A shattered kidney in grade V trauma consists of multiple fragments of disorganized tissue with associated hemorrhage without normal renal architecture and urine collection in the renal bed.

10. Conclusion

Typical US features of the normal kidney and normal anatomic variants are very important to prevent over diagnosis and to recognize pathologic lesions. Moreover, typical US findings of benign lesions are extremely important to prevent unnecessary additional imaging and interventions. Although US is the first-line imaging and the second-line cross-sectional imaging modalities (CT and MRI) are performed in malignant disorders, radiologists and clinicians should be familiar with typical US appearances to narrow down differential diagnosis, to guide for most appropriate second-line imaging and for comprehensive follow-up.

Acknowledgements

The images are obtained from the archives of Istanbul Medeniyet University and Bingol State Hospital radiology archives.

Conflict of interest

The author declares no conflict of interest about this chapter.

Author details

Ercan Ayaz
Department of Radiology, Hacettepe University School of Medicine, Ankara, Turkey

Available from : https://dx.doi.org/10.5772/intechopen.86246

References

[1] Zweyer M. Embryology of the kidney. In: Quaia E, editor. Radiological Imaging of the Kidney. Medical Radiology. Berlin, Heidelberg: Springer; 2010. pp. 3-16

[2] Moore KL, Dalley AF, Agur AMR. Clinically Oriented Anatomy. 6th ed. Philedelphia: Wolters Kluwer/Lippincott Williams & Wilkins; 2010

[3] Quaia E, Martingano P, Cavallaro M, Zappetti R. Normal radiological anatomy and anatomical variants of the kidney. In: Quaia E, editor. Radiological Imaging of the Kidney. Medical Radiology. Berlin, Heidelberg: Springer; 2014. pp. 17-74

[4] Emamian SA, Nielsen MB, Pedersen JF, Ytte L. Kidney dimensions at sonography: Correlation with age, sex, and habitus in 665 adult volunteers. American Journal of Roentgenology. 1993;**160**:83-86

[5] Netter FH. Anatomy, structure, and embryology. In: Shapter RK, Yonkman FF, editors. The CIBA Collection of Medical Illustrations, Vol. 6. Kidneys, Ureters, and Urinary Bladder. Summit, NJ, USA: CIBA Pharmaceutical; 1973. pp. 2-35

[6] Friedenberg RM, Dunbar JS. Excretory urography. In: Pollack HM, editor. Clinical Urography. Philadelphia: Saunders; 1990. pp. 101-243

[7] Platt JF, Rubin JM, Bowerman RA, Marn CS. The inability to detect kidney disease on the basis of echogenicity. American Journal of Roentgenology. 1988;**151**:317-319

[8] Kasap B, Soylu A, Türkmen M, et al. Relationship of increased renal cortical echogenicity with clinical and laboratory findings in pediatric renal disease. Journal of Clinical Ultrasound. 2006;**34**:339-342

[9] Yeh HC, Halton KP, Shapiro RS, et al. Junctional parenchyma: Revised definition of hypertrophic column of Bertin. Radiology. 1992;**185**:725-732

[10] Leekam RN, Matzinger MA, Brunelle M, et al. The sonography of renal columnar hypertrophy. Journal of Clinical Ultrasound. 1983;**11**:491-494

[11] Quaia E. Ultrasound of the kidney. In: Quaia E, editor. Radiological Imaging of the Kidney. Medical Radiology. Berlin, Heidelberg: Springer; 2014. pp. 83-121

[12] Friedland GW, Devries PA, Nino-Murcia M, et al. Congenital anomalies of the urinary tract. In: Pollack HM, editor. Clinical Urography: An Atlas and Textbook of Urologic Imaging. Philadelphia, USA: Saunders; 1990. pp. 559-787

[13] Talner LB. Specific causes of obstruction. In: Pollack HM, editor. Clinical Urography: An Atlas and Textbook of Urological Imaging. Philadelphia: Saunders; 1990. pp. 1629-1751

[14] Menon M, Resnick MI. Urinary lithiasis: Etiology, diagnosis, and medical management. In: Walsh PC, Retik AB, Darracott VE Jr, editors. Campbell's Urology. Philadelphia, USA: WB Saunders; 2002. pp. 3229-3305

[15] Sandhu C, Anson KM, Patel U. Urinary tract stones–Part I: Role of radiological imaging in diagnosis and treatment planning. Clinical Radiology. 2003;**58**:415-421

[16] Phillips S, Tudor GR. Nephrocalcinosis and nephrolithiasis. In: Quaia E, editor. Radiological Imaging of the Kidney. Medical Radiology. Berlin, Heidelberg: Springer; 2014. pp. 391-410

[17] Freeman SJ, Sells S. Investigation of loin pain. Imaging. 2008;**20**:38-56

[18] Fowler KA, Locken JA, Duchesne JH, et al. US for detecting renal calculi with nonenhanced CT as a reference standard. Radiology. 2002;**222**:109-113

[19] Ozdemir H, Demir MK, Temizöz O, et al. Phase inversion harmonic imaging improves assessment of renal calculi: A comparison with fundamental gray-scale sonography. Journal of Clinical Ultrasound. 2008;**36**:16-19

[20] Lee JY, Kim SH, Cho JY, Han D. Color and power Doppler twinkling artifacts from urinary stones: Clinical observations and phantom studies. American Journal of Roentgenology. 2001;**176**:1441-1445

[21] Banner M. Nephrocalcinosis. In: Pollack HM, editor. Clinical Urography: An Atlas and Textbook of Urological Imaging. Philadelphia, USA: Saunders; 1990. pp. 1768-1775

[22] Khoory BJ, Andreis IA, Vino L, Fanos V. Transient hyperechogenicity of the renal medullary pyramids: Incidence in the healthy term newborn. American Journal of Perinatology. 1999;**16**:463-468

[23] Bae KT, Furlan A, Mileto A. Renal cystic disease. In: Quaia E, editor. Radiological Imaging of the Kidney. Medical Radiology. Berlin, Heidelberg: Springer; 2014. pp. 305-334

[24] Tada S, Yamagishi J, Kobayashi H, et al. The incidence of simple renal cyst by computed tomography. Clinical Radiology. 1983;**34**:437-439

[25] Tublin M, Thurston W, Wilson SR. The kidney and urinary tract. In: Rumack CM, Wilson SR, Charboneu JW, Levine D, editors. Diagnostic Ultrasound. 4th ed. Philadelphia, PA, USA: Elsevier Mosby; 2011. pp. 317-391

[26] Bosniak MA. The small (≤3.0 cm) renal parenchymal tumor: Detection, diagnosis, and controversies. Radiology. 1991;**179**:307-317

[27] Kozar RA, Crandall M, Shanmuganathan K, Zarzaur BL, Coburn M, Cribari C, et al. Organ injury scaling 2018 update: Spleen, liver, and kidney. The Journal of Trauma and Acute Care Surgery. 2018;**85**:1119-1122

[28] Harris PC, Bae KT, Rossetti S, et al. Cyst number but not the rate of cystic growth is associated with the mutated gene in autosomal dominant polycystic kidney disease. Journal of the American Society of Nephrology. 2006;**17**:3013-3019

[29] Pei Y, Obaji J, Dupuis A, et al. Unified criteria for ultrasonographic diagnosis of ADPKD. Journal of the American Society of Nephrology. 2009;**20**:205-212

[30] Turkbey B, Ocak I, Daryanani K, et al. Autosomal recessive polycystic kidney disease and congenital hepatic fibrosis (ARPKD/CHF). Pediatric Radiology. 2009;**39**:100-111

[31] Slywotzky CM, Bosniak MA. Localized cystic disease of the kidney. American Journal of Roentgenology. 2001;**176**:843-849

[32] Bakir AA, Hasnain M, Young S, et al. Dialysis-associated renal cystic disease resembling autosomal dominant polycystic kidney disease: A report of two cases. American Journal of Nephrology. 1999;**19**:519-522

[33] Hains DS, Bates CM, Ingraham S, et al. Management and etiology of the unilateral multicystic dysplastic kidney: A review. Pediatric Nephrology. 2009;**24**:233-241

[34] Vester U, Kranz B, Hoyer PF. The diagnostic value of ultrasound in cystic kidney diseases. Pediatric Nephrology. 2010;**25**:231-240

[35] Shibata S, Nagata M. Pathogenesis of human renal dysplasia: An alternative scenario to the major theories. Pediatrics International. 2003;**45**:605-609

[36] Roque A, Heredia V, Ramalho M, et al. MR findings of lithium related kidney disease: Preliminary observations in four patients. Abdominal Imaging. 2012;**37**:140-146

[37] Quaia E. Benign solid renal tumors. In: Quaia E, editor. Radiological Imaging of the Kidney. Medical Radiology. Berlin, Heidelberg: Springer; 2014. pp. 501-535

[38] Silverman SG, Israel GM, Herts BR, et al. Management of the incidental renal mass. Radiology. 2008;**249**:16-31

[39] Lee WK, Lau EW, Duddalwar VA, et al. Abdominal manifestations of extranodal lymphoma: Spectrum of imaging findings. American Journal of Roentgenology. 2008;**191**:198-206

[40] Rappaport A, Oyen RH. Renal lymphoma and renal sarcoma. In: Quaia E, editor. Radiological Imaging of the Kidney. Medical Radiology. Berlin, Heidelberg: Springer; 2014. pp. 631-643

[41] Hayashi D, Guermazi A, Holalkere NS. Imaging in renal cell carcinoma. In: Quaia E, editor. Radiological Imaging of the Kidney. Medical Radiology. Berlin, Heidelberg: Springer; 2014. pp. 537-570

[42] Blandino A, Mazziotti S, Minutoli F, Ascenti G, Gaeta M. Acute renal infections. In: Quaia E, editor. Radiological Imaging of the Kidney. Medical Radiology. Berlin, Heidelberg: Springer; 2014. pp. 411-436

[43] Quaia E, Giarraputo L, Martingano P, Cavallaro M. Chronic renal infections and renal fungal infections. In: Quaia E, editor. Radiological Imaging of the Kidney. Medical Radiology. Berlin, Heidelberg: Springer; 2014. pp. 437-467

[44] Mirvis SE. Imaging of renal trauma. In: Quaia E, editor. Radiological Imaging of the Kidney. Medical Radiology. Berlin, Heidelberg: Springer; 2014. pp. 483-498

[45] Behrman RE, Kliegman RM, Arvin AM. Nelson Textbook of Pediatrics. 15th ed. Philadelphia: WB Saunders; 1996

Chapter

Ultrasound of the Kidneys: Application of Doppler and Elastography

Moawia Gameraddin

Abstract

Doppler ultrasound of the kidneys is essential in the assessment and diagnosis of kidney diseases. There are several diseases involving the kidneys. Some are functional, diffuse and systematic. Using Doppler imaging provides an assessment of vascular changes which is easily evaluated. Doppler investigation is widely used for assessment of the perfusion of renal arteries. The Doppler indexes; resistive index, pulsatility index, peak systolic are utilized for evaluating the blood flow of the renal arteries. Doppler analysis provides useful diagnostic data that can predict early damage of the kidney tissue. In recent years, ultrasound elastography showed advanced development. It is a new promising technique that is used for assessing the renal tissue characterization. Elastography is an effective imaging for assessing kidney diseases. In the future, clinicians can use elastography instead of biopsy. In this chapter, we highlighted the applications of Doppler ultrasound and elastography in evaluation of various kidney diseases.

Keywords: Doppler, renal elastography, kidney disease, renal artery

1. Introduction

Doppler ultrasound is widely used in medical imaging. It is an application of diagnostic ultrasound utilized for assessing the blood flow speed and direction. These measurements depend on the Doppler effect is used to measure changes in the frequency of the echoes reflected from moving blood cells. In many cases, Doppler ultrasound replaces X-ray angiography. The most important advantage of Doppler ultrasound over other imaging methods that it provides a real-time assessment of blood flow.

The Doppler renal resistive index (RRI) is the most common Doppler parameter that is used to assess a variety of renal diseases such as assessment of rejection of transplanted kidney, detection of renal artery stenosis in hypertensive patients and evaluation of chronic kidney disease (CKD).

Ultrasound elastography is an advanced imaging method which is sensitive to tissue stiffness. In recent years, elastography has been further developed to enable quantitative assessments of tissue stiffness. Elastography is capable to assess changed elasticity of soft tissues resulting from specific pathological processes. It can differentiate between malignant and benign renal masses which may replace the need of biopsy. The combination of Doppler and elastography provide rich diagnostic data about the pathological processes with kidney tissue which is essential for management and treatment.

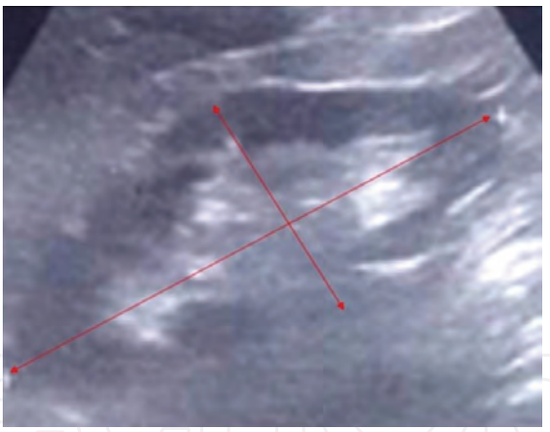

Figure 1.
The length and width of the kidney.

1.1 Ultrasound examination technique

The kidneys are examined with ultrasound in longitudinal and transverse scans planes using 3.5 and 5 MHz transducers. The organ is examined in supine position combined with the lateral decubitus. Then various planes are performed to demonstrate the entire kidney. Preferably, longitudinal and transverse planes are taken to determine the length and size of the kidney, as shown in **Figure 1**.

In the adult patient, a curved array transducer with of 2.5–3.5 MHz is used, while high-frequency 5–7 MHz is used in the pediatric patients.

Artifacts of the lowest ribs and gastric gases may obscure the upper poles of the kidneys. However, the whole kidney can be investigated during either normal respiration or breath hold, since the kidney will follow the diaphragm movement and change position accordingly [1].

2. The Doppler ultrasound: a general review

Doppler ultrasound has been extensively utilized in assessing reno-vascular diseases since it is a safe, non-invasive, available and cheap. These measurements depend on the Doppler effect is used to measure changes in the frequency of the echoes reflected from moving blood cells. In many cases, Doppler ultrasound replaces X-ray angiography. The most important advantage of Doppler ultrasound over other imaging methods that it provides a real-time assessment of blood flow.

2.1 Types of Doppler ultrasound imaging

All kinds of Doppler sonography are widely used in medical imaging. The advantages of these types are high accuracy in measurements, non-invasive nature, accessibility, and no harmful biological effects. Today, there are three types:

a. Color Doppler

b. Power Doppler

c. Pulse wave Doppler

The color Doppler (CD) converts Doppler shifts to an array of colors and form a picture of blood vessels to display the speed and direction of blood flow through

the vessels. The Doppler shift is the difference between the incident frequency and reflected frequency. Positive Doppler shift occurs when the reflector is moving away from the probe, and a negative shift occurs when the reflector moving toward the source of ultrasound. Thus, the Doppler shift is directly proportional to the velocity of the blood flow.

$$FD = \frac{2F0v\ cos\ 0}{C} \quad (1)$$

where F_0: is the transmitted ultrasound frequency; V: is the reflector velocity; C: is the speed of sound; Cos 0: is the cosine of the angle between the transmitted beam and the reflector path.

2.1.1 Factors influencing color flow image

1. Power: transmitted power into tissue*

2. Gain: affect sensitivity to flow signals

3. Frequency: affect sensitivity and resolution. High frequency provides better sensitivity to low flow while lower frequency has better penetration and lesser aliasing.

4. Pulse repetition frequency (PRF): called scale: low PRF concerns at low velocities and high PRF reduces aliasing.

5. Area of investigation: larger area reduces frame rate. Thus, reducing the color box of the flow area under examination will usually improve frame rate and may allow a higher color scan line density with improved spatial resolution

6. Focus: should be coincide to the region of interest [2].

2.1.2 Practical guidelines of color Doppler flow imaging

1. Choose the set-up key. This improve Doppler parameters for specific investigations.

2. Apply power within the study area and then adjust color gain. Ensure focus is set at the level of region of investigation. Adjust gain to improve color signal.

3. Position beam steering to get satisfactory beam angle for the selected artery or vein.

4. Adjust PRF to synchronize the flow status. Low PRF are very sensitive to low flows or velocities but may cause aliasing. High PRF decrease aliasing but are less sensitive to low flows/velocities [2].

5. Set the color flow area to suitable size. A small color flow 'box' or region may lead to a better frame rate and better resolution.

2.1.3 Spectral wave Doppler

Pulsed wave Doppler (PWD) ultrasound is used to generate a sonogram of a blood vessel (vein or artery) under study (**Figure 2**). PWD provides a measure of

the flow changing velocity throughout the cardiac cycle and display distribution of velocities in the sample volume (gate) as demonstrate in **Figure 3**. Velocities can be measured when an accurate angle correction is made.

2.1.4 Factors affecting the spectral Doppler image

1. Power: set the transmitted power to study area.

2. Gain: influence sensitivity to flow signals.

3. PRF: low PRF is used to detect low velocities while high PRF decrease aliasing.

4. Gate size: beam steering allows improved beam angle for accuracy of calculation of flow velocity.

2.1.5 Guidelines for practical spectral Doppler image

1. Set power to the selected study area.

2. Place the Doppler cursor on the artery/vein to be examined.

3. Gain should be adjusted so that the image is clearly visible and noiseless.

4. Apply the beam steering to get a satisfactory angle. Remember that angles approaching to 90° will give ambiguous image or unclear data. The beam angle must be 60° or less when velocity measurements are to be maintained.

5. Adjust the PRF/scale and baseline to suit flow conditions. The sonogram should be clear and not subjected to aliasing.

6. Adjust the sample volume (SV) to correct and suitable size coincided with area under investigation. Correct the angle to obtain accurate velocities. Use the B-mode and color flow image of the vessel to make the angle correction [2].

2.2 Doppler ultrasound of the kidneys

Doppler ultrasound is essential for evaluation of the kidneys. Doppler is considered more accurate than conventional sonography since it provides functional and

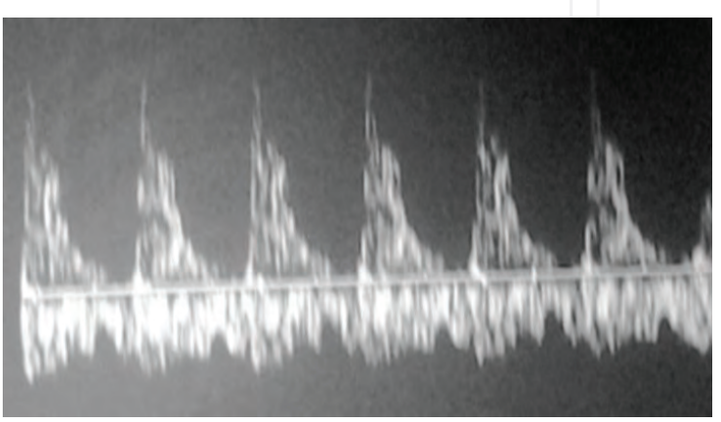

Figure 2.
Spectral wave Doppler. Renal arterial velocity waveform.

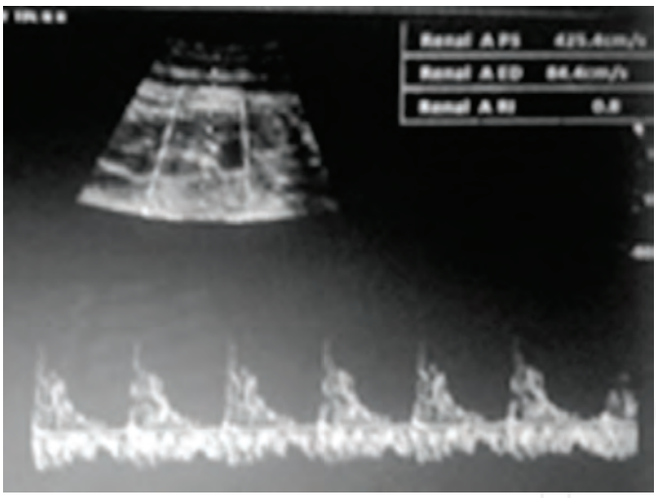

Figure 3.
Renal artery spectral Doppler demonstrates renal artery stenosis; PSV is 452.4 cm/s, RI= 0.80 in a 25-years male with hypertension and abnormal renal function (the sonogram taken by Dr. Moawia Gameraddin).

vascular information which are lacked in grayscale ultrasound. Doppler ultrasound assesses patterns of renal and extrarenal vascularization [3].

Doppler investigations must be performed properly to gain useful data. It allows information about the presence and direction of blood flow in renal vessels. Renal artery stenosis can be assessed by Doppler indices; resistive index (RI), pulsatility index (PI) and systolic to diastolic ratio (S/D). These indices provide hemodynamic and predictive information regarding the renal arteries. Analysis of the RI may provide helpful clinical information in various renal diseases [3].

2.2.1 Doppler procedure of the renal arteries

The investigation starts with the patient in the supine position using a low-frequency probe (2.5–5.0 MHz) to depict the abdominal aorta (AA) and renal arteries (RAs). The two main approaches for imaging the renal arteries are through the anterior abdominal wall. In most situations the anterior approach is used to assess the main RAs [4, 5].

The RAs arise from the lateral borders of the abdominal aorta (AA) at the level of the second lumbar vertebra, almost 1–2 cm inferior to the superior mesenteric artery (SMA) origin. The right RA arises from the anterolateral aspect of the abdominal aorta and it courses under the inferior vena cava (IVC) [8–10]. From this view, RA flow is in a direction that is parallel to the Doppler beam, optimizing signal reception. The patient usually needs to be placed in the opposite lateral decubitus position [4, 6].

A 3.5 MHz curvilinear array transducer with variable focal zone are used. The Doppler examination is usually performed in supine positions as stated by the renal ultrasound protocols. Each Kidney will be examined firstly with B-mode ultrasound in at least two planes to maintain the renal length for each kidney. The Doppler indices (RI and PI) are measured at interlobular or arcuate artery in the upper, middle, and lower portions of the kidney and the mean values were calculated for each kidney.

2.2.2 Normal vascularity of the renal artery

Doppler RI is efficient to detect intrarenal vascular pathological processes. Several studies have demonstrated that a normal mean renal RI is approximately 0.60. It was reported that a mean RI of 0.60 ± 0.01 for individuals without

pre-existing renal disease [7]. Other studies also reported normal mean RI values of 0.64 ± 0.05, 0.58 ± 0.05 [8], and 0.62 ± 0.04 [8, 9]. In addition, most sonographers have considered 0.70 to be the upper threshold of the normal RI in adults [10, 11].

2.2.3 The importance of Doppler resistive index

Doppler sonographic analysis of renal artery waveforms was empirically applied to disease characterization (**Figure 4**). Despite RI is a good predictor of several renal abnormalities, there are factors that affect the arterial waveform such as vascular resistance, vascular compliance, and heart rate. In a previous study, it was reported that renal RI was associated with "histological changes and poor renal outcome during chronic kidney disease". It was shown that RI ≥ 0.65 is associated with arteriosclerosis, severe interstitial fibrosis and renal function decline. Therefore, RI is essential Doppler parameter that contribute to diagnose patients at high risk of end-stage renal disease (ESRD) [12].

2.2.4 Application of Doppler in renal diseases

2.2.4.1 The role of Doppler in hypertension

Hypertension involves approximately 25–30% of the adult population and it was reported that the prevalence will increase. It is considered a main risk factor for the development of renal failure and cardiovascular disease. It was reported that 80% of patients with chronic kidney disease (CKD) are hypertensive. The relationship between hypertension and kidney disease is complex and it is attributed to the interrelated pathophysiology. Renal hypertension or renovascular hypertension means hypertension due to renal artery stenosis and kidney disease. Thus, patients who newly diagnosed hypertension must be screened for underlying kidney disease [13].

2.2.4.2 The role of Doppler RI in renal hypertension

The Doppler RI has been utilized for many years in a variety of clinical situations. Doppler ultrasonography detects renal abnormalities at macrovascular and microvascular levels. Assessment of renal RI at different regions of the renal parenchyma may suggest physiological or morphological changes within the kidneys. Therefore, it provides useful information for diagnosis and prognosis of the disease.

Recent studies revealed an increased renal resistive index (RRI) in patients with primary hypertension not only reflects vascular changes in intrarenal supply, but that it is also associated with atherosclerosis and systemic hemodynamics. Therefore, it provides useful prognostic information.

2.2.5 Doppler assessment of non-obstructive diseases

2.2.5.1 Acute and chronic kidney disease

Acute kidney injury: Acute kidney injury (AKI) was reported to associate with a high morbidity, long-term mortality and apparent economic impact [14].

Doppler ultrasound has been widely used in the assessment of renal diseases for diagnosis, prognosis and management. Doppler ultrasound is non-invasive, low cost and safe method for the evaluation of the renal blood flow. Recent studies reported different incidence of AKD among hospitalized patients classified as

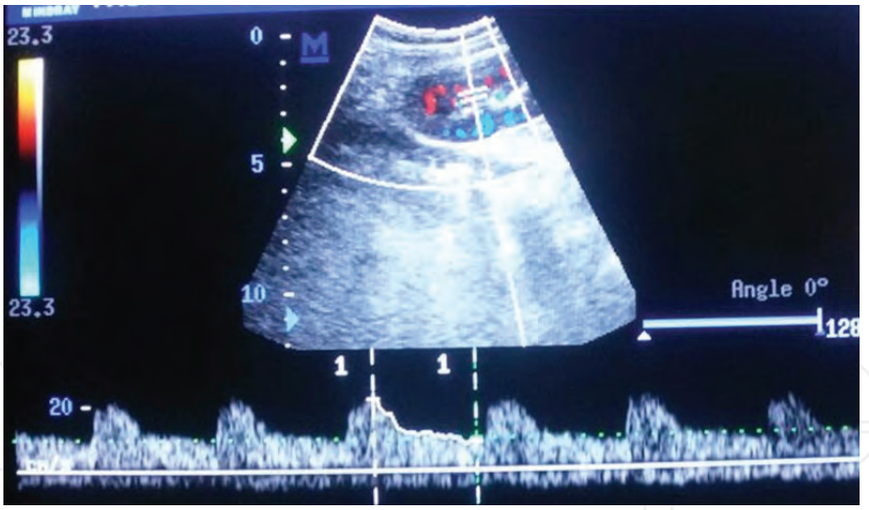

Figure 4.
Duplex Doppler reveals normal waveform of the renal artery (a sonogram taken from Awadia Gareeballah and Moawia Gameraddin researches).

"KDIGO classification (18.3 %), followed by AKIN (16.6 %) and RIFLE (16.1 %) and CK (7.0 %)."

2.2.5.2 Doppler evaluation of acute kidney injury

In gray scale ultrasound, AKD reveals increased renal parenchymal echogenicity which attributed to inflammatory states (acute glomerulonephritis, acute interstitial nephritis, acute tubular necrosis, HIV nephropathy) or infiltrative diseases (lymphoma, monoclonal, myeloma and gammopathies) decreased thickening of kidney cortex and echogenicity are also significant findings of AKI [15]. Color Doppler identifies the renal vessels localization to calculate RRI to monitor renal perfusion. In late stages of AKI, RRI usually exceed 0.7, and a threshold of 0.75 is reported as optimal in recognizing between renal and prerenal disease. However, RRI values lower than 0.7 are related to a good recovery after fluid rehydration, while RRI >0.7 suggest a developing ischemic acute tubular necrosis (ATN) and worse prognosis [16]. In conclusion, RRI play an effective role in different types of AKI.

2.2.6 Doppler assessment of chronic kidney disease

Chronic kidney disease (CKD) is considered as one of the public health problems worldwide [17]. According to the report of Global Burden of Disease in 2010 [2], CKD had been ranked the first cause of death worldwide at 27th to 18th over two decades. It was reported that "the surge of the CKD epidemic over these decades produced an 82% increase in years of life lost related to CKD, a disease toll of the same magnitude of that attributable to diabetes".

Ultrasonography of the kidneys is essential imaging modality among other renal imaging methods since it is available, low cost and safe. US can easily assess a CKD by measuring the length of the kidneys and evaluating the echogenicity of the kidney cortex. The reduction of size and increased echogenicity reflect pathological processes within the kidney.

The normal kidney length is about 11–12 cm (the left kidney is about 3 mm longer than the right kidney) in younger adults and a progressive atrophy with aging. Normal kidney is always as bright as normal liver or spleen tissue [18]. When the kidney cortex became brighter (echogenic) than hepatic tissue or splenic tissue,

this reflects inflammatory changes in the kidney tissues. CKD is often associated with increased echogenicity of the renal cortex since fibrous tissue such as glomerulosclerosis interstitial fibrosis, increases echogenicity.

However, those inflammatory conditions such as glomerulonephritis and acute interstitial nephritis (ATN) are associated with hyperechoic aspect of the renal parenchyma. In most cases, small and echogenic kidneys always suggest CKD instead of AKI.

Doppler ultrasound plays effective role in defining CKD and its progression to ESRD. Renal RI is reported to be correlated with arteriolosclerosis, glomerulosclerosis and tubulointerstitial lesions more than others morphologic parameters like kidney length and cortex area [19]. In general, higher values of renal RI (>0.7) ordinary reflects more severe arteriolosclerosis than normal values (<0.65) or high normal RRI ($0.65 \leq RI < 0.7$) [20]. However, patients with high-normal renal RI revealed good response to steroid therapy compared to a RRI > 0.7 [19]. Additionally, patients with advanced CKD stage showed significant higher RI than patients with earlier CKD stage.

2.2.7 Renal masses

Ultrasound plays a key role in screening renal cancer in asymptomatic patients. Most renal tumors remain are not accurately diagnosed on US and require CT for further characterization. However, US help to characterize cystic RCC that remain unclear on computerize tomography (CT). Recent technology in gray-scale imaging have improved the accuracy of US in the diagnosis and staging of kidney cancer. In addition, solid renal masses can grossly be categorized as completely solid, multifocal, or partially cystic tumors. The cystic appearance is mainly due to necrosis.

2.2.7.1 Ultrasound evaluation kidney cancer

Computed tomography (CT) is the gold standard for imaging the kidneys. It is accurate for detecting and characterizing renal neoplasms and staging renal cell carcinoma (RCC). On the other hand, ultrasound (US) has a less sensitivity in detecting small renal lesions, but it plays a key role in the early diagnosis of kidney cancer since it is routinely used in the evaluation of the abdomen. Renal masses were identified on US as a distortion of the normal tissue echotexture. Previous studies reported that RCC is detected incidentally in asymptomatic patients. Only 10% of patients with RCC present with the classic triad of hematuria, pain and a flank mass. Most of these patients often have advanced disease. More than 40% of the present with none of these three symptoms [21]. The RCC might be detected incidentally during abdominal sonography. The majority of RCC measure less than 3 cm or less on US. Early detection of RCC improves prognosis and survival rate.

The sonographic appearance of renal tumors vary between isoechoic-, hypoechoic, and hyperechoic compared with the normal renal parenchyma [22]. Doppler US assesses the blood flow patterns of vascularity in renal tumor tissue. It reveals vessels with high velocities. In RCC, the hypervascularity is attributed to neovascularization. The Doppler RI on spectral Doppler US was reported to be useful in detecting RCC in patients with ESRD [23].

2.2.8 The Doppler assessment of transplanted kidney

US is the most imaging modality for assessment of the transplanted kidneys (TK) (**Figure 5**). The TR is located in the right or left iliac fossa. The superficial location of the graft make the US examination accurate and ideal. The renal graft

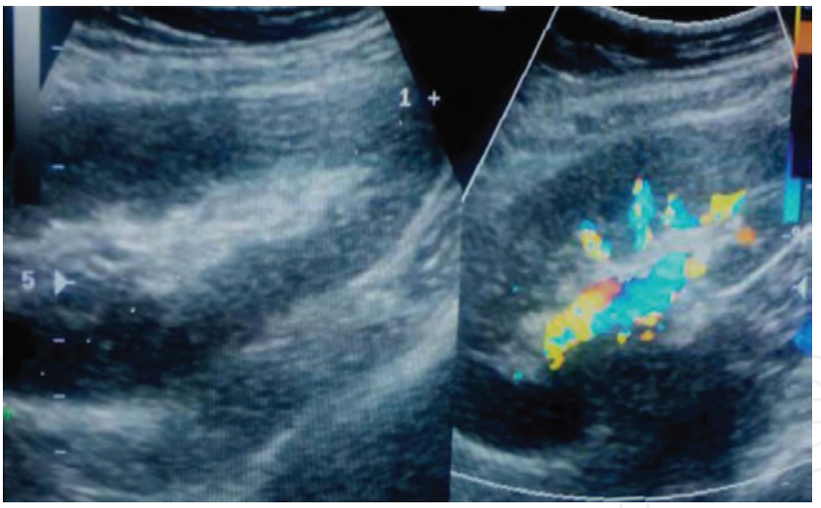

Figure 5.
A sonogram of a transplanted kidney shows normal size and normal color flow.

is vulnerable to several pathologic changes which might occur immediately or later. The sonographic appearance for evaluation of immediate post-plant pathologies may not be specific such as acute tubular necrosis (ATN), acute rejection, and toxicity associated with immunosuppressive calcineurin inhibitors [24].

The Doppler renal RI has a significant correlation with renal allograft size. It was reported that RI of 0.8 or higher was considered a strong predictor of graft failure and morphological changes [25]. The increase of RI was reported to correlate with presence of acute rejection and ATN [26]. On the other hand, elevated serum creatinine levels in renal transplant patient reveals high RI values. Therefore, the renal RI was a good predictor of graft function.

3. Renal elastography

Ultrasound elastography (USE) was first described in the 1990s. It is an imaging technology which is sensitive to tissue stiffness. In recent years, elastography has been further developed to enable quantitative assessments of tissue stiffness. Elastography is capable to assess changed elasticity of soft tissues resulting from specific pathological or physiological processes [27]. For example, tissue of solid tumors tends to differ mechanically from surrounding healthy tissues. Furthermore, fibrosis makes diseased tissue to be stiffer than normal ones. The role of elastography is to differentiate diseased tissue from normal one for diagnostic applications.

Ultrasound elastography (USE) of the kidneys is a potential application is an advanced imaging tool that may become a clinical biomarker for disease. However, elastography of renal transplant cortex and the corticomedullary strain ratio have been studied and they were found to correlate with renal cortical fibrosis [28, 29]. Shear-wave elastography (SWE) of the kidney utilizing acoustic radiation force impulse (ARFI) is a potential clinical application which was reported to demonstrate successful clinical applications in human organs [29]. In the kidney, SWE has shown promise in the evaluation of CKD, renal transplant function, and renal vein thrombosis (RVT).

3.1 Renal fibrosis

USE is clinically useful to detect and assess fibrosis in CKD and transplanted kidneys. USE with both strain imaging and SWI methods are noninvasively to

Criteria	Doppler ultrasound	Elastography
Main principle	Evaluates vascularity	Assesses elasticity
Renal transplantation	Renal blood resistivity index (renal RI) above 0.8 indicates renal graft dysfunction.	Assesses cortical fibrosis in early stage. Additionally, elastography assesses the grades of fibrosis; distinguish mild from moderate fibrosis.
Obstructive and non-obstructive hydronephrosis	Doppler US distinguishes between obstructive and non-obstructive hydronephrosis. Obstructive hydronephrosis reveals higher RI values than non-obstructive hydronephrosis.	Measurements did not enable distinguishing of obstructive hydronephrosis from non-obstructive hydronephrosis in children
Differentiation between malignant and benign tumors	Doppler US is useful in characterization of renal pseudotumors. Doppler allows differentiation of normal vascularity from tumor neovascularity. On the other hand, benign renal masses characterized by less or peripheral vascularity, homogeneous echotextures and well-defined margins.	Malignant tumors are stiffer than benign masses.

Table 1.
Comparison between Doppler ultrasound and elastography in evaluation of abnormalities of the kidney.

detect, stage and monitor kidney fibrosis, thus, reducing the need for renal biopsy [30]. SWI is preferable to strain imaging in evaluating kidney fibrosis in both renal graft and native kidneys since it is independent of external compression [30]. A previous study reported that SWE renal stiffness was higher in patients affected with CKD than in healthy controls [31]. Therefore, tissue stiffness measured by USE was significantly correlated with histopathologic renal fibrosis. This finding concluded that, USE is a non-invasive tool for predicting kidney fibrosis.

3.2 Characterization of focal renal lesions using elastography

USE is useful for characterizing focal renal masses since US features are not specific for malignancy. Assessment of renal masses with USE have shown controversial results. Some results found SW velocity values could differentiate between benign and malignant masses. Another study compared between malignant and benign renal masses concluded that malignant tumors are 2.8 times stiffer than benign masses [32]. A previous study reported that USE can differentiate between renal cell carcinoma (RCC) and transitional cell carcinoma (TCC) [33]. In general, quantification of kidney tissue using USE is more complex than other organs since the high heterogeneity of the renal tissue. However, the combination of doppler ultrasound and elastography will provide better assessment of kidney abnormalities as compared in **Table 1**.

4. Conclusion

In summary, Doppler ultrasound and USE are very effective imaging method to the kidneys. Doppler assesses vascularity of the kidneys while elastography evaluates tissue elasticity. USE is a new developing method and various studies have been made using elastography in kidneys. It is very effective on the transplanted and CKD kidneys to evaluate the corticomedullary fibrosis to prevent invasive biopsy.

Conflict of interest

The author declares there was no conflict of interest regarding this chapter.

Author details

Moawia Gameraddin
Department of Diagnostic Radiologic Technology, Faculty of Applied Medical Sciences, Taibah University, Almadinah, Kingdom of Saudi Arabia

References

[1] Hansen KL, Nielsen MB, Ewertsen C. Ultrasonography of the kidney: A pictorial review. Diagnostics (Basel). 2015;**6**(1):2. DOI: 10.3390/diagnostics6010002

[2] Available from: https://sonoworld.com/client/fetus/html/doppler/capitulos-html/chapter_01.htm [Accessed: 27 Jan. 2019]

[3] Granata A, Fiorini F, Andrulli S, et al. Doppler ultrasound and renal artery stenosis: An overview. Journal of Ultrasound. 2009;**12**(4):133-143

[4] Zubarev AV. Ultrasound of renal vessels. European Radiology. 2001;**11**:1902-1915

[5] Meola M, Petrucci I. Color Doppler sonography in the study of chronic ischemic nephropathy. Journal of Ultrasound. 2008;**11**(2):55-73

[6] Korst MB, Joosten FB, Postma CT, Jager GJ, Krabbe JK, Barentsz JO. Accuracy of normal-dose contrast-enhanced MR angiography in assessing renal artery stenosis and accessory renal artery stenosis and accessory renal arteries. American Journal of Roentgenology. 2000;**174**:629-634. [PubMed]

[7] Keogan M, Kliewer M, Hertzberg B, DeLong DM, Tupler RH, Carroll BA. Renal resistive indexes: Variability in Doppler US measurement in a healthy population. Radiology. 1996;**199**:165-169

[8] Norris C, Pfeiffer J, Rittgers S, Barnes RW. Noninvasive evaluation of renal artery stenosis and renovascular resistance: Experimental and clinical studies. J Vasc Surg. 1984;**1**:192-201

[9] Kim S, Kim W, Choi B, Kim CW. Duplex sonography of the native kidney: Resistive index vs serum creatinine. (abstract). Journal of Ultrasound in Medicine. 1990;**9**:S25

[10] Platt J, Ellis J, Rubin J. Examination of native kidneys with duplex Doppler ultrasound. Seminars in Ultrasound, CT, and MR. 1991;**12**:308-318

[11] Platt J. Doppler evaluation of native kidney dysfunction: Obstructive and nonobstructive disease. AJR. 1992;**158**:1035-1042

[12] Bigé N, Lévy PP, Callard P, et al. Renal arterial resistive index is associated with severe histological changes and poor renal outcome during chronic kidney disease. BMC Nephrology. 2012;**13**:139. DOI: 10.1186/1471-2369-13-139

[13] Grendelmeier I. Renal hypertension—The role of the kidneys in blood pressure regulation and the kidneys as end-organ. Therapeutische Umschau. 2015;**72**(6):369-374. DOI: 10.1024/0040-5930/a000688

[14] Nisula S, Kaukonen KM, Vaara ST, Korhonen AM, Poukkanen M, Karlsson S, et al. Intensive Care Medicine. 2013;**39**:420-428. DOI: 10.1007/s00134-012-2796-5

[15] Legrand MM, Darmon M. Renal imaging in acute kidney injury. In: Acute Nephrology for the Critical Care Physician. 2015

[16] Pozzi Mucelli R, Bertolotto M, Quaia E. Imaging techniques in acute renal failure. Contributions to Nephrology. 2001;**132**:76-91. DOI: 10.1159/000060076

[17] Neuen BL, Chadban SJ, Demaio AR, Johnson DW, Perkovic V. Chronic kidney disease and the global NCDs agenda. BMJ Global Health.

2017;**2**(2):e000380. DOI: 10.1136/bmjgh-2017-000380

[18] Spatola L, Andrulli S. Doppler ultrasound in kidney diseases: A key parameter in clinical long-term follow-up. Journal of Ultrasound. 2016;**19**:243-250

[19] Hanamura K, Tojo A, Knugasa S, Asaba K, Fujita TT. The resistive index is a marker of renal function, pathology, prognosis, and responsiveness to steroid therapy in chronic kidney disease patients. International Journal of Nephrology. 2012;**2012**:139565

[20] Gibbons RP, Monte JE, Correa RJ Jr, Mason JT. Manifestations of renal cell carcinoma. Urology. 1976;**8**:201-206

[21] Ikee R, Kobayashi S, Hemmi N, et al. Correlation between the resistive index by Doppler ultrasound and kidney function and histology. American Journal of Kidney Diseases. 2005;**46**(4):603-609

[22] Rumack CM, Wilson SR, Charboneau JW, Levine D. Diagnostic Ultrasound. St Louis, MO, USA: Elsevier Health Sciences; 2005

[23] Kim SY, Woo S, Hwang SI, et al. Usefulness of resistive index on spectral Doppler ultrasonography in the detection of renal cell carcinoma in patients with end-stage renal disease. Ultrasonography. 2014;**33**(2):136-142

[24] Piyasena RV, Hamper UM. Doppler evaluation of renal transplants. Applied Radiology. Available from: https://www.appliedradiology.com/articles/doppler-ultrasound-evaluation-of-renal-transplants [Accessed: 20 Jan. 2019]

[25] Gameradin M, Malik BA, Yousef M, Gareeballah A, Siddig S, Burai M, et al. Renal transplantation: Sonography and Doppler assessment of transplanted kidneys in adult Sudanese patients. Australasian Medical Journal. 2017;**10**(6):489-496. DOI: 10.21767/AMJ.2017.2994

[26] Radermacher J, Mengel M, Ellis S. The renal arterial resistance index and renal allograft survival. The New England Journal of Medicine. 2003;**349**:115-124

[27] Shiina T, Nightingale KR, Palmeri ML, Hall TJ, Bamber JC, Barr RG, et al. WFUMB guidelines and recommendations for clinical use of ultrasound elastography: Part 1: Basic principles and terminology. Ultrasound in Medicine & Biology. 2015;**41**:1126-1147

[28] Gao J, Weitzel W, Rubin JM, Hamilton J, Lee J, Dadhania D, et al. Renal transplant elasticity ultrasound imaging: Correlation between normalized strain and renal cortical fibrosis. Ultrasound in Medicine & Biology. 2013;**39**:1536-1542

[29] Gao J, Min R, Hamilton J, Weitzel W, Chen J, Juluru K, et al. Corticomedullary strain ratio: A quantitative marker for assessment of renal allograft cortical fibrosis. Journal of Ultrasound in Medicine. 2013;**32**:1769-1775

[30] Anvari A, Barr RG, Dhyani M, Samir AE. Clinical application of sonoelastography in thyroid, prostate, kidney, pancreas, and deep venous thrombosis. Abdominal Imaging. 2015;**40**:709-722

[31] Samir AE, Allegretti AS, Zhu Q, et al. Shear wave elastography in chronic kidney disease: A pilot experience in native kidneys. BMC Nephrology. 2015;**16**:119. DOI: 10.1186/s12882-015-0120-7

[32] Onur MR, Poyraz AK, Bozgeyik Z, Onur AR, Orhan I. Utility of

semiquantitative strain elastography for differentiation between benign and malignant solid renal masses. Journal of Ultrasound in Medicine. 2015;**34**:639-647

[33] Inci MF, Kalayci TO, Tan S, Karasu S, Albayrak E, Cakir V, et al. Diagnostic value of strain elastography for differentiation between renal cell carcinoma and transitional cell carcinoma of kidney. Abdominal Radiology (NY). 2016;**41**(6):1152-1159. DOI: 10.1007/s00261-016-0658-2

Chapter

Ultrasound Modality in the Evaluation and Management of Gallbladder Polyps

Haithem Zaafouri, Meryam Mesbahi, Nizar Khedhiri, Wassim Riahi, Mouna Cherif, Dhafer Haddad and Anis Ben Maamer

Abstract

Gallbladder polyps (GBP) are defined as developed masses inside the wall of the gallbladder; most of them (90%) are nontumor lesions. Abdominal ultrasound is the main and the first line radiological modality for their diagnosis and their risk lamination. We conducted a 12 year retrospective study between 2009 and 2020, which included patients who had preoperative transabdominal ultrasonography showing gallbladder polyps and had undergone cholecystectomy, and for whom postoperative pathology results were available, as well as patients who had at least one polyp discovered on the histopathological exam and who were not determined preoperatively. A total of 70 patients were identified. Preoperative diagnosis of vesicular polyp by ultrasound was carried in 82.9% of patients. The number of ultrasounds performed per person was 1.2 ± 0.47. The polyps' size in mm was on average 6.14 ± 2.6 with extremes between 3 and 13 mm. On anatomopathological examination, a polyp was objectified in 33.3% of cases. In our series, abdominal ultrasound had a low sensitivity at 36.4%. We aim to provide the accuracy of abdominal ultrasound for the diagnosis of GBP, as a low-cost modality, and to evaluate the concordance of preoperative ultrasound imaging with postoperative pathology.

Keywords: gallbladder polyps, abdominal ultrasound, sensitivity, cholecystectomy, management

1. Introduction

Gallbladder polyps (GBP) are defined as developed masses inside the wall of the gallbladder; most of them (90%) are nontumor lesions [1]. They have been firstly classified in 1976 as benign tumors, pseudotumors, and malignant tumors [2].

Abdominal ultrasound is the main and the first line radiological modality for their diagnosis and their risk lamination [3]. It has been proven in the literature, the superiority of ultrasound by comparing it to other imaging techniques such as CT scan [4].

Ultrasound diagnosis of GBP is founded on two criteria—the lack of posterior acoustic shadow and immobility when changing the patient's position [1, 5].

Transabdominal ultrasound represents also an essential modality for the follow-up of GBP [6].

Nowadays, plenty of radiological modalities, such as transabdominal ultrasonography, endoscopic ultrasonography, magnetic resonance imaging (MRI), CT scan, or PET-CT have been employed for the diagnosis of GBP [7].

GBP are potentially malignant lesions so that it is mandatory to be precise whether the polyp is a high or low risk of malignancy and to lead undoubtedly to their perfect management [8].

We aim to provide the accuracy of abdominal ultrasound for the diagnosis of GBP, as a low-cost modality, and to evaluate the concordance of preoperative ultrasound imaging with postoperative pathology.

2. Methods

We conducted a 12 year retrospective study between 2009 and 2020, which included patients who had preoperative transabdominal ultrasonography showing gallbladder polyps and had undergone cholecystectomy, and for whom postoperative pathology results were available, as well as patients who had at least one polyp discovered on the histopathological exam and who were not determined preoperatively.

Epidemiological, clinical, morphological, and ultrasound data were then collected, as well as data from anatomy pathology interventions and reports.

3. Results

A total of 70 patients were identified. The sex ratio (male:female) was 0.34. The average age was 53.4 years with extremes ranging from 28 to 78 years. A total of 35 patients had a medical history, such as high blood pressure (25.7%), dyslipidemia (11.4%), and diabetes (8.6%). A total of 45 patients had a surgical history. The ASA score was 1 in 62.9%, 2 in 34.3%, and 3 in 2.9%.

Abdominal ultrasound was performed in all patients.

Preoperative diagnosis of vesicular polyp by ultrasound was carried in 82.9% of patients. Either due to symptoms in 68.6% of cases—right hypochondrium pain (48.4%), liver colic (35.5%), vomiting (9.7%) or fortuitous discovery in 8.6% of cases during an abdominal ultrasound for other pathology, or systematically in 5.7% of cases (four cases) as part of the preoperative assessment of an umbilical hernia.

In 17.1% of cases, the polyp was discovered perioperatively.

The number of ultrasounds performed per person was 1.2 ± 0.47.

Characteristics	
Age (years)	53.4
Symptoms, (%)	68.8%
Diabetes mellitus	8.6%
Size of gallbladder polyp (mm)	6.14 ± 2.6
No. of polyps per patient	1.59 ± 0.79
Coexistin ggallstones	4

Table 1.
Demographic and clinical characteristics of the study population.

The number of gallbladder polyps per patient was 1.59 ± 0.79.

The polyps' size in mm was on average 6.14 ± 2.6 with extremes between 3 and 13 mm. Gallbladder polyp and gallbladder stones were found in four patients (**Table 1**).

Other additional tests were performed: abdominal CT scan in 17.1% of cases, MRI in 5.7% of cases, upper endoscopy in 14.3% of cases, especially before gastric pain.

The surgical indication was retained especially when there were symptomatic polyps whatever the size, which was in 67.6% of cases.

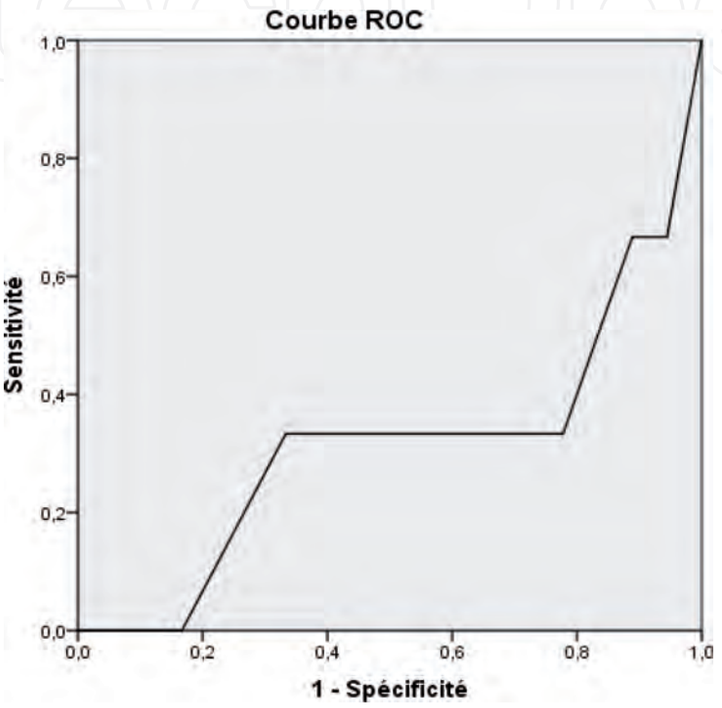

Figure 1.
Correlation between the size of the polyp on the abdominal ultrasound and the presence of polyp on the piece of cholecystectomy.

Positive if >=	Sensibility	Specificity
2.00	1000	1000
3.35	667	944
3.85	667	889
4.25	333	778
4.75	333	722
5.25	333	611
5.75	333	556
7.00	333	333
8.25	000	167
9.75	000	111
12.00	000	056
14.00	000	000

Table 2.
Sensibility and specificity of the abdominal ultrasound in function of the size of the polyp.

Cholecystectomy was performed by laparoscopy in 82.9% of cases.

On anatomopathological examination, a polyp was objectified in 33.3% of cases. The average size was 8.83 ± 10.8 mm. Dysplasia was found in 72.7% of all polyps.

In 22.7% of cases, cholesterolosis was noted.

In our series, abdominal ultrasound had a low sensitivity at 36.4%.

Using the ROC curve (**Figure 1**) to study the correlation between the size of the polyp on the abdominal ultrasound and the presence of polyp on the piece of cholecystectomy, we found that the area under the curve was 0.315, which corresponds to a low discriminating power.

The study of the coordinates of the curve showed that a size of 7 mm would have the best specificity and sensitivity (**Table 2**).

4. Discussion

This cohort study is based on the effectiveness of transabdominal ultrasound on the detection of GBP.

GBP is the frequent vesicular lesions, which are found frequently on abdominal ultrasonography [8]. Asymptomatic GBP is present in 5% of adults [9].

The abdominal ultrasonography presents the first line radiological means for the diagnosis of gallbladder diseases and the perfect examination for diagnosing polyps [4, 8]. Considering that it has the lower cost-effectiveness, convenient accessibility, the lack of radiation, and because of its higher sensitivity 93% and specificity 95.3% [8–10].

On the ultrasound, GBP appears as an elevated, immobile lesion of the wall, it has a posterior acoustic shadow, and it appears as a sessile lesion [11, 12].

Despite the routine use of ultrasound, it seems that its positive predictive value in diagnosing polyps is still low [13].

It can present some limitations because it is operator-dependent [14], and it can provide errors in the determination of polyps, their numbers, and their size [8].

As an example, a gallstone can be easily mistaken for a polyp on ultrasonography [15], as it can be only identified on ultrasound if it measures over 5 mm [15].

Many hypotheses have been studied to explain the poor sensitivity of ultrasound in determining true polyps, Kratzer proposed in this case, that the initial diagnosis of a polyp might be incorrect [7]. As seen in the Cochrane review that the cause of false diagnoses by ultrasound was generally a result of misinterpretation of gallstones as polyps [10].

However, Ostapenko [13] has concluded that seven patients of 34 with GBP did not have a detectable polyp, supporting the argument that the initial diagnosis was a false positive.

In our series, ultrasound had a sensitivity of 36.4%. Several factors could explain this result. Since ultrasound is a dependent operator examination, gall bladder stones, especially those of small size, could be taken on account of a polyp. The polyp's migration to the bile ducts could be another explanation and would probably be the cause of the hepatic colic. The absence of polyp on the histological examination could also be explained by the manipulation of the gallbladder during cholecystectomy.

In case of diagnostic difficulties, and mainly when malignancy is suspected, other complementary investigations can be more helpful [14, 16, 17] presenting by:

Contrast-enhanced sonography: which is an ultrasound enhanced by the injection of a medium non-irradiating ultrasonic contrast (microbubbles), is more specific in the study of vascularity, showing hyper-echoic contrast during the arterial phase and iso-echoic images during the venous phase. So, it is more

useful to identify gallbladder polyps of multiple stones and from other polypoid lesions [9, 14].

Magnetic resonance imaging (MRI): It is a particular modality used in the differentiation between gallbladder polyps from other polypoid lesions, especially adenomyomatosis [14].

Positron emission tomography (PET): It is used to evaluate the malignancy diagnosis in polyps rising more than 10 mm by hypermetabolism [14].

Endoscopic ultrasound (EUS): It is determined to be better than ultrasound, it is the best modality in diagnosing gallbladder polyps [15], especially when there is suspicion of regional lymph nodes, providing the staging of polypoid lesions [14, 15].

Conventional ultrasound is sufficient to investigate GBP compared to other modalities, however, it has been proven in some studies that endoscopic ultrasound is more specific and exact, especially in the differentiation between true and pseudopolyps [11].

Guo [8] confirmed the accuracy of ultrasound for polyps diagnosis which was 78.8% in their work, and its accuracy for differentiation between benign and malignant polyps, which was confirmed in the Cochrane review [10]. Our results are in line with these cohort studies.

On ultrasonography, the polyp echogenicity is used to distinguish between true, pseudopolyps, and gallstones [18].

Its main role is to identify prematurely the progression of polyps to malignant carcinomas [13]. Polyps size is considered the main indicator of potential malignancy [16].

According to the guidelines, an arbitrary cut-off of 10 mm is confirmed to indicate cholecystectomy, which is justified by the increased incidence of gallbladder carcinoma in the polyps rising sharply from 10 mm and upwards [11, 16, 18, 19].

Polyps can cause symptoms and the relationship between symptoms and risk of malignancy is still controversial according to the literature, so cholecystectomy is wisely indicated when GBP are symptomatic [11].

Many factors that influence the therapeutic strategy of GBP were studied, including mainly the polyp size on radiological findings [18].

Referring to the literature (recent guidelines by the ESGAR group), the main factors that determine malignancy included primarily—the size greater than 10 mm, the sessile morphology, the presence of symptoms, the age 50 years and older, the Indian ethnicity, and the associated primary sclerosing cholangitis (**Figure 2**) [14, 18, 20].

Several retrospective studies showed controversial results about factors influencing malignancy and indicating cholecystectomy, which are—concomitant gallstones, elevated CA 19-9 marker, rapid polyp growth, and the number of polyps [14, 18, 20].

Gallbladder polyps are generally diagnosed and monitored by ultrasonography which is debated in the literature, discussing its accuracy [16]. Some studies confirmed its failure for the diagnosis, seen the absence of polyps at numerous histological examinations [16].

Several series have studied the correlation between ultrasound findings and histopathology results, concluded significant conjunction for the size determination between both modalities [15].

Elmasry [16] showed a significant number of gallbladder polyps that were not seen at histological examination postcholecystectomy, with an incidence of 16.4% of all histological results. This can be explained that polyps may be destroyed by the mechanical action of the gallbladder wall [7].

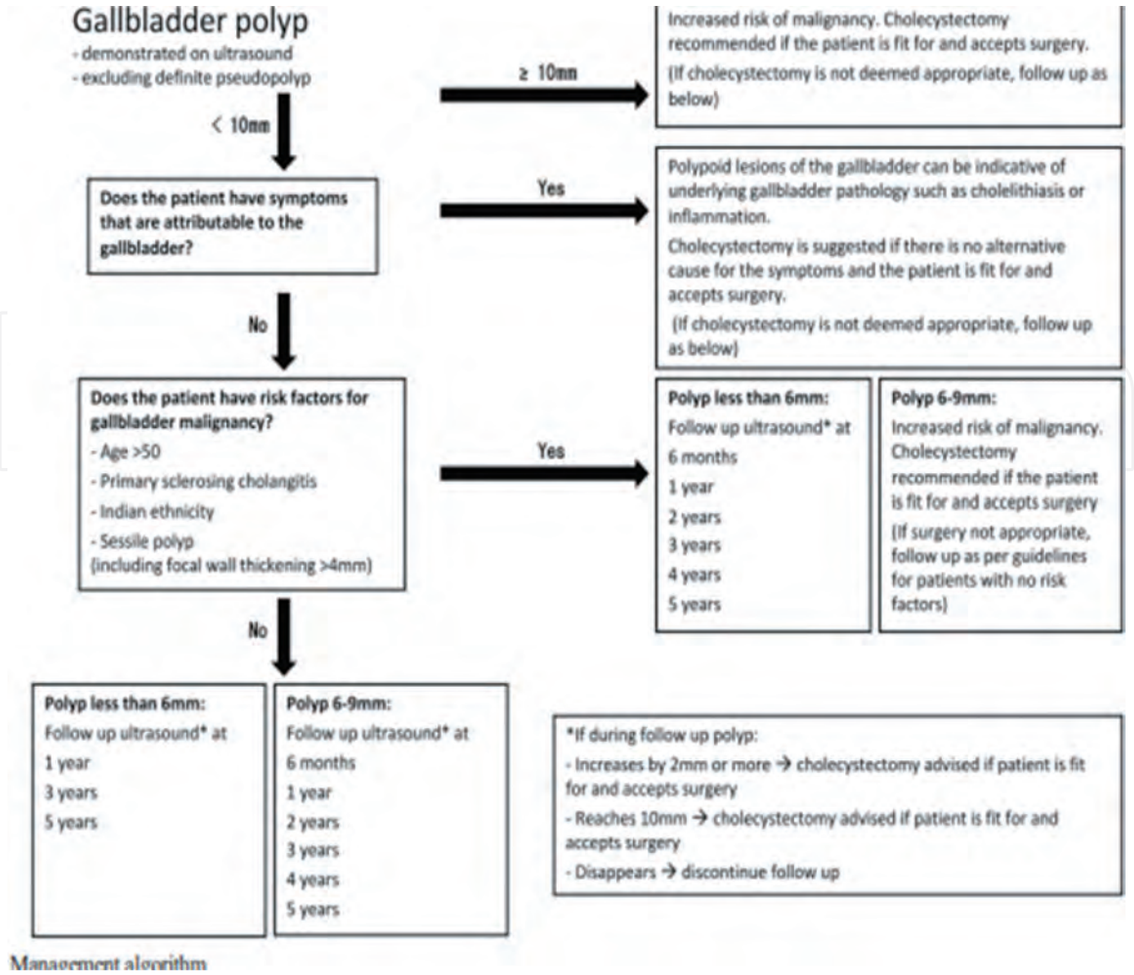

Figure 2.
Management algorithm for gallbladder polyps [11].

Nonresected GBP which are smaller than 10 mm are recommended to be followed up regularly with serial ultrasound imagery [15], every 6 months–1 year for those under 5 mm, every 3–6 months for those with a dimension of 5–10 mm [1].

Follow-up strategy of GBP is not yet based on any consensus on the size of polyps, neither on its frequency or duration. Recently, the guidelines of ESGAR states recommend that polyps of 6–9 mm should be supervised prudently than polyps of less than 6 mm [18]. So that the measurement of polyps size is mandatory during the follow up of GBP—it was found that 6.9% of polyps increased their size during the monitoring period [12].

It has been proven that there was no evidence data published to define the increasing size of the polyps during surveillance, which may be an indicator for cholecystectomy [2].

5. Conclusion

Preoperative diagnosis of GBP distinguishing malignant from benign lesions is challenging. Literature has highlighted the accuracy of ultrasound as the key modality for GBP detection.

It is used to be the gold standard, seeing it has relatively low-cost, low-risk, and widely available techniques. However, many studies discussed its ineffectiveness in polyp diagnosis, despite its major role in European guidelines. Leading to the essential role of other modalities such as magnetic resonance imaging, and endoscopic

ultrasound. In the upcoming, studies should investigate more on the utility of these newer imaging techniques to enhance a new multimodal strategy to gallbladder polyp investigation.

Author details

Haithem Zaafouri*, Meryam Mesbahi, Nizar Khedhiri, Wassim Riahi, Mouna Cherif, Dhafer Haddad and Anis Ben Maamer
Department of General Surgery, Habib Thameur Hospital, Tunis, Tunisia

References

[1] Pirraci DA. Evaluation and Ultrasound Follow-up of Gallbladder Polyps. Webmed Central Radiology. 2013;**4**(6):WMC004297

[2] Morera-Ocón FJ, Ballestín-Vicente J, Calatayud-Blas AM, Cataldo de Tursi-Rispoli L, Bernal-Sprekelsen JC. Surgical indications in gallbladder polyps Cirugía Española. 2013;**91**(5): 324-330

[3] Choi TW. Risk stratification of gallbladder polyps larger than 10 mm using high-resolution ultrasonography and texture analysis. European Radiology. 2018;**28**(1):196-205

[4] Liu L-N, Xu H-X, Lu M-D, Xie X-Y, Wang W-P, Hu B, et al. Contrast-enhanced ultrasound in the diagnosis of gallbladder diseases: A multi-center experience. PLoS One. 2012;**7**(10):13

[5] Bae JS. Quantitative contrast-enhanced US helps differentiating neoplastic vs non-neoplastic gallbladder polyps. European Radiology. 2019; **29**(7):3772-3781

[6] Martin E, Gill R, Debru E. Diagnostic accuracy of transabdominal ultrasonography for gallbladder polyps: Systematic review. Canadian Journal of Surgery. 2018;**61**(3):200-207

[7] Kratzer W, Haenle MM, Voegtle A, Mason RA, Akinli AS, Hirschbuehl K, et al. Ultrasonographically detected gallbladder polyps: A reason for concern? A seven-year follow-up study. BMC Gastroenterology. 2008;**8**:41-49

[8] Guo J, Wu G, Zhou Z. Polypoid lesions of the gallbladder: report of 160 cases with special reference to diagnosis and treatment in China. International Journal of Clinical and Experimental Pathology. 2015;**8**(9):11569-11578

[9] Yuan Z. Is contrast-enhanced ultrasound superior to computed tomography for differential diagnosis of gallbladder polyps? A cross-sectional study. Frontiers in Oncology. 2021;**11**:12

[10] Sarah ZW, Mark PL, Marcello DM, Joost Ph D, Kurinchi SG, Cornelis Jhm van L. et al. Transabdominal ultrasound and endoscopic ultrasound for diagnosis of gallbladder polyps (review). Cochrane Database of Systematic Reviews. 2018;**8**(8):CD012233

[11] Wiles R. Management and follow-up of gallbladder polyps. European Radiology. 2017;**27**(9):3856-3866.

[12] Rafaelsen SR, Otto PO, Pedersen MRV. Long-term ultrasound follow-up in patients with small gallbladder polyps. Danish Medical Journal. 2020;**67**(10):1-7

[13] Ostapenko A, Liechty S, Kim M, Kleiner D. Accuracy of ultrasound in diagnosing gallbladder polyps at a community hospital. JSLS. 2020; **24**(4):1-5

[14] Valibouze C. The management of gallbladder polyps. Journal of Visceral Surgery 2020;**157**(5):410-417

[15] Andrén-Sandberg Å. Diagnosis and management of gallbladder polyps. North American Journal of Medicine and Science. 2012;**4**(5):10

[16] Elmasry MM, Mrcs M. The risk of malignancy in ultrasound detected gallbladder polyps: A systematic review. International Journal of Surgery. 2016;**33**:28-35

[17] Babu BI, Dennison AR, Garcea G. Management and diagnosis of gallbladder polyps: A systematic review. Langenbeck's Archives of Surgery. 2015;**400**(4):455-62

[18] McCain RS, Diamond A, Jones C, Coleman HG. Current practices and future prospects for the management of gallbladder polyps: A topical review. World Journal of Gastroenterology. 2018;**24**(26):2844-2852

[19] Jeong Y, Kim JH, Chae HD, Park SJ, Bae JS, Joo I, et al. Deep learning-based decision support system for the diagnosis of neoplastic gallbladder polyps on ultrasonography: Preliminary results. Scientific Reports 2020;**10**(1): 1-10

[20] Sun Y, Yang Z, Lan X, Tan H. Neoplastic polyps in gallbladder: A retrospective study to determine risk factors and treatment strategy for gallbladder polyps. Hepatobiliary Surgery and Nutrition. 2019;**8**(3):9

9

Ultrasonography of the Stomach

Laurence Trahair and Karen L. Jones
University of Adelaide, Discipline of Medicine, Royal Adelaide Hospital
Adelaide, South Australia,
Australia

1. Introduction

Ultrasound is a versatile imaging modality with the potential to provide much quantitative and qualitative information in both clinical and research settings. Ultrasound has the capacity to provide both anatomical and physiological information in real-time, and also offers images with high temporal and spatial resolution. Furthermore, ultrasound is relatively non-invasive and is not associated with a radiation burden to the patient. These advantages, as well as the capacity to provide this information in a simple, fast and pain free examination has meant that there has been a huge increase in the number of applications of ultrasound since its introduction in the early 1960s. It was not until the 1980s that ultrasonographic assessment of the stomach and its contents were explored, and, since that time, a number of new techniques have been developed which can provide more comprehensive information in a single ultrasonographic exam.

This chapter will describe a number of these techniques, specifically, ultrasound imaging of the fundus and antrum (including area and volume), 2D and 3D assessment of gastric emptying, measurement of antropyloroduoenal motility and transpyloric flow as well as gastric strain rate imaging. Within each of these sections both clinical and research applications will be discussed. Strengths and limitations of the techniques, as well as comparisons with other methodological or diagnostic techniques will also be addressed.

2. Scanning techniques

Generally, no specific patient preparation is necessary (Nylund *et al.*, 2009). Fasting for a period of time prior to the examination will minimise the fluid and air present in the stomach and small intestine, resulting in better quality images (Folvik *et al.*, 1999; Nylund *et al.*, 2009), this is, however, not strictly necessary. If air is present, the ultrasonographer can apply gentle pressure with the transducer to move the air away from the area being scanned (Tarjan *et al.*, 2000). Additionally, it is important to minimise respiration effects when scanning, and this can be achieved by taking images at a constant point throughout the respiration cycle, or by asking patients to hold their breath as images are acquired (Jones *et al.*, 1997).

The patient should be positioned comfortably, in a supine position; however, measurement of gastric emptying (with both 2D and 3D ultrasound) should be performed seated or

semirecumbent position, to allow better visualisation of the entire stomach, and to reflect gastric emptying in a physiological situation (Hveem *et al.*, 1996; Gilja *et al.*, 1997a; Gilja *et al.*, 2005). Scanning should be performed with a 3.5 – 5 MHz transducer, allowing for complete visualisation of the area of interest (Nylund *et al.*, 2009).

The transducer should be placed on the surface of the skin in such a way as to acquire an image of the entirety of the region being examined, as this varies from individual to individual, and is easily modified throughout the exam. This location is normally in the region of the epigastrium, down to the subcostal margins, or over the umbilicus (Hveem *et al.*, 1996; Gilja *et al.*, 1997a; Gilja *et al.*, 2005).

The use of colour and power Doppler should be considered, as well as duplex ultrasonography. These can add additional anatomical information, particularly relating to the vasculature, which can be impossible to see with B-mode ultrasonography (Nylund *et al.*, 2009).

3. Imaging of the antrum

The way in which the stomach regulates the emptying of food to optimise digestion and absorption is complex. The function of the proximal stomach is generally recognised as a storage facility relaxing to accommodate food which is then passed down into the antrum where it is ground down into particles <1mm in size before emptying into the small intestine. Several techniques have been used to provide insights into the mechanisms regulating this process. Ultrasonographic imaging of the antrum can be used to provide information relating to the volume or area of the distal stomach both in the fasted state and postprandially, thereby providing information about distension of this region.

Imaging should ideally be performed with the subject seated, and the transducer positioned vertically to obtain a sagittal image of the antrum, with the superior mesenteric vein and the abdominal aorta in a longitudinal section (Hveem *et al.*, 1996) (Figure 1). Images should be taken at the end of inspiration to minimise the effects of the normal motion of the stomach which occurs with regular breathing (Jones *et al.*, 1997). The area of the antrum is defined by a region of interest drawn around the cross section of the antrum and is expressed in cm^2.

The use of ultrasound to assess the antrum is appealing in both the clinical and research setting due to the ease and simplicity with which it can be applied, especially in favour of other imaging modalities that are more expensive and time consuming.

The ability to assess gastric distension is of particular relevance in patients with diabetes mellitus and functional dyspepsia in whom the prevalence of upper gastrointestinal symptoms is substantial (Hausken & Berstad, 1992; Undeland *et al.*, 1996). Studies using 2D ultrasound have demonstrated in these patient populations that antral area is increased; both in the fasted and postprandial state (Hausken & Berstad, 1992; Undeland *et al.*, 1996).

The use of ultrasound to assess gastric distension can also be applied to evaluate mechanisms relating to appetite regulation. For example, in both healthy young (Jones *et al.*, 1997), and older (Sturm *et al.*, 2004) subjects, antral distension (as measured by antral area on a 2D ultrasound image) following a meal has been shown to correlate with perceptions of fullness and energy intake indicating the importance of antral distension in appetite regulation (Figure 2).

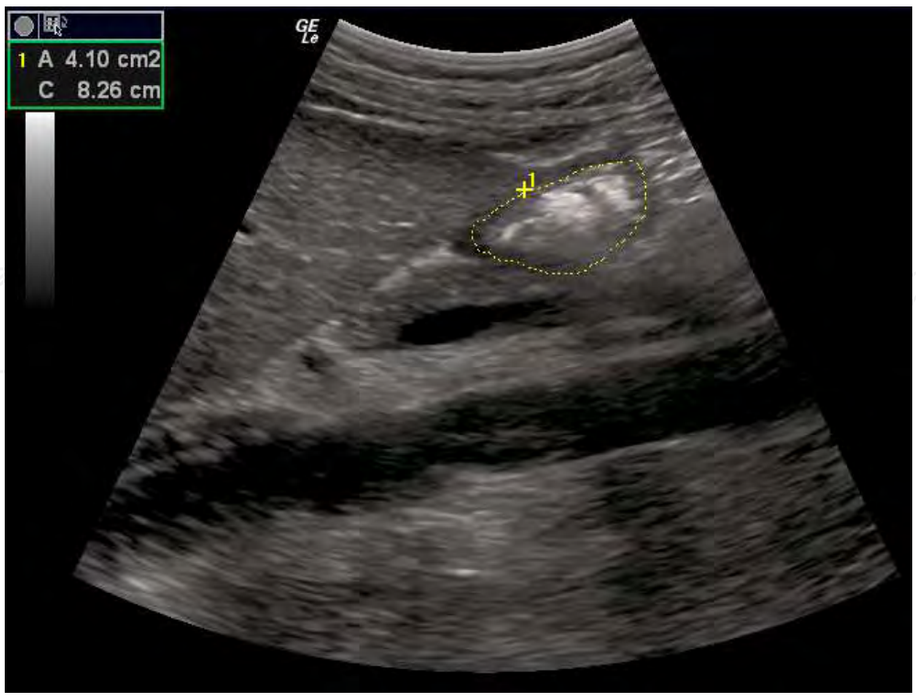

Fig. 1. 2D image of the antrum, with area calculation. The abdominal aorta and superior mesenteric vein are visible in the longitudinal section of the image.

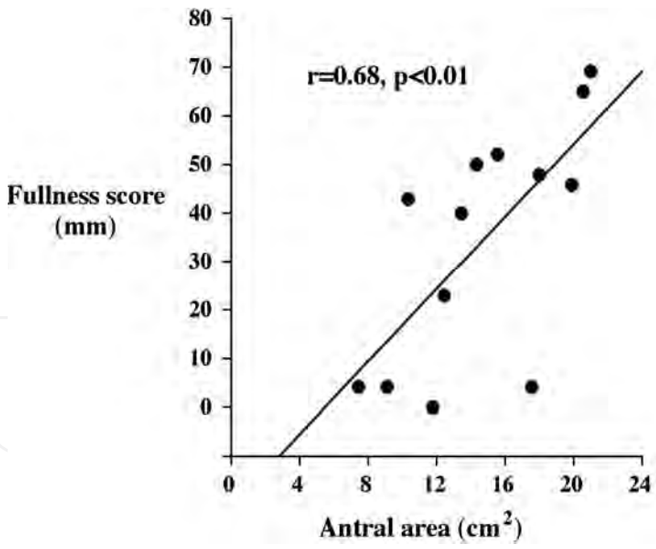

Fig. 2. Relationship between fullness score as measured by a visual questionnaire and antral area, measured by 2D ultrasound, 45 minutes after the consumption of a high-nutrient dextrose drink (75g dextrose dissolved in 350mL water) (n=14 healthy, young volunteers). (Am. J. Clin. Nutr. (1997;66:127-32), American Society for Nutrition).

Ultrasonographic assessment of the antrum has also been used pre-operatively to assess the likelihood of perioperative complications arising from the aspiration of gastric contents during surgery (Perlas *et al.*, 2009). Physicians acquiring a single image of the antrum were

able to distinguish between a fasted and fed stomach 2 hours following the ingestion of either a solid or a liquid meal (Bouvet *et al.*, 2009).

4. Imaging of the proximal stomach

Ultrasonographic imaging of the proximal stomach was first described in 1995 (Gilja *et al.*, 1995). With the patient seated, leaning backwards slightly, the transducer is be placed on the epigastrium, by the left subcostal margin, and tilted cranially (Gilja *et al.*, 2007). Two images are acquired, the first being a sagittal slice of the proximal stomach, with the left renal pelvis in the longitudinal section of the image, using the left lobe of the liver and pancreas as anatomical landmarks. The area of the fundus is defined as a region from the top margin of the fundus to a point 7 cm downward, along the axis of the stomach (Gilja *et al.*, 1995). A second image, taken in the oblique plane can be acquired with the transducer in the same location. The top margin of the fundus should remain clearly visible in this image. The diameter of the fundus can be calculated on this image and is defined as the maximum diameter of the fundus kept within 7 cm along the axis of the proximal stomach (Gilja *et al.*, 1995). Proximal stomach volume can be derived using these measurements. In addition to measurements of diameter, area and volume, this ultrasound technique also enables the calculation of the initial emptying fractions of the proximal stomach, if imaging is performed soon after ingestion of a meal (Gilja *et al.*, 1995).

Imaging of the proximal stomach and estimation of fundic accommodation was traditionally performed with either a gastric barostat or scintigraphy. Currently, the 'gold standard' for assessment of proximal stomach accommodation is the use of a barostat device, a thin, plastic, inflatable balloon attached to an orogastric catheter, which, when positioned correctly and inflated in the proximal stomach, can measure gastric wall relaxation, and from this the tone of the muscle can be inferred (Azpiroz & Malagelada, 1987). Unlike ultrasonographic assessment, the barostat technique only measures the volume of a sealed balloon, therefore it offers no information about the size or true muscle tone of the stomach (Szarka & Camilleri, 2009). The barostat device can be uncomfortable, is highly invasive and has been shown to influence gastric motor patterns (Moragas *et al.*, 1993; Parys *et al.*, 1993). The barostat bag has also been shown to cause dilation of the antrum due to its placement, which may affect gastric emptying (Mundt *et al.*, 2002), an effect clearly overcome with ultrasound. Ultrasound enables the accommodation of the proximal stomach to be assessed with high inter- and intra-observer agreement (De Schepper *et al.*, 2004) with the added advantage of also assessing gastric emptying, antral motility and transpyloric flow, if desired, in a single examination (De Schepper *et al.*, 2004).

Scintigraphic single photon emission computed tomography (SPECT) scanning has the capacity to non-invasively provide information about gastric volume (Vasavid *et al.*, 2010), without interfering with gastric motor patterns. The technique requires intravenous administration of radioactive technetium pertechnetate which is taken up by the gastric mucosa to facilitate imaging. Gastric accommodation can be assessed using this technique in a reproducible fashion, however, there is evidence that SPECT is not very sensitive in detecting fundic relaxation when compared to the gastric barostat (van den Elzen *et al.*, 2003). Ultrasonographic imaging of the proximal stomach has similar advantages to that of imaging of the antrum, in that its cost, absence of radiation burden, accessibility and simplicity makes it more approachable than other imaging modalities. In addition,

ultrasound imaging is performed in the sitting position, which is more reflective of the 'physiological' way one would be positioned when eating as opposed to SPECT, which requires the patient to be scanned in the supine position (De Schepper *et al.*, 2004; Hausken & Gilja, 2006).

While ultrasound has several advantages over the barostat technique, there remains some controversy as to whether measurements acquired by ultrasound, or even SPECT, can be compared directly to those acquired with a barostat device. The barostat, when inflated, can adjust to the changes in gastric pressure by adjusting the intrabag volume, therefore, changes in intrabag volume are said to reflect changes in muscle tone (Azpiroz & Malagelada, 1987). Ultrasound and scintintigraphic imaging methods, however, measure the physical size of the proximal stomach, which can only be used to infer movements of contraction and relaxation of the stomach (Hausken & Gilja, 2006). Whilst this information is not directly comparable, both changes in gastric volume, as well as the contraction and relaxation of the stomach provide valuable information about disordered motility (Hausken & Gilja, 2006).

Ultrasonographic imaging of the fundus has largely been used in the research setting while clinical applications of this type of imaging remain to be explored. Patients with functional dyspepsia and diabetes studied with ultrasound have demonstrated reduced proximal stomach accommodation (Gilja *et al.*, 1996b; Undeland *et al.*, 1998) when compared to healthy subjects. In patients with functional dyspepsia, glyceryl trinitrate (an exogenous donor of NO, a key neurotransmitter in mediating the relaxation of the smooth muscle of the stomach), administered sublingually has been shown to improve the accommodation of the proximal stomach, as measured by ultrasound, and reduce the postprandial symptoms associated with this condition (Gilja *et al.*, 1997b). In patients with reflux esophagitis, the area of the fundus has been shown to be significantly greater after a meal when compared to healthy controls, and these patients experienced greater epigastric fullness (Tefera *et al.*, 2001; Tefera *et al.*, 2002).

5. 2D assessment of gastric emptying

Scintigraphy is currently the 'gold standard' for clinical measurement of gastric emptying (Collins *et al.*, 1983; Collins *et al.*, 1991); however, it requires access to expensive equipment and carries a radiation burden to the patient and operator. Other techniques involve the use of an orogastric catheter, which is invasive and associated with a high degree of discomfort (Sheiner, 1975), or stable radioisotopes such as C^{14}-octanoic acid, which are not as readily available as ultrasound and requires specialised equipment to analyse (Vantrappen, 1994). Ultrasonography of the stomach has the ability to overcome these disadvantages. It provides an indirect measurement of gastric emptying by quantifying changes in antral area over time (Holt *et al.*, 1980; Bolondi *et al.*, 1985; Holt *et al.*, 1986).

The skills to acquire 2D ultrasound images are relatively easy to learn from an experienced operator. To optimise measurement, the subject should remain seated in approximately the same position for the duration of the examination, and ultrasound images of antral area should be taken at consistent times through the respiration cycle (Jones *et al.*, 1997). A variety of both liquid and semi-solid test meals, including low-nutrient beef soup, beans, pasta, orange juice and dextrose (Holt *et al.*, 1980; Bolondi *et al.*, 1985; Holt *et al.*, 1986; Brown

et al., 1993; Benini *et al.*, 1994; Hveem *et al.*, 1996) have been used to assess gastric emptying. The rate of gastric emptying, or gastric emptying half time (T50), defined as the time it takes for 50% of a given meal to empty from the stomach, can be calculated (Collins *et al.*, 1983) and the retention of a meal, expressed as a percentage of the total meal, at any given time, is defined as in equation (1) below.

$$\text{Retention } (\%) = \frac{AA(t) - AA(f)}{AA(max) - AA(f)} x100 \quad (1)$$

Where AA(t) is the antral area measured at any given time point, AA(f) is the fasting antral area and AA(max) is the maximum antral area recorded after drink ingestion (Hveem *et al.*, 1996).

Ultrasonographic assessment of gastric emptying has been validated against scintigraphy. Studies comparing emptying of a low nutrient beef soup (Holt *et al.*, 1986) and high nutrient dextrose drink (Hveem *et al.*, 1996; Jones *et al.*, 1997) demonstrate good correlation and agreement between techniques (Figure 3).

Studies using 2D ultrasonography in the research setting are particularly attractive as several measurements can be taken over a given time frame or in a single exam. Research studies have shown an overall delayed rate of gastric emptying in functional dyspepsia, with occasional, more rapid initial emptying (Lunding *et al.*, 2006) and an overall delayed rate of gastric emptying in patients with longstanding type 1 (Darwiche *et al.*, 1999) and type 2 (Bian *et al.*, 2011) diabetes.

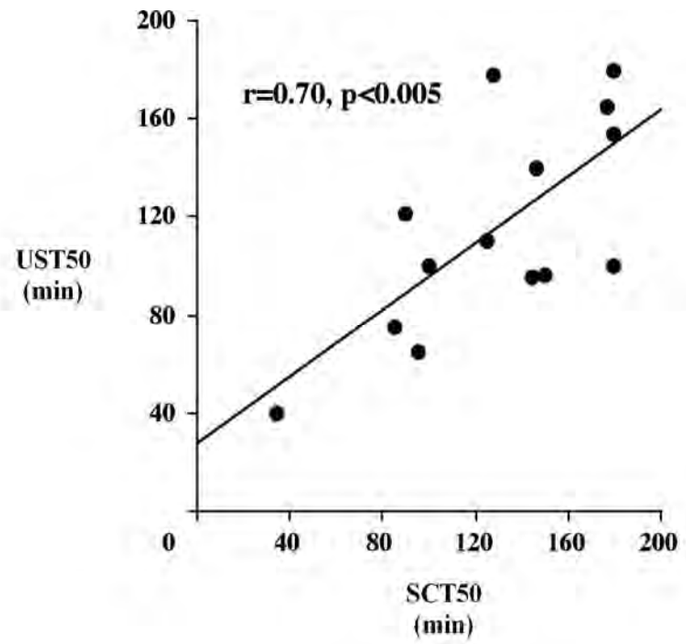

Fig. 3. Relationship between the gastric emptying half times (T50) of a high-nutrient dextrose drink (75g dextrose dissolved in 350mL water) as measured by 2D ultrasound and scintigraphy (n=14 healthy, young volunteers). (Am. J. Clin. Nutr. (1997;66:127-32), American Society for Nutrition).

Despite numerous advantages, 2D ultrasonographic assessment of gastric emptying is associated with some limitations. It is not a direct measure of gastric emptying but rather an assessment of changes in antral area (Holt *et al.*, 1980; Bolondi *et al.*, 1985; Holt *et al.*, 1986). Additionally, it does not take into account the full geometrical shape or distribution of the contents of the stomach (Gilja *et al.*, 2005).

6. 3D assessment of gastric emptying

Initially, assessment of gastric emptying with ultrasound was limited to the abovementioned 2D technique; however, 3D examinations of the stomach, including the emptying and distribution of its contents, have been developed with the increasing availability of suitable technology (Gilja *et al.*, 2005).

The concept was originally pioneered in the 1980s (Snyder *et al.*, 1986), and further developed by the Bergen group in Norway. 3D volume estimation of organs by ultrasound was originally only possible with a transducer mechanically tilted through 90° with a motor device whilst scanning continuously, with the ultrasonographic data transferred to a separate workstation for 3D reconstruction and processing (Hausken *et al.*, 1994; Gilja *et al.*, 1996a; Thune *et al.*, 1996; Gilja *et al.*, 1998). Obviously limited by the pre-determined scanning range and position of the sensor, a magnetometer based position and orientation measurement (POM) device was developed (Detmer *et al.*, 1994) providing precision mapping of points in space (Detmer *et al.*, 1994) and was validated as an accurate method of volume estimation (Hodges *et al.*, 1994; Matre *et al.*, 1999).

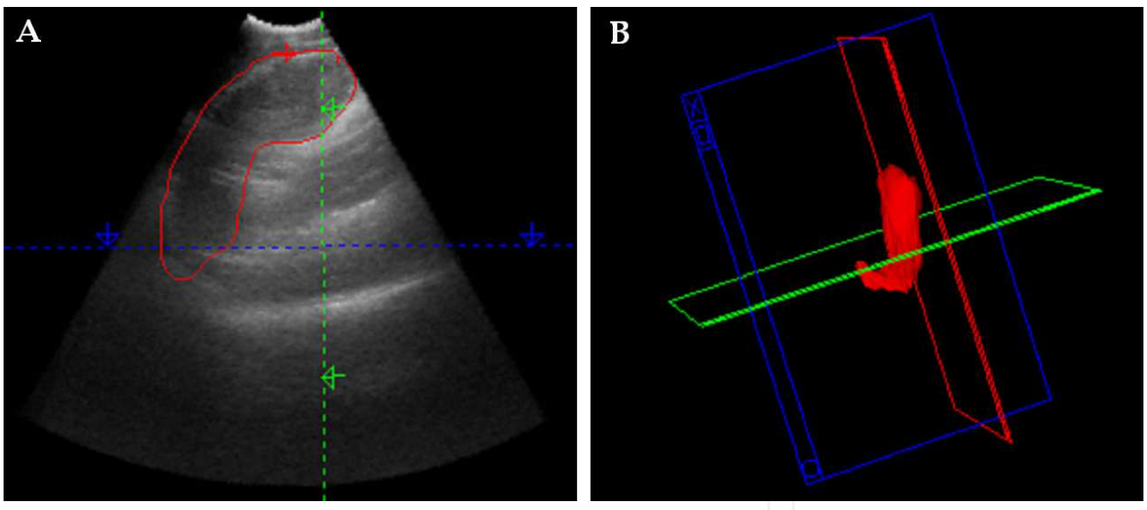

Fig. 4. 3D ultrasound to measure gastric emptying (A) a region of interest drawn around the stomach (B) reconstructed volumetric image of the stomach.

A series of sagittal slices are acquired with a continuous sweeping motion towards the midline, beginning with the transducer at the left subcostal margin, tilted cranially, to image the most proximal part of the stomach, through to the distal stomach and ceasing at the gastro-duodenal junction (Gilja *et al.*, 1997a; Gilja *et al.*, 2005). The resulting images can be analysed with specialised software (EchoPAC-3D) to provide 3D reconstruction and volume estimation (Martens *et al.*, 1997) (Figure 4), this software also enables intragastric distribution to be studied by dividing the stomach into proximal and/or distal volumes (Gilja *et al.*, 1997a).

Currently, 3D ultrasound to measure gastric emptying is restricted to work in the research setting. This method has been applied to stomach volumes and validated against scintigraphy in both the healthy elderly (Gentilcore *et al.*, 2006) and in patients with diabetic gastroparesis (Stevens *et al.*, 2011) (Figure 5 and 6).

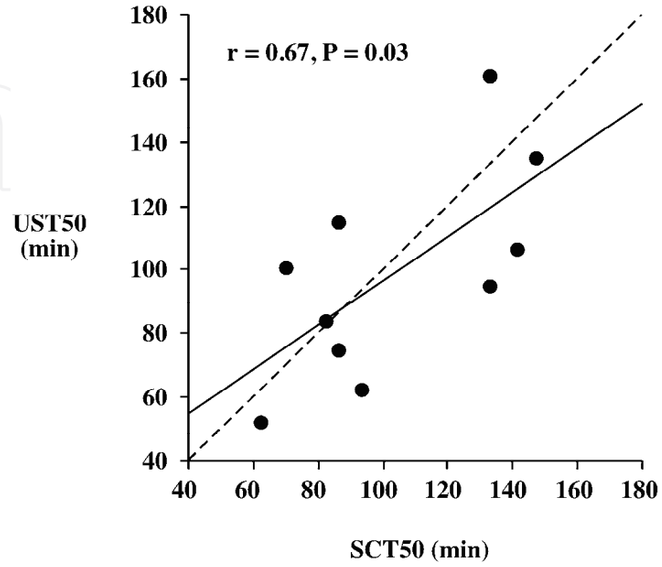

Fig. 5. Relationship between the gastric emptying half times ($T_{1/2}$) of a high-nutrient dextrose drink (75g dextrose dissolved in 300mL water) as measured by 3D ultrasound and scintigraphy (n=10 diabetic patients with gastroparesis). (Neurogastroenterol Motil (2011;23:220-e114)).

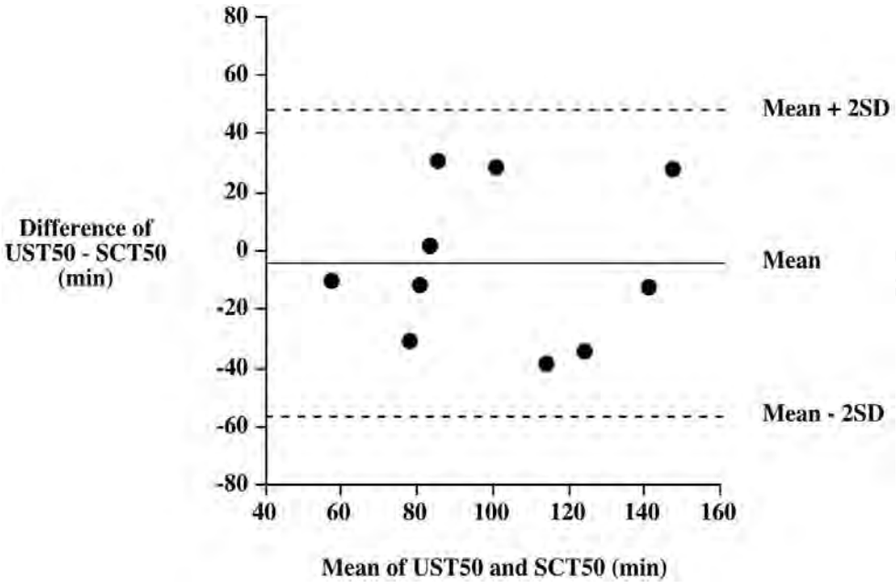

Fig. 6. Limits of agreement for scintigraphic (SCT50) and 3D ultrasonographic (UST50) 50 % emptying times (T50s) for the drink (75 g dextrose in 300 mL water) (n=10 diabetic patients with gastroparesis). (Neurogastroenterol Motil (2011;23:220-e114)).

3D ultrasound has also been shown to have higher accuracy and less variability than 2D ultrasound of the stomach (Gilja *et al.*, 1997a) and in a study with a fluid-filled barostat bag, has correlated well with true stomach volumes with low inter-observer variation (Tefera *et al.*, 2002).

3D ultrasound is limited by the complexities of scanning technique and technological availability. Additionally, difficulties in imaging due to the presence of intragastric gas may limit accuracy.

7. Measurement of antropyloroduoenal motility

Gastric emptying in humans is predominantly a pulsatile phenomenon in which the contents of the stomach move across the pylorus in response to either a local increase in the pressure between the antrum and duodenum caused by an increase in local antropyloric pressure waves (i.e., peristaltic flow), or non-peristaltic flow caused by differences in pressure between the distal antrum and duodenum (Berstad *et al.*, 1994; Gilja *et al.*, 2007).

Much information about gastric emptying can be obtained by evaluating the physical contractions of the antropylorodudodenal region. While manometric apparatus have been traditionally used to assess antropyloric pressure changes during these events, the technique is limited to assessment of lumen occlusive contractions (Gilja *et al.*, 2007). Following ingestion of a low nutrient soup with simultaneous ultrasound, approximately 45% of pyloric contractions which were visible on ultrasound images were not correlated to manometric pressure changes (Hveem *et al.*, 2001; Hausken *et al.*, 2002). While providing more comprehensive information about the timing and magnitude of antropyloric pressure contractions, ultrasound has the added benefit of also providing visual information about the movement of gastric contents across the pylorus in relation to individual peristaltic contractions (King *et al.*, 1984; Hausken *et al.*, 1992). Additionally, intubation with a manometric catheter is invasive, associated with significant patient discomfort, and is not always practical.

Ultrasongraphic measurement of antropylorodudodenal contractions, whilst beneficial in that it overcomes the limitations of manometry, is restricted in that it requires a well trained operator. Currently, use is restricted to the research setting (Gilja *et al.*, 2007).

8. Measurement of transpyloric flow

Ultrasonography can be used to both quantify and qualify the movement of the contents of the stomach across the pylorus, into the duodenum. This normal movement of the stomach contents into the duodenum is normally followed by a short period of duodenogastric reflux immediately prior to the closing of the pylorus (Berstad *et al.*, 1994; Hausken *et al.*, 2001; Gilja *et al.*, 2007).

Transpyloric imaging employs duplex ultrasonography (simultaneous Doppler and B-mode imaging) of the pylorus enabling the motion and velocity of gastric contents to be assessed (Hausken *et al.*, 1992; Berstad *et al.*, 1994; Hausken *et al.*, 1998a). Gastric emptying is said to occur when there is flow across the pylorus with a mean velocity of 10 cm/s or more, lasting for at least one second (Gilja *et al.*, 2007). Contraction of the antrum occurs when there is visible movement of the antral wall which propagates with time and is not caused by pulsation of nearby vessels or the adjacent intestine, or by respiration (Gilja *et al.*, 2007).

A technique involving 3D ultrasonography of transpyloric flow has been developed by Hausken et al. to assess flow during the abovementioned duodenogastric reflux period. This technique enables quantification of duodenogastric stroke volume (Hausken *et al.*, 2001). High intra and inter individual correlations of stroke volume have been shown (Hausken *et al.*, 2001).

Whilst there are substantial operational and technical demands of this type of ultrasound, the significant insight into the normal physiological movements involved in digestion it provides has proven invaluable in the research setting (King *et al.*, 1984; Hausken & Berstad, 1992; Hausken *et al.*, 1998a; Jones *et al.*, 2006). Transpyloric flow has been shown to be greater in a sitting position, compared to a supine position, with no effect on the overall emptying of a standardised drink consisting of 600mL of water and 75g of glucose (Jones *et al.*, 2006). Measurements of transpyloric flow have been shown to be decreased, along with the overall rate of gastric emptying, in older, when compared with young, subjects (O'Donovan *et al.*, 2005). In studies of patients with type 2 diabetes, with and without autonomic neuropathy, reduced transpyloric flow was shown (Kawagishi *et al.*, 1994). Additionally, altered movement of the contents of the stomach across the pylorus may be responsible for postprandial symptoms in patients with functional dyspepsia (Hausken *et al.*, 1998b).

9. Gastric strain rate imaging

The deformation of the gastric wall due to mechanical stress (strain) can be imaged with B-mode ultrasonography (Gilja *et al.*, 2002). Gastric strain is of interest for a number of reasons; mechanoreceptors respond to changes in stress in a muscular wall, not changes in pressure or volume so it allows these direct effects to be studied, it provides information on the elastic properties of the muscular walls of the stomach, it can differentiate phasic motions from passive changes in muscle tone (which is of particular importance in a research setting) and it allows the normal geometry of the stomach to be maintained while assessing these parameters (Gregersen *et al.*, 2002).

Gastric strain rate imaging (SRI) involves the recording of tissue velocity to obtain strain, and the strain rate is defined by the gradient of the velocity component of two points along the ultrasound beam (Gilja *et al.*, 2007; Ahmed *et al.*, 2009). SRI is able to distinguish between contraction of the circular and longitudinal muscle layers, even when not distinctly visible on the 2D ultrasound image (Gilja *et al.*, 2002).

Technically, continuous imaging is necessary and a small sample size (~2 mm) should be selected (Gilja *et al.*, 2007; Ahmed *et al.*, 2009). Cine imaging should be acquired over the antral lumen whenever a change in luminal cross-section or antral circularity is observed (Gilja *et al.*, 2007; Ahmed *et al.*, 2009).

SRI has been validated *in vivo* with a silicone phantom to mimic moving tissue (Matre *et al.*, 2003) and in an *in vitro* porcine model (Ahmed *et al.*, 2006). In a study involving the artificial distension of the antrum with a barostat device, there was a significant inverse correlation between balloon pressure and gastric strain (Gilja *et al.*, 2002).

The use of SRI has been applied in patients with functional dyspepsia (Ahmed *et al.*, 2008), and in these patients, divided into subgroups of 'epigastric pain syndrome' (EPS) and

'postprandial distress syndrome' (PDS), antral strain was shown to be higher in EPS patients, compared with PDS patients and normal controls, both in the fasting and postprandial state (Ahmed *et al.*, 2008; Ahmed *et al.*, 2009).

Due to the relatively novel nature of this type of imaging, and the requirement for a well trained operator, SRI imaging is still largely reserved for the research setting. Further studies would be required to assess potential clinical applications for this type of imaging.

10. Conclusion

Ultrasonography remains a safe and effective means by which the structure and function of the stomach can be assessed in an accurate and reproducible manner. Ultrasonography offers several advantages over other imaging modalities in that it is easy to perform, readily accessible, cheap and not associated with a radiation burden.

The techniques described in this chapter have been applied in a meaningful way in either the clinical or research setting, or in some cases, both. 2D ultrasonography of the stomach stands out as a simple and well-validated means by which antral area, proximal stomach accommodation and gastric emptying can be assessed, whereas 3D ultrasonography offers added information about the physiology of the stomach. New techniques involving the imaging of the flow of the stomach contents across the pylorus, motility of the pylorus, and the mechanical stress placed on the gastric wall, continue to be developed.

It should be recognised that for these techniques to be effective, they require the hand of a skilled, well trained operator, and are only applicable in situations where there is relevance or interest in the added information that ultrasonography of the stomach has to offer. Whilst at this time, this is often limited to the research setting, as these techniques are more widely adopted, clinical use will become more widespread.

Provided the limitations of each ultrasonographic technique discussed in this chapter are observed, ultrasound has the ability to provide significant anatomical and physiological information about the stomach and its contents in both the clinical and research setting.

11. References

Ahmed AB, Gilja OH, Gregersen H, Odegaard S & Matre K. (2006). In vitro strain measurement in the porcine antrum using ultrasound doppler strain rate imaging. *Ultrasound Med Biol* 32, 513-522.

Ahmed AB, Gilja OH, Hausken T, Gregersen H & Matre K. (2009). Strain measurement during antral contractions by ultrasound strain rate imaging: influence of erythromycin. *Neurogastroenterol Motil* 21, 170-179.

Ahmed AB, Matre K, Hausken T, Gregersen H & Gilja OH. (2008). T1326 ROME III Subgroups of Functional Dyspepsia Exhibit Different Characteristics of Antral Strain Measured By Strain Rate Imaging. *Gastroenterology* 134, A-531.

Azpiroz F & Malagelada JR. (1987). Gastric tone measured by an electronic barostat in health and postsurgical gastroparesis. *Gastroenterology* 92, 934-943.

Benini L, Brighenti F, Castellani G, Brentegani MT, Casiraghi MC, Ruzzenente O, Sembenini C, Pellegrini N, Caliari S, Porrini M & et al. (1994). Gastric emptying of solids is markedly delayed when meals are fried. *Dig Dis Sci* 39, 2288-2294.

Berstad A, Hausken T, Gilja OH, Thune N, Matre K & Odegaard S. (1994). Volume measurements of gastric antrum by 3-D ultrasonography and flow measurements through the pylorus by duplex technique. *Dig Dis Sci* 39, 97S-100S.

Bian RW, Lou QL, Gu LB, Kong AP, So WY, Ko GT, Ouyang XJ, Mo YZ, Ma RC, Chan JC & Chow CC. (2011). Delayed gastric emptying is related to cardiovascular autonomic neuropathy in Chinese patients with type 2 diabetes. *Acta Gastroenterol Belg* 74, 28-33.

Bolondi L, Bortolotti M, Santi V, Calletti T, Gaiani S & Labo G. (1985). Measurement of gastric emptying time by real-time ultrasonography. *Gastroenterology* 89, 752-759.

Bouvet L, Miquel A, Chassard D, Boselli E, Allaouchiche B & Benhamou D. (2009). Could a single standardized ultrasonographic measurement of antral area be of interest for assessing gastric contents? A preliminary report. *Eur J Anaesthesiol* 26, 1015-1019.

Brown BP, Schulze-Delrieu K, Schrier JE & Abu-Yousef MM. (1993). The configuration of the human gastroduodenal junction in the separate emptying of liquids and solids. *Gastroenterology* 105, 433-440.

Collins PJ, Horowitz M, Cook DJ, Harding PE & Shearman DJ. (1983). Gastric emptying in normal subjects--a reproducible technique using a single scintillation camera and computer system. *Gut* 24, 1117-1125.

Collins PJ, Houghton LA, Read NW, Horowitz M, Chatterton BE, Heddle R & Dent J. (1991). Role of the proximal and distal stomach in mixed solid and liquid meal emptying. *Gut* 32, 615-619.

Darwiche G, Almer LO, Bjorgell O, Cederholm C & Nilsson P. (1999). Measurement of gastric emptying by standardized real-time ultrasonography in healthy subjects and diabetic patients. *J Ultrasound Med* 18, 673-682.

De Schepper HU, Cremonini F, Chitkara D & Camilleri M. (2004). Assessment of gastric accommodation: overview and evaluation of current methods. *Neurogastroenterol Motil* 16, 275-285.

Detmer PR, Bashein G, Hodges T, Beach KW, Filer EP, Burns DH & Strandness DE, Jr. (1994). 3D ultrasonic image feature localization based on magnetic scanhead tracking: in vitro calibration and validation. *Ultrasound Med Biol* 20, 923-936.

Folvik G, Bjerke-Larssen T, Odegaard S, Hausken T, Gilja OH & Berstad A. (1999). Hydrosonography of the small intestine: comparison with radiologic barium study. *Scand J Gastroenterol* 34, 1247-1252.

Gentilcore D, Hausken T, Horowitz M & Jones KL. (2006). Measurements of gastric emptying of low- and high-nutrient liquids using 3D ultrasonography and scintigraphy in healthy subjects. *Neurogastroenterol Motil* 18, 1062-1068.

Gilja OH, Detmer PR, Jong JM, Leotta DF, Li XN, Beach KW, Martin R & Strandness DE, Jr. (1997a). Intragastric distribution and gastric emptying assessed by three-dimensional ultrasonography. *Gastroenterology* 113, 38-49.

Gilja OH, Hatlebakk JG, Odegaard S, Berstad A, Viola I, Giertsen C, Hausken T & Gregersen H. (2007). Advanced imaging and visualization in gastrointestinal disorders. *World J Gastroenterol* 13, 1408-1421.

Gilja OH, Hausken T, Bang CJ & Berstad A. (1997b). Effect of glyceryl trinitrate on gastric accommodation and symptoms in functional dyspepsia. *Dig Dis Sci* 42, 2124-2131.

Gilja OH, Hausken T, Odegaard S & Berstad A. (1995). Monitoring postprandial size of the proximal stomach by ultrasonography. *J Ultrasound Med* 14, 81-89.

Gilja OH, Hausken T, Odegaard S & Berstad A. (1996a). Three-dimensional ultrasonography of the gastric antrum in patients with functional dyspepsia. *Scand J Gastroenterol* 31, 847-855.

Gilja OH, Hausken T, Odegaard S & Berstad A. (2005). Ultrasonography and three-dimensional methods of the upper gastrointestinal tract. *Eur J Gastroenterol Hepatol* 17, 277-282.

Gilja OH, Hausken T, Olafsson S, Matre K & Odegaard S. (1998). In vitro evaluation of three-dimensional ultrasonography based on magnetic scanhead tracking. *Ultrasound Med Biol* 24, 1161-1167.

Gilja OH, Hausken T, Wilhelmsen I & Berstad A. (1996b). Impaired accommodation of proximal stomach to a meal in functional dyspepsia. *Dig Dis Sci* 41, 689-696.

Gilja OH, Heimdal A, Hausken T, Gregersen H, Matre K, Berstad A & Odegaard S. (2002). Strain during gastric contractions can be measured using Doppler ultrasonography. *Ultrasound Med Biol* 28, 1457-1465.

Gregersen H, Gilja OH, Hausken T, Heimdal A, Gao C, Matre K, Odegaard S & Berstad A. (2002). Mechanical properties in the human gastric antrum using B-mode ultrasonography and antral distension. *Am J Physiol Gastrointest Liver Physiol* 283, G368-375.

Hausken T & Berstad A. (1992). Wide gastric antrum in patients with non-ulcer dyspepsia. Effect of cisapride. *Scand J Gastroenterol* 27, 427-432.

Hausken T & Gilja OH. (2006). Functional Ultrasound of the Gastrointestinal Tract. *Ultrasound of the Gastrointestinal Tract* Springer.

Hausken T, Gilja OH, Odegaard S & Berstad A. (1998a). Flow across the human pylorus soon after ingestion of food, studied with duplex sonography. Effect of glyceryl trinitrate. *Scand J Gastroenterol* 33, 484-490.

Hausken T, Gilja OH, Undeland KA & Berstad A. (1998b). Timing of postprandial dyspeptic symptoms and transpyloric passage of gastric contents. *Scand J Gastroenterol* 33, 822-827.

Hausken T, Li XN, Goldman B, Leotta D, Odegaard S & Martin RW. (2001). Quantification of gastric emptying and duodenogastric reflux stroke volumes using three-dimensional guided digital color Doppler imaging. *Eur J Ultrasound* 13, 205-213.

Hausken T, Mundt M & Samsom M. (2002). Low antroduodenal pressure gradients are responsible for gastric emptying of a low-caloric liquid meal in humans. *Neurogastroenterol Motil* 14, 97-105.

Hausken T, Odegaard S, Matre K & Berstad A. (1992). Antroduodenal motility and movements of luminal contents studied by duplex sonography. *Gastroenterology* 102, 1583-1590.

Hausken T, Thune N, Matre K, Gilja OH, ØDegaard S & Berstad A. (1994). Volume estimation of the gastric antrum and the gallbladder in patients with non-ulcer dyspepsia and erosive prepyloric changes, using three-dimensional ultrasonography. *Neurogastroenterology & Motility* 6, 263-270.

Hodges TC, Detmer PR, Burns DH, Beach KW & Strandness DE, Jr. (1994). Ultrasonic three-dimensional reconstruction: in vitro and in vivo volume and area measurement. *Ultrasound Med Biol* 20, 719-729.

Holt S, Cervantes J, Wilkinson AA & Wallace JH. (1986). Measurement of gastric emptying rate in humans by real-time ultrasound. *Gastroenterology* 90, 918-923.

Holt S, McDicken WN, Anderson T, Stewart IC & Heading RC. (1980). Dynamic imaging of the stomach by real-time ultrasound--a method for the study of gastric motility. *Gut* 21, 597-601.

Hveem K, Jones KL, Chatterton BE & Horowitz M. (1996). Scintigraphic measurement of gastric emptying and ultrasonographic assessment of antral area: relation to appetite. *Gut* 38, 816-821.

Hveem K, Sun WM, Hebbard G, Horowitz M, Doran S & Dent J. (2001). Relationship between ultrasonically detected phasic antral contractions and antral pressure. *Am J Physiol Gastrointest Liver Physiol* 281, G95-101.

Jones KL, Doran SM, Hveem K, Bartholomeusz FD, Morley JE, Sun WM, Chatterton BE & Horowitz M. (1997). Relation between postprandial satiation and antral area in normal subjects. *Am J Clin Nutr* 66, 127-132.

Jones KL, O'Donovan D, Horowitz M, Russo A, Lei Y & Hausken T. (2006). Effects of posture on gastric emptying, transpyloric flow, and hunger after a glucose drink in healthy humans. *Dig Dis Sci* 51, 1331-1338.

Kawagishi T, Nishizawa Y, Okuno Y, Shimada H, Inaba M, Konishi T & Morii H. (1994). Antroduodenal motility and transpyloric fluid movement in patients with diabetes studied using duplex sonography. *Gastroenterology* 107, 403-409.

King PM, Adam RD, Pryde A, McDicken WN & Heading RC. (1984). Relationships of human antroduodenal motility and transpyloric fluid movement: non-invasive observations with real-time ultrasound. *Gut* 25, 1384-1391.

Lunding JA, Tefera S, Gilja OH, Hausken T, Bayati A, Rydholm H, Mattsson H & Berstad A. (2006). Rapid initial gastric emptying and hypersensitivity to gastric filling in functional dyspepsia: effects of duodenal lipids. *Scand J Gastroenterol* 41, 1028-1036.

Martens D, Hausken T, Gilja OH, Steen E, Alker H & Odegaard S. (1997). 3D processing of ultrasound images using a novel EchoPac-3D® software. *Ultrasound Med Biol* 23 (suppl 1), 136.

Matre K, Ahmed AB, Gregersen H, Heimdal A, Hausken T, Odegaard S & Gilja OH. (2003). In vitro evaluation of ultrasound Doppler strain rate imaging: modification for measurement in a slowly moving tissue phantom. *Ultrasound Med Biol* 29, 1725-1734.

Matre K, Stokke EM, Martens D & Gilja OH. (1999). In vitro volume estimation of kidneys using three-dimensional ultrasonography and a position sensor. *Eur J Ultrasound* 10, 65-73.

Moragas G, Azpiroz F, Pavia J & Malagelada JR. (1993). Relations among intragastric pressure, postcibal perception, and gastric emptying. *Am J Physiol* 264, G1112-1117.

Mundt MW, Hausken T & Samsom M. (2002). Effect of intragastric barostat bag on proximal and distal gastric accommodation in response to liquid meal. *Am J Physiol Gastrointest Liver Physiol* 283, G681-686.

Nylund K, Odegaard S, Hausken T, Folvik G, Lied GA, Viola I, Hauser H & Gilja OH. (2009). Sonography of the small intestine. *World J Gastroenterol* 15, 1319-1330.

O'Donovan D, Hausken T, Lei Y, Russo A, Keogh J, Horowitz M & Jones KL. (2005). Effect of aging on transpyloric flow, gastric emptying, and intragastric distribution in healthy humans--impact on glycemia. *Dig Dis Sci* 50, 671-676.

Parys V, Bruley des Varannes S, Ropert A, Roze C & Galmiche JP. (1993). [Use of an electronic barostat for measurement of motor response of the proximal stomach to feeding and different nervous stimuli in man]. *Gastroenterol Clin Biol* 17, 321-328.

Perlas A, Chan VW, Lupu CM, Mitsakakis N & Hanbidge A. (2009). Ultrasound assessment of gastric content and volume. *Anesthesiology* 111, 82-89.

Sheiner HJ. (1975). Gastric emptying tests in man. *Gut* 16, 235-247.

Snyder JE, Kisslo J & von Ramm O. (1986). Real-time orthogonal mode scanning of the heart. I. System design. *J Am Coll Cardiol* 7, 1279-1285.

Stevens JE, Gilja OH, Gentilcore D, Hausken T, Horowitz M & Jones KL. (2011). Measurement of gastric emptying of a high-nutrient liquid by 3D ultrasonography in diabetic gastroparesis. *Neurogastroenterol Motil* 23, 220-225, e113-224.

Sturm K, Parker B, Wishart J, Feinle-Bisset C, Jones KL, Chapman I & Horowitz M. (2004). Energy intake and appetite are related to antral area in healthy young and older subjects. *Am J Clin Nutr* 80, 656-667.

Szarka LA & Camilleri M. (2009). Methods for measurement of gastric motility. *Am J Physiol Gastrointest Liver Physiol* 296, G461-475.

Tarjan Z, Toth G, Gyorke T, Mester A, Karlinger K & Mako EK. (2000). Ultrasound in Crohn's disease of the small bowel. *Eur J Radiol* 35, 176-182.

Tefera S, Gilja OH, Hatlebakk JG & Berstad A. (2001). Gastric accommodation studied by ultrasonography in patients with reflux esophagitis. *Dig Dis Sci* 46, 618-625.

Tefera S, Gilja OH, Olafsdottir E, Hausken T, Hatlebakk JG & Berstad A. (2002). Intragastric maldistribution of a liquid meal in patients with reflux oesophagitis assessed by three dimensional ultrasonography. *Gut* 50, 153-158.

Thune N, Gilja OH, Hausken T & Matre K. (1996). A practical method for estimating enclosed volumes using 3D ultrasound. *European journal of ultrasound : official journal of the European Federation of Societies for Ultrasound in Medicine and Biology* 3, 83-92.

Undeland KA, Hausken T, Gilja OH, Aanderud S & Berstad A. (1998). Gastric meal accommodation studied by ultrasound in diabetes. Relation to vagal tone. *Scand J Gastroenterol* 33, 236-241.

Undeland KA, Hausken T, Svebak S, Aanderud S & Berstad A. (1996). Wide gastric antrum and low vagal tone in patients with diabetes mellitus type 1 compared to patients with functional dyspepsia and healthy individuals. *Dig Dis Sci* 41, 9-16.

van den Elzen BD, Bennink RJ, Wieringa RE, Tytgat GN & Boeckxstaens GE. (2003). Fundic accommodation assessed by SPECT scanning: comparison with the gastric barostat. *Gut* 52, 1548-1554.

Vantrappen G. (1994). Methods to study gastric emptying. *Dig Dis Sci* 39, 91S-94S.

Vasavid P, Chaiwatanarata T & Gonlachanvit S. (2010). The Reproducibility of Tc-Pertechnetate Single Photon Emission Computed Tomography (SPECT) for Measurement of Gastric Accommodation in Healthy Humans: Evaluation of the Test Results Performed at the Same Time and Different Time of the Day. *J Neurogastroenterol Motil* 16, 401-406.

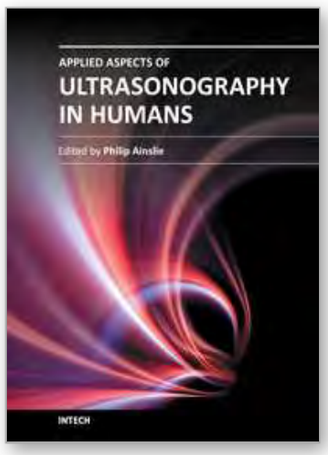

Applied Aspects of Ultrasonography in Humans
Edited by Prof. Philip Ainslie

ISBN 978-953-51-0522-0
Hard cover, 190 pages
Publisher InTech
Published online 25, April, 2012
Published in print edition April, 2012

Written by international experts, this publication provides the reader with the present knowledge and future research directions of diagnostic and therapeutic ultrasound and spectroscopy. Focused topics include Duplex ultrasound, transcranial color Duplex, MRA guided Doppler ultrasonography and near-infrared spectroscopy. New directions in the use and application of transcranial and color Duplex ultrasound are provided, as well as the use of ultrasound and arterial stiffness for measuring human vascular health and circulatory control. Novel use of ultrasound for the detection of intra-cardiac and intra-pulmonary shunts is also described along with its utility for the assessment of gastric regulation and emptying.

INTECH
open science | open minds

InTech Europe
University Campus STeP Ri
Slavka Krautzeka 83/A
51000 Rijeka, Croatia
Phone: +385 (51) 770 447
Fax: +385 (51) 686 166
www.intechopen.com

InTech China
Unit 405, Office Block, Hotel Equatorial Shanghai
No.65, Yan An Road (West), Shanghai, 200040, China
中国上海市延安西路65号上海国际贵都大饭店办公楼405单元
Phone: +86-21-62489820
Fax: +86-21-62489821

IntechOpen

Chapter

Anatomy, Sonographic Features, and Dimensional Variations of Spleen among Individuals with Different Sociodemographic and Anthropometric Measurement

Solomon Demissie, Mulatie Atalay and Yonas Derso

Abstract

The spleen is a vital lymphoid soft organ located in the left hypochondrium region. It is a multi-dimensional organ that enlarges in all dimensions during some disease conditions. Recently, splenomegaly prevalence has been increasing throughout the world. Due to the lack of attention in clinical practice, splenomegaly has become quite a common problem in all parts of the world. The detection of the spleen by palpation is not approval of enlarged spleen because normal spleen may be palpable. A detailed knowledge of morphometric variations of the spleen is of great value in diagnosing splenomegaly clinically, radiologically, and for surgical procedures. Measurement of spleen size by sonography is important as it gives true result than splenic palpation and for identification of disorders present with enlargement or reduction of the spleen. Therefore, this study aimed to assess the anatomy, sonography, and dimensional variation of spleen among individuals with different sociodemographic and anthropometric measurements. The current study reviews different types of literature conducted on spleen all over the world. The result from overall spleen dimensions review shows measurements vary: spleen length (7–14 cm), spleen width (2–7.5 cm), spleen thickness (2–7 cm), and spleen volume (20–350 cm^3). The literature revealed that spleen dimensions are affected by geographical differences, races, nutritional status, physical exercise, and anthropometric measurements. The result from reviews shows that spleen dimensions are larger in males than females. As age increases, spleen dimensions significantly decrease. Spleen dimensions positively correlate with height, weight, body mass index, and body surface of individuals. The spleen dimensions were higher in males than in females and have significant positive correlation with height, weight, body mass index, and body surface area. Clinicians, radiologists, and surgeons should confirm splenomegaly by both palpation and sonography. Spleen dimensions variation due to geographical sex, age, and other anthropometric measurements should be taken into consideration during their clinical investigation. Radiologists should measure all dimensions of spleen rather than the length to rule out splenomegaly correctly.

Keywords: spleen, anatomy, sonography, dimensional variation

1. Introduction

The spleen is the largest lymphoid soft organ that lies in the left hypochondrium between the fundus of the stomach and the diaphragm [1]. Its long axis extends from 9th to 11th ribs on the left side with its long axis running parallel to the 10th rib (**Figure 1**) [2].

The shape of the spleen is ovoid-like pulpy mass about the size + shape of one's fist with a convex outer diaphragmatic surface and an indented inner visceral surface [3]. The diaphragmatic surface of spleen is convex and smooth to fit the concavity of the diaphragm, while the visceral surface is irregular and related to the stomach, left kidney, left suprarenal gland, and left colic flexure [4]. The medial end (apex) lies in line with the spine of 10th thoracic vertebra about 4 cm from the midline, and the lateral end (base) does not descend beyond the midaxillary line [5].

The functions of the spleen are centered on the systemic circulation [6]. It contains two functionally and morphologically distinct compartments: the red pulp and the white pulp. The red pulp functions as a blood filter that removes foreign material and damaged erythrocytes, and the white pulp initiates immune responses to blood-borne antigens (**Figure 2**) [7].

The spleen is involved and enlarged in a variety of clinical conditions. Its size is mostly affected by infections, hematological disorders, infiltrative states, and immunological and malignant diseases [8, 9]. A variety of diseases condition alters spleen dimensions, where splenomegaly and its consequence become a primary clinical concern in developing countries [10]. It is commonly seen in about 63% of patients with pulmonary arterial hypertension [11], infectious mononucleosis [12], malaria [13], lymphoma [14], kala-azar [15], typhoid fever [16], liver disease (hepatitis and cirrhosis) [17], hematological diseases, metabolism diseases, and cancer [18]. The altered splenic dimensions and structure during these diseases result in asymptomatic enlargement and complications such as hematoma formation, rupture, hypersplenism, ectopic spleen, and torsion that affect other adjacent organs [19].

Splenic atrophy is also another common problem seen in diseases like sickle cell anemia, where progressive atrophy as a result of repeated attacks of vaso-occlusion and infarction caused by these diseases leads to auto splenectomy [20].

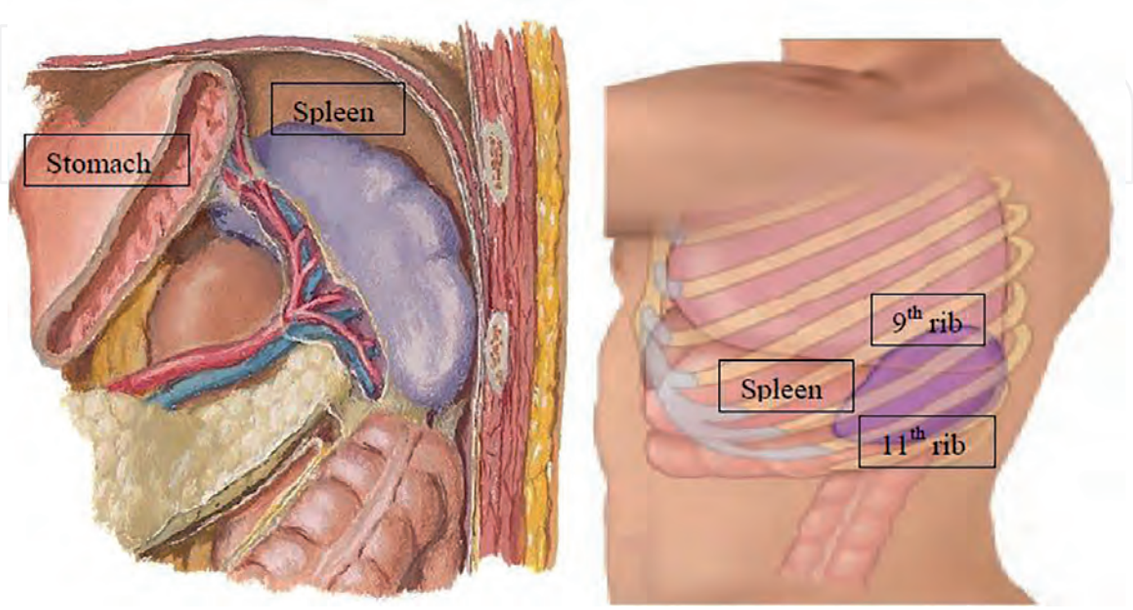

Figure 1.
Spleen anatomical location.

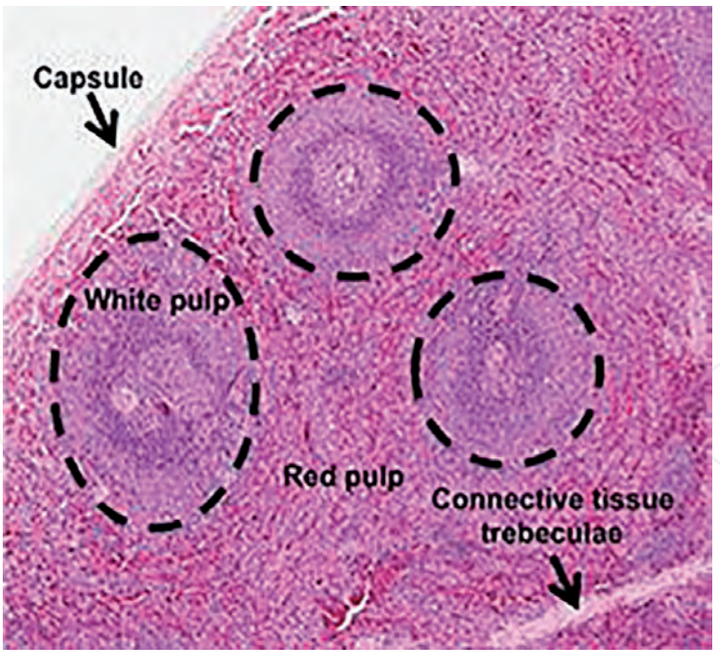

Figure 2.
Spleen histological features.

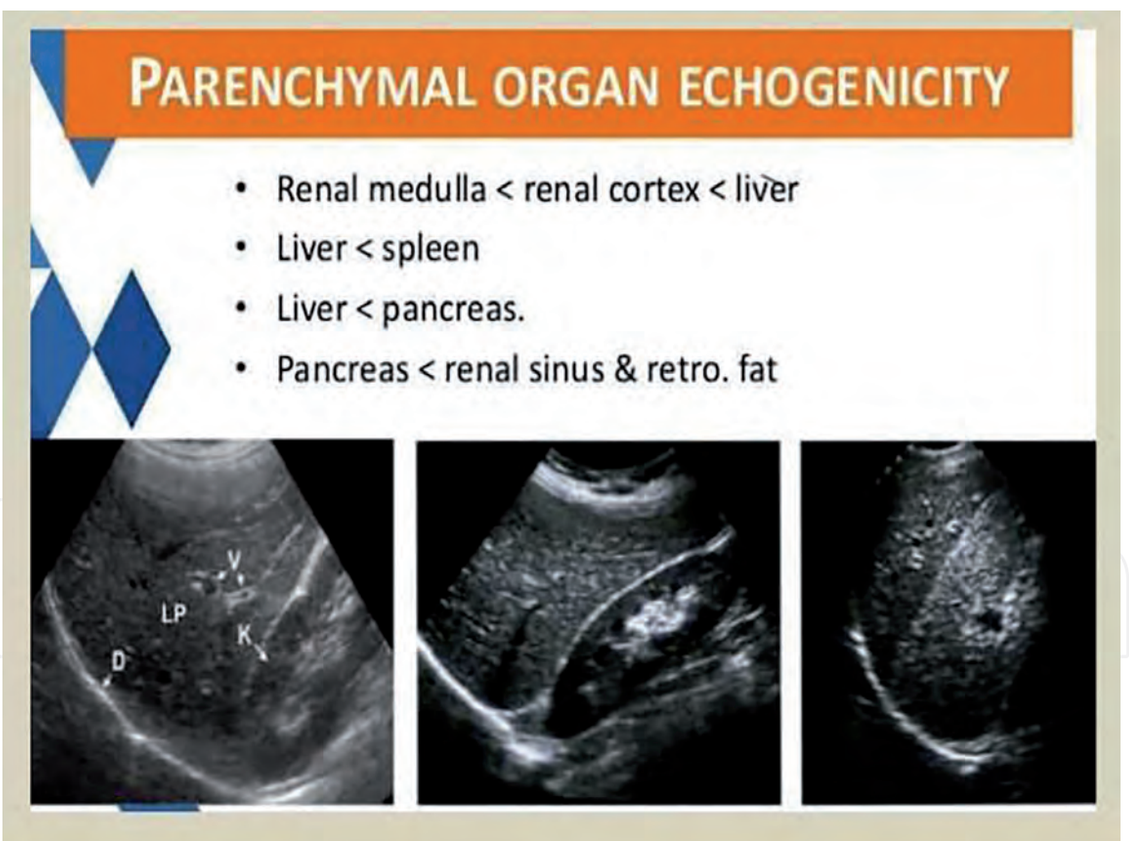

Figure 3.
Spleen sonographic comparison with kidney and liver.

The dimension of the spleen is evaluated using conventional radiography, ultrasonography, scintigraphy, computed tomography, and magnetic resonance imaging [21]. However, ultrasonography is a non-invasive, safe, quick, and accurate method for measurement of spleen size [22]. On sonography spleen is characterized as crescent-shaped with outer convexity is smooth, whereas the inner margin is

indented. Its echo structure is homogeneous and more echogenic than healthy liver tissue and markedly hyperechoic compared to kidney tissue (**Figure 3**) [23].

The average dimensions of the spleen are 12.5 cm, 7.5 cm, and 2.5 cm in length, width, and thickness, respectively, and 150–200 g in weight, but its dimensions vary considerably [20]. The literature revealed that spleen dimensions are affected by geographical differences, races, nutritional status, and anthropometric measurements [21–23]. The following are types of literature reviewed.

2. Literature reviews

2.1 Overall morph metric evaluation of normal dimension of spleen

Average overall dimension of spleen varies from race to race and region to region. The study designed to evaluate splenic size by ultrasonography (US) of healthy Turkish men found the average splenic length to be 10.76 (±1.84) cm [24]. Study conducted in Istanbul Turkey found that the mean spleen volume (SV), splenic length (SL), width (SW), and thickness (ST) were 198 (±88) cm^3, 9.96 (±2.1) cm, 8.87 (±1.6) cm, and 4.58 (±0.8) cm, respectively [25]. In another study conducted on North Indian adult population, splenic dimensions were 10.67 (±1.62) cm in length, 6.26 (±1.66) cm in width, and 4.86 (±1.22) cm in thickness [26]. Recent study conducted in North West Ethiopia also found that the mean dimensions of spleen, the mean splenic length, width, thickness, and volume with (±SD), were 9.95 cm (±1.12), 4.3 cm (±0.7), 3.8 cm (±0.8), and 92.0(±38.4) cm^3, respectively [27].

2.2 Normal spleen dimensions in correlation with sex

Different literature states that spleen dimension varies in relation to sex, with more studies indicating that males have larger spleen dimensions than females. Ultrasound assessment of spleen size in collegiate athletes conducted in Kentucky, USA, shows that spleen length and width (cm) 9.91 (±1.27) cm, 4.74 (±0.91) cm and 11.29 (±1.49) cm, 5.54 (±1.28) cm in female and male, respectively. The study concludes that men have larger spleen size than females [28].

In a study conducted on Saudi Arabian adult, the average splenic volume of males was 196.95 (±48.70) cm^3 and that of females was 196.95 (±26.97) cm^3. The study concludes that a significant difference was found between sex [29].

In a study conducted on sonological evaluation of the spleen in an adult Southern Nigerian population, lengths of the spleen were 9.62 (±1) cm and 9.12 (±1.22) cm for the males and females, respectively. A significant difference ($p < 0.05$) was found between the sex, and it is significantly larger in the males [30].

Measurement of normal spleen dimensions in adult Sudanese using ultrasonography revealed that the mean values of spleen length, width, thickness, and volume were 10.3 (±1.2), 3.3 (±0.4), 3.9 (±0.6), and 73.3 (±23) respectively for males and 9.2 (±0.9), 3.1 (±0.3), 3.6 (±0.6), and 56.5 (±18.0) respectively for female. The study concludes that men have larger spleens than females in relation of spleens to sex [31].

2.3 Normal spleen dimensions in correlation with age

The study conducted in Pakistan to determine the normal spleen parameters in adults shows that the mean spleen sizes of the participants were 9.81 ± 1.73 cm, and a significant positive correlation was observed between age and spleen size of the individuals ($r = 0.053$, $p = 0.012$) [32].

The splenic dimension study conducted in Western Nepal revealed that in age groups of 16–30, 31–45, 46–60, and 61–75 years, respectively, revealed that spleen length for males (10.07 ± 0.7 cm, 10.1 ± 0.54 cm, 9.5 ± 0.7 cm, and 9.0 ± 0.43 cm, respectively) and for the females (9.83 ± 0.53 cm, 9.58 ± 0.58 cm, 9.2 ± 0.64 cm, and 8.8 ± 0.36 cm, respectively). The spleen thickness for males (4.1 ± 0.5 cm, 4.05 ± 0.58 cm, 3.43 ± 0.38 cm, and 3.0 ± 0.36 cm, respectively) and for the females (4.06 ± 0.47 cm, 3.78 ± 0.48 cm, 3.38 ± 0.35 cm, and 2.29 ± 0.23 cm, respectively). The results show that the splenic length and thickness decreased with increase in age in both males and females [33].

In a study conducted on adults of Tripura, India, with age groups of (15–30 years), (31–45 years), (46–60 years), (61–75 years), and (>75 years), the spleen lengths were 9.00 ± 1.07 cm, 8.79 ± 1.44, 9.15 ± 1.04, 8.63 ± 1.55, and 7.64 ± 1.06 cm, respectively. Correlation analysis showed that spleen length was negatively correlated with age in all adults. So, with increasing age, spleen length was found to be decreasing, which is significant ($p < 0.05$) [34].

A study conducted to establish the normal range of the splenic dimensions in North Indian adult population revealed that the splenic length, width, and thickness decreased with increase in age in both males and females. The results show that in both males and females, the splenic length decreased at a slow rate up to the age of 50 years, after which it decreased rapidly; the splenic width decreased with age up to 30 years; thereafter, it remained relatively constant up to the age of 50 years and after that the splenic width decreased. It also shows that in both males and females, splenic thickness was constant up to the age of 50 years, after which there was a fall in the splenic thickness [35].

The studies from Rajasthan, India, revealed that the length was 8.69 ± 0.93 cm in adults and 9.64 ± 0.64 cm in older subjects. The width was 3.59 ± 0.55 cm in adults, while in older subjects, the width was 3.38 ± 0.38 cm [36].

2.4 Normal spleen dimensions in correlation with height, weight, BSA, and BMI

In a study conducted in Saudi in Jordanian population, ultra-sonographic assessment of splenic volume revealed that splenic dimensions were 10.72 ± 1.37 cm in length, 7.40 ± 1.52 cm in width, 4.40 ± 1.47 cm in depth, and 184.15 ± 79.56 cm^3 in volume. Moderate positive linear relationships were found between the splenic dimension and body height, weight, BSA, and BMI ($r > 0.3$). This correlation was statistically significant ($p < 0.0001$) [37].

Study conducted in the United States revealed that spleen length and volume were associated with body height in which body height alone accounted for 17.3% of spleen length variability and 14.9% of spleen volume variability [38].

Sonographic evaluation of spleen size in athletes conducted in Canada revealed that the mean splenic dimensions were 11.4 ± 1.7 cm length (range, 8.2–16.1 cm), 10.8 ± 1.4 cm width (range, 8–14 cm), 5.0 ± 0.8 cm in thickness, and 333.6 ± 116.1 cm^2 in volume. All splenic measurements correlated better with height than weight [39].

Assessment of dimensions of spleen in normal adult Kashmiri population revealed that the mean length of the spleen was 10.20 + 1.40 cm and the width was 8.63 + 1.57 cm. The study found a statistically significant correlation of splenic dimensions with body weight and BMI [40].

3. Dimensional measurement on sonography

The dimension of spleen is measured as follows.

Spleen length: the maximum distance measured in longitudinal plane at hilum between the dome of the spleen and the splenic tip.

Apparently healthy individual: individuals with no signs and symptoms of disease.

Spleen width: the maximum dimension measured in a plane perpendicular to the length at hilum between the medial and lateral borders of the spleen.

Spleen thickness: the maximum AP dimension measured on the transverse section.

Spleen volume: calculated using the standard ellipsoid formula (length × width × depth × 0.523); this formula is frequently used for estimating the volume of many irregularly shaped organs (**Figures 4–6**) [41].

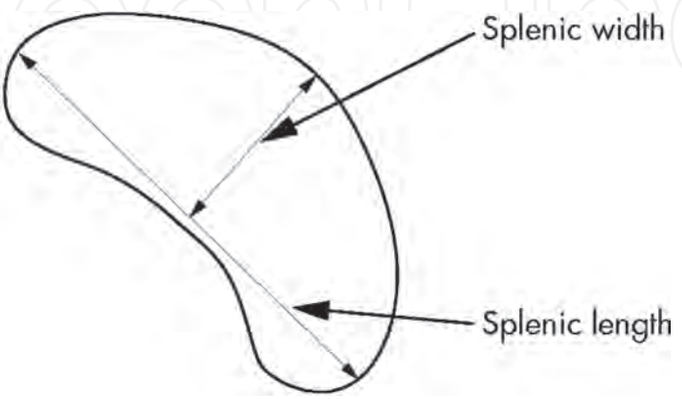

Figure 4.
Spleen length and width measurement.

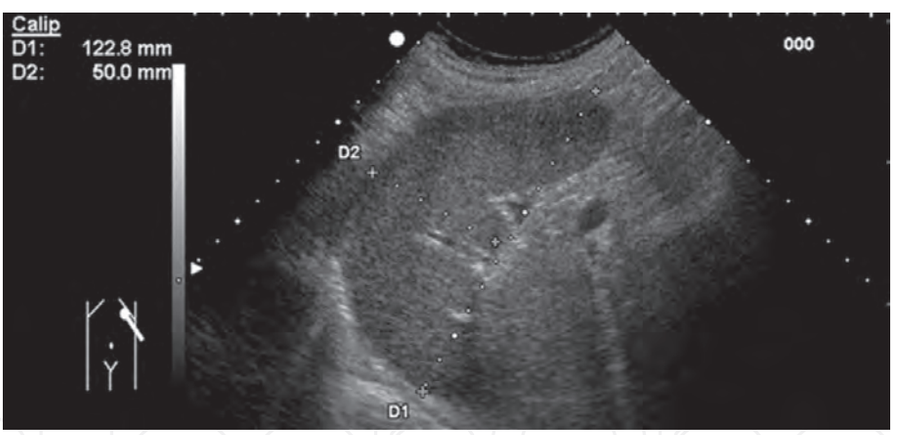

Figure 5.
Spleen sonographic length and width measurement.

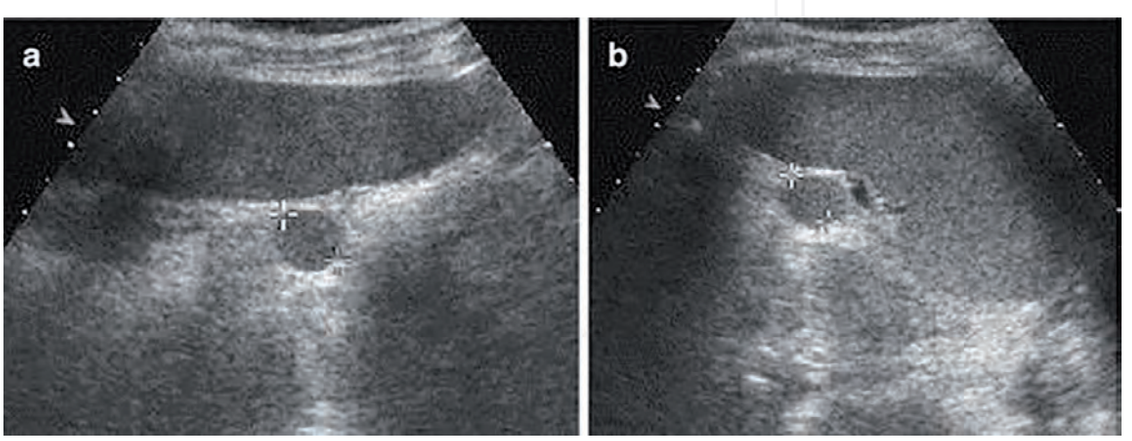

Figure 6.
Spleen thickness sonographic measurement.

4. Discussion

This study describes the morphometry of spleen dimensions and compares the presence of a significant difference between sex and age as well as dimensional correlations with anthropometric measurements. The sonography assessment of spleen dimensions provides essential inputs for clinicians in daily clinical practice for the proper diagnosis of splenomegaly [33, 35, 42]. This study provides estimates of spleen to help radiologists for the diagnosis of diseases related to splenomegaly and atrophy, also used by hematologists and immunologists for the diagnosis of various gastrointestinal and hematological diseases, in addition to forensic studies [43–45].

The result from overall spleen dimensions review shows that measurements vary as follows: spleen length (7–14 cm), spleen width (2–7.5 cm), spleen thickness (2–7 cm), and spleen volume (20–350 cm^3). The average dimensional difference between studies is probably due to age group differences, geographical differences, nutritional status, physical exercise, and race differences, which were stated in different literature [25, 42, 45–48].

In most of studies reviewed, the spleen dimensions were lower in females than males. This is due to histological and genetic differences of spleens between males and females. On histological studies, females have fewer total red cell mass, when compared to males [38, 49]. Studies conducted in Turkey, Saudi, Nigeria, Sudan, and Ethiopia support this idea [30, 31, 45, 50, 51]. But, one study conducted in Egypt showed the length was higher among females than males. This may be due to nutritional status where Egyptian culture recommends women to gain weight for fertility purposes [52, 53].

In most of the study reviewed, as age increases the spleen length, width, thickness, and volume are reduced. This is from the fact that as age increases, the number and size of B cell follicles of the white pulp of the spleen decrease. This implies a decrease of germinal center of spleen, which reduces overall spleen dimension [54–56]. This review is supported by the studies conducted in Iraq, Nepal, and India [33, 35, 36, 42, 57]. But, this summary of review does not agree with the studies conducted in Pakistan, Jordan, and Nigeria [32, 37, 51, 58]. The difference is maybe due to nutritional status where larger anthropometric measurements and obesity were observed in the studies of Pakistan, Jordan, and Nigeria.

Physiological studies indicate that as individual's height, weight, BMI, and BSA increase, the blood volume increases. This increase of blood volume requires larger spleens for filtration. This fact is supported by most of literature reviewed where all dimensions were positively correlated with height, weight, BMI, and BSA. The studies conducted in Jordan, the United States, India, Sudan, and Ethiopia were some of the studies that support this idea [26, 37, 38, 59].

5. Conclusion

This chapter gives baseline information for clinicians as well as for academicians about the morphometric variation of spleen dimensions. Hence, it helps in diagnosing pathological cases associated with spleen, both splenomegaly as well as splenic atrophy. Therefore, clinicians should consider this variation during their diagnosis. Radiology professionals also should measure all dimensions rather than the length alone to rule out splenomegaly correctly.

Funding

No specific funding was received for the study from any organization.

Competing interests

No competing interest.

Consent for publication

Not applicable.

Availability of data and materials

All relevant data are included in the article.

Author details

Solomon Demissie[1*], Mulatie Atalay[1] and Yonas Derso[2]

1 Department of Clinical Anatomy, College of Medicine and Health Science, Arba Minch University, Arba Minch, Ethiopia

2 Department of Physiology, College of Medicine and Health Science, Arba Minch University, Arba Minch, Ethiopia

Available from https://dx.doi.org/10.5772/intechopen.101900

References

[1] Singh V. Textbook of Anatomy Abdomen and Lower Limb. Volume II. 2nd ed. India: Elsevier Health Sciences; 2014. 93p.

[2] Sinnatamby CS. Last's Anatomy e-Book: Regional and Applied. 12th ed. India: Elsevier Health Sciences; 2011. 560p.

[3] Nayak BN, Buttar HS. Health benefits of tryptophan in children and adults. Journal of Pharmaceutical Sciences and Technology Management. 2015;**1**:8-12

[4] Chaudhry SR, Panuganti K. Anatomy, Abdomen and Pelivs. Spleen StatPearls Treasure Island (FL): StatPearls Publishing StatPearls Publishing LLC; 2019

[5] Moore K, Dalley I. AF & Agur, AMR Clinically Oriented Anatomy. Philadelphia, Wolters Kluwer Health/ Lippincott Williams & Wilkins; 2014

[6] Haley PJ. The lymphoid system: A review of species differences. Journal of Toxicologic Pathology. 2017;**30**(2): 111-123

[7] Nolte MA, Hamann A, Kraal G, Mebius RE. The strict regulation of lymphocyte migration to splenic white pulp does not involve common homing receptors. Immunology. 2002;**106**(3): 299-307

[8] Levy AD, Mortele KJ, Yeh BM. Gastrointestinal Imaging: Oxford University Press, USA; 2015

[9] Niederau C, Sonnenberg A, Müller J, Erckenbrecht J, Scholten T, Fritsch W. Sonographic measurements of the normal liver, spleen, pancreas, and portal vein. Radiology 1983;**149**(2):537-540

[10] Lv Y, Lau WY, Li Y, Deng J, Han X, Gong X, et al. Hypersplenism: History and current status. Experimental and Therapeutic Medicine. 2016; **12**(4):2377-2382

[11] Tonelli AR, Yadav R, Gupta A, Arrossi AV, Heresi GA, Dweik RA. Spleen size in idiopathic and heritable pulmonary arterial hypertension. Respiration. 2013;**85**(5):391-399

[12] Kinderknecht JJ. Infectious mononucleosis and the spleen. Current Sports Medicine Reports. 2002; **1**(2):116-120

[13] Alkadarou T, Musa A, Alkadarou A, Mahfouz MS, Troye-Blomberg M, Elhassan AM, et al. Immunological characteristics of hyperreactive malarial splenomegaly syndrome in Sudanese patients. Journal of Tropical Medicine. **2013**;2013:1-5

[14] Smeltzer J, Habermann TM, Timucin T, Nagorney D, Ristow K, Colgan JP, et al. Long term clinical outcomes in patients with massive splenomegaly and non-Hodgkin's lymphoma treated with splenectomy American Society of Hematology; 2012;**120**(21):2692

[15] Varma N, Naseem S. Hematologic changes in visceral leishmaniasis/kala azar. Indian Journal of Hematology and Blood Transfusion. 2010;**26**(3):78-82

[16] Sahu N, Rath S, Padhy RN. Role of abdominal ultrasound in the diagnosis of typhoid fever in pediatric patients. Journal of Medical Ultrasound. 2016; **24**(4):150-153

[17] Chapman J, Bansal P, Goyal A, Azevedo AM. Splenomegaly. In: StatPearls. Treasure Island (FL): StatPearls Publishing; 2021. PMID: 28613657

[18] Kienle DL. The spleen in hematologic malignancies.

Therapeutische Umschau Revue Therapeutique. 2013;**70**(3):163-169

[19] Aubrey-Bassler FK, Sowers N. 613 cases of splenic rupture without risk factors or previously diagnosed disease: A systematic review. BMC Emergency Medicine. 2012;**12**(1):1-14

[20] Babadoko A, Ibinaye P, Hassan A, Yusuf R, Ijei I, Aiyekomogbon J, et al. Autosplenectomy of sickle cell disease in Zaria, Nigeria: An ultrasonographic assessment. Oman Medical Journal. 2012;**27**(2):121

[21] Poulin E, Thibault C. The anatomical basis for laparoscopic splenectomy. Canadian Journal of Surgery Journal Canadien de Chirurgie. 1993;**36**(5):484-488

[22] Megremis SD, Vlachonikolis IG, Tsilimigaki AM. Spleen length in childhood with US: Normal values based on age, sex, and somatometric parameters. Radiology 2004;**231**(1): 129-134

[23] Ahmed OF. Ahmed of assesment of normal hepatosplenic span using ultrasound in egyptian population. Natural Sciences. 2017;**15**(8):215-219

[24] Serter S, Ceylan C, Tunçyürek Ö, Örgüç Ş, Pabuçcu Y. Sonographic evaluation of spleen size and prevalence of accessory spleen in a healthy male Turkish population. Turkish Journal of Hematology. 2010;**27**(1):25-28

[25] Caglar V, Alkoc O, Uygur R, Serdaroglu O, Ozen O. Determination of normal splenic volume in relation to age, gender and body habitus: A stereological study on computed tomography. Folia Morphologica. 2014;**73**(3):331-338

[26] Asghar A, Naaz S, Agrawal D, Sharma P. Morphometric study of spleen in North Indian adult population: CT Scan image based study. Journal of Clinical and Diagnostic Research. 2011;**5**(5):974-977

[27] Tekle Y, Gudadhe DR, Abreha M, Muche A, Tegegne Z, Hiware SD. Morphometric assessment of the normal dimensions of the adult spleen in North-west Ethiopia region—A radiological study. Annals of International Medical and Dental Research. 2018;**4**(4):34-37

[28] Hosey RG, Mattacola CG, Kriss V, Armsey T, Quarles J, Jagger J. Ultrasound assessment of spleen size in collegiate athletes. British Journal of Sports Medicine. 2006;**40**(3):251-254

[29] Siddiqui MA, Ali AHA, Bedewi MA, Serhan OO. Estimation of standard splenic volume in Saudi Arabian adult population: Using 3D reconstruction of Abdominal CT scan Images. Open Journal of Internal Medicine. 2014;**4**(01):7

[30] Udoaka A, Enyi C, Agi C. Sonological evaluation of the liver, spleen and the kidneys in an adult southern Nigerian population. Asian Journal of Medical Sciences. 2013; **5**(2):33-36

[31] Yousif JM. Measurement of Normal Spleen in Sudanese by Using Ultrasonography. Sudan: Sudan University of Science and Technology; 2016. 61p

[32] Khan SA, Yasmeen S, Adil H, Adil SO, Huda F, Khan S. Sonographic evaluation of normal liver, spleen, and renal parameters in adult population: A multicenter study. Journal of the College of Physicians and Surgeons Pakistan. 2018;**28**(11):834

[33] Sharma K, Lamichhane P, Sharma B, Sharma B. Sonographic measurement of spleen in relation to age: A prospective study among adult Nepalese people in Western Nepal. Journal of Gandaki Medical College-Nepal. 2017;**10**(1):11-16

[34] Chakraborti S, Saha N, Debbarma B, Das S, Leishram D. Normal spleen length by ultrasonography in adults of Tripura. Journal of Dental and Medical Sciences. 2016;**1**:55-60

[35] Arora N, Sharma P, Sahai A, Singh R. Sonographic measurements of the spleen in relation to age; a prospective study in north Indian adults. Journal of Anatomical Society of India. 2010;**59**(2):177-181

[36] Mittal R, Chowdhary D. A pilot study of the normal measurements of the liver and spleen by ultrasonography in the Rajasthani population. Journal of Clinical and Diagnostic Research. 2010;**4**(4):2733-2736

[37] Badran DH, Kalbouneh HM, Al-Hadidi MT, Shatarat AT, Tarawneh ES, Hadidy AM, et al. Ultrasonographic assessment of splenic volume and its correlation with body parameters in a Jordanian population. Saudi Medical Journal. 2015;**36**(8):967

[38] Chow KU, Luxembourg B, Seifried E, Bonig H. Spleen size is significantly influenced by body height and sex: Establishment of normal values for spleen size at US with a cohort of 1200 healthy individuals. Radiology. 2015;**279**(1):306-313

[39] Gul S, Itoo MS, Jahangir M, Kamal Y. Sonologic Assessment of Dimensions of Spleen in Normal Adult Kashmiri Population and their Correlation with Weight and Height. Autopsies Forensic Medicine and Anatomy Research. 2014;**2**:63-69

[40] Paul L, Talhar S, Sontakke B, Shende M, Waghmare J. Relation between Renal Length and Renal Volume with Patient's BMI: A Critical Appraisal. Anatomy & Physiology. 2016;**6**(246):1-7

[41] De Odorico I, Spaulding KA, Pretorius DH, Lev-Toaff AS, Bailey TB, Nelson TR. Normal splenic volumes estimated using three-dimensional ultrasonography. Journal of Ultrasound in Medicine. 1999;**18**(3):231-236

[42] Chakraborti S, Saha N, Debbarma B, Das S, Leishram D. Normal spleen length by ultrasonography in adults of Tripura. IOSR Journal of Dental and Medical Sciences. 2016;**15**(1):55-60

[43] Okuma H, Gonoi W, Ishida M, Shirota G, Kanno S, Shintani Y, et al. Comparison of volume and attenuation of the spleen between postmortem and antemortem computed tomography. International Journal of Legal Medicine. 2016;**130**(4):1081-1087

[44] Palmiere C, Tettamanti C, Scarpelli MP, Tse R. The forensic spleen: Morphological, radiological, and toxicological investigations. Forensic Science International. 2018;**291**:94-99

[45] Çeliktas M, Özandaç S, Göker P, Bozkir MG. Sonographic determination of normal spleen size in Turkish adults. International Journal of Morphology. 2015;**33**(4):1401-1405

[46] Sonmez G, Ozturk E, Basekim CC, Mutlu H, Kilic S, Onem Y, et al. Effects of altitude on spleen volume: Sonographic assessment. Journal of Clinical Ultrasound. 2007;**35**(4):182-185

[47] Purdy GM, James MA, Rees JL, Ondrus P, Keess JL, Day TA, et al. Spleen reactivity during incremental ascent to altitude. Journal of Applied Physiology. 2019;**126**(1):152-159

[48] Shephard RJ. Responses of the human spleen to exercise. Journal of Sports Sciences. 2016;**34**(10):929-936

[49] Murphy WG. The sex difference in haemoglobin levels in adults—Mechanisms, causes, and consequences. Blood Reviews. 2014;**28**(2):41-47

[50] Siddiqui MA, Ali A, Serhan O. Estimation of standard splenic volume in Saudi Arabian adult population: Using 3D reconstruction of Abdominal CT scan Images. Journal of Morphological Sciences. 2015; **32**(04):227-230

[51] Ehimwenma O, Tagbo MT. Determination of normal dimension of the spleen by ultrasound in an endemic tropical environment. Nigerian Medical Journal: Journal of the Nigeria Medical Association. 2011;**52**(3):198

[52] Ahmed OF, Assessment of normal hepatosplenic span using ultrasound in Egyptian population. Natural Science. 2017;**15**(8):215-219

[53] Galal OM. The nutrition transition in Egypt: Obesity, undernutrition and the food consumption context. Public Health Nutrition. 2002;**5**(1a):141-148

[54] Himamoni D, Das T, Talukdar K. Age related histological changes of human spleen. IJHRMLP. 2016; **3**(1):59-61

[55] Turner VM, Mabbott NA. Influence of ageing on the microarchitecture of the spleen and lymph nodes. Biogerontology. 2017;**18**(5):723-738

[56] Alex L, Rajan ML, Xavier B, Jacob P, Rani KD, Lakshmi GV. Microscopic study of human spleen in different age groups. International Journal of Research in Medical Sciences. 2015;**3**(7):1701-1706

[57] Estephan MF, Al-Saadi WI, Funjan MM. Possible anthropometric explanation of age-related changes in splenic volume in a sample of healthy Iraqi individuals using ultrasonography Iraqi Journal of Medical Sciences. 2012;**10**(4):312-320

[58] Mustapha Z, Tahir A, Tukur M, Bukar M, Lee W-K. Sonographic determination of normal spleen size in an adult African population. European Journal of Radiology. 2010;**75**(1): e133-e1e5

[59] Yousef M. Local reference of splenic volume in healthy sudanese subjects sonographically. Journal of Biomedical Engineering and Medical Imaging. 2018;**5**(4):30

3

Prostate

Ragab Hani Donkol[1] and Ahmad Al Nammi[2]
[1]*Cairo University*
[2]*Aseer Central Hospital*
[1]*Egypt*
[2]*Saudi Arabia*

1. Introduction

The value of prostatic sonography has dramatically increased in the past three decades. Transrectal ultrasound (TRUS) imaging is currently an integral part of prostate cancer diagnosis and treatment procedures, providing high-resolution anatomical detail of the prostate region. In this chapter we review the anatomy and sonographic methods in imaging of the prostate and prostatic diseases. Also we emphasize the role of new sonographic techniques, such as color and power Doppler, the use of contrast agents, 3D sonography and elastography for diagnosis of different prostate diseases especially prostate cancer. We also discuss the use of systematic and targeted sonographic-guided biopsies as gold standard for prostate cancer detection. Finally, we will elaborate the new role of ultrasound in management of prostate cancer.

2. Anatomy of the prostate

2.1 Embryology of the prostate

In the 4th week of gestation, the urogenital septum divides the cloaca into two parts: The rectum posteriorly and the primitive urogenital sinus anteriorly. In the 5th week, the distal portions of the Wolffian canal and the Mullerian canal attach to the posterior aspect of the primitive urogenital sinus (Fig. 1) to form an elevation called Mullerian tubercle. The tubercle divides the primitive urogenital sinus into vesico-urethral canal superiorly and definitive urogenital sinus inferiorly.The Wolffian canal forms the vas deferens, the ampulla of the vas and the seminal vesicle. The Mullerian canal regresses to form the utricle. Formation of the prostate begins at the 10th week of gestation by proliferation of the epithelium of the posterior urethra around the orifices of the Wolffian canal, to surround the urethral circumference. The prostatic glands formed anterior to the urethra regress and are replaced by fibromuscular stroma. The secretory function of the glands starts about the 13th week of gestation. (Brandes, 1989).

2.2 Gross anatomy of the prostate and its relations

The term "prostate" was originally derived from the Greek word "prohistani", meaning "to stand in front", and has been used to describe the organ located in front of the urinary bladder (Lowsley, 1912). The prostate is conical in shape with its long axis directed

inferiorly and anteriorly. The shape and size of the prostate may vary with age. The prostate of an adult man measures 20 – 25 gms in weight. The base of the prostate is directed superiorly and in contact with the bladder base. The apex is directed inferiorly and in contact with the external sphincter above the deep fascia of the urogenital membrane. The anterior border is separated from the symphysis pubis and pubic bones by the retropubic space which contains loose areolar tissue, preprostatic venous plexus, lymphatics, nerves and puboprostatic ligament. The trapezoid area is an extraprostatic area of anatomic weakness. It may be involved by carcinoma extending through the inferior neurovascular pedicle. This area bounded by the prostate proximally, the rectourethralis muscle distally, the membranous urethra anteriorly and the rectum posteriorly (Mayers et al, 1987). Posteriorly, the prostate is related to the rectum and is separated from it by the Denoviller's fascia which extends superiorly, behind the seminal vesicles up to the peritoneal reflection. At each posterolateral aspect of the prostate, the hypogastric pelvic fascia contains the neurovascular bundle of the prostate, seminal vesicles and bladder neck (Fig. 2).

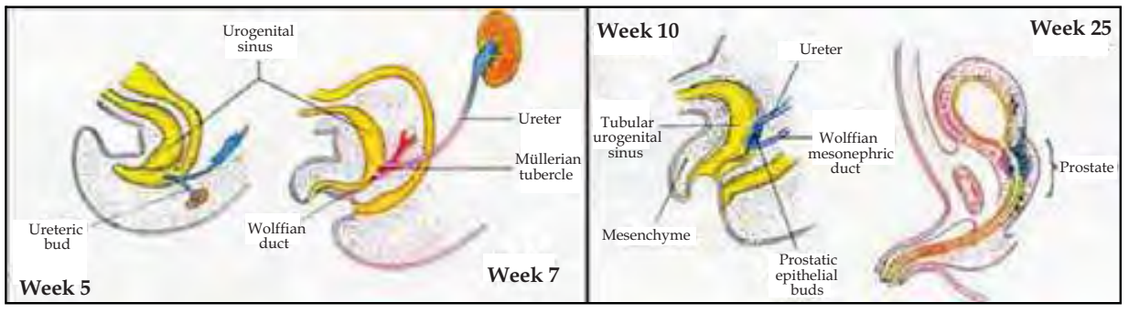

Fig. 1. The embryological origin and development of the prostatic urethra and the prostate (adapted from Delmas, 1991)

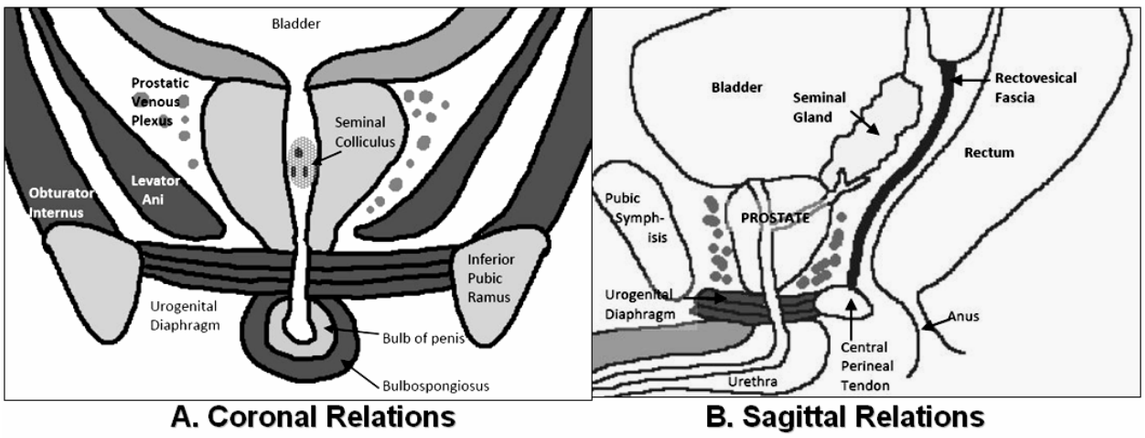

Fig. 2. Relations of the prostate in the coronal (A) and sagittal planes (B)

2.3 The distal seminal tract

It is formed of two seminal vesicles, ampullae of the vasa differentia and ejaculatory ducts. The seminal vesicle is a cystic structure, measuring about 35 mm in length and 15 mm in width. It is related anteriorly to the urinary bladder and posteriorly to the the rectum.The ampula of the vas is located medial to the seminal vesicle. The vassal ampula joins the

seminal vesicle to form the ejaculatory duct. Each duct enters the base of the prostate, passes through central zone to end in the urethra below the utricle (Brandes, 1989).

2.4 Lobar concept of intraprostatic anatomy

In 1912, Lowsley demonstrated the first detailed description of the anatomy of the prostate. This traditional concept which is no longer used, divided the prostate into lobes: an anterior, posterior, middle and two lateral lobes. This method has been used to identify the prostate and prostatic disease for about 60 years. The anterior lobe was situated from the anterior margin of the gland to the level of the prostatic urethra. The middle lobe was a small area between the proximal prostatic urethra and the ejaculatory ducts. This lobe extnds form the base of the prostate to the level of verumontanum. The posterior lobe was situated posterior to the ejaculatory ducts and extends to the posterior margin of the gland. The two lateral lobes extend from the lateral margin of the gland bilaterally toward the middle part of the gland. None of these lobes has clearly defined medial margin (Lowsley, 1912).

2.5 Zonal concept of intraprostatic anatomy

The understanding of the gross and microscopic anatomy of the prostate has changed during the past few decades. Since 1965, a zonal concept of anatomy has evolved initially developed by McNeal and then modified over about three decades. The prostate is best considered to be a fusion of different glandular regions contained within a discontinuous capsule (McNeal, 1968, 1988). The prostate is composed of four glandular regions and a non-glandular region which is the anterior fibromuscular stroma (Fig. 3). The fibromuscular stroma (FMS) is the anteromedial portion of the gland is devoid of glandular tissue. This region is generally considered to be of less clinical significance. The peripheral zone (PZ) comprises the largest portion of the glandular prostate in young man (70%). The PZ is

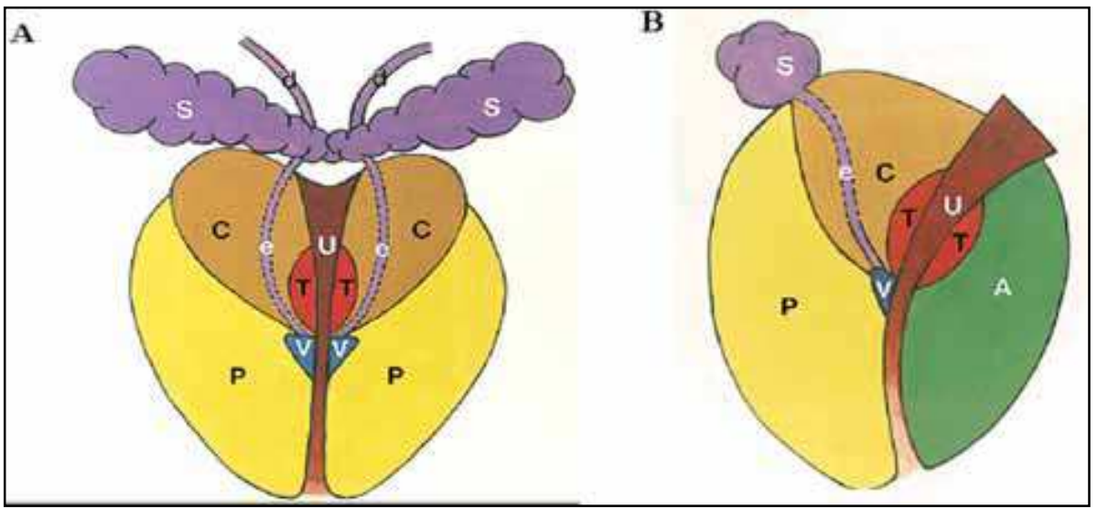

Fig. 3. Zonal anatomy of the prostate in coronal and sagittal planes showing the central zone (C), peripheral zone (P), transition zone (T) and anterior fibromuscular stroma (A). It also shows the distal seminal tract formed of the ampula of the vas deference (d) which joins the seminal vesicle (S) to form ejaculatory duct (e) which opens at vera montanium (v) (adapted from McNeal 1968)

situated posteriorly, posterolaterally and a thin layer of this tissue also extends up laterally and anterolaterally. Distal to the verumontanum, the PZ often surrounds the urethra and occupies the apical region if the prostate. The transition zone (TZ) is situated on both sides of the proximal prostatic urethra and comprises only 5 to 10% of the glandular tissue in the non hyperplastic prostate. The surgical capsule is an interface between the PZ and TZ. In the aging prostate where the TZ can show marked glandular hyperplasia and may constitute the majority of prostatic glandular elements. The periurethral glandular zone (PUG) consists of mucosal glands in the prostatic urethra itself and represents only a tiny fraction of the glandular prostate. This zone may become hyperplastic with age to form the "median lobe" which may obstruct the bladder neck. The central zone (CZ) is cone-shaped with its base forms the base of prostate, bordering the urinary bladder and seminal vesicles and its apex is at the verumontanum The CZ forms about 25% of the glandular prostatic tissue. The CZ surrounds the ejaculatory ducts throughout their entire courses in the prostate. The site where the ejaculatory ducts enter the CZ is devoid of prostatic capsule. The extraprostatic space invaginates around the ejaculatory ducts down to the verumontanum forming the "invaginated extra prostatic space". If the ejaculatory ducts are invaded by carcinoma, the tumor will have a ready "highway" to the seminal vesicles and extraprostatic space.

2.6 Correlation of the lobar and zonal concepts of anatomy of the prostate

A comparison of Lowsley lobar and McNeal zonal concepts of anatomy is possible and important to compare the clinical findings. Clinicians may still refer to lobar anatomy while radiologists use zonal anatomy. So, the anterior lobe correlates with the anterior fibro-muscular stroma. The medial lobe and the CZ are similar. The sum of the posterior and two lateral lobes correlated to a large extent with the PZ.

2.7 Correlation of the zonal anatomy and origin of prostatic diseases

With the development of cross sectional – imaging studies like transrectal ultrasound (TRUS) and magnetic resonance imaging (MRI), the zonal concept of anatomy becomes useful technique to apply because the different areas can be definite (Rifkin et al, 1990). The zonal concept of anatomy is also useful because it incorporated a clearer understanding if the development of disease. The origin of prostatic disease was poorly understood under Lowsley's concept of lobar anatomy. It was previously thought that cancer only arises in the posterior lobe and BPH develops predominantly in the lateral and, to a lesser degree in the median lobe. It is now understood that the prostate cancer develops in the acinar tissue predominantly the peripheral prostate. Although the PZ is three times larger in volume that the CZ, prostate cancer develops seven times more often in the PZ. It was shown that about 50% of cancer arises in the anterior half of the prostate, including all those cancers from the TZ (20% of the total), CZ (10%) and anteriorly situated portions of the PZ. In contrast, BPH develops exclusively from the central gland, approximately 95% from the TZ and 5% from the periurethral glandular tissue. Prostatitis (when not due to surgical manipulation) starts mainly in the PZ similar to the prostatic cancer (McNeal et al 1988).

3. Techniques and approaches of prostatic ultrasonography

Ultrasonography is firmly established diagnostic tool in prostatic imaging. Recent development in US technology has led to significant improvements in image quality,

consistency and resolution. Additionally, dynamic scanners, color flow imaging and real time imaging have allowed appreciation of blood flow, reduced examination time and improved quality of the image. These advances combined with the portability, relative low cost and lack of risks of iodinated contrast media and irradiation have made US one of the most useful modality in evaluation of the prostate. Many approaches can be used to image the prostate as trans-abdominal, trans-urethral, trans-perineal and transrectal US. The common two approaches are transabdominal and transrectal ultrasound.

3.1 Trans-abdominal ultrasound

Transabdominal US of the prostate is nearly universally available and provides excellent anatomic information using the urine-filled bladder as an acoustic window. Prostate size, weight, shape and intravesical extent can be determined. Caudal angulation of the transducer to accommodate the public bone is often required. The normal prostate appears as a homogenous, round or ovoid structure with uniform low level echoes. The intraglandular zonal anatomy can not be visualized (Fig. 4). The relation between the prostate, bladder and seminal vesicles can be demonstrated (Abu-Yosef & Noryana 1982).

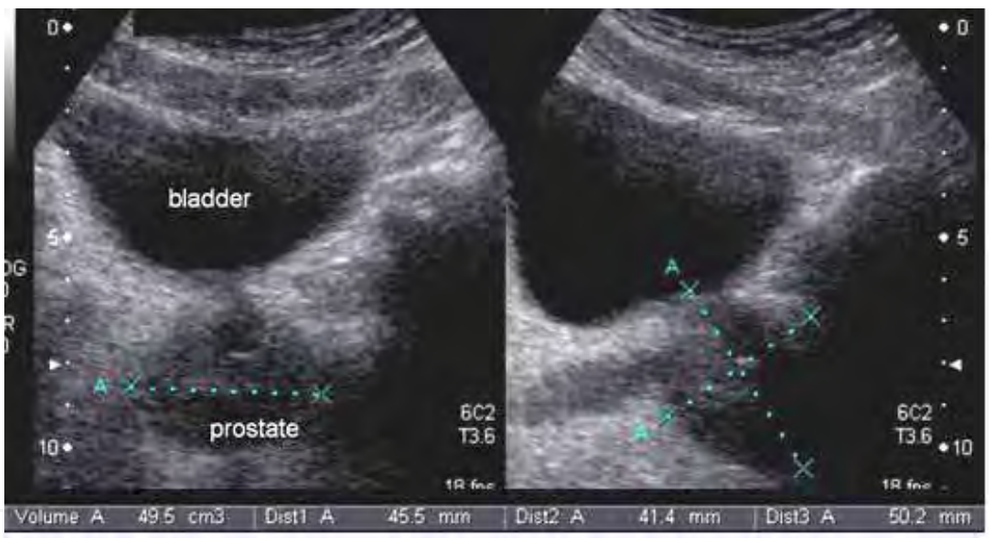

Fig. 4. Transabdonal US of a moderately enlarged prostate in axial and sagittal planes

3.2 Transrectal ultrasound (TRUS)

In 1963, Takahashi and Ouchi were the first to describe the use of TRUS to evaluate the prostate. The first clinically applicable images of the prostate obtained with TRUS were described in 1967 by Watanabe et al, they used a 3.5 MHz transducer, which at that time was considered to be state of the art, to obtain images that were clinically meaningful. As US technology has become more refined, the use of TRUS in the evaluation of prostatic disease has increased. By the mid 1980s.TRUS had become a standard diagnostic instrument of the urologists and radiologists. Most investigators today prefer equipment using hand-held transducers which are available in frequencies ranging from 3.5 MHz up to 10 MHz with the optimum frequency being around 7.0 MHz. Transrectal probes are available in different sizes and shapes with diameters ranging from 1.2 to 2 cm.

4. Sonographic anatomy of the normal prostate

Transrectal US of the prostate has revolutionized our ability to examine this organ. It provides excellent visualization of the prostate in the axial and sagittal planes.

In the axial plane, scanning usually begins at a level just above the seminal vesicles and by sequential withdrawing of the transducer in a caudal direction, the base, mid gland and the apex is visualized (Fig. 5). When scanning the most cephalad areas, the vas deferens will be visualized. They will appear as bilateral round cystic structures. Then the seminal vesicles will come into view as the vas deferens joins with them superior to the prostate. They usually appear as bow-tie configuration, but they may be rounded, lobulated or flattened. At the level of the base of the prostate, the prostate appears as a symmetrical crescent-shaped with triangular postero-lateral margin. The normal prostate will appear hyperechoic to the sminal vesicles and will have a homogenous echopattern. The CZ and TZ cannot be individually distinguished by their echogenicity. However the PZ appears more echogenic with homogenous echotexture. At the level of mid gland, the prostate becomes ovoid in shape. The anterior fibromuscular tissue is seem and has an echogenicity equal to or less than that of the glandular areas. The hypoechoic periurethral glandular tissue is demonstrated as hypoechoic area in the midline. Posterior and lateral to the PUG tissue, the PZ appears more echogenic and homogenous. The apex of the prostate appears more rounded. The obturator internus and levator anu muscles appear as hyperechoic structures lateral to the prostate apex. The prostate is surrounded by hyperegenic layer comprising the prostatic capsule and surrounding fat and fascia. The normal prostatic urethra is rarely visualized. The advantages of axial scanning include visualization of the left-right symmetry and echotexture,visualization of the anterior lateral portions of the PZ in a single view and assessment the lateral extracapsular spread of carcinoma (Rifkin, 1997).

In the sagittal plane scanning starts in the midline where the entire prostate can be visualized in one image. The seminal vesicle will be superior and posterior to the base of the prostate, and the vas deferens will be seen anterior to the seminal vesicles. The seminal vesicles will be less echogenic than the prostate and will appear rounded in shape. In the midline sagittal plane, the hypoechoic periurethral tissue will be seen and may be difficult to differentiate form the anterior fibromuscular stroma. The rest of the prostate will be homogenous in echogenicity with the PZ slightly more echogenic than the CZ and TZ (fig. 6). By tilting the transducer slightly to the right or the left of midline, the lateral aspects of the prostate and seminal vesicles will be visualized. The lateral aspects of the prostate are normally more rounded and homogenous in ehcogenicity. The ejaculatory ducts can be identified as hypoechoic lines structures between two parallel echogenic lines as the course from the seminal vesicles through the CZ into prostatic urethra. The advantages of sagittal scanning include evaluation of the base and apex of the prostate in a single view, accurate measurement of the cranio-caudal diameter of the prostate or of a lesion within the prostate and better demonstration of the prostatic urethra and ejaculatory ducts ((Rifkin, 1997)

Estimation of prostate volume may be useful in a variety of clinical settings. In cases of BPH, most urologists prefer to perform transurethral resections for glands under 60 grams, while open prostatectomy is preferred for glands over 60 grams (Narayan & Foster 1991). Other potential users include the comparison of the prostate volume with levels of PSA for early detection of the prostatic cancer. PSA density is an index calculated by dividing PSA by the volume of the prostate measured by TRUS. In absence of cancer, prostatic volume is directly

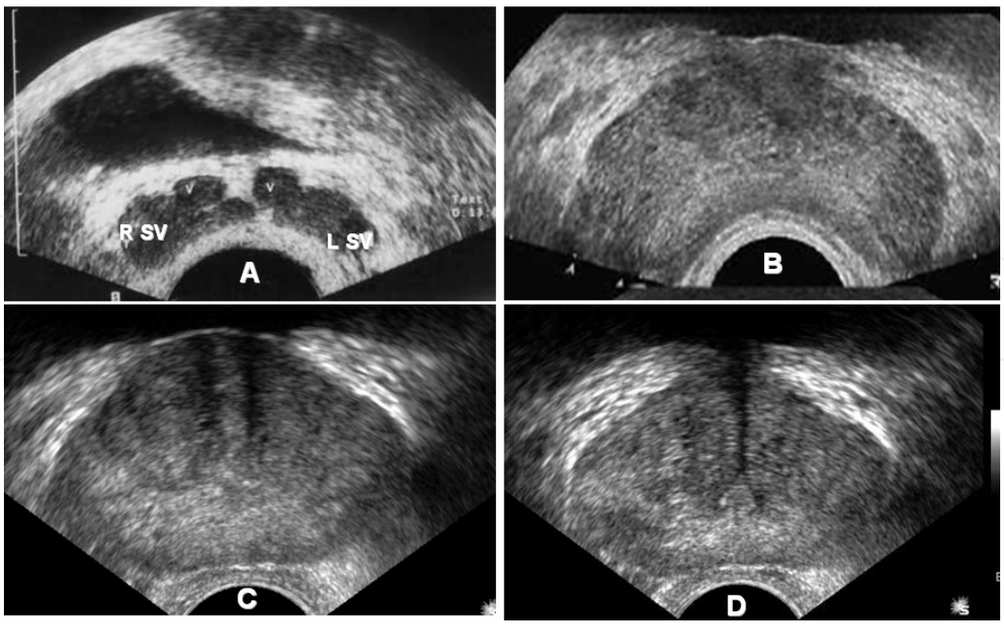

Fig. 5. TRUS axial images. (A) the level of distal seminal tract; showing seminal vesicle (SV) and vasl ampulla (V), (B) level of prostate base, (C) level of mid gland and (D) level of vera montanum showing its appearance as tour Eiffel

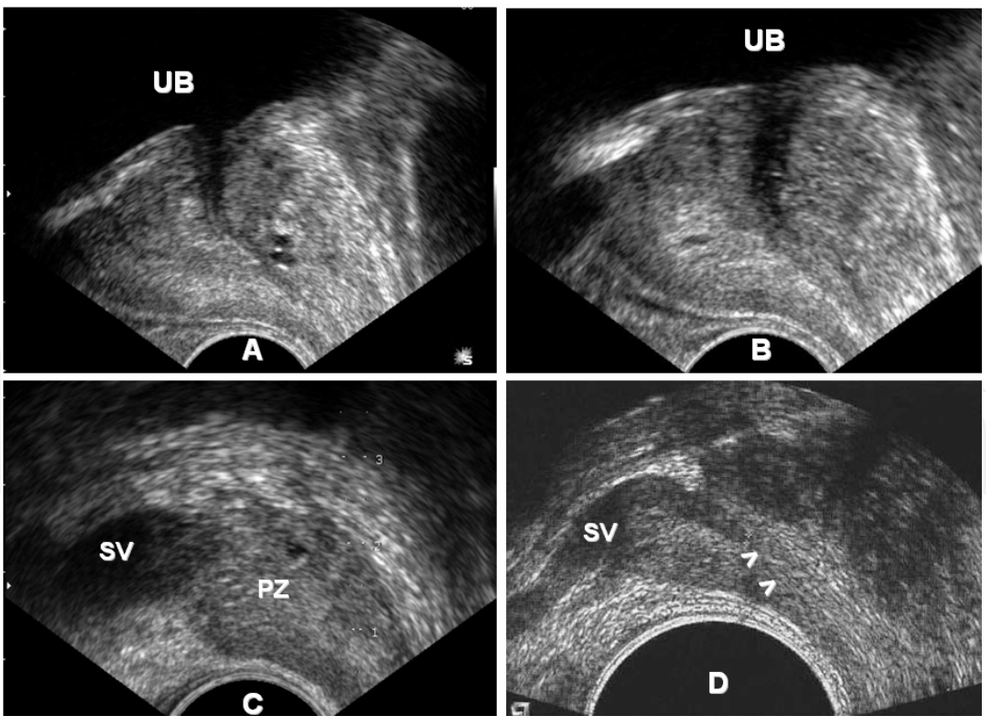

Fig. 6. TRUS sagittal images; (A) in midline; (B) in paramedical region; (C) peripheral part of the gland which is formed mainly of peripheral zone (PZ) and above it the body of seminal vesicle (SV) and (D) shows the confluence of vas and seminal vesicle (SV) to form the ejaculatory duct (arrowhead)

proportional to circulating serum PSA (Benson et al., 1992). Benign prostatic hyperplasia is associated with, on average, only 0.26 ng/ mL PSA per gram of tissue, whereas cancer results in a density 10-fold higher (Hammerer et al., 1995). Any PSA value greater than that predicted by gland volume should raise a suspicion of prostate cancer. Also, the pre-treatment estimation of the volume of prostate cancer can provide important prognostic information after hormonal or radiation therapy. (Terris & Stamey 1991). The commonly used method in measuring prostate volume is the elliptical method. This formula can be transformed into volume = $0.523 \times d_1 \times d_2 \times d_3$. Maximal width and height diameters are obtained at the largest appearing mid gland axial image section. The length dimension can be obtained on midline sagittal plane (Fig. 9). This method is widely used because it is easy and fast method. The fact that it is slightly less accurate than other methods is not documented (Terris & Stamey,1990).

5. Diseases of the prostate and their sonographic appearance

5.1 Cysts of the prostate

Cysts of the prostate are confusing abnormalities because they are uncommon and their origin is uncertain. Small cysts are asymptomatic while large cysts may present with symptoms of urinary tract irritation, obstruction or hypofertility. The cysts may be complicated by infection, and stone formation. They may be turned malignant in about 3% of cases (Litirup et al., 1988). The cysts are usually unilocular, sharply defined, thin walled and anechoic. They vary size from 0.5 cm to 3.0 cm in diameters (Fig. 7). Prostatic cysts are either midline prostatic cysts like utricle cyst and Mullerian duct cyst or lateral prostatic cysts as cysts of the ejaculatory ducts or acquired cysts which are associated with prostate cancer, PBH, and prostatic abscess (Patel et al., 2002). Utricle cysts are dilatation of the prostatic utricle which may be congenital (megautricle) or acquired due to obstruction of its orifice by inflammation (utriclocele). The utricle cysts are small intraprostatic midline cysts.. Mullerian duct cysts are remnants of Mullerian duct. These cysts are relatively large, extends superiorly and inferiorly from the level of the verumontanum even outside the prostate. Ejaculatory ducts cysts are present along the course of the ejaculatory ducts within the CZ. They are usually paramedian and unilateral. They are complex cysts with solid and cystic components.They containing spermatozoa. Extra-prostatic cysts are either cysts of the seminal vesicles or the ampulae of the vas. They are congenital in origin and associated with urinary tract anomalies. Some patients are manifested by obstructive azospermia and TRUS can classify the patients without cysts where TRUS-guided aspiration and seminal vesiculography can be performed and patients with cyst where TRUS-guided cyst aspiration and opacification can be performed (Donkol, 2010).

5.2 Inflammatory diseases the prostate

Acute prostatitis is acute bacterial inflammation of the prostate. The clinical diagnosis usually is not difficult. The patient has fever, perineal and low back pain; pain with defecation of after ejaculation; urethral discharge associated with dysuria, urgency, frequency, or retention. On examination, the prostate is swollen, boggy and tender. Griffiths and associates in 1984 described three characteristic sonographic features seen in a group of 40 patients with an acute inflammation of the prostate as a periurethral echo-poor halo, a

prominent periprostatic venous plexus and hypoechoic areas within the prostate, predominantly in the peripheral zone (Griffiths et al., 1984).

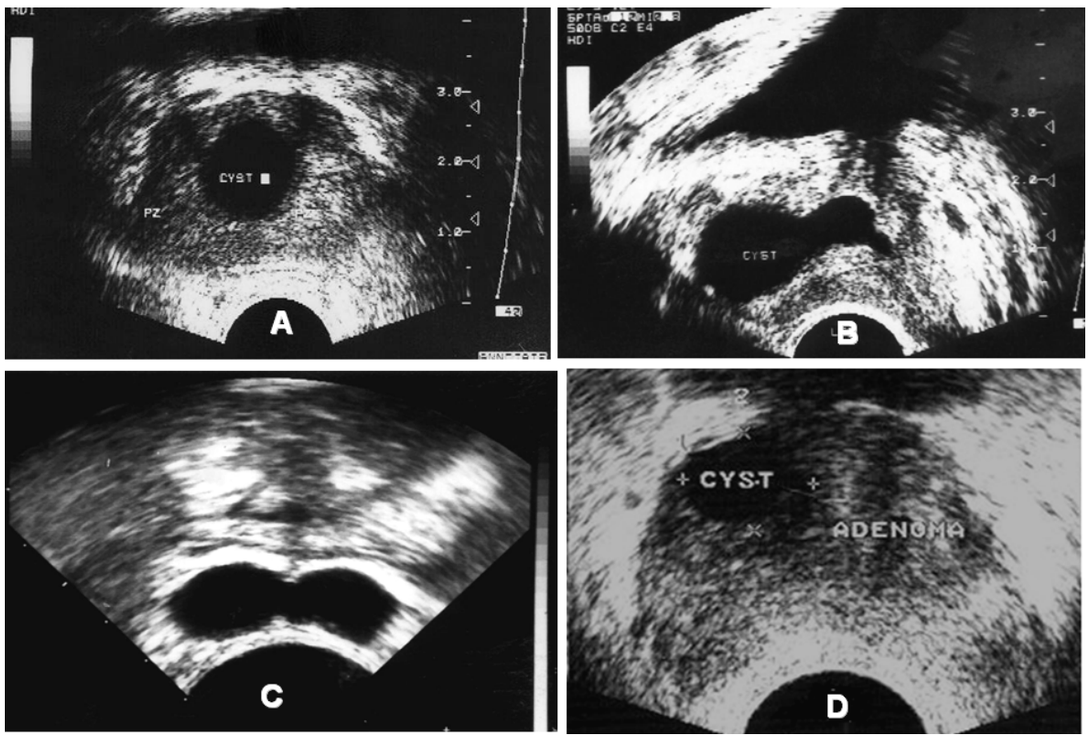

Fig. 7. TRUS of different prostatic cysts. (A) Axial TRUS of a utricle cyst; the cyst is midline and intraprostatic. (B) Sagittal TRUS of Mullerian duct cyst; the cyst is midline is midline with supraprostatic extension. (C) Axial TRUS of bilateral seminal vesicles cysts in a patient with obstructive azospermia. (D) Axial TRUS shows an acquired intraprostatic cyst in the in the right part of adenoma of benign prostatic hypertrophy

Chronic prostatitis may be infective as a complication of acute prostatitis or noninfective secondary to congestion of the prostate or urinary reflux into the prostate resulting in inflammatory or fibrotic reaction or both within the prostate. Chronic prostatitis has varied sympthomatology and lack of physical signs. The diagnosis currently rests on the finding of excessive leukocytes in prostatic secretions. Sonographic findings include high density echoes, mid range echoes, echo-lucent zones, ejaculatory duct calcifications, capsular irregularity, capsular thickening and periurethral zone irregularity (Fig. 8 A&B). The sensitivity and specificity of these signs are low (Doble & Carter, 1989)

Prostatic abscesses have been reported in an older age group due bladder outlet obstruction and urinary tract infection. Iatrogenic prostatic abscess have been reported after biopsy or instrumentation. Half of the patients presenting in acute retention and half presenting with irritative voiding symptoms. Of the patients 40% have fever, 25% have associated epididymo-orchitis. On examination, the majority showed enlarged prostate but only 20% present with the classic signs of prostatic fluctuance and tenderness on DRE (Sohlberg et al., 1991). Abscess can be identified as irregular hypoechoic area containing diffuse mid-range echoes within an enlarged gland (Fig. 8 C). Once identified, the lesions may be aspirated transperineally under ultrasound control (Doble & Carter, 1989).

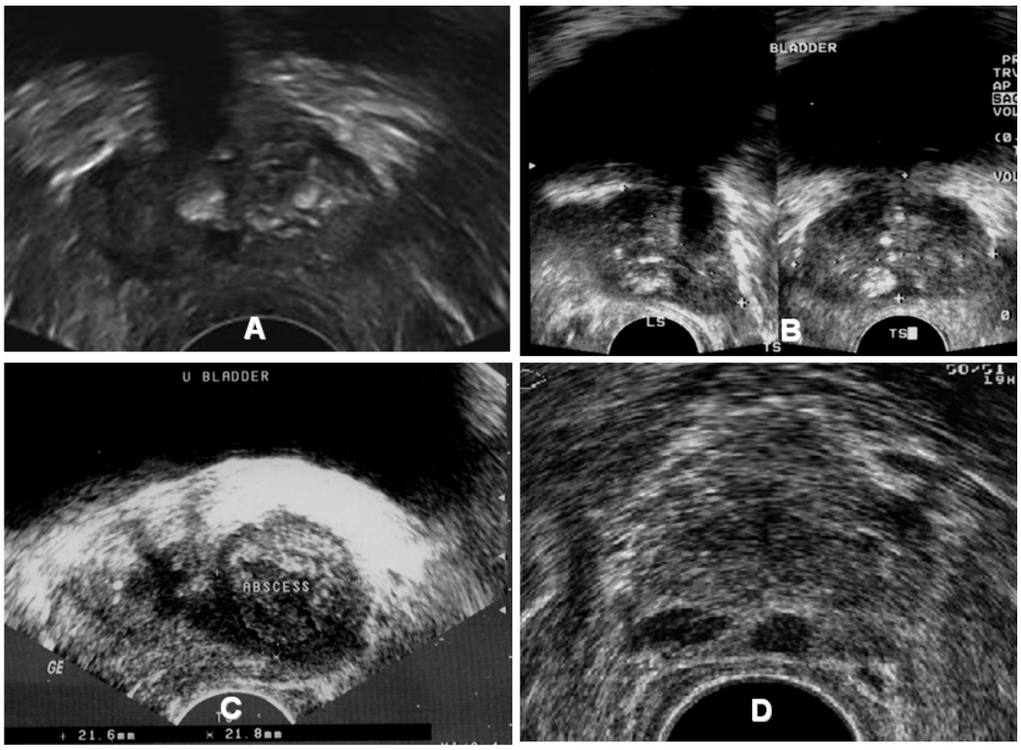

Fig. 8. (A) TRUS of a patient with chronic prostatitis shows calcification of periurethral tissue. (B) TRUS of another patient with chronic prostatitis shows calcification of peripheral zone. (C) TRUS of a case of prostatic abscess with a relatively thick wall and echogenic fluid content. (D) TRUS of a patient with granulomatous prostatitis shows multifocal hypoechoic lesions in the peripheral zone mimicking prostatic cancer

The exact aetiology of granulomatous prostatitis remains undetermined. It is thought to be due to ductal obstruction and ectasia with subsequently extravasation of luminal contents into the glandular stroma. In most patients, these changes are thought to be idiopathic but in others, it can be also linked with specific infecting agents (tuberculosis, schistosomiasis, and fungi). In patients with granulomatous prostatitis, the prostate is usually firm, nodular or indurated on DRE, PSA may be elevated. Patients may present with symptoms of outflow tract obstruction, acute retention or urinary infection. Sonographic findings are single or multiple areas of low echogenicity in the peripheral zone (Fig. 8 D) or heterogeneous echotexture of the gland. The hypoechoic areas are indistinguishable from carcinoma and diagnosis must be established by biopsy (Clements et al., 1993).

5.3 Prostatic calcifications and calculi

Primary prostatic calculi develop in the prostatic ducts and acini. They are usually multiple and small (1-5mms). Secondary dystrophic calcifications are associated with infection, obstruction, necrosis in a prostatic adenoma or radiation therapy. They are usually larger and more irregular than primary calculi. It needs to be emphasized that dystrophic prostatic calculi are not precancerous (Hricak, 1990). Sonographically calcifications appear as bright echogenic foci with or without posterior acoustic shadowing. Calculi can be seen within the seminal vesicles, vassal ampulae or ejaculatory ducts (Fig. 9).

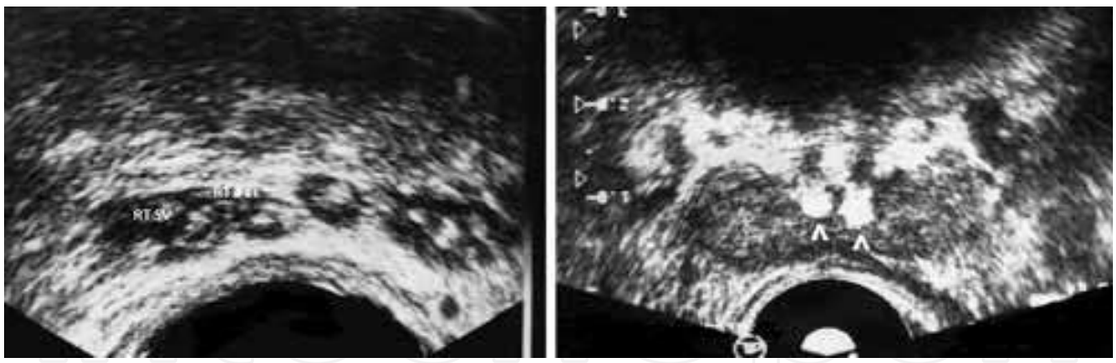

Fig. 9. (A) TRUS shows multiple flecks of calcifications seen in both seminal vesicles (SV) and vassal ampulae. (B) TRUS shows bilateral ejaculatory ducts calculi (arrow heads) in a patient with obstructive azospermia

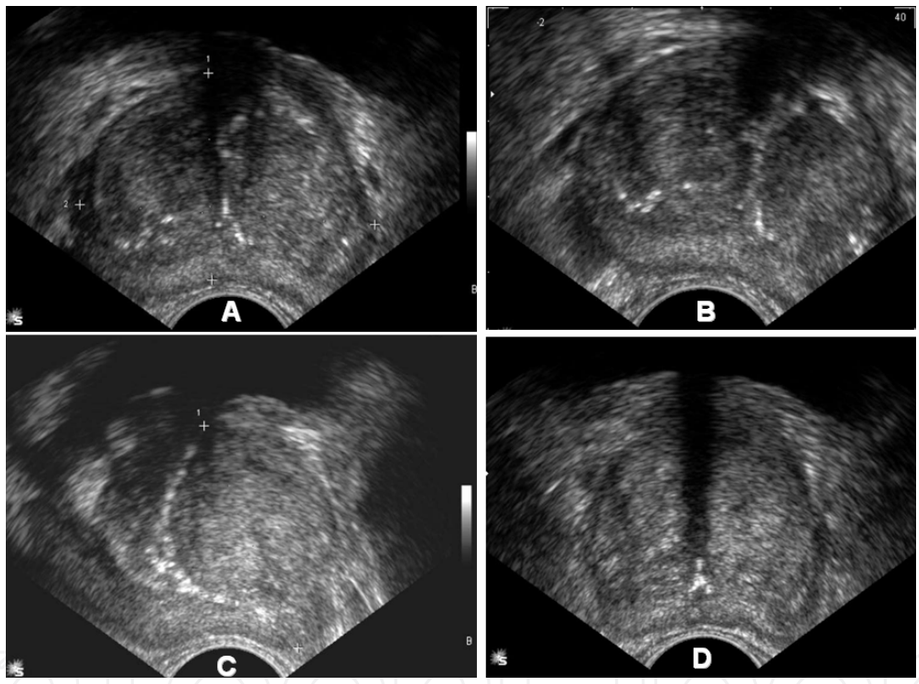

Fig. 10. (A) & (B) TRUS of BPH shows bilobed adenoma causing compression and flattening of the PZ. (C) TRUS of another case of BPH shows calcified surgical capsule separating the adenoma from the PZ. (D) TRUS of another patient with BPH shows large bilobed adenoma separating from the flattened PZ by hypoechoic surgical capsule

5.4 Benign prostatic hyperplasia

Benign prostatic hyperplasia (BPH) is rarely seen in males less than 40 years of age. It affects 50 to 70% of men older than 60, and 80 to 85% of men older than 80 years. BPH begins in the inner region of the prostate adjacent to the urethra. BPH may be diffuse or focal; forming prostatic adenoma. The normal prostatic tissue is displayed caudally and posteriorly to form the surgical capsule (Mc Neal, 1983). Ultrasound is the primary imaging modality for evaluation of the aging men with known or suspected BPH. By transabdominal US prostatic

size, weight, shape and intravesical extent can be determined. Uncomplicated BPH usually produce a diffusely – altered inhomogenous echotexture, but distinct nodular enlargement cannot be differentiated from the surrounding gland (Fig. 5). Residual urine and bladder volume can be measured by the same formula used for estimating prostatic size (volume=0.52 x d1 x d2 X d3. Upper tract changes secondary to BPH are best evaluated using abdominal US. TRUS provides the best cross-sectional anatomy of the prostate and it is more accurate than transabdominal US to assess volume of the prostate and adenoma. BPH has a varied echotexture but is usually homogenous solitary or multiple adenomas (hyperplastic nodules) may be imaged, confined or extending outwards from the central gland often compressing the peripheral zone (Fig. 10). Although symmetry is the rule asymmetrical increase in size, especially near the bladder neck are common. Cysts, calcifications, prostatitis, infarctions and carcinoma may be coincident with BPH. The thick surgical capsule interposed between the central and peripheral gland can be appreciated. (Naryan & Foster, 1991).

5.5 Prostatic cancer

Carcinoma of the prostate is the most common human cancer, found at autopsy in 30% of men at age 50, 60% of men at age 80 – 90 up to 100% in those over age 90. It is now the second most common cancer in men. Pathological evidence of prostate cancer is found in 10-20% of patients undergoing surgery for BPH. 68% of prostatic carcinomas originate in the PZ, 24% in the TZ, and 8% in the CZ. Carcinoma of the prostate is often adenocarcinoma with varying grades of differentiation in 95% (Mc Neal, 1983). Unlike lung and colon cancer, prostatic cancer is predominantly latent. The patient may present with the symptoms and signs of prostatism and occasionally haematuria. It has been speculated that prostatic cancer disseminates first by invading into the periprostatic tissues, then by lymphatic embolization, and finally by hematogenous dissemination. Prostatic cancer can also spread by direct local invasion and through vascular and lymphatic channels. Seminal vesicle invasion almost always results from direct spread of the tumor into the ejaculatory duct while crossing inside and prostate. The primary field of lymphatic drainage of the prostate includes the perivesical, hypogastric, obturator, presacral and preciatic lymph nodes. The obturator nodes are the commonest site of involvement (Mc Laughlin et al., 1976). Osseous metastases are present in about 85 percent of patients dying of prostatic cancer. Osseous metastases involve the cancellous bone, altering the normal internal architecture with proliferating osteoblasts and new bone formation. The commonest sites for visceral metastases from prostatic cancer lung, liver and adrenal gland, but virtually any organ may be involved. Pulmonary metastases, occurring in 25 to 38 percent of patients dying of prostatic cancer. Metastases to the central nervous system usually occur in the meninges and may be clinically silent. Other neurogenic manifestations of prostatic cancer include organic brain syndrome, raduculopathy, and paraneoplastic syndromes (Jacobs, 1983).

5.5.1 Detection of prostate cancer

TRUS is useful for early detection of prostate cancer, guided biopsy, local staging, and follow up after treatment. Its role in screening of asymptomatic men is still controversial. (Clements et al., 1993).The first step in any sonographic examination of the prostate should be to gain an overall impression of the gland's shape and size. An irregular asymmetric

gland often signals malignancy even in the absence of the identifiable lesion. Even small prostatic cancer often alters the shape of the prostate. Distortion or bulging of the posterior boundary of the prostate is suggestive of the presence of cancer. Lateral distortion is of less significance because hyperplastic nodules of the TZ cause considerable asymmetric bulging. In advanced cancer, discontinuity of the capsule or seminal vesicles irregularity often can be seen (Shinohara et al.., 1989).

Prostate cancer has different echotexture; it may be hypoechoic, isoechpic or hyperechoic (Fig. 11). Most cancers consist of a dense mass of cells which destroys the normal glandular structure. The malignant tissue contains few sonographically detectable interfaces and therefore appears hyperechoic region in relation to the adjacent normal tissue. The most common feature of all visible cancer is a central hypoechoic region relative to the peripheral zone of the normal prostate. The margins of the tumor all ill defined as the malignant cells invade between normal prostatic acini (Shinohara et al., 1989). The hypoechoic tumors represent 70-75% of prostate tumors (Hamper & Sheth, 1993). Approximately 30-35% of clinically detected prostate cancer cannot be distinguished from the normal surrounding prostatic tissue and is termed isoechoic. Several features may contribute to cancer being undetectable by US: tumor size, grade, location, and stage, technique of the study, equipment used and the experience of the operator. Absence of the normal margin between the PZ and TZ in a rounded prostate should alert the sonographer to the possibility of a large infiltrating tumor. Also, a palpable abnormality in the presence of an apparently normal US scan should be biopsied to avoid missing an isoechoic cancer (Shabsigh et al., 1989). In case of presence of large adenoma of BPH, the PZ is compressed. So, it is less easy to detect a PZ cancer (Shinohara et al., 1989). Hyperechoic tumors are rare. Prostatic calculi that have been engulfed by cancer may account for a mixed echogenic pattern. Hyperechoic foci within the tumor correspond pathologically to comedonecrosis and calcification within highly undifferentiated anaplastic tumors or unusual deposits of intraluminal crystalloid secretions.

The sonographic appearance of early prostate cancer is not specific. The positive predictive value for a hypoechoic focal lesion to be cancer has ranged from 0% to 50%. Overall, the incidence of malignancy in US suspicious lesion is 20% to 255 (Hamper & Sheth, 1993). Information from US-guided biopsy of the prostate has shown that many suspicious areas seen on TRUS do not correspond to cancer: negative biopsy rated of 58 to 70.8% has been reported (Shabsigh et al., 1989). There is a big list of differential diagnosis of intraprostatic hypoechoic lesions. First anatomic structures as periurethral tissue, ejaculatory duct complex, periprostatic veins and neuovascular bundles. Second are benign prostatic diseases as hyperplastic nodule (stromal types), prostatitis, abscess, cysts and hematoma. Lastly sonographic artifacts as inappropriate use of the focal range of transducer, acoustic shadowing, reverberation artifacts and edge effect (Shinhara et al., 1989). Mc Neal and associates have emphasized the importance of measurement of the volume of prostate cancer as a determinant of pathologic stage and prognosis. They described a strong association between tumor volume and the incidence of extracapsular extension and lymph node metastases (Mc Neal et al., 1986). Estimation of tumor volume by TRUS is often inaccurate for two reasons. Tumor size is usually underestimated, as the tumor tends to infiltrate invade between normal prostatic tissues. So, the margin of the tumor may therefore be indistinguishable from normal prostate. Second is prostate cancer is often

multifocal. So, U.S underestimates the maximum diameter of a focus of cancer by an average of 4.2 mm (Shinohara et al., 1989).

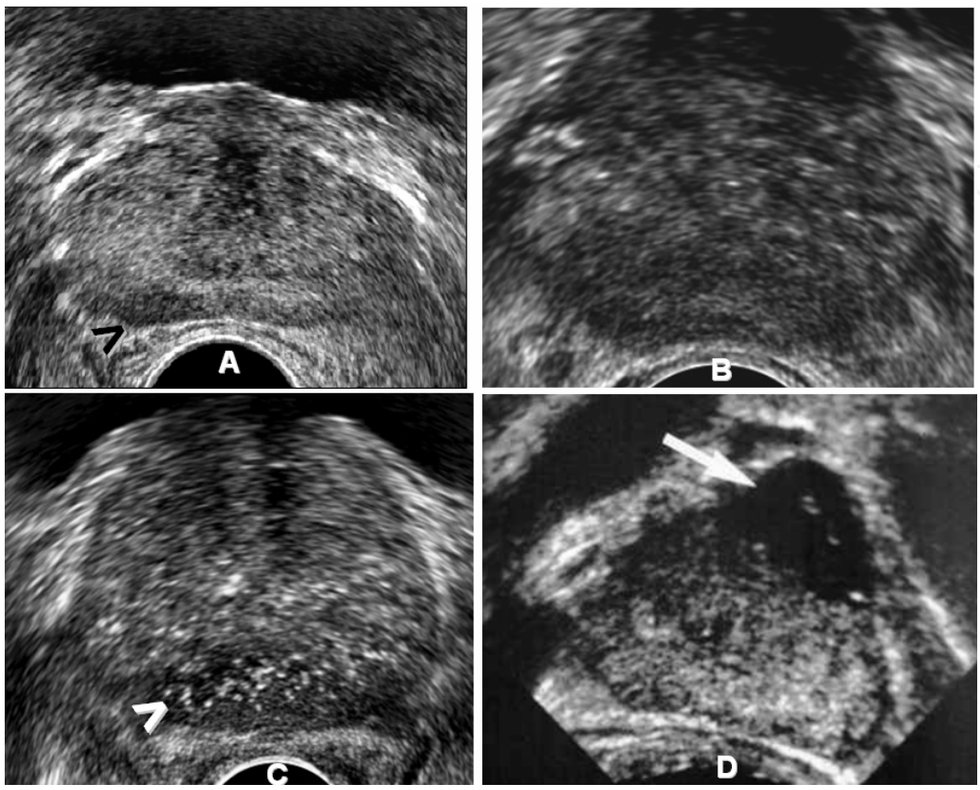

Fig. 11. TRUS of four different patients with prostate cancer. The carcinoma appears as focal hypoechoic area (arrow head) in the right PZ (A), diffuse hypoechogenicity of the whole gland (B), focal hyperechoic area (arrow head) in the posterior PZ (C) and focal hypoechoic area (arrow) in the central gland (D)

5.5.2 Extra capsular extension of prostate cancer

Prostate cancer spreads locally through pathways of least resistance. The areas of local spread include the invaginated extraprostatic area around the ejaculatory duct to the seminal vesicles, at the apex where the capsule is deficient, areas of capsule penetration by superior and inferior neurovascular bundles. The prostatic capsule usually cannot be distinguished sonographically from the prostatic parenchyma. Consequently, the continuos hyperechoic border around the normal prostate, (usually referred as the "capsule"), is actually represents the acoustic interface between the prostate and the periprostatic fat (Scardino et al., 1989). Sonographic signs of capsular penetration include bulge or irregularity of the prostate contour and disruption or discontinuity of the echogenic periprostatic boundary echo (Hamper & Sheth, 1993). Spread of the cancer to the neurovascular bundle is suspected if the tumor is close to the posterolateral aspect of the prostate with irregularity of the contour at this region as well as interruption of the echogenic periprostatic boundary echo. TRUS is able to detect neurovascular involvement with sensitivity of 66% and specificity of 78% (Fig. 12 and 13).

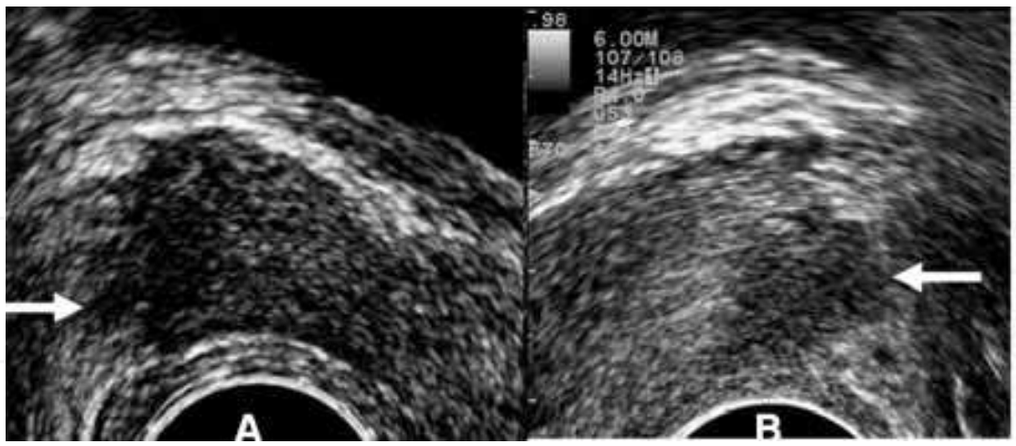

Fig. 12. Two different patients with right and left lateral extracapsular extension (arrows)

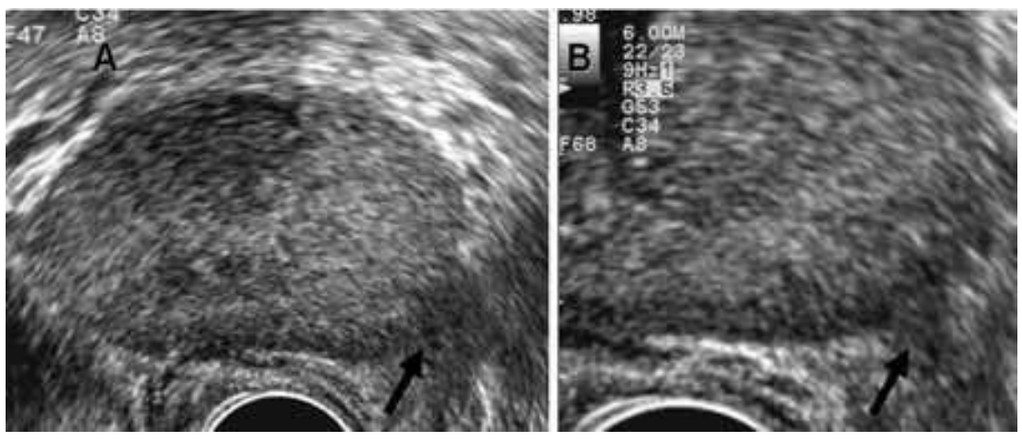

Fig. 13. A case of prostate cancer with left posterolateral extension through the neurovascular bundle (arrows)

The pattern and extent of seminal vesicle invasion vary widely. Type I is the most common pattern. It shows invasion along the ejaculatory ducts into the seminal vesicle. Type II is the second most common pattern. The invasion of seminal vesicle occurs from a tumor that penetrates the capsule and invades the seminal vesicles in continuity. Type III is the least common pattern, where small isolated foci of tumor in the seminal vesicles. The sonographic criteria for seminal vesicles invasion have traditionally been described as asymmetry in size, irregularity in outline, atrophy and distension, but the validity of these signs has rarely been substantiated by surgical or pathological staging (Shinohora et al., 1988). The accuracy of detection seminal vesicle invasion using sonography is 86% (Terries et al., 1990). The apex of the prostate must be carefully assessed sonographically to detect involvement of the rhamoboid area. This area bounded by the prostate proximally, the rectourethralis muscle distally, the membranous urethra anteriorly and the rectum posteriorly. It is best demonstrated by TRUS on the sagittal view. TRUS has no role in nodal staging. Also, it had limited role in detection of invasion of neighboring tissue, e.g. bladder, rectum and muscles of the pelvic side wall. These disadvantages of TRUS can be explained by its limited field of view (Scardino et al., 1989).

5.5.3 Response to treatment of prostate cancer

After treatment by ochidectomy and hormonal therapy, the gland becomes smaller and assumes a more circular shape. Most of the decrease in volume occurred within the first three months. A variable series of changes in the US appearance of the gland may be seen. In some patients, the area of abnormal echogenicity may persist. In others, it disappears. The integrity of the capsule may appear to be resorted in patients with previous capsule breech. It may be extremely difficult to demonstrate U.S whether the active cancer is still present or not (Clements et al., 1989). Following radiotherapy for cancer, the prostate becomes small and echogenic. Anechoic or hypoechoic lesions following radiotherapy frequently represent persistent cancer and the positive predictive value of such lesions for cancer is 91%. Most foci of cancer with marked radiation effect tend to be isoechoic. The non malignant prostate tissue generally retains its normal echogenic appearance after irradiation. Lesions over 5mm in the diameter persisting for 12 months following radiotherapy are suspicious of malignancy and should be biopsied (Egawa et al., 1991). A decrease in total prostate volume is not a reliable indicator of prognosis as normal and malignant prostatic tissue will shrink in response to radiotherapy. Measuring PSA is probably more useful in the follow up of the prostate cancer (Richards, 1992). After radical retropubic prostatectomy (for clinically non invasive prostatic cancer), the patients are routinely followed up at periodic interval with DRE and measuring PSA. Elevation of PSA above the female range indicates either local progression, recurrence of distant metastases. Post-operative mature fibrotic tissue at the site of operation is difficult of distinguish form recurrent tumors by means of TRUS. The main value of TRUS in case of presence of post operative palapable mass may be in accurate positioning of the biopsy needle about the vesico-urethral anastomosis (Wasserman et., 1992).

6. Ultrasound guided prostatic biopsy

The most important role for TRUS is to provide visual guidance for biopsy. Approximately 25% to 30% of cancers are isoechoic, random biopsies of the PZ, in addition to sampling all suspicious lesions should be done. In the technique of random prostatic biopsies, multiple samples are taken from different parts of the gland mainly apex, mid gland and base bilaterally (Hamper & Sheth 1993). In general, TRUS guided prostate needle biopsy should be performed in men with an abnormal DRE, an elevated PSA (>4.0 ng/ ml) or PSA velocity (rate of PSA change) >0.4 to 0.75ng/ ml/ yr. Also, men who were diagnosed with high-grade prostatic intraepithelial neoplasia (PIN) or atypia on a previous prostate needle biopsy should undergo a repeat biopsy 3 to 12 months later. Less commonly agreed upon recommendations for TRUS guided prostate needle biopsy include, age-specifi c PSA elevation, low percentage free PSA (< 22% to 25%), and prostate specifi c antigen density (PSAD) > 0.15, which is a measure of the amount of PSA relative to the overall prostatic volume (Hamper & Sheth 1993).US- guided prostate biopsies can be performed either transperineally or transrectally.

Transperineal approach is the first way described for US-guided prostate biopsy in 1981. The probe is fixed to a stabilizing biopsy stand. The perineum should be infiltrated local anesthetic. The entire gland is inspected and once a suspected area is identified, the biopsy needle is inserted and the track of the needle is monitored on the viewing screen. When the

needle tip approaches the area to be biopsied, the needle is positioned so that the cutting section can be passed through the abnormal area under visual guidance (Muldoon & Resnick, 1989). The drawbacks of transperineal U.S guided biopsy are difficult needle due to relatively long transperineal needle path, it is time consuming procedure, and patients tolerate the procedure poorly because of perineal pain and side effects of local anaesthesia. (Clements et al., 1993). Transperineal approach is preferable if prostate abscess or inflammatory disease is suspected.

Transrecta approach was first described in 1987, since then, this technique has been described as a superior method of performing a core biopsy of the prostate (Weaver et al., 1991). The transrectal approach offers the advantage of a shorter needle with easier needle placement, and quicker and relatively painless procedure. Local anesthesia is not required and it is done on an out-patients basic (Clements et al,. 1993). Hodge et al reported that systematic sampling of the prostate guided by TRUS improved the detection rate of prostate cancer over merely sampling hypoechoic or other lesions. By taking sextant biopsies from the mid lobe (parasagittal) of each side of the prostate at the apex, middle, and base (Fig. 14), the cancer detection rate was superior to lesion-directed biopsies (Hodge et al., 1989). This technique was accepted over the time as the standard of care and helped to emphasize that TRUS was more useful for biopsy than for imaging. In the current PSA era, though, most men who are undergoing prostate biopsy do not have palpable abnormalities or hypoechoic lesions This has lead investigators to question the sampling adequacy of the standard sextant prostate biopsy template and to propose alternate "extended pattern" biopsy schemes to improve prostate cancer detection. The alternate prostate biopsy templates aim to improve sampling of the prostate by either increasing the number of core biopsies taken and/ or by directing the biopsies more laterally to better sample the anterior horn (Chen et al, 1999, Naughton et al., 2000). During biopsy, the puncture path is shown on the monitor as electric dotted line. The probe should be positioned so that the puncture path passes through the designated area. Without moving the probe, the needle is introduced through the needle guide and the needle tip is positioned proximal to the suspicious area. A trigger action biopsy gun is used to obtain a core specimen in an instance once the biopsy needle in place. The biopsies performed while the biopsy needle is directed parallel to the transducer in the sagittal plane so the needle seen as an echogenic linear structure approaching the suspicious area, instead of an echogenic dot in the axial plane (Lee et al., 1988).

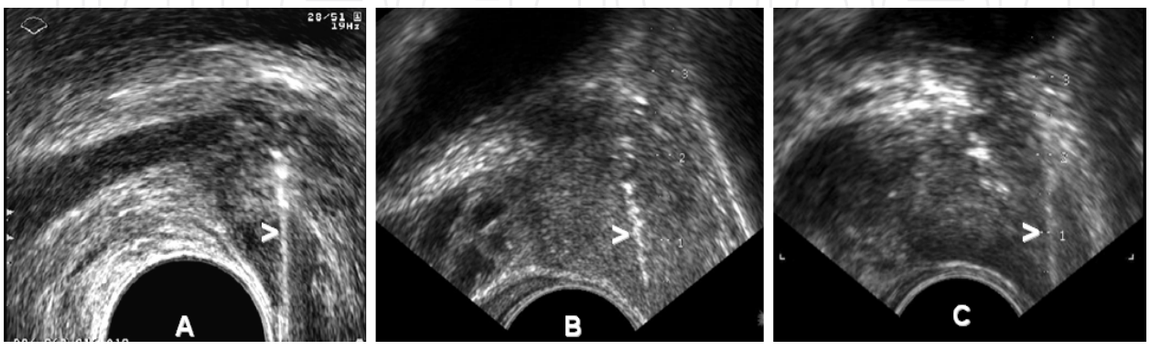

Fig. 14. Systematic TRUS –guided biopsy of the upper (A), middle (B) and lower (C) parts of the lateral regions peripheral zone (arrowheads)

7. Role of new ultrasound techniques in diagnosis of prostate cancer

Conventional gray-scale US has low sensitivity and specificity and is mainly used for guiding systematic prostate biopsies. With the development of new US techniques, such as three dimensional US color and power Doppler US, the use of US contrast agents and elastography, the role of US for prostate cancer detection has dramatically improved.

7.1 Three dimensional (3D) US of the prostate

It gives views of the prostate in the 3 orthogonal planes; sagital, transverse and coronal and in any other oblique planes (Fig. 15). The detection rates of prostate cancer were significantly improved with 3D- TRUS. Also it may improve the biopsy yield by determining appropriate sites for target and systematic biopsies (Cool et al., 2008, Shen et al., 2008). With 3D imaging, spatial relationships much clearer, so radiologist/ urologist can better assess the extent of disease. It may make it easier to determine whether the "prostate capsule" has been penetrated to detect possible extra-capsular tumor extension which is a key factor in staging of prostate cancer. It provides valuable information to plan for alternative therapies, like radiotherapy of the prostate and robotic prostatectomy. The 3D images are saved and they can be reviewed as many times as needed. Diagnosis can be achieved by retrieving the saved images which is most convenient for the operator and patient, leading to faster patient turnaround (Liang et al., 2010, Bax et al., 2008).

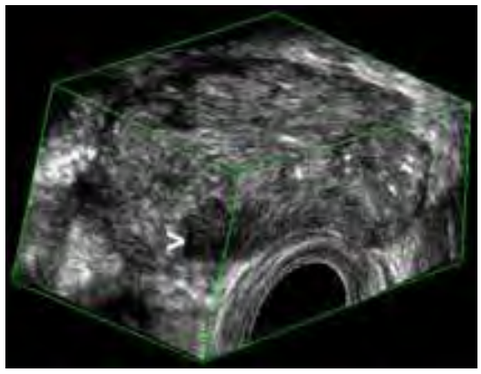

Fig. 15. 3D images of a prostate with cancer. The image has been 'sliced' to reveal a hypoechoic lesion in the right side of the PZ (arrowhead) proved to be a cancer

7.2 Color Doppler sonography of the prostate

Color Doppler TRUS (CD-TRUS) has been applied to evaluate the vascularity within the prostate and the surrounding structures. Preliminary studies demonstrated increased flow within or surrounding prostate neoplasm, whereas prostatitis and BPH showed a diffusely abnormal flow.However, the flow of focal prostatitis was not significantly different from cancer. By using objective measures, as resistive indices, no statistically significant difference was found between cancer and benign conditions (Rifkin et al, 1993). CD-TRUS may help in determining the site of biopsy. If the level of PSA is elevated with DRE normal in one patient, the presence of hypervascular focal lesion in PZ makes the lesion the target of the biopsy. But, if the nodule is hypovascular, we have to biopsy the anterior part of the gland to detect carcinoma of the TZ. (Cornud et al., 1993). Early results have suggested that up to 85% of men with prostate cancers greater than 5 mm in size have visibly increased

flow in the area of tumor involvement. In addition, hypervascularity may be seen in patients with more difficult to identify, isoechoic and hyperechoic lesions (Fig. 16). Unfortunately, subsequent studies suggested that some prostate cancers are hypovascular. Many studies prove the benefits of CD-TRUS for the evaluation of prostatic disease, especially carcinoma. The motivation behind the application of color Doppler US is to detect tumor neovascularity. Cancerous tissue generally grows more rapidly than normal tissue and demonstrates increased blood flow; as compared to normal tissue and benign lesions. Color Doppler US may demonstrate an increased number of visualized vessels, as well as an increase in flow rate, size and irregularity of vessels within prostate cancer (Newman et al., 1995 Littrup et al., 1995, Ismail et al., 1997)

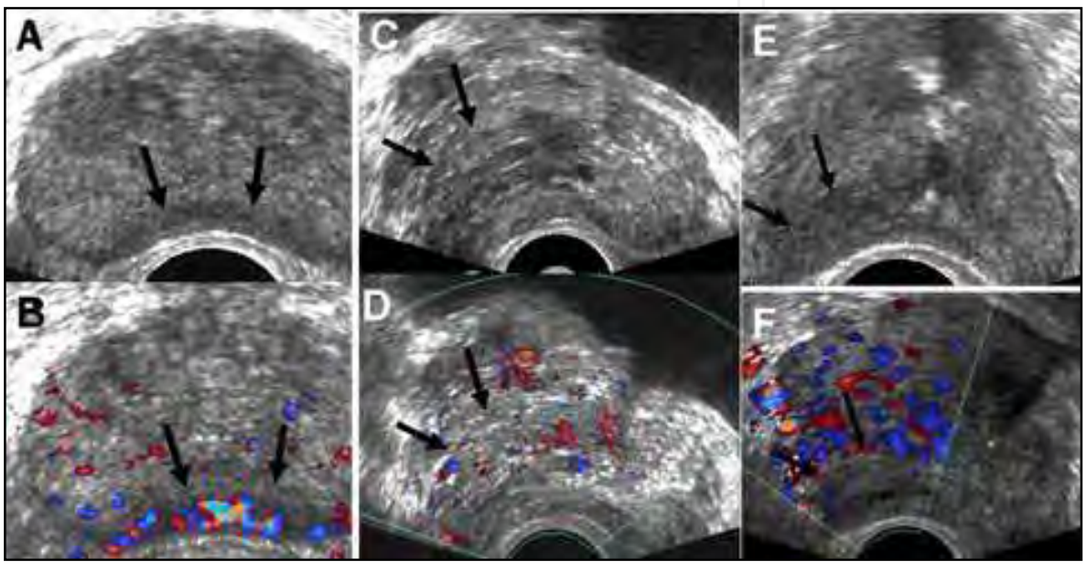

Fig. 16. (A) TRUS shows hypoechoic areas proved to be cancer (arrows). (B) Color-Doppler shows the same area to be of high vascularity (arrows). (C) TRUS of another patient with prostate cancer appears as hypoechoic area (arrows). (D) The same area appears with normal vascularity in color Doppler. (E) TRUS of a third patient with hypoechoic lesion of prostate cancer appears as hypoechoic (arrows). (F) The same lesion appears of low vascularity in color Doppler

7.3 Power Doppler sonography of the prostate

Power Doppler US is an amplitude-based technique for the detection of flow. It is more sensitive to slow flow and is less angle-dependent than color Doppler US. This technique has been less commonly applied to the assessment of prostate tumor vascularity, and there are few papers addressing its use. Some studies showed that prostate cancer are hypervascular by power Doppler (Fig. 17) so it may be useful in detection of prostate cancer (Inahara et al., 2004). Halpern et al assessed the value of gray-scale, color and power Doppler US for detection of prostatic cancer. They investigated 251 patients prior to biopsy and they hey concluded that power Doppler may be useful for targeted biopsies when the number of biopsy passes must be limited but that there is no substantial advantage of power Doppler over color Doppler (Halpern et al., 2000).

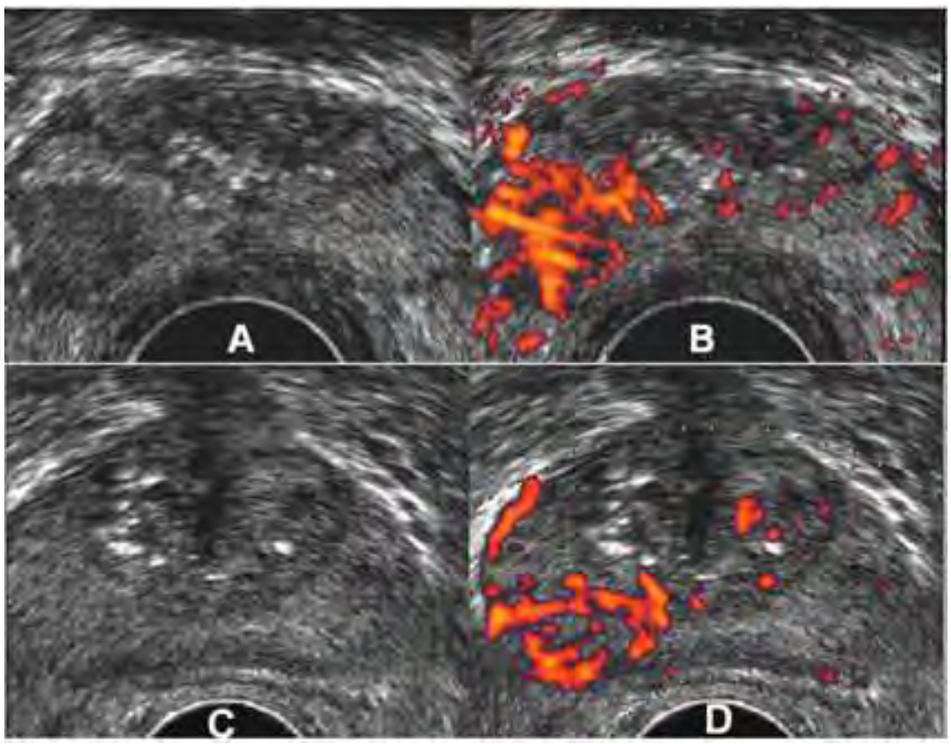

Fig. 17. (A) TRUS show a hypoechoic lesion in the right posterolateral aspect of the peripheral zone proved to be cancer. (B) The same area is hypervascular in power Doppler (C) TRUS in another patient with prostate cancer shows no evident focal lesion in grey scale US. (D) Power Doppler of the same patient show focal area of increased vascularity in the right side of the peripheral zone proved to be carcinoma by targeted biopsy

7.4 Contrast enhanced ultrasound imaging

Recently developed US contrast agents can improve the detection of low-volume blood flow by increasing the signal-to-noise ratio. Unlike radiographic contrast media, which diffuse into the tissue and may obscure smaller vessels, microbubble echo-enhancing agents are confined to the vascular lumen, where they persist until they dissolve. They have two important acoustic properties, first, they are many times more reflective than blood, thus improving flow detection. Second, their vibrations generate higher harmonics to a much greater degree than surrounding tissues (Forsberg et al, 1998). Bree RL and De Dreu SE showed that contrast enhanced color Doppler US had a sensitivity of 53%, specificity of 72%, and a positive predictive value of 70% in distinguishing prostate cancer from benign lesions in 72 patients identified by PSA screening (Bree RL & DeDreeu SE,1998). Most investigators showed increased sensitivity in detection of prostate cancer after the use of contrast enhanced US (Fig. 20). In the study of Bogers et al, they showed that sensitivity of enhanced images was 85% (specificity 80%) compared with 38% for unenhanced images (specificity 80%) and 77% for conventional gray-scale transrectal US (specificity 60%) (Bogers et al., 1999). Frauscher et al reported the value of contrast enhanced color Doppler in a prospective study in 90, and 230 male screening volunteers (Frauscher et al., 2001, 2002). They found that targeted biopsies based on contrast enhanced color Doppler detected as many cancers as

systematic biopsies, with fewer than half the number of biopsy cores. Halpern et al, in their prospective study of contrast-enhanced transrectal US in 60 patients who underwent sextant biopsy of the prostate concluded that the sensitivity increased from 38% at baseline to 65% after contrast injection (Fig. 18). However there was no significant change of specificity between baseline study (83%) and during contrast aging (80%) in the same study (Halpern et al., 2001).

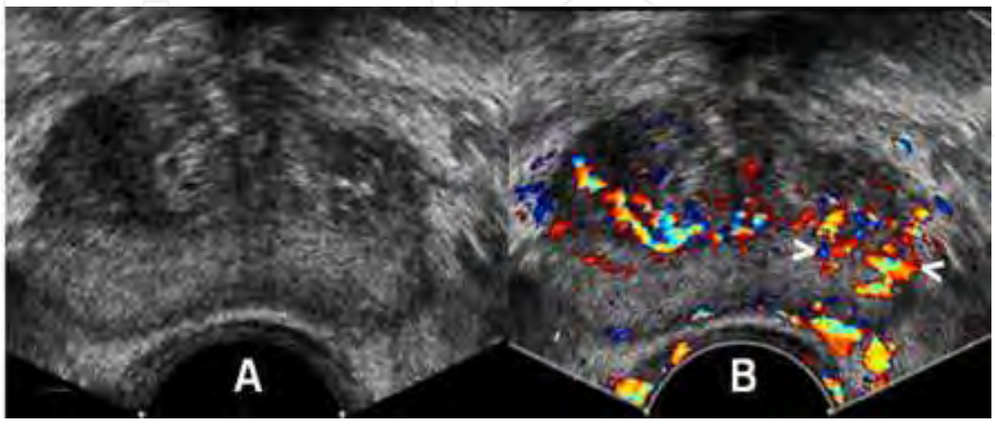

Fig. 18. (A) TRUS of a patient with prostate cancer show no evident focal lesions in grey scale US. (B) Contrast enhanced TRUS shows focal area of hypervascularity in the left side of the peripheral zone (arrowheads) proved to be carcinoma by targeted biopsy

7.5 Elastography of the prostate

Elastography or strain imaging was first described in 1991 (Ophir et al., 1991). This technique can be used to detect degree of stiffness of the tissues. In a pilot study done by Klauser et al, patients with clinically localized prostate cancer who underwent radical prostatectomy were examined prospectively. They found that elastography detected 28 of 32 cancer foci (sensitivity 88%) and they concluded that elastography is a sensitive new imaging modality for the detection of prostate cancer (Klauser et al., 2003). Konig et al. evaluated elastography for biopsy guidance for prostate cancer detection in 404 men underwent systematic sextant biopsy. They found that in 127 of the cancer proved 151 cases (84.1%), prostate cancer was detected using elastography as an additional diagnostic feature. They concluded that it is possible to detect prostate cancer with a high degree of sensitivity using real-time elastography in conjunction with conventional diagnostic methods for guided prostate biopsies (Konig et al., 2005). Supersonic shear imaging (SSI) is a new US-based technique for real-time visualization of soft tissue elastographic properties. Using ultrasonic focused beams, it is possible to remotely generate mechanical vibration sources radiating low-frequency, shear waves inside tissues (Bercoff et al., 2004). Athanasiou et al studied quantitative ultrasonographic elastography of breast lesions in 46 women. They concluded that SSI provides quantitative elasticity measurements, thus adding complementary information that potentially could help in breast lesion characterization with B-mode US (Athanasiou et al., 2010). Recently a preliminary study by Correas et al done to evaluated the feasibility of TRUS quantitative Shear Wave Elastography (SWE) for prostate cancer evaluation in 21 patients presenting with increased PSA values (Fig. 19). Elasticity measurements and ratios between nodules and adjacent parenchyma were

calculated. They found that signals were obtained in both the peripheral and the transition zones with good correlation to anatomical areas, macro-calcifications exhibited very high stiffness values and prostate cancer nodules exhibited a high stiffness than the adjacent peripheral gland. Also they noticed that peripheral adenomatous hyperplasia and focal prostatitis exhibited a significantly lower stiffness. They concluded that TRUS quantitative SWE is a feasible technique for prostate cancer evaluation. It provides additional information about stiffness of nodules localized in the peripheral zone (Correas et al., 2011). These preliminary results are encouraging but a larger multicentric evaluation remains necessary.

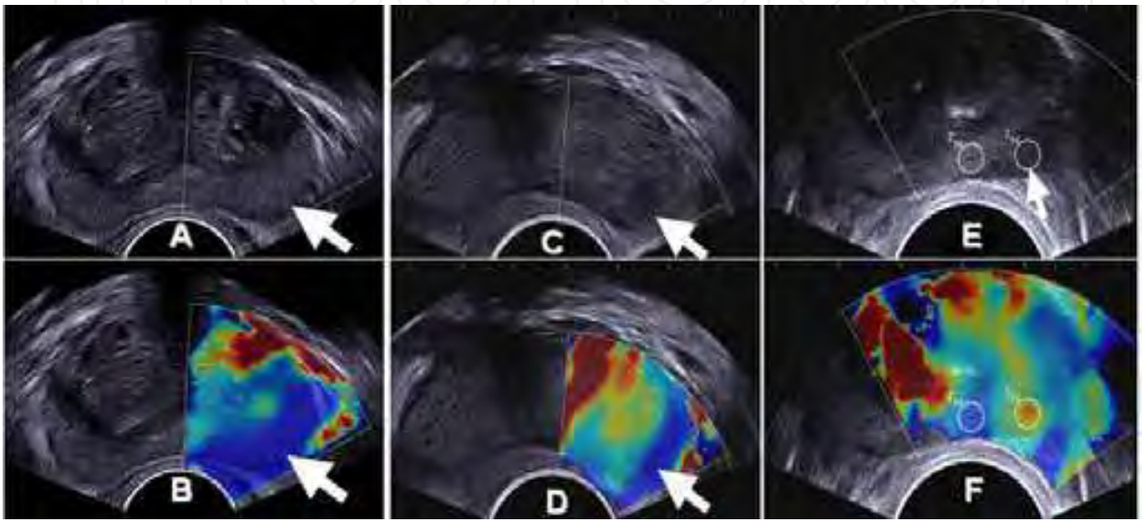

Fig. 19. (A) TRUS of a normal homogeneous PZ. (B).TRUS-SWE shows homogeneous blue coding of PZ (arrow) indicating its soft texture. (B) TRUS of another patient shows a hypoechoic area in left PZ proved to be carcinoma (atypical pattern). (D) TRUS-SWE of the same patient shows the focal area has blue coding (arrow) indicating its soft texture. (E) TRUS of another patient with a hypoechoic nodule in the left PZ proved to be carcinoma (arrow). (F) TRUS-SWE of the same patient shows a strong increase in stiffness values of the focal area (red) with a ratio of 2.8 compared to the surrounding PZ (typical pattern) (adapted from Correas et al 2011)

8. Role of ultrasound in prostate cancer treatment

Recent interest in focal therapy for localized prostate cancer has been driven by downward stage migration, improved biopsy and imaging techniques. Several techniques have potential for focal ablation of prostate cancer.

8.1 TRUS-guided cryotherapy for prostate cancer

Cryotherapy is tissue ablation by local induction of extremely cold temperatures. The first use cryoablation in urological disorders started in the 1960s for management of benign prostatic hyperplastic tissue (Gonder et al., 1966). This was followed shortly thereafter by the treatment of prostate cancer via an open perineal approach (Fig. 20). The major impediment to early acceptance of the modality, however, was the inability to accurately

monitor cryoprobe placement and ice-ball formation. Major advances in the past 20 years, which have reinvigorated investigation into the use of cryotherapy for prostate cancer, have included the use of TRUS monitoring of probe placement and freezing (Onil et al,1993). A significant recent development was the introduction of cryotherapy probes that use argon gas rather than liquid nitrogen (De La Taille et al., 2000). Outcomes have now been reported as late as 7 years following treatment of prostate cancer and seem to compare favorably with contemporary series of patients who receive radiation therapy (Bahn et al., 2002). Marberger et al reported that cryotherapy has been used for some time as a form of first-line therapy for complete ablation of the prostate or and as a second-line therapy for local recurrence after radiotherapy (Marberger et al., 2008).

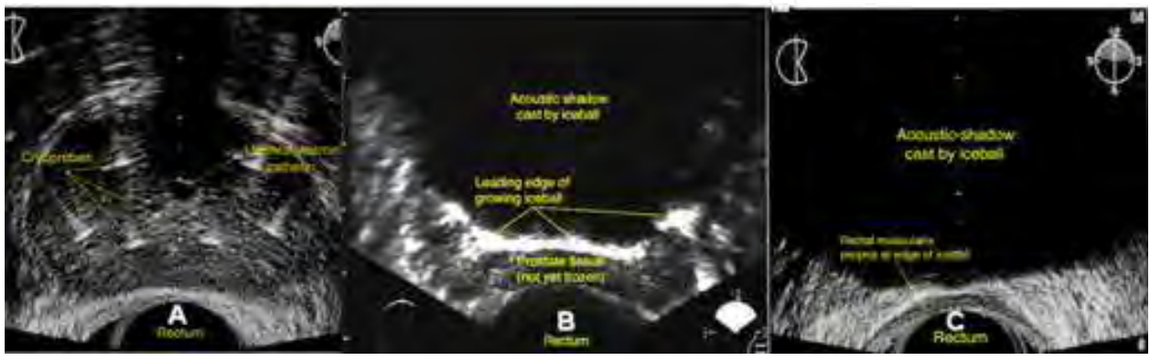

Fig. 20. (A) TRUS of the prostate illustrating placement of the cryoprobes and urethral-warming catheter. (B) TRUS of the prostate during cryoablation showing the ice ball, growing posteriorly, is echodense and casts a dark acoustic shadow. (C) The ice ball extends posteriorly to include the whole prostate tissue. Transrectal sonogram of the prostate illustrating placement of the cryoprobes and urethral-warming catheter

8.2 High-intensity focused ultrasound (HIFU)

HIFU is one of the newer methods that have been developed to treat early stage prostate cancers. High energy is delivered to the affected area by ultrasound, this result in the targeted cancerous cells heating up and being destroyed. Using extracorporeal HIFU, temperatures of greater than 60°C can be achieved in the target tissue. The prostate can be easily treated with this modality via a transrectal probe. Gelet et al pioneered the use of transrectal HIFU in the treatment of localized prostate cancer. Prostates smaller than 40 mL or those with an anteroposterior diameter of less than 5 cm are best suited for this treatment. During the procedure, the whole gland is treated. They reported that 78% of low-risk patients were disease-free and had negative biopsy results at an actuarial 5-year follow-up (Gelet et al., 2004). Some of the advantages of HIFU are that it is able to be repeated if cancer reappears; it can destroy cancer in targeted areas of the prostate without destroying other areas of the prostate; and it can be given to patients who may not be able to take other forms of prostate treatment such as brachytherapy. Marberger et al reported that HIFU has been used widely in Europe for complete ablation of the prostate, especially in elderly men who are unwilling or unable to undergo radical therapy. For low- or intermediate-risk cancer, the short- and intermediate-term results have been acceptable. Focal use of HIFU should reduce the adverse sexual and urinary side effects of whole gland ablation (Marberger et al., 2008).

8.3 Vascular-targeted photodynamic therapy (VTFT)

VTFP is a minimally invasive ablative treatment for localized prostate cancer and may represent a preferred option for men with low-risk disease who want to balance the risks and benefits of treatment. (Lepor, 2008). VTPT has been used for whole gland ablation of locally recurrent cancer after radiotherapy and for focal ablation of previously untreated cancer. In combination with a new, systemically administered photodynamic agent, laser light is delivered through fibers introduced into the prostate under TRUS. This technique does not heat the prostate but destroys the endothelial cells and cancer by activating the photodynamic agent. Damage to surrounding structures appears to be limited and can be controlled by the duration and intensity of the light. (Marberger et al., 2008).

8.4 TRUS-guided prostate brachytherapy

Brachytherapy is an effective treatment for localized prostate cancer with high patient tolerability and acceptable morbidity outcome data. It delivers a high dose of radiation to a small target volume of tissue, minimizing radiation side-effects to adjacent structures. Brachytherapy is an alternative to radical surgery and external beam radiotherapy and can be delivered in two different ways: permanent seed implants using iodine or palladium seeds or using temporary removable implants with iridium wires. TRUS is essential for accurate imaging guidance to place the radioactive sources into the prostate (Fig. 21). Prostate brachytherapy data has now matured as a treatment with consistent results reported from major centers in the US and Europe (Henry et al., 2010, Battermann et al., 2008).

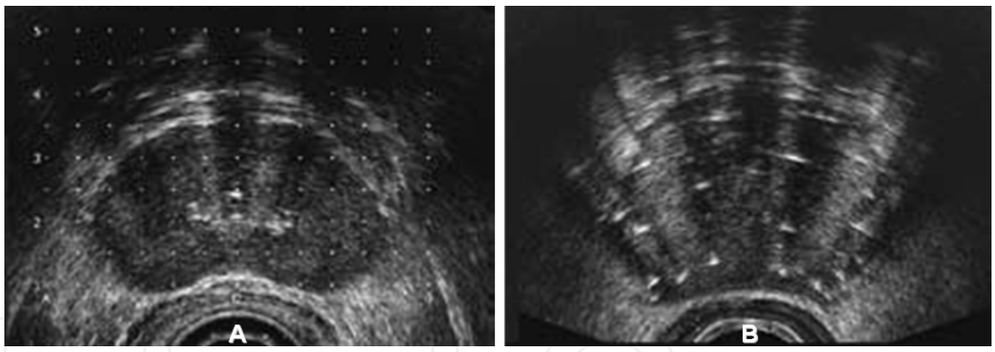

Fig. 21. Prostate brachytherapy. (A) Transrectal ultrasound set-up: transverse image of the prostate with 5mm template overlay. (B) Transverse image of the prostate after seed implant (echogenic areas)

9. Conclusion

One of the major advances that have greatly improved our understanding of prostatic diseases is the development of sonography especially TRUS. It is considered the first imaging modality in diagnosis of prostate diseases. Improvement of the application of the new advances in US for the detection and clinical staging of prostate cancer is promising. TRUS-guided procedures are now widely used in diagnosis and treatment of prostate cancer. Radiologists and urologists should be well trained in the application of these new US techniques and should therefore play an important role in the management of prostate cancer in the future.

10. References

Abou Yousef M M and Naryana AS (1982). Tran rectal ultrasound in the evaluation of the prostatic size. J. Clin ultrasound. 10: 275-278.

Athanasiou A, Tardivon A, Tanter M, Sigal-Zafrani B, Bercoff J, Deffieux T, Gennisson JL, Fink M, Neuenschwander S (2010). Breast lesions: quantitative elastography with supersonic shear imaging--preliminary results. Radiology. Jul; 256(1):297-303.

Babaian RJ, Toi A, Kamoi K, Troncoso P, Sweet J, Evans R, Johnston D, Chen M. (2000). A comparative analysis of sextant and an extended 11-core multisite directed biopsy strategy. JUrol; 163:152-157.

Bahn DK, Lee F, Badalament R, Kumar A, Greski J, Chernick M (2002). Targeted cryoablation of the prostate: 7-year outcomes in the primary treatment of prostate cancer. Urology Aug; 60(2 Suppl 1):3-11.

Battermann J, Boon T, Moerland M (2004). Results of permanent prostate brachytherapy, 13 years of experience at a single institution Radiother Oncol; 71:23-28

Benson MC, Whang IS, Pantuck A, Ring K, Kaplan SA, Olsson CA, et al (1992). Prostate specific antigen density: a means of distinguishing benign prostatic hypertrophy and prostate cancer. JUrol; 147:815-9.

Bax J, Cool D, Gardi L, Knight K, Smith D, Montreuil J, Sherebrin S, Romagnoli C, Fenster A (2008). Mechanically assisted 3D ultrasound guided prostate biopsy system. Med Phys. Dec ;35(12):5397-410.

Bercoff J, Tanter M, Fink M (2004). Supersonic shear imaging: a new technique for soft tissue elasticity mapping. IEEE Trans Ultrason Ferroelectr Freq Control. Apr;51(4):396-409

Bogers HA, Sedelaar JP, Beerlage HP, de la Rosette JJ, Debruyne FM, Wijkstra H, Aarnink RG (1999). Contrast enhanced three-dimensional power Doppler angiography of the human prostate: correlation with biopsy outcome. Urology; 54: 97–104.

Brandes D. (1984) prostate gland embryology, anatomy and histology. In: G. Hills. Uropathology. Chirchill, Livingstone, New York; 1165-1180.

Bree RL, De Dreu SE (1998). Contrast enhanced color Doppler of the prostate as an adjunct to gray-scale identification of cancer prior to biopsy. Radiology; 209: 418.

Correas1 J.-M., KHAIROUNE A., Tissier A.-M, Vassiliu V., EISS D., Hélénon O (2011). Trans-rectal quantitative Shear Wave Elastrography: application to prostate cancer - A feasibility study.Poster No.: C-1748 Congress: ECR 2011.

Chen ME, Troncoso P, Tang K, Babaian RJ, Johnston D (1999). Comparison of prostate biopsy schemes by computer simulation. Urology; 53:951-960.

Clements R, Gower TK, Griffeth GT, Peeling WB (1993) Transrectal ultrasound appearance of granulomatous prostatitis. Clinc. Radiol; 47: 174-176.

Gonder MJ, Soanes WA, Shulman S (1966). Cryosurgical treatment of the prostate. Invest Urol. Jan; 3(4):372-8

Cool D, Sherebrin S, Izawa J, Chin J, Fenster A (2008). Design and evaluation of a 3D transrectal ultrasound prostate biopsy system. Med Phys. Oct; 35(10):4695-707.

Cornud F, Belin X, Fromont G. (1993). Prostate normale. In: Imaging de la prostate, H. Nahum ed. Medecine – Sciences Flammavior, Paris; 3-18.

Delmas V, Dauge MC (1991). Embryology of the prostate- current state of knowledge. In: Khoury S CC, Murphy G, Denis L, ed. Prostate cancer in questions. Edinburgh, UK: ICI publications;16-17.

De La Taille A, Benson MC, Bagiella E, Burchardt M, Shabsigh A, Olsson CA, et al (2000). Cryoablation for clinically localized prostate cancer using an argon-based system: complication rates and biochemical recurrence. BJU Int. Feb; 85(3):281-6.

Doble A, Carter SS. (1989) Ultrasonographic findings in prostatitis. Urol Clinc. North Am; 18, 4.

Donkol, RH (2010). Imaging in male-factor obstructive infertility.World J Radiol 2(5):172-179.

Egawa S, Wheeler TM, Scardino PT (1991). The sonographic appearances of irradiated prostate cancer. Brit J. Urol; 172-177.

Forsberg F, Merton DA, Liu JB et al (1998). Clinical applications of ultrasound contrast agents. Ultrasonics; 36: 695–701.

Frauscher F, Klauser A, Halpern EJ, Horninger W, Bartsch G (2001). Detection of prostate cancer with a microbubble ultrasound contrast agent. Lancet; 357: 1849–50.

Frauscher F, Klauser A, Volgger H,Halpern EJ, Pallwein L, Steiner H, Schuster A, Horninger W, Rogatsch H, Bartsch G (2002). Comparison of contrast enhanced color Doppler targeted biopsy with conventional systematic biopsy: impact on prostate cancer detection. JUrol; 167: 1648–52.

Gelet A, Chapelon JY, Poissonnier L, Bouvier R, Rouvière O, Curiel L (2004). Local recurrence of prostate cancer after external beam radiotherapy: early experience of salvage therapy using high-intensity focused ultrasonography. Urology.Apr;63 (4):625-629.

Giffiths GJ, Grooks AJR, Roberts EE, Evans KT, Buck AC, Thomas PJ, Peeling WB (1984) Ultrasonic appearance associated with prostatic inflammation: a preliminary study. Clinc Radiol., 35 : 343- 345.

Hammerer PG, McNeal JE, Stamey TA (1995). Correlation between serum prostate specific antigen levels and the volume of the individual glandular zones of the human prostate. JUrol ;153:111- 114.

Halpern EJ, Rosenberg M, Gomolla LG (2001). Contrast enhanced sonography of the prostate. Radiology; 219: 219–25.

Hamper UM, Sheth S (1993). Prostate ultrasonography. Semin roentg; 28, 1: 57 – 73.

Henry AM, Al-Qaisieh B, Gould K, Bownes P, Smith J, Carey B, Bottomley D, Ash D (2010). Outcomes following iodine-125 monotherapy for localized prostate cancer: the results of leeds 10-year single-center brachytherapy experience. Int J Radiat Oncol Biol Phys. Jan 1; 76(1):50-56.

Hodge KK, McNeal JE, Terris MK, Stamey TA (1989). Random systematic versus directed ultrasound guided transrectal core biopsies of the prostate. JUrol ;142:71-75.

Hricak H (1990). The prostate gland. In: Hricak H, Carrington BM (eds.). MRI of the pelvis. A text atlas. California Martin Dunitz:

Inahara M, Suzuki H, Nakamachi H, Kamiya N, Shimbo M, Komiya A, Ueda T, Ichikawa T, Akakura K, Ito H (2004). Clinical evaluation of transrectal power doppler imaging in the detection of prostate cancer. Int Urol Nephrol ;36(2):175-80.

Ismail M, Petersen RO, Alexander AA, Newschaffer C, Gomella LG (1997). Color Doppler imaging in predicting the biologic behavior of prostate cancer: correlation with disease-free survival. Urology; 50: 906–12.

Jacobs S, C (1983). Spread of prostatic cancer to bone. Urology 21 : 337.

Klauser A, Koppelstaetter F, Berger AP, Horninger W,Lorenz A, Frauscher F (2003). Real-time elastography for prostate cancer detection: preliminary experience. Radiology; 229 (Suppl): 1395

Konig K, Scheipers U, Pesavento A, Lorenz A, Ermert H,Senge T (2005). Initial experiences with real-time elastography guided biopsies of the prostate. JUrol; 174: 115–17.

Lee F, Littrup PJ, Torp-Pedersen ST, Mettlin C, McHugh TA, Gray JM, Kumasaka GH, McLeary RD (1988) Prostate cancer: Comparison of transrectal US and digital rectal examination for screening. Radiology; 168 : 389- 394.

Lepor H (2008).Vascular targeted photodynamic therapy for localized prostate cancer.Rev Urol. fall; 10(4): 254–261.

Liang K, Rogers AJ, Light ED, Von Allmen D, Smith SW (2010). Simulation of autonomous robotic multiple-core biopsy by 3D ultrasound guidance. Ultrason Imaging. Apr; 32(2):118-27.

Littrup PJ, Klein RM, Gross ML, Sparschu RA, Segel MC, Zingas AP (1995). Color Doppler of the prostate: histologic and racial correlations. Radiology; 197: 365

Lowsley OS (1912). The development of human prostate gland with reference to the development of other structures of the neck of the urinary bladder. Am JAnat, 13: 299-349.

Marberger M, Carroll PR, Zelefsky MJ, Coleman JA, Hricak H, Scardino PT, Abenhaim LL (2008). New treatments for localized prostate cancer. Urology. Dec;72(6 Suppl):S36-43.

Mc Langhin AP, Saltzstein SL McCullough, DL and Gittes RF (1976) prostatic carcinoma: Incidence location of unsuspected lymphatic metastasis. J. Urol. 115 – 89.

Mc Neal JE (1968). Regional morphology and pathology of the prostate. Am J Clinc Pathol, 49: 347 – 357.

Mc Neal JE (1983). The prostate gland; morphology and pathology. Monogr. Urol., 4: 5 -13.

Mc Neal JE (1988). Normal anatomy of the prostate and changes in benign prostatic hypertrophy and carcinoma. Semin US CT, MRI, 9: 329 -334.

Muldoon L and Resnick Ml. Result of ultrasonography of the prostate (1989). Urol Clinc North Am, 16, 4: 693 – 701.

Myers RP, Geollner JR, Cahil DR (1987) Prostate shape, external striated urethral sphincter and radical prostatectomy: The apical dissection. JUrol, 138: 543-548.

Naughton CK, Miller DC, Mager DE, Ornstein DK, Catalona WJ (2000). A prospective randomized trial comparing 6 versus 12 prostate biopsy cores: impact on cancer detection. JUrol.; 164:388-392.

Naryan P, Foster L (1991). The rule of intravenous urography and magnetic resonance imaging in the evaluation of men with symptomatic benign prostatic hyperplasia. Probl urol, 5, 3: 369-379.

Newman JS, Bree RL, Rubin JM (1995). Prostate cancer: diagnosis with color Doppler sonography with histologic correlation of each biopsy site. Radiology; 195: 86–90.

Ophir J, Cespedes I, Ponnekanti H, Yazdi Y, Li X (1991). Elastography: a quantitative method for imaging the elasticity of biological tissues. Ultrason Imaging; 13:111–34.

Onik GM, Cohen JK, Reyes GD, Rubinsky B, Chang Z, Baust J (1993). Transrectal ultrasound-guided percutaneous radical cryosurgical ablation of the prostate. Cancer. Aug 15; 72(4):1291-9.

Patel U, Rickards D (2002). Handbook of Transrectal Ultrasound and Biopsy of the Prostate. Martin.Dunitz Ltd, London.

Richards D (1992). Transrectal ultrasound, 1992. Brit JUrol; 69, 449-465.

Rifkin MD, Dahnert W, Kurtz AB (1990). State of the art: endorectal sonography of the prostate gland. AJR; 154:691-700

Rifkin MD (1997). Ultrasound of the Prostate. 2nd edn.Philadelphia, PA: Lippincott-Raven.
Rifkin MD, Sudakoff GS, Alexander AA (1993). Prostate: techniques, results, and potential applications of color Doppler US scanning. Radiology; 186: 509–13.
Scardino PT, Shinohara K, Wheeler TM, Carter SS (1989). Staging of prostate cancer: Value of ultrasonography. Urol Clinc North AM; 16, 713-733.
Shabsigh R, Kadmon D, Fishman IJ (1989). Ultrasonographically guided transperineal prostate biopsy in patients with suspicious glands and previously negative digitally guided biopsies. J. Endourol., 3: 185.
Shen F, Shinohara K, Kumar D, Khemka A, Simoneau AR, Werahera PN, Li L, Guo Y, Narayanan R, Wei L, et al (2008). Three-dimensional sonography with needle tracking: role in diagnosis and treatment of prostate cancer. J Ultrasound Med. Jun; 27(6):895-905.
Shinohara K, Scardino PT, Carter ST, Wheeler TM (1989). Pathological basis of the sonographic appearance of the normal and malignant prostate. Urol Clinc North AM; 16, 4: 675-691.
Sohlberg OE, Chetner M, Ploch N, Brawer MK (1991). Prostatic abscess after transrectal ultrasound guided biopsy. J Urol; 146, 420-422.
Takahashi H, Ouchi T. The ultrasonic diagnosis in the field of urology (1963). Proc Jap Soc Ultrasonics Med; 3:7.
Terris MK, McNeal JE, Stamey TA (1990). Invasion of the seminal vesicles by prostatic cancer: Detection by transrctal sonography. AJR; 155; 811-815.
Terris MK, and Stamey TA (1991). Determination of prostatic volume by transrectal ultrasound. J Urol, 145: 984-987.
Wasserman NF, Kapoor DA, Hildebrandt WC, et al (1992) Transrectal ultrasound in evalaaution of patients after radical prostatectomy.Radiology; 185; 361-372.
Watanabe H, Igari D, Tanahasi Y, Harada K, Saito M. Development and application of new equipment for transrectal ultrasonography. J Clin Ultrasound. 1974; 2:91-98.
Weaver RP, Noble MJ, Weigle JW (1991). Correlation of ultrasound guided and digitally directed transrectal biopsies of palpable prostatic abnormalities. J Urol.; 145:516-518.

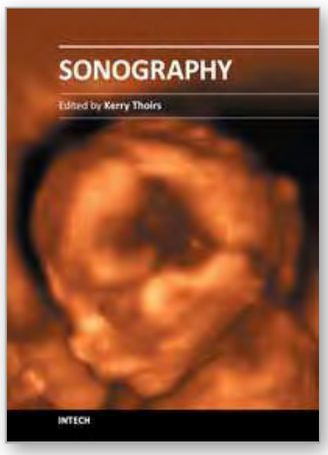

Sonography

Edited by Dr. Kerry Thoirs

ISBN 978-953-307-947-9
Hard cover, 346 pages
Publisher InTech
Published online 03, February, 2012
Published in print edition February, 2012

Medical sonography is a medical imaging modality used across many medical disciplines. Its use is growing, probably due to its relative low cost and easy accessibility. There are now many high quality ultrasound imaging systems available that are easily transportable, making it a diagnostic tool amenable for bedside and office scanning. This book includes applications of sonography that can be used across a number of medical disciplines including radiology, thoracic medicine, urology, rheumatology, obstetrics and fetal medicine and neurology. The book revisits established applications in medical sonography such as biliary, testicular and breast sonography and sonography in early pregnancy, and also outlines some interesting new and advanced applications of sonography.

How to reference

In order to correctly reference this scholarly work, feel free to copy and paste the following:

Ragab Hani Donkol and Ahmad Al Nammi (2012). Prostate, Sonography, Dr. Kerry Thoirs (Ed.), ISBN: 978-953-307-947-9, InTech, Available from: http://www.intechopen.com/books/sonography/prostate

INTECH
open science | open minds

InTech Europe
University Campus STeP Ri
Slavka Krautzeka 83/A
51000 Rijeka, Croatia
Phone: +385 (51) 770 447
Fax: +385 (51) 686 166
www.intechopen.com

InTech China
Unit 405, Office Block, Hotel Equatorial Shanghai
No.65, Yan An Road (West), Shanghai, 200040, China
中国上海市延安西路65号上海国际贵都大饭店办公楼405单元
Phone: +86-21-62489820
Fax: +86-21-62489821

IntechOpen

1

Sonography of the Scrotum

Chee-Wai Mak and Wen-Sheng Tzeng
Department of Medical Imaging, Chi Mei Medical Center, Tainan, Taiwan
Central Taiwan University of Science and Technology, Taichung, Taiwan
Chung Hwa University of Medical Technology, Tainan, Taiwan
Republic of China

1. Introduction

Although the development of new imaging modality such as computerized tomography and magnetic resonance imaging have open a new era for medical imaging, high resolution sonography remains as the initial imaging modality of choice for evaluation of scrotal disease. Many of the disease processes, such as testicular torsion, epididymo-orchitis, and intratesticular tumor, produce the common symptom of pain at presentation, and differentiation of these conditions and disorders is important for determining the appropriate treatment. High resolution ultrasound helps in better characterize some of the intrascrotal lesions, and suggest a more specific diagnosis, resulting in more appropriate treatments and avoiding unnecessary operation for some of the diseases.

2. Imaging technique

For any scrotal examination, thorough palpation of the scrotal contents and history taking should precede the sonographic examination. Patients are usually examined in the supine position with a towel draped over his thighs to support the scrotum. Warm gel should always be used because cold gel can elicit a cremasteric response resulting in thickening of the scrotal wall; hence a thorough examination is difficult to be performed. A high resolution, near-focused, linear array transducer with a frequency of 7.5 MHz or greater is often used because it provides increased resolutions of the scrotal contents. Images of both scrotum and bilateral inguinal regions are obtained in both transverse and longitudinal planes. Color Doppler and pulsed Doppler examination is subsequently performed, optimized to display low-flow velocities, to demonstrate blood flow in the testes and surrounding scrotal structures. In evaluation of acute scrotum, the asymptomatic side should be scanned first to ensure that the flow parameters are set appropriately. A transverse image including all or a portion of both testicles in the field of view is obtained to allow side-to-side comparison of their sizes, echogenicity, and vascularity. Additional views may also be obtained with the patient performing Valsalva maneuver.

3. Anatomy

The normal adult testis is an ovoid structure measuring 3 cm in anterior-posterior dimension, 2–4 cm in width, and 3–5 cm in length. The weight of each testis normally ranges

from 12.5 to 19 g. Both the sizes and weights of the testes normally decrease with age. At ultrasound, the normal testis has a homogeneous, medium-level, granular echotexture. The testicle is surrounded by a dense white fibrous capsule, the tunica albuginea, which is often not visualized in the absence of intrascrotal fluid. However, the tunica is often seen as an echogenic structure where it invaginates into the testis to form the mediastinum testis [Fig. 1]. In the testis, the seminiferous tubules converge to form the rete testes, which is located in the mediastinum testis. The rete testis connects to the epididymal head via the efferent ductules. The epididymis is located posterolateral to the testis and measures 6–7 cm in length. At sonography, the epididymis is normally iso- or slightly hyperechoic to the normal testis and its echo texture may be coarser. The head is the largest and most easily identified portion of the epididymis. It is located superior-lateral to the upper pole of the testicle and is often seen on paramedian views of the testis [Fig. 2]. The normal epididymal body and tail are smaller and more variable in position.

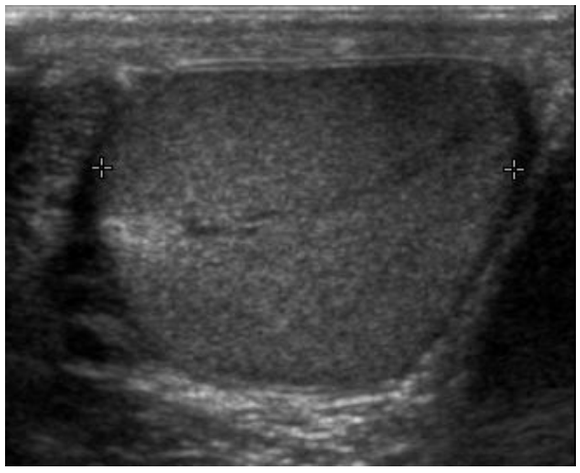

Fig. 1. Sonography of a normal testis. The normal testis presents as a structure having homogeneous, medium level, granular echotexture. The mediastinum testis appears as the hyperechoic region located at the periphery of the testis as seen in this figure

The testis obtains its blood supply from the deferential, cremasteric and testicular arteries. The right and left testicular arteries, branches of the abdominal aorta, arise just distal to the renal arteries, provide the primary vascular supply to the testes. They course through the inguinal canal with the spermatic cord to the posterior superior aspect of the testis. Upon reaching the testis, the testicular artery divides into branches, which penetrate the tunica albuginea and arborize over the surface of the testis in a layer known as tunica vasculosa. Centripetal branches arising from the capsular arteries carry blood toward the mediastinum, where they divide to form the recurrent rami that carry blood away from the mediastinum into the testis. The deferential artery, a branch of the superior vesicle artery and the cremasteric artery, a branch of the inferior epigastric artery, supply the epididymis, vas deferens, and peritesticular tissue.

Four testicular appendages have been described: the appendix testis, the appendix epididymis, the vas aberrans, and the paradidymis. They are all remnants of embryonic ducts (Dogra et al 2003, as cited in Cook and Dewbury, 2000). Among them, the appendix testis and the appendix epididymis are usually seen at scrotal US. The appendix testis is a

mullerian duct remnant and consists of fibrous tissue and blood vessels within an envelope of columnar epithelium. The appendix testis is attached to the upper pole of the testis and found in the groove between the testis and the epididymis. The appendix epididymis is attached to the head of the epididymis. The spermatic cord, which begins at the deep inguinal ring and descends vertically into the scrotum is consists of vas deferens, testicular artery, cremasteric artery, deferential artery, pampiniform plexuses, genitofemoral nerve, and lymphatic vessel.

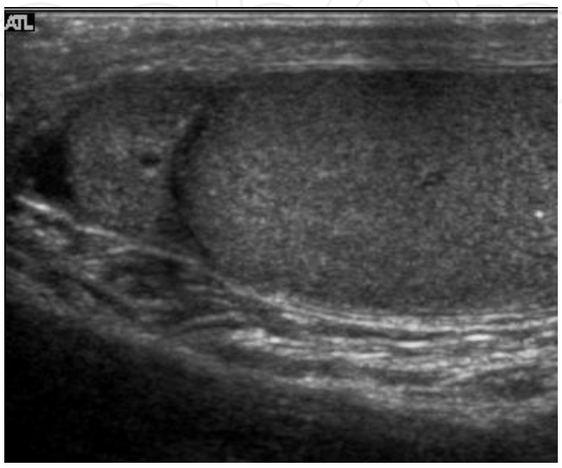

Fig. 2. Normal epididymal head. The epididymal head, usually iso- or slightly hyperechoic than the testis is seen located cephalad to the testis

4. Intratesticular tumors

One of the primary indications for scrotal sonography is to evaluate for the presence of intratesticular tumor in the setting of scrotal enlargement or a palpable abnormality at physical examination. It is well known that the presence of a solitary intratesticular solid mass is highly suspicious for malignancy. Conversely, the vast majority of extratesticular lesions are benign.

4.1 Germ cell tumors

Primary intratesticular malignancy can be divided into germ cell tumors and non–germ cell tumors. Germ cell tumors are further categorized as either seminomas or nonseminomatous tumors. Other malignant testicular tumors include those of gonadal stromal origin, lymphoma, leukemia, and metastases.

4.1.1 Seminoma

Approximately 95% of malignant testicular tumors are germ cell tumors, of which seminoma is the most common. It accounts for 35%–50% of all germ cell tumors (Woodward et al, 2002). Seminomas occur in a slightly older age group when compared with other nonseminomatous tumor, with a peak incidence in the forth and fifth decades. They are less aggressive than other testicular tumors and usually confined within the tunica albuginea at presentation. Seminomas are associated with the best prognosis of the germ cell tumors because of their high sensitivity to radiation and chemotherapy (Kim et al, 2007).

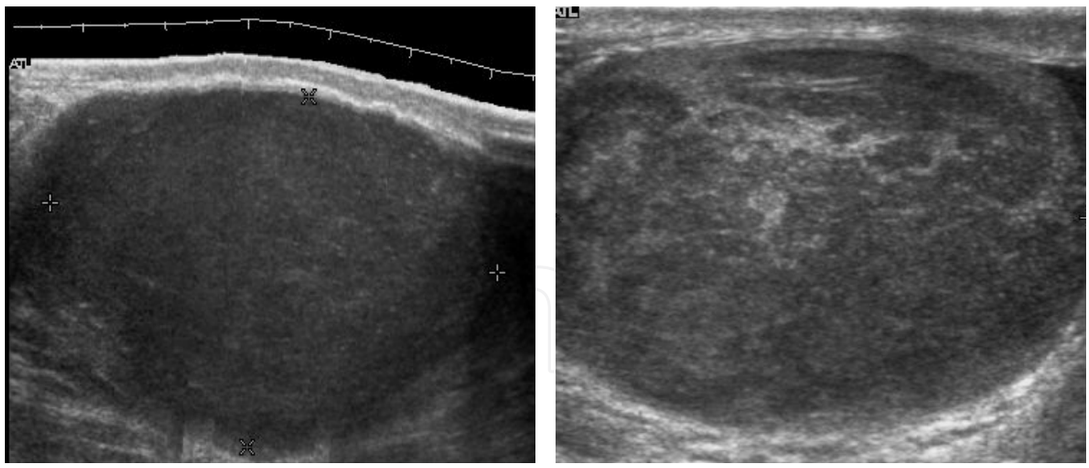

(a) (b)

Fig. 3. Seminoma. (a) Seminoma usually presents as a homogeneous hypoechoic nodule confined within the tunica albuginea. (b) Sonography shows a large heterogeneous mass is seen occupying nearly the whole testis but still confined within the tunica albuginea, it is rare for seminoma to invade to peritesticular structures

Seminoma is the most common tumor type in cryptorchid testes. The risk of developing a seminoma is increased in patients with cryptorchidism, even after orchiopexy. There is an increased incidence of malignancy developing in the contralateral testis too, hence sonography is sometimes used to screen for an occult tumor in the remaining testis.

On US images, seminomas are generally uniformly hypoechoic, larger tumors may be more heterogeneous [Fig. 3]. Seminomas are usually confined by the tunica albuginea and rarely extend to peritesticular structures. Lymphatic spread to retroperitoneal lymph nodes and hematogenous metastases to lung, brain, or both are evident in about 25% of patients at the time of presentation (Dogra et al 2003, as cited in Guthrie & Fowler, 1992)

4.1.2 Nonseminomatous germ cell tumors

Nonseminomatous germ cell tumors most often affect men in their third decades of life. Histologically, the presence of any nonseminomatous cell types in a testicular germ cell tumor classifies it as a nonseminomatous tumor, even if most of the tumor cells belong to seminona. These subtypes include yolk sac tumor, embryonal cell carcinoma, teratocarcinoma, teratoma, and choriocarcinoma. Clinically nonsemionatous tumors usually present as mixed germ cell tumors with variety cell types and in different proportions.

Embryonal cell carcinoma --- Embryonal cell carcinomas, a more aggressive tumor than seminoma usually occurs in men in their 30s. Although it is the second most common testicular tumor after seminoma, pure embryonal cell carcinoma is rare and constitutes only about 3 percent of the nonseminomatous germ cell tumors. Most of the cases occur in combination with other cell types.

At ultrasound, embryonal cell carcinomas are predominantly hypoechoic lesions with ill defined margins and an inhomogeneous echotexture. Echogenic foci due to hemorrhage, calcification, or fibrosis are commonly seen. Twenty percent of embryonal cell carcinomas

have cystic components (Dogra et al, 2003). The tumor may invade into the tunica albuginea resulting in contour distortion of the testis [Fig. 4].

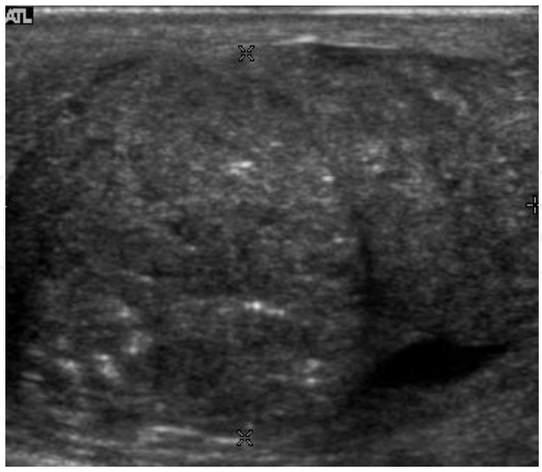

Fig. 4. Embryonal cell carcinoma. Longitudinal ultrasound image of the testis shows an irregular heterogeneous mass that forms an irregular margin with the tunica albuginea

Yolk sac tumor --- Yolk sac tumors also known as endodermal sinus tumors account for 80% of childhood testicular tumors, with most cases occuring before the age of 2 years (Woodward et al, 2002, as cited in Frush & Sheldon 1998)**.** Alpha-fetoprotein is normally elevated in greater than 90% of patients with yolk sac tumor (Woodward et al, 2002, as cited in Ulbright et al, 1999). In its pure form, yolk sac tumor is rare in adults; however yolk sac elements are frequently seen in tumors with mixed histologic features in adults and thus indicate poor prognosis. The US appearance of yolk sac tumor is usually nonspecific and consists of inhomogeneous mass that may contain echogenic foci secondary to hemorrhage.

Choriocarcinoma --- Choriocarcinoma is a highly malignant testicular tumor that usually develops in the 2nd and 3rd decades of life. Pure choriocarcinomas are rare and represent only less than 1 percent of all testicular tumors (Woodward et al, 2002). Choriocarcinomas are composed of both cytotrophoblasts and syncytiotrophoblasts, with the latter responsible for the clinical elevation of human chorionic gonadotrophic hormone level. As microscopic vascular invasion is common in choriocarcinoma, hematogeneous metastasis, especially to the lungs is common (Dogra et al, 2003, as cited in Geraghty et al, 1998). Many choriocarcinomas show extensive hemorrhagic necrosis in the central portion of the tumor; this appears as mixed cystic and solid components (Dogra et al 2003, as cited in Hamm, 1997) at ultrasound.

Teratoma --- Although teratoma is the second most common testicular tumor in children, it affects all age groups. Mature teratoma in children is often benign, but teratoma in adults, regardless of age, should be considered as malignant. Teratomas are composed of all three germ cell layers, i.e. endoderm, mesoderm and ectoderm. At ultrasound, teratomas generally form well-circumscribed complex masses. Echogenic foci representing calcification, cartilage, immature bone and fibrosis are commonly seen [Fig. 5]. Cysts are also a common feature and depending on the contents of the cysts i.e. serous, mucoid or keratinous fluid, it may present as anechoic or complex structure [Fig. 6].

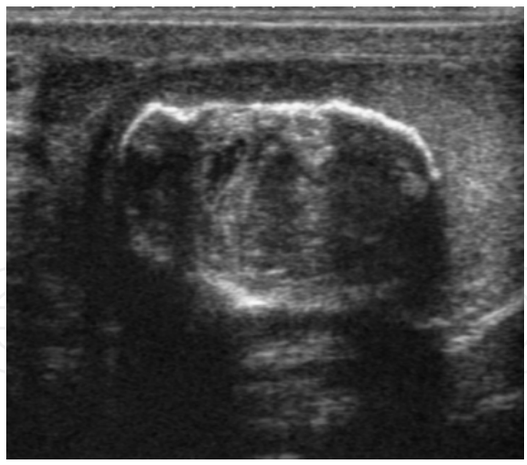

Fig. 5. Teratoma. A plaque like calcification with acoustic shadow is seen in the testis

4.2 Non-germ cell tumours

4.2.1 Sex cord-stromal tumours

Sex cord-stromal (gonadal stromal) tumors of the testis, account for 4 per cent of all testicular tumors (Dogra et al, 2003). The most common are Leydig and Sertoli cell tumors. Although the majority of these tumors are benign, these tumors can produce hormonal changes, for example, Leydig cell tumor in a child may produce isosexual virilization. In adult, it may have no endocrine manifestation or gynecomastia, and decrease in libido may result from production of estrogens. These tumors are typically small and are usually discovered incidentally. They do not have any specific ultrasound appearance but appear as well-defined hypoechoic lesions. These tumors are usually removed because they cannot be distinguished from malignant germ cell tumors.

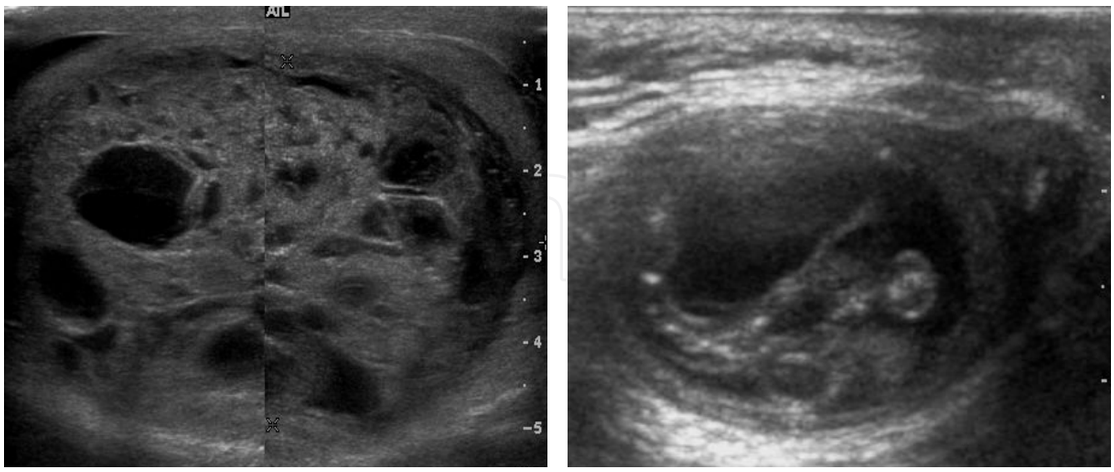

(a) (b)

Fig. 6. Mature cystic teratoma. (a) Composite Image. Mature cystic teratoma in a 29 year-old man. Longitudinal sonography image of the right testis shows a multilocular cystic mass. (b) Mature cystic teratoma in a 6 year-old boy. Longitudinal sonography of the right testis shows a cystic mass contains calcification with no obvious acoustic shadow

Leydig cell tumors are the most common type of sex cord–stromal tumor of the testis, accounting for 1%–3% of all testicular tumors. They can be seen in any age group, they are generally small solid masses, but they may show cystic areas, hemorrhage, or necrosis (Woodward et al 2002, as cited in Ulbright et al, 1999). Their sonographic appearance is variable and is indistinguishable from that of germ cell tumors (Woodward et al 2002, as cited in Avery et al, 1991)

Sertoli cell tumors are less common, constituting less than 1% of testicular tumors. They are less likely than Leydig cell tumors to be hormonally active, but gynecomastia can occur (Woodward et al 2002, as cited in Ulbright et al, 1999). Sertoli cell tumors are typically well circumscribed, unilateral, round to lobulated masses.

4.2.2 Lymphoma

Clinically lymphoma can manifest in one of three ways: as the primary site of involvement, or as a secondary tumor such as the initial manifestation of clinically occult disease or recurrent disease. Although lymphomas constitute 5% of testicular tumors and are almost exclusively diffuse non-Hodgkin B-cell tumors, only less than 1 % of non-Hodgkin lymphomas involve the testis (Doll and Weiss 1986).

Patients with testicular lymphoma are usually old aged around 60 years of age, present with painless testicular enlargement and less commonly with other systemic symptoms such as weight loss, anorexia, fever and weakness. Bilateral testicle involvements are common and occur in 8.5% to18% of cases (Dogra et al, 2003, as cited in Horstman et al, 1992). At sonography, most lymphomas are homogeneous and diffusely replace the testis [Fig. 7]. However focal hypoechoic lesions can occur, hemorrhage and necrosis are rare. At times, the sonographic appearance of lymphoma is indistinguishable from that of the germ cell tumors [Fig. 8], then the patient's age at presentation, symptoms, and medical history, as well as multiplicity and bilaterality of the lesions, are all important factors in making the appropriate diagnosis.

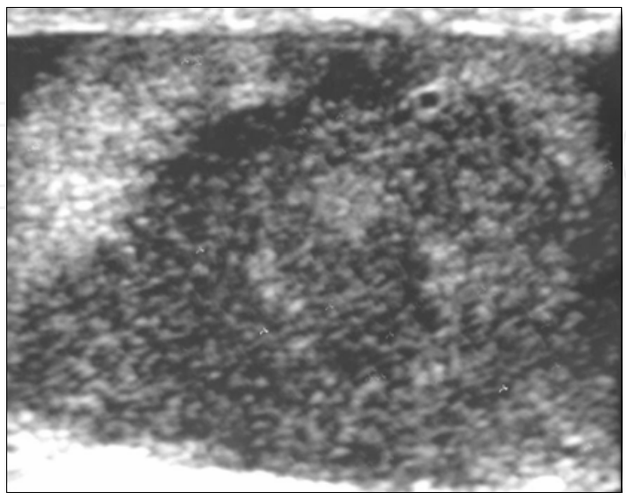

Fig. 7. Lymphoma. Lymphoma in a 61 year-old man. Longitudinal sonography shows an irregular hypoechoic lesion occupied nearly the whole testis

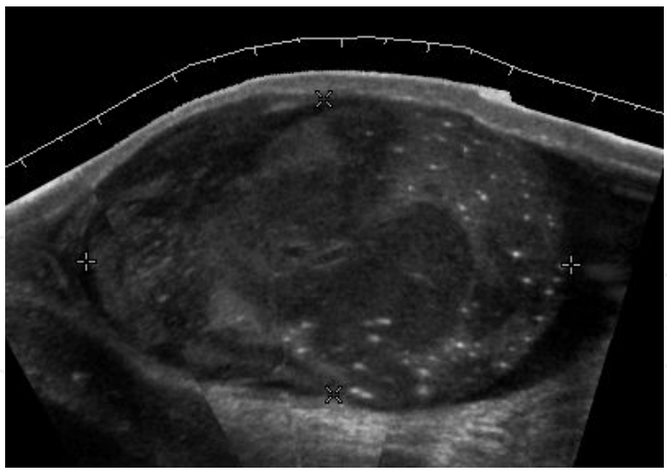

Fig. 8. Primary Lymphoma. Longitudinal sonography of a 64 year-old man shows a lymphoma mimicking a germ cell tumor

4.2.3 Leukemia

Primary leukemia of the testis is rare. However due to the presence of blood-testis barrier, chemotherapeutic agents are unable to reach the testis, hence in boys with acute lymphoblastic leukemia, testicular involvement is reported in 5% to 10% of patients, with the majority found during clinical remission (Dogra et al, 2003). The sonographic appearance of leukemia of the testis can be quite varied, as the tumors may be unilateral or bilateral, diffuse or focal, hypoechoic or hyperechoic (Woodward et al, 2002). These findings are usually indistinguishable from that of the lymphoma [Fig. 9].

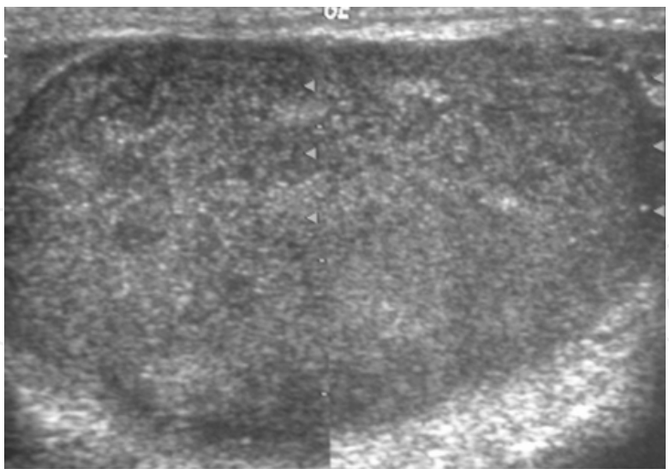

Fig. 9. Leukemia. Diffuse hypoechoic infiltrative lesions are seen involving the whole testis, indistinguishable from that of the lymphoma

4.3 Epidermoid cyst

Epidermoid cysts, also known as keratocysts, are benign epithelial tumors which usually occur in the second to fourth decades and accounts for only 1–2% of all intratesticular

tumors. As these tumors have a benign biological behavior and with no malignant potential, preoperative recognition of this tumor is important as this will lead to testicle preserving surgery (enucleation) rather than unnecessary orchiectomy.

Clinically, epidermoid cyst cannot be differentiated from other testicular tumors, typically presenting as a non-tender, palpable, solitary intratesticular mass. Tumor markers such as serum beta-human chorionic gonadotropin and alpha-feto protein are negative.

The ultrasound patterns of epidermoid cysts are variable and include:

i. A mass with a target appearance, i.e. a central hypoechoic area surrounded by an echolucent rim (Mak et al, 2007a, as cited in Maxwell & Mamtora, 1990);
ii. An echogenic mass with dense acoustic shadowing due to calcification; (Mak et al, 2007a, as cited in Meiches & Nurenberg 1991);
iii. A well-circumscribed mass with a hyperechoic rim (Mak et al, 2007a, as cited in Cohen 1984);
iv. Mixed pattern having heterogeneous echotexture and poor-defined contour (Mak et al, 2007a, as cited in Atchley & Dewbury, 2000) and
v. An onion peel appearance consisting of alternating rings of hyperechogenicities and hypoechogenicities (Mak et al, 2007a, as cited in Malvica, 1993).

However, these patterns, except the latter one, may be considered as non-specific as heterogeneous echotexture and shadowing calcification can also be detected in malignant testicular tumors (Mak et al, 2007a). The onion peel pattern of epidermoid cyst [Fig. 10] correlates well with the pathologic finding of multiple layers of keratin debris produced by the lining of the epidermoid cyst. This sonographic appearance should be considered characteristic of an epidermoid cyst and corresponds to the natural evolution of the cyst. Absence of vascular flow is another important feature that is helpful in differentiation of epidermoid cyst from other solid intratesticular lesions.

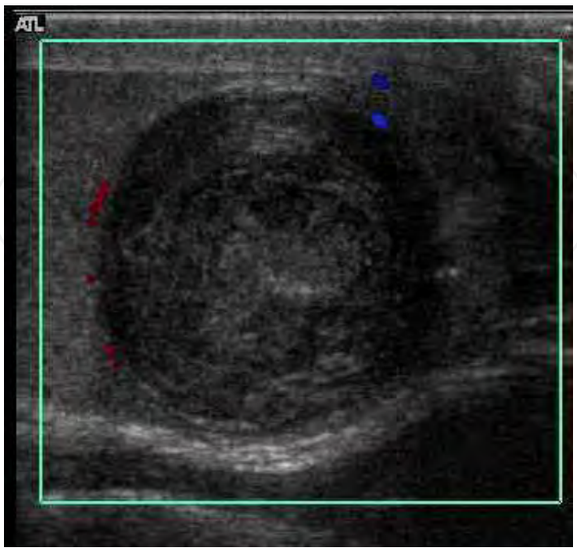

Fig. 10. Epidermoid cyst. Onion peel appearances of the tumor together with absence of vascular flow are typical findings of epidermoid cyst

5. Extratesticular tumors

Although most of the extratesticular lesions are benign, malignancy does occur; the most common malignant tumors in infants and children are rhabdomyosarcomas (Mak et al 2004, as cited in Green, 1986). Other malignant tumors include liposarcoma, leiomyosarcoma, malignant fibrous histiocytoma and mesothelioma.

5.1 Rhabdomyosarcoma

Rhabdomyosarcoma is the most common tumor of the lower genitourinary tract in children in the first two decades, it may develop anywhere in the body, and 4% occur in the paratesticular region (Mak et al 2004a, as cited in Hamilton et al, 1989) which carries a better outcome than lesions elsewhere in the genitourinary tract. Clinically, the patient usually presents with non-specific complaints of a unilateral, painless intrascrotal swelling not associated with fever. Transillumination test is positive when a hydrocele is present, often resulting in a misdiagnosis of epididymitis, which is more commonly associated with hydrocele.

The ultrasound findings of paratesticular rhabdomyosarcoma are variable. It usually presents as an echo-poor mass [Fig. 11a] with or without hydrocele (Mak et al 2004a, as cited in Solvietti et al, 1989). With color Doppler sonography [Fig. 11b] these tumors are generally hypervascular (Mak et al, 2004a).

5.2 Mesothelioma

Malignant mesothelioma is an uncommon tumor arising in body cavities lined by mesothelium. The majority of these tumors are found in the pleura, peritoneum and less frequently pericardium. As the tunica vaginalis is a layer of reflected peritoneum, mesothelioma can occur in the scrotal sac. Although trauma, herniorrhaphy and long term

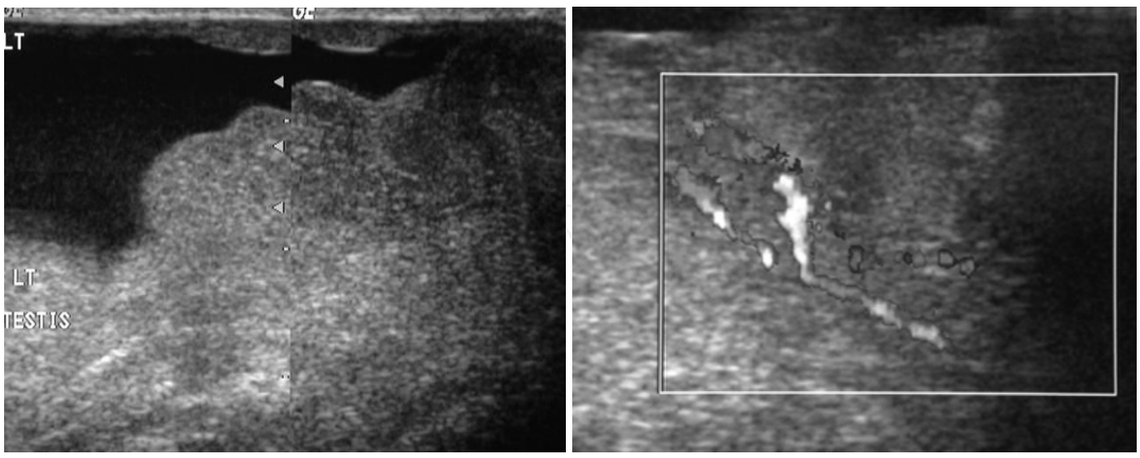

(a) (b)

Fig. 11. Rhabdomyosarcoma (Reproduced with permission from British Institute of Radiology, British Journal of Radiology 2004; 77: 250–252). (a) Longituidinal section (composite image) of high resolution ultrasound of a 14 year-old boy shows a well defined hypoechoic extratesticular mass is found in the left scrotum, hydrocele is also present. (b) Color Doppler ultrasound shows that the mass is hypervascular

hydrocele (Mak et al, 2004b, as cited in Gurdal & Erol, 2001) have been considered as the predisposing factors for development of malignant mesothelioma, the only well established risk factor is asbestos exposure (Boyum & Wasserman, 2008). Patients with malignant mesothelioma of the tunica vaginalis frequently have a progressively enlarging hydrocele and less frequently a scrotal mass, rapid re-accumulation of fluid after aspiration raises the suggestion of malignancy (Mak et al, 2004b, as cited in Wolanske & Nino-Murcia, 2001).

The reported ultrasound features of mesothelioma of the tunica vaginalis testis are variable. Hydrocele, either simple or complex is present and may be associated with: (1) multiple extratesticular papillary projections of mixed echogenicity (Boyum & Wasserman 2008, as cited in Fields et al, 1992); (2) multiple extratesticular nodular masses of increased echogenicity (Boyum & Wasserman, 2008, as cited in Bruno et al, 2002 and Tyagi et al, 1989); (3) focal irregular thickening of the tunica vaginalis testis (Bruno et al, 2002); (4) a simple hydrocele as the only finding (Boyum & Wasserman, 2008, as cited in Jalon et al, 2003) and (5) A single hypoechoic mass located in the epididymal head (Boyum & Wasserman, 2008; Mak et al, 2004b). With color Doppler sonography, mesothelioma is hypovascular [Fig. 12] (Bruno et al, 2002; Mak et al, 2004b; Wang et al, 2005).

5.3 Leiomyoma

Leiomyomas are benign neoplasms that may arise from any structure or organ containing smooth muscle. The majority of genitourinary leiomyomas are found in the renal capsule, but this tumor has also been reported in the epididymis, spermatic cord, and tunica albuginea. Scrotal leiomyomas have been reported in patients from the fourth to ninth decades of life with most presenting during the fifth decade. These tumors are generally slow growth and asymptomatic. The sonographic features of leiomyomas have been reported as solid hypoechoic or heterogeneous masses that may or may not contain

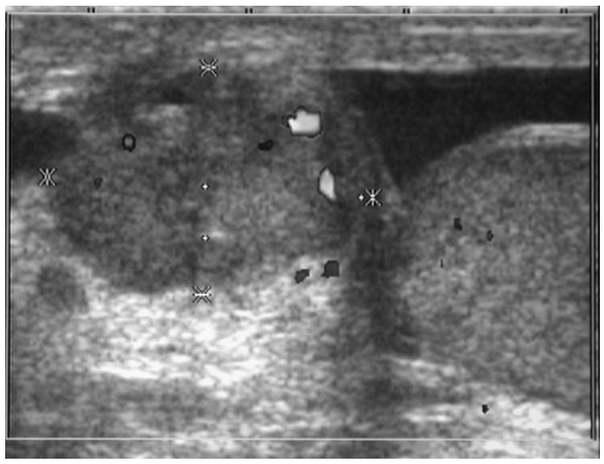

Fig. 12. Mesothelioma arising from the tunica vaginalis (Reproduced with permission from British Institute of Radiology, British Journal of Radiology 2004:77:780–781). Color Doppler ultrasound demonstrates a well-defined hypoechoic nodule occupying the left epididymal head, with a few areas of color flow demonstrated. The left testis is intact with no focal nodule detected. Hydrocele is also present

shadowing calcification (Mak et al, 2004c, as cited in Hricak & Filly, 1983 & Leonhardt, 1993). Other findings include whorl shaped configuration [Fig. 13a] of the nodule (Mak et al, 2004c) and multiple, narrow areas of shadowing not cast by calcifications [Fig. 13b], but corresponding to transition zones between the various tissue components of the mass (Mak et al, 2004c, as cited in Hertzberg et al, 1996) are characteristic of leiomyoma and may help differentiate it from other scrotal tumors.

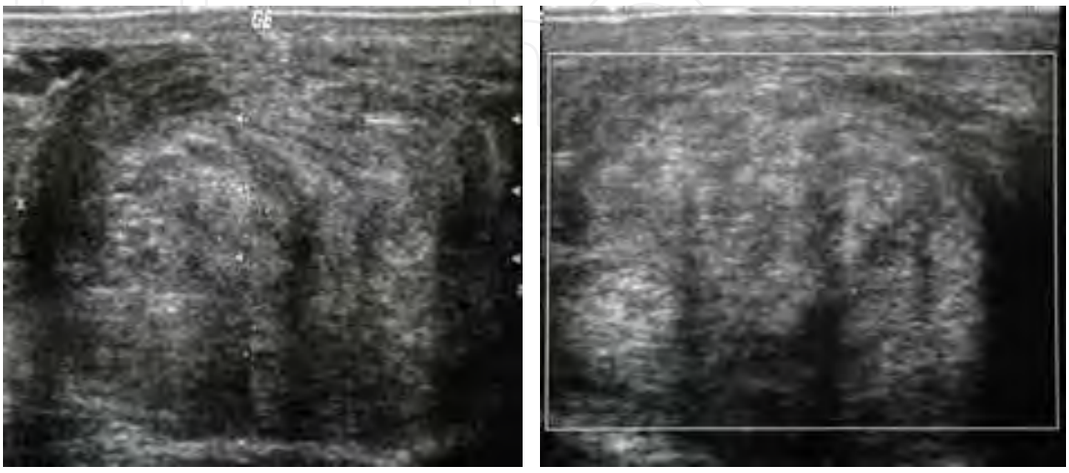

(a) (b)

Fig. 13. Leiomyoma arising from tunica albuginea (Reproduced with permission from John Wiley and Sons publishing company License number 2643411100095, Journal of Clinical Ultrasound 2004; 32:309–311). (a) Montage of 2 contiguous sonograms of a 67 year-old man shows a well-defined extratesticular mass with a whorl-shaped echotexture. (b) Color Doppler sonogram shows no internal vascularity. Note the presence of multiple shadows not associated with echogenic foci in the mass

5.4 Fat containing tumors

5.4.1 Lipoma

Lipoma is the most common nontesticular intrascrotal tumor. It can be divided into 3 types depending upon the site of origination and spread:

1. Originate in the spermatic cord with spread to the scrotum;
2. Originate and develop within the cord (most common type) and
3. Originate and develop within the scrotum (Rosenberg & Williamson, 1989).

At ultrasound, lipoma is a well–defined, homogeneous, hyperechoic paratesticular lesion of varying size [Fig. 14]. The simple finding of an echogenic fatty mass within the inguinal canal, while suggestive of a lipoma, should also raise a question of fat from the omentum secondary to an inguinal hernia. However lipomas are well-defined masses, whereas herniated omentum appears to be more elongated and can be traced to the inguinal area, hence scanning along the inguinal canal as well as the scrotum is necessary to make the differential diagnosis. Magnetic resonance imaging and computerized tomography are helpful in doubtful cases.

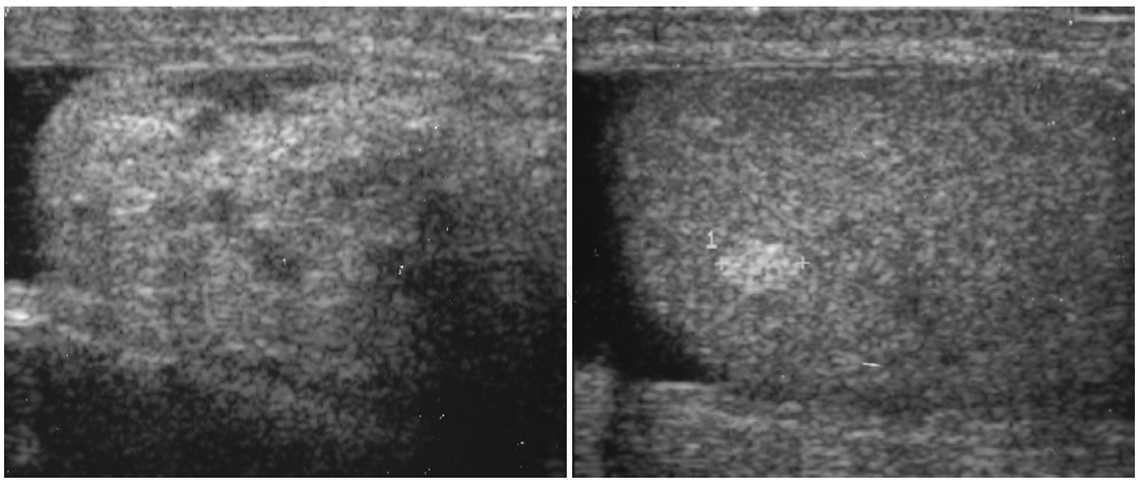

(a) (b)

Fig. 14. Lipoma at spermatic cord and testiscle. (a) Longitudinal scrotal sonography of a 61 year-old patient shows a well defined hyperechoic nodule is seen in the scrotum. (b) Scrotal sonography of the same patient shows a hyper echoic nodule in the left testis, pathology proved that this is a lipoma too

5.4.2 Liposarcoma

Malignant extratesticular tumors are rare. Most of the malignant tumors are solid and have nonspecific features on ultrasonography. The majority of the malignant extratesticular tumors arise from spermatic cord with liposarcoma being the most common in adults (Woodward et al, 2003). On gross speciemen, liposarcoma is a solid, bulky lipomatous tumor with heterogeneous architecture, often containing areas of calcification (Bostwick & Eble, 1997). Although the sonographic appearances of liposarcoma are variable and nonspecific, it still provides a clue about the presence of lipomatous matrix. Echogenic areas corresponding to fat often associated with poor sound transmission and areas of heterogeneous

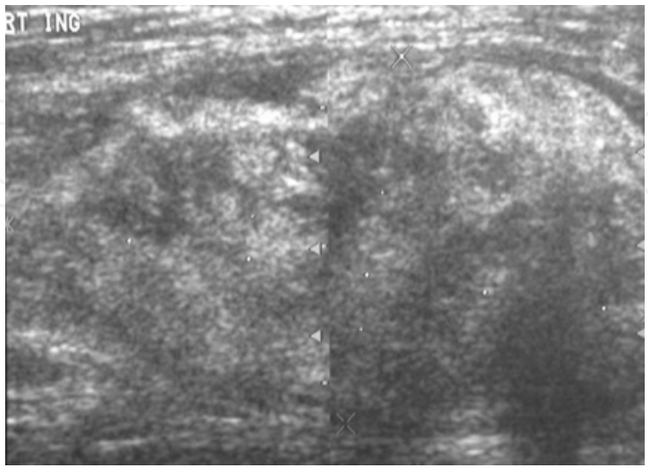

Fig. 15. Liposarcoma. A heterogeneous mass consists of an upper hyperechoic portion corresponds to lipomatous matrix and areas of hypoechogenicity corresponds to nonlipomatous component is seen

echogenicity corresponding to nonlipomatous component are present [Fig. 15]. Some liposarcomas may also mimic the sonographic appearance of lipomas [Fig. 16] and hernias that contain omentum, but lipomas are generally smaller and more homogeneous and hernias are elongated masses that can often be traced back to the inguinal canal. CT and MR imaging are more specific, as they can easily recognize fatty component along with other soft tissue component more clearly than ultrasound.

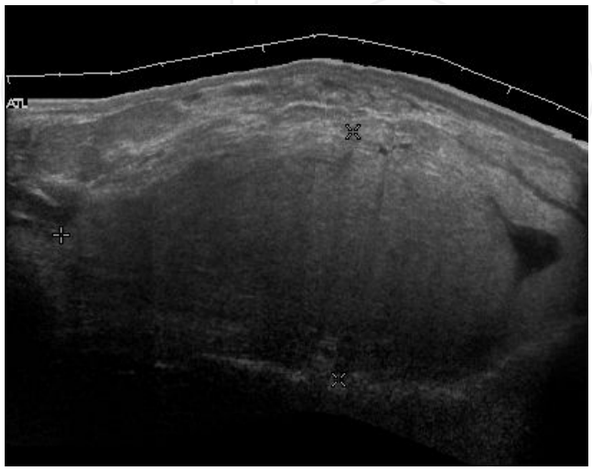

Fig. 16. Liposarcoma mimicking lipoma. A homogeneous hypoechoic mass presents with the same appearance of lipoma, rapid growth of this tumors grants surgical intervention with pathology proved to be well differentiated liposarcoma

5.5 Adenomatoid tumor

Adenomatoid tumors are the most common tumors of the epididymis and account for approximately 30% of all paratesticular neoplasms, second only to lipoma (Bostwick & Eble, 1997). They are usually unilateral, more common on the left side, and usually involve the epididymal tail. Adenomatoid tumor typically occurs in men during the third and fourth decades of life. Patients usually present with a painless scrotal mass that is smooth, round and well circumscribed on palpation. They are believed to be of mesothelial origin and are universally benign. Their sonographic appearance is that of a round shaped, well-defined, homogeneous mass with echogenicity ranging from hypo- to iso- to hyperechoic [Fig. 17] (Mak et al, 2001).

5.6 Fibrous pseudotumor

Fibrous pseudotumors, also known as fibromas are thought to be reactive, nonneoplastic lesions. They can occur at any age, about 50% of fibromas are associated with hydrocele, and 30% are associated with a history of trauma or inflammation (Akbar et al, 2003). Although the exact cause of this tumor is not completely understood, it is generally believed that these lesions represent a benign reactive proliferation of inflammatory and fibrous tissue, in response to chronic irritation (Garriga et al, 2009).

Sonographic evaluation generally shows one or more solid nodules arising from the tunica vaginalis, epididymis, spermatic cord and tunica albuginea [Fig. 18]. A hydrocele is frequently present too. The nodules may appear hypoechoic or hyperechoic, depending on the amount

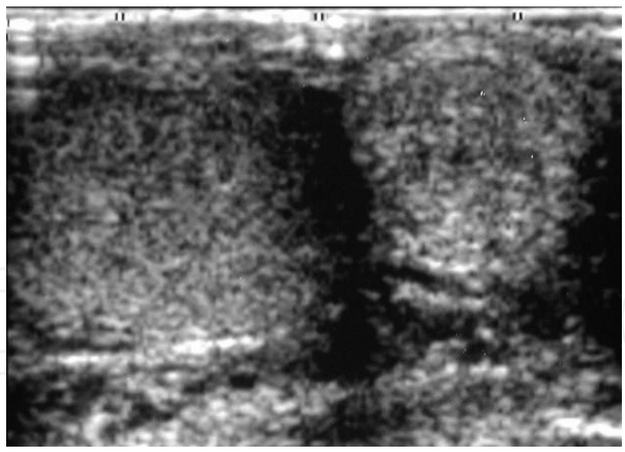

Fig. 17. Adenomatoid tumor at epididymis. A nodule that is isoechoic to the testis is seen occupying nearly the entire epididymal tail

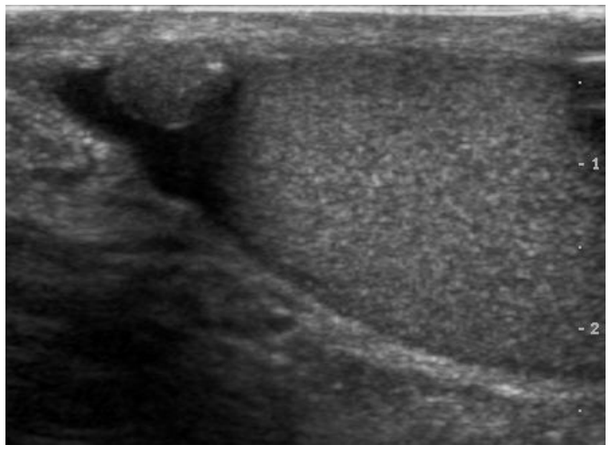

Fig. 18. Fibrous pseudotumor. A homogeneous hypoechoic nodular lesion is seen attached to the tunica associated with minimal amount of hydrocele

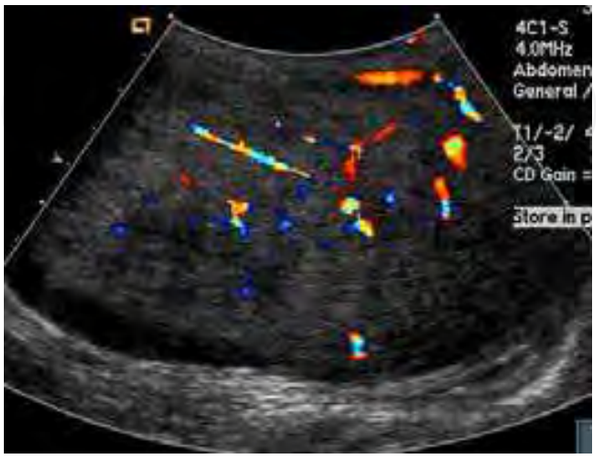

Fig. 19. Fibrous pseudotumor. With color Doppler, a little vascular flow is seen in this fibrous pseudotumor

of collagen or fibroblast present (Garriga et al, 2009, as cited in Tobias-Machado et al, 2000). Acoustic shadowing may occur in the absence of calcification due to the dense collagen component of this tumor. With color Doppler sonography, a small to moderate amount of vascularity may be seen (Garriga et al 2009, as cited in Germaine and Simerman, 2007) [Fig. 19].

6. Inflammation

6.1 Epididymitis and epididymo-orchitis

Epididymitis and epididymo-orchitis are common causes of acute scrotal pain in adolescent boys and adults. At physical examination, they usually are palpable as tender and enlarged structures. Clinically, this disease can be differentiated from torsion of the spermatic cord by elevation of the testes above the pubic symphysis. If scrotal pain decreases, it is more likely to be due to epidiymitis rather than torsion (Prehn's sign). Most cases of epididymitis are secondary to sexually transmitted disease or retrograde bacteria infection from the urinary bladder. The infection usually begins in the epididymal tail and spreads to the epididymal body and head. Approximately 20% to 40 % of cases are associated with orchitis due to direct spread of infection into the testis (Kim et al, 2007, as cited in Horstman et al, 1991).

At ultrasound, the findings of acute epididymitis include an enlarged hypoechoic or hyperechoic (presumably secondary to hemorrhage) epididymis [Fig. 20a]. Other signs of inflammation such as increased vascularity, reactive hydrocele, pyocele and scrotal wall thickening may also be present. Testicular involvement is confirmed by the presence of testicular enlargement and an inhomogeneous echotexture. Hypervascularity on color Doppler images [Fig. 20b] is a well-established diagnostic criterion and may be the only imaging finding of epididymo-orchitis in some men (Kim et al, 2007, as cited in Horstman et al, 1991).

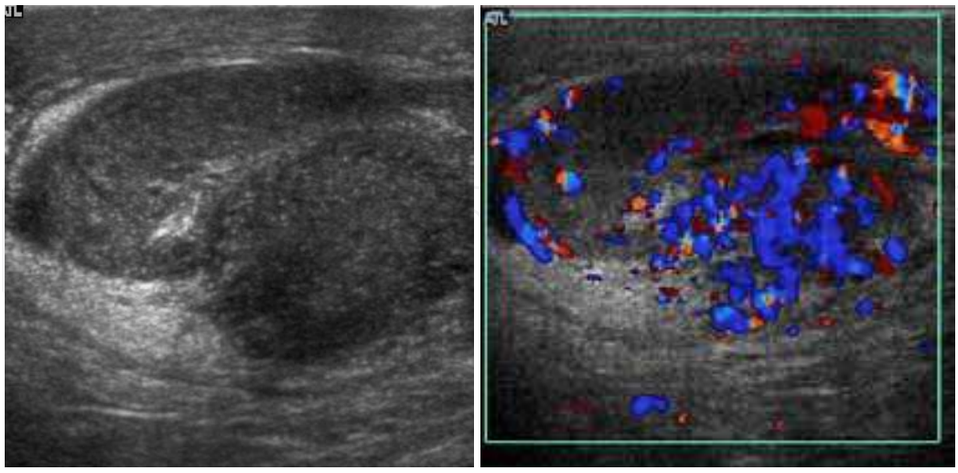

(a) (b)

Fig. 20. Epididymo-orchitis in a 77 year-old man. (a) Transverse sonography shows enlargement of the epididymis with hypoechogenicity noted over the testis and epididymis associated with scrotal wall thickening. (b) Color Doppler sonography showed hyperemic change of the testis and epididymis, presenting as an "inferno" vascular flow pattern

6.2 Tuberculous epididymo-orchitis

Although the genitourinary tract is the most common site of extra-pulmonary involvement by tuberculosis, tuberculous infection of the scrotum is rare and occurs in approximately 7% of patients with tuberculosis (Muttarak and Peh, 2006, as cited in Drudi et al, 1997). At the initial stage of infection, the epididymis alone is involved. However if appropriate antituberculous treatment is not administered promptly, the infection will spreads to the ipsilateral testis. The occurrence of isolated testicular tuberculosis is rare (Muttarak and Peh, 2006, as cited in Riehle & Jayaraman, 1982). Clinically patients with tuberculous epididymo-orchitis may present with painful or painless enlargement of the scrotum, hence they cannot be distinguished from lesions such as testicular tumor, testicular infarction and may mimic testicular torsion.

At ultrasound, tuberculous epididymitis is characterized by an enlarged epididymis with variable echogenicity. The presence of calcification, caseation necrosis, granulomas and fibrosis can result in heterogeneous echogenicity [Fig. 21a]. The ultrasound findings of tuberculous orchitis are as follow: (a) diffusely enlarged heterogeneously hypoechoic testis (b) diffusely enlarged homogeneously hypoechoic testis (c) nodular enlarged heterogeneously hypoechoic testis and (d) presence of multiple small hypoechoic nodules in an enlarged testis [Fig. 21b] (Muttarak and Peh, 2006).

Although both bacterial and tuberculous infections may involve both the epididymis and the testes, an enlarged epididymis with heterogeneously hypoechoic pattern favors a diagnosis of tuberculosis (Muttarak and Peh, 2006, as cited in Kim et al, 1993 and Chung et al, 1997). With color Doppler ultrasound, a diffuse increased blood flow pattern is seen in bacterial epididymitis, whereas focal linear or spotty blood flow signals are seen in the peripheral zone of the affected epididymis in patients with tuberculosis (Muttarak and Peh, 2006, as cited in Yang et al, 2000).

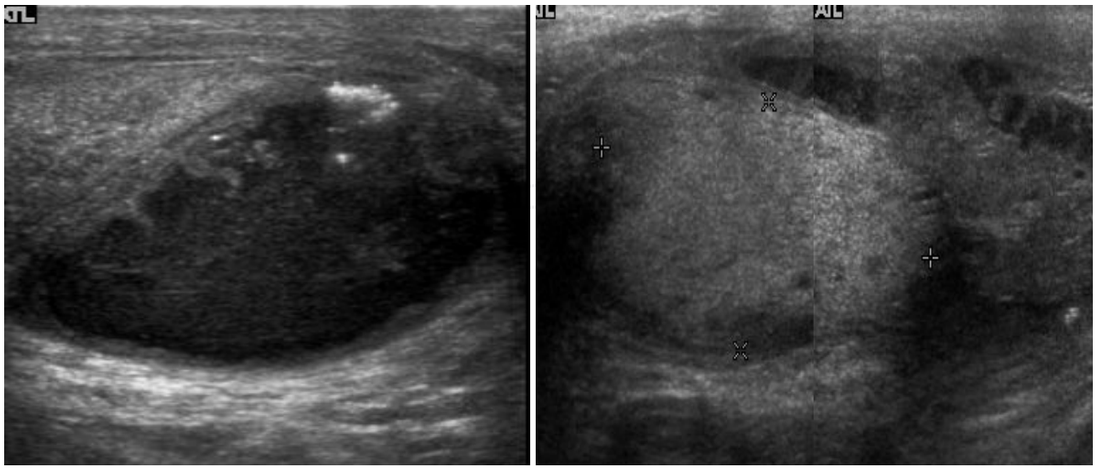

(a) (b)

Fig. 21. Tuberculous epididymo-orchitis. (a) Transverse sonography of a surgically proved tuberculous epididymitis shows an enlarged epididymis containing calcification and necrosis. (b) Composite image: Transverse sonography of the same patient shows multiple hypoechoic nodules in the left testis associated with surrounding reactive hydrocele

6.3 Fournier gangrene

Fournier gangrene is a polymicrobial necrotizing fascitis involving the perineal, perianal, or genital regions and constitutes a true surgical emergency with a potentially high mortality rate. It usually develops from a perineal or genitourinary infection, but can arise following local trauma with secondary infection of the wound. 40–60% of patients are being diabetic. Although the diagnosis of Fournier gangrene is often made clinically, diagnostic imaging is useful in ambiguous cases.

The sonographic hallmark of Fournier gangrene is presence of subcutaneous gas within the thickened scrotal wall. At ultrasound, the gas appears as numerous, discrete, hyperechoic foci with reverberation artifacts [Fig. 22]. Evidence of gas within the scrotal wall may be seen prior to clinical crepitus. The only other condition manifesting with gas at sonographic examination is an inguinoscrotal hernia. This can be differentiated from Fournier gangrene by the presence of gas within the protruding bowel lumen and away from the scrotal wall. (Levenson et al, 2008).

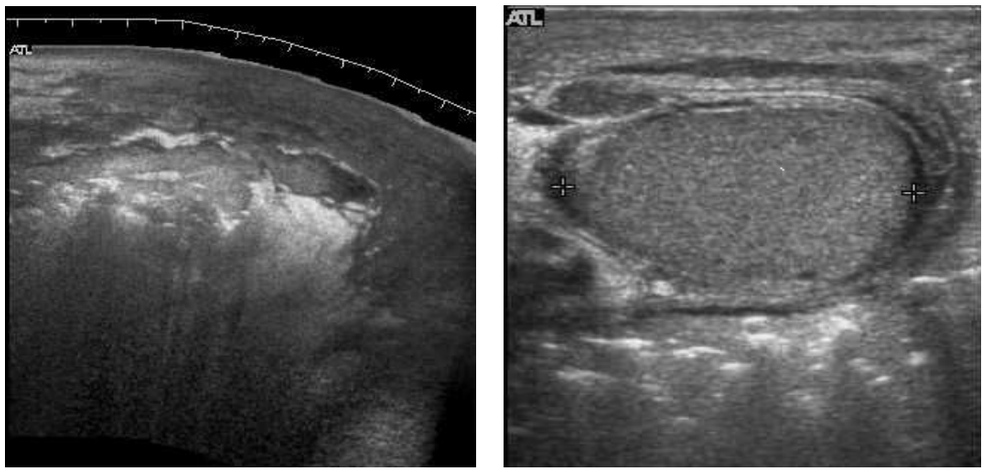

(a) (b)

Fig. 22. Fournier gangrene. (a) Transverse sonography image shows echogenic areas with dirty shadowing representing air in the perineum. (b) Gas presented as numerous, discrete, hyperechoic foci with reverberation artifacts are seen at scrotal wall

7. Other benign lesions of the scrotum

7.1 Tubular ectasia

The normal testis consists of several hundred lobules, with each lobule containing several seminiferous tubules. The seminiferous tubules of each lobule merge to form the straight tubes, which in turn converge to form the rete testis. The rete testis tubules, which lie within the mediastinum testis, are an anastomosing network of irregular channels with a broad lumen, which then empties into the efferent ductules to give rise to the head of the epididymis. Obstruction in the epididymis or efferent ductules may lead to cystic dilatation of the efferent ductules, which usually presents as an epididymal cyst on ultrasound. However, in the more proximal portion this could lead to the formation of an intratesticular

cyst or dilatation of the tubules, so called tubular ectasia. Factors contributing to the development of tubular ectasia include epididymitis, testicular biopsy, vasectomy or an aging process (Mak et al 2007b). Clinically this lesion is usually asymptomatic. The ultrasound appearance of a microcystic or multiple tubular-like lesions located at the mediastinal testis [Fig. 23] and associated with an epididymal cyst in a middle-aged or elderly patient should alert the sonographer to the possibility of tubular ectasia.

The differential diagnosis of a multicystic lesion in testis should include a cystic tumor, especially a cystic teratoma. A cystic teratoma is usually a palpable lesion containing both solid and cystic components; and the cysts are normally larger than that of tubular ectasia, which appear microcystic [Fig. 24]. Furthermore, the location of tubular ectasia in the mediastinum testis is also helpful in making the differential diagnosis.

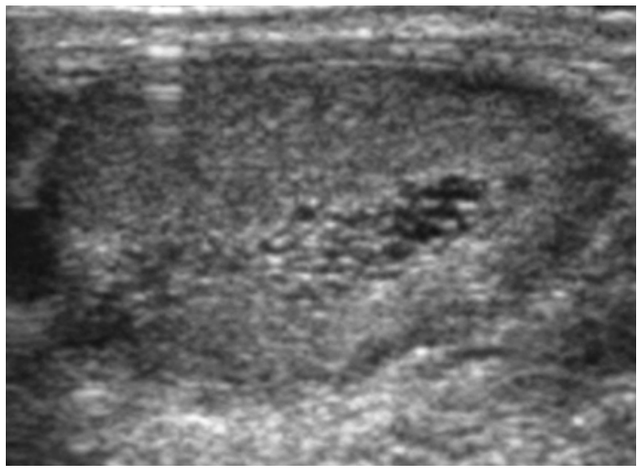

Fig. 23. Tubular ectasia of the testis. Honey-comb shaped cystic lesion at mediastinum testis

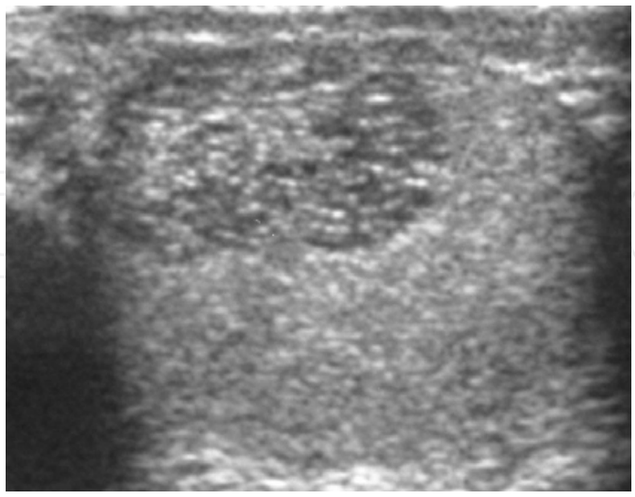

Fig. 24. Tubular ectasia of the testis (Reproduced with permission from British Institute of Radiology, British Journal of Radiology 2007; 80: 67-68). Lesion in the testis mimicking testicular tumor, but the microcystic appearance of this lesion is suggestive of tubular ectasia

7.2 Testicular microlithiasis

Histologically, testicular microlithiasis refers to the scattered laminated calcium deposits in the lumina of the seminiferous tubules. These calcifications arise from degeneration of the cells lining the seminiferous tubules. At ultrasonography, microliths appear as tiny punctate echogenic foci, which typically do not shadow. Although minor microcalcification within a testis is considered normal, the typical US appearance of testicular microlithiasis is of multiple nonshadowing echogenic foci measuring 2–3 mm and randomly scattered throughout the testicular parenchyma [Fig. 25] (Dogra et al, 2003, as cited in Janzen et al, 1992). The clinical significance of testicular microlithiasis is that it is associated with increased risk of testicular malignancy, thus follow up of affected individuals with scrotal sonography is necessary to ensure that a testicular tumor does not develop.

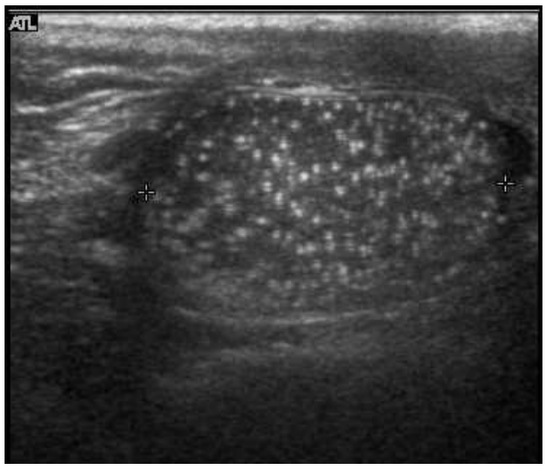

Fig. 25. Testicular microlithiasis. Multiple hyperechoic foci without acoustic shadow presenting as a starry sky appearance is seen in the testis

7.3 Testicular torsion

The normal testis and epididymis are anchored to the scrotal wall. If there is a lack of development of these attachments, the testis is free to twist on its vascular pedicle. This will result in torsion of the spermatic cord and interruption of testicular blood flow. Testicular torsion occurs most commonly at 12 to 18 years but can occur at any age. Torsion results in swelling and edema of the testis, and as the edema increases, testicular perfusion is further altered. The extent of testicular ischemia depends on the degree of torsion, which ranges from 180° to 720° or greater. The testicular salvage rate depends on the degree of torsion and the duration of ischemia. A nearly 100% salvage rate exists within the first 6 hours after the onset of symptoms; a 70% rate, within 6–12 hours; and a 20% rate, within 12–24 hours (Dogra et al, 2003, as cited in Patriquin et al, 1993). Therefore testicular torsion is a surgical emergency and the role of ultrasound is to differentiate it from epididymitis as both disease presents with acute testicular pain clinically.

There are two types of testicular torsion: extravaginal and intravaginal. Extravaginal torsion occurs exclusively in newborns. Ultrasound findings include an enlarged heterogeneous testis, ipsilateral hydrocele, thickened scrotal wall and absence of vascular flow in the testis and spermatic cord (Dogra et al 2003, as cited in Brown et al, 1990). The ultrasound findings

of intravaginal torsion vary with the duration and the degree of rotation of the spermatic cord. Gray scale ultrasound may appear normal if the torsion is just occurred. At 4-6 hours after onset of torsion, enlarged testis with decreased echogenicity is seen. At 24 hours after onset, the testis appears heterogeneous due to vascular congestion, hemorrhage and infarction (Dogra et al, 2003). As gray scale ultrasound is often normal during early onset of torsion, Doppler sonography is considered as essential in early diagnosis of testicular torsion. The absence of testicular flow at color and power Doppler ultrasound is considered diagnostic of ischemia [Fig. 26], provided that the scanner is set for detection of slow flow, the sampling box is small and the scanner is adjusted for the lowest repetition frequency and the lowest possible threshold setting.

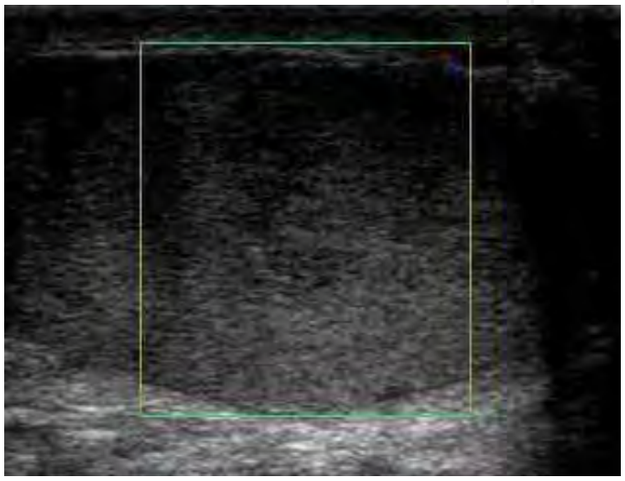

Fig. 26. Testicular torsion of the right testis. Absence of vascular flow and ill-defined hypoechoic lesions are seen in the testis

7.4 Varicocele

Varicocele refers to an abnormal dilatation of the veins of the spermatic cord due to incompetence of valve in the spermatic vein. This results in impaired blood drainage into the spermatic vein when the patient assumes a standing position or during Valsalva's maneuver. Varicoceles are more common on the left side due to the following reasons (a) The left testicular vein is longer; (b) the left testicular vein enters the left renal vein at a right angle; (c) the left testicular artery in some men arches over the left renal vein, thereby compressing it; and (d) the descending colon distended with feces may compress the left testicular vein (Mehta and, Dogra, 1998).

The US appearance of varicocele consists of multiple, hypoechoic, serpiginous, tubular like structures of varying sizes larger than 2 mm in diameter that are usually best visualized superior or lateral to the testis [Fig. 27a]. Color flow and duplex Doppler US optimized for low-flow velocities help confirm the venous flow pattern, with phasic variation and retrograde filling during a Valsalva's maneuver [Fig. 27b]. Intratesticular varicocele may appear as a vague hypoechoic area in the testis or mimics tubular ectasia. With color Doppler, this intratesticular hypoechoic area also showed reflux of vascular flow during Valsalva's maneuver [Fig. 28]

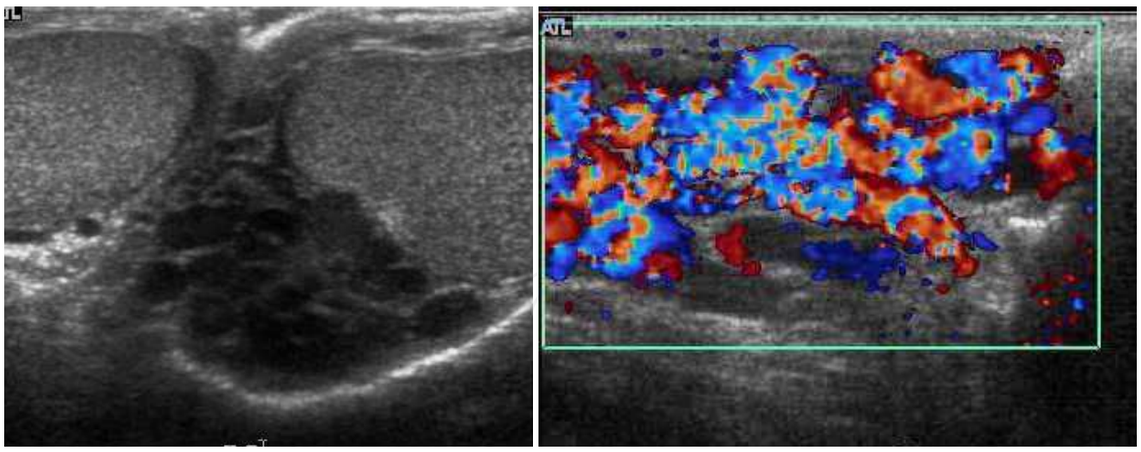

(a) (b)

Fig. 27. Varicocele. (a) Multiple tortuous tubular like structure are seen in the left scrotum. (b) Color Doppler sonography shows vascular reflux during Valsalva's maneuver

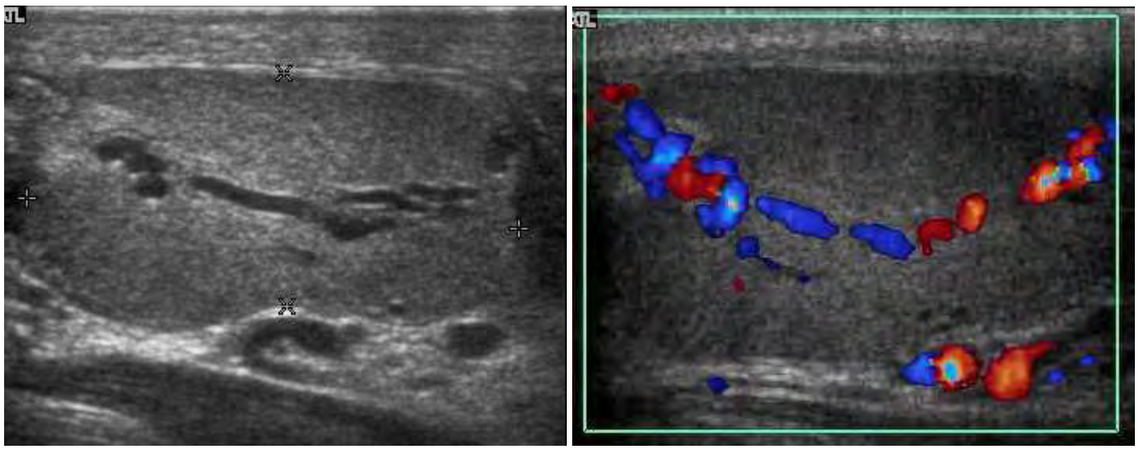

(a) (b)

Fig. 28. Intratesticular varicocele. (a) Dilated tubular structures are seen within the testis. (b) Presence of vascular reflux is noted during Valsalva's maneuver

7.5 Undescended testis (Cryptorchidism)

Normally the testes begin its descent through the inguinal canal to the scrotum at 36 weeks' of gestation and completed at birth. Failure in the course of testes descent will result in undescended testes. Undescended testis is found in 4% of full-term infants and only 0.8% of males at the age of 1 year have true cryptorchidism. Although an undescended testis can be found anywhere along the pathway of descent from the retroperitoneum to the scrotum, the inguinal canal is the most common site for an undescended testis. Deviation of testis from the normal pathway of descent will result in ectopic testis that is commonly seen in pubopenile, femoral triangle and perineal regions.

Besides infertility, undescended testes carry an increased risk of malignancy even for the normally located contralateral testis. The risk of malignancy is estimated to be as high as 10

times the normal individual with seminoma being the most common malignancy. The incidence of infertility is decreased if surgical orchiopexy is carried out before the 1-3 years but the risk of malignancy does not change.

Because of the superficial location of the inguinal canal in children, sonography of undescended testes should be performed with a high frequency transducer. At ultrasound, the undescended testis usually appears small, less echogenic than the contralateral normal testis and usually located in the inguinal region [Fig. 29]. With color Doppler, the vascularity of the undescended testis is poor.

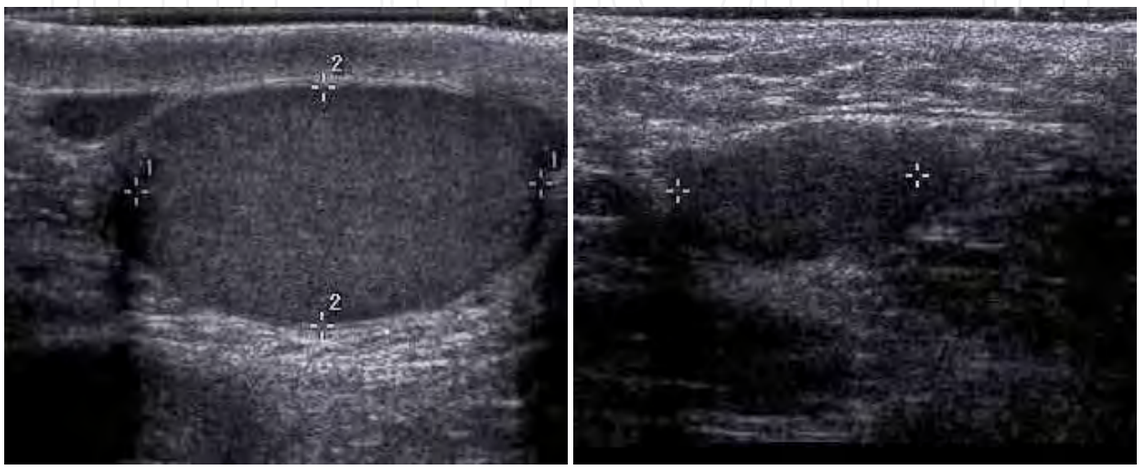

(a) (b)

Fig. 29. Undescended testis. (a) Normal testis in the scrotum. (b) Atrophic and decreased echogenicity of the contralateral testis of the same patient seen in the inguinal region

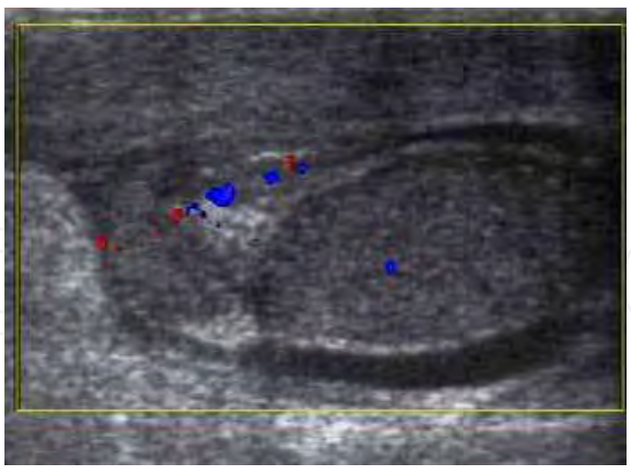

Fig. 30. Testicular appendiceal torsion. A hyperechoic lesion with surrounding vascularity is seen in the groove between the testis and epididymis

7.6 Testicular appendiceal torsion

At sonography, the appendix testis usually appears as a 5 mm ovoid structure located in the groove between the testis and the epididymis. Normally it is isoechoic to the testis but at

times it may be cystic. The appendix epididymis is of the same size as the appendix testis but is more often pedunculated. Clinically pain may occur with torsion of either appendage. Physical examination showed a small, firm nodule is palpable on the superior aspect of the testis and a bluish discoloration known as ''blue dot'' sign may be seen on the overlying skin (Dogra and Bhatt 2004, as cited in Skoglund et al 1970). Torsion of the appendiceal testis most frequently involved in boys aged 7-14 years (Dogra and Bhatt 2004).

The sonographic features of testicular appendiceal torsion includes a circular mass with variable echogenicity located adjacent to the testis or epididymis [Fig. 30], reactive hydrocele and skin thickening of the scrotum is common, increased peripheral vascular flow may be found around the testicular appendage on color Doppler ultrasound. Surgical intervention is unnecessary and pain usually resolves in 2 to 3 days with an atrophied or calcified appendages remaining.

8. Conclusion

Ultrasound remains as the mainstay in scrotal imaging not only because of its high accuracy, excellent depiction of scrotal anatomy, low cost and wide availability, it is also useful in determining whether a mass is intra- or extra-testicular, thus providing us useful and valuable information to decide whether a mass is benign or malignant even though malignancy do occur in extratesticular tumors and vice versa. Furthermore, ultrasound also provides information essential to reach a specific diagnosis in patients with testicular torsion, testicular appendiceal torsion and inflammation such as epididymo-orchitis, Fournier gangrene etc, thus enabling us to avoid unnecessary operation.

9. Acknowledgments

The authors acknowledge Miss Lee Ying-Fang for her expert technical support in preparation of this manuscript. We are also thankful to British Institute of Radiology and John Wiley and Sons publishing company in granting us permission to reuse some of the figures previously published in British Journal of Radiology and Journal of Clinical Ultrasound.

10. References

Akbar SA (2003), Sayyed TA, Jafri SZ, Hasteh F & Neill JS. Multimodality Imaging of Paratesticular Neoplasms and Their Rare Mimics. *Radiographics*, Vol. 23, No. 6, (November-December 2003), pp. 1461-1476, ISSN 0271-5333

Bostwick DG (1997). Spermatic Cord and Testicular Adnexa, In: *Urologic Surgical Pathology* , Bostwick DG, Eble JN, pp. 647-674 Mosby, ISBN 978080167 St Louis, Missouri.

Boyum J(2008) & Wasserman NF. Malignant Mesothelioma of the Tunica Vaginalis Testis. *Journal of ultrasound in Medicine*, Vol. 27, No. 8, (August 2008), pp.1249-1255. ISSN 0278-4297

Bruno C (2002), Minniti S & Procacci C. Diagnosis of Malignant Mesothelioma of the Tunica Vaginalis Testis by Ultrasound Guided Fine Needle Aspiration. *Journal of Clinical Ultrasound*, Vol. 30, No.3, (March-April 2002), pp.181-183. ISSN 0091-2751

Dogra VS (2003), Gottlieb RH, Oka M & Rubens DJ. Sonography of the Scrotum. *Radiology*, Vol.227, No.1, (April 2003), pp.18–36. ISSN 0033-8419

Dogra V (2004) & Bhatt S. Acute Painful Scrotum. *Radiologic Clinics of North America*, Vol.42, (2004), pp. 349– 363, ISSN 0033-8389

Doll DC (1986) & Weiss RB Malignant Lymphoma of the Testis. *American Journal of Medicine*, Vol.81, No. 3, (September 1986), pp.515-524, ISSN 0002-9343

Garriga V (2009), Serrano A, Marin A, Medrano S, Roson N & Pruna X. US of the Tunica Vaginalis Testis: anatomic relationships and pathologic conditions. *Radiographics*, Vol.29, No.7, pp.2017-2032, (November, 2009), ISSN0271-5333

Kim W (2007), Rosen MA, Langer JE, Banner MP, Siegelman ES & Ramchandani P. US–MR Imaging Correlation in Pathologic Conditions of the Scrotum. *Radiographics,* Vol.27, No.5, (September 2007), pp.1239–1253, ISSN 0271-5333.

Levenson RB (2008), Singh AK & Novelline RA. Fournier Gangrene: Role of Imaging. *Radiographics*, Vol.28, No.2, (March-April 2008), pp.519-528, ISSN0271-5333

Mak CW (2001), Wu TC, Chou CK, Tzeng WS, Sia YL, Chang JM & Lin CN. Ultrasonographic Appearance of an Adenomatoid Tumor in the Epididymis: Report of a Case. *Journal of Medical Ultrasound*, Vol.9, No.4, (December 2001), pp. 202-205, ISSN 0929-6441

Mak CW (2004a), Chou CK, Su CC, Huan SK & Chang JM. Ultrasound Diagnosis of Paratesticular Rhabdomyosarcoma. *British Journal of Radiology*, Vol.77, No. 915, (March 2004), pp.250–252, ISSN 0007-1285

Mak CW (2004b), Cheng TC, Chuang SS, Wu RH, Chou CK & Chang JM. Malignant Mesothelioma of the Tunica Vaginalis Testis. *British Journal of Radiology*, Vol.77, No.921, (September2004), pp.780–781, ISSN 0007-1285

Mak CW (2004c), Tzeng WS, Chou CK, Chen CY, Chang JM & Tzeng CC. Leiomyoma Arising from the Tunica Albuginea of the Testis: Sonographic Findings. *Journal of Clinical Ultrasound*, Vol.32, No.6, (July-August 2004), pp.309–311, ISSN 0091-2751

Mak CW (2007a), Chen CY, Tzeng WS & Li CF. Epidermoid Cyst of the Testis. *Australasian Radiology*, Vol.51, No.Supplement S1, (October 2007), pp.B74–B76, ISSN 0004-8461

Mak CW (2007b), Tzeng WS & Chou CK. Microcystic Lesion of the Testis. *British. Journal. Radiology*, Vol.80, No. 949, (January 2007) pp.67-68, ISSN 0007-1285.

Mehta AL (1998) & Dogra VS. Intratesticular Varicocele. *Journal of Clinical Ultrasound*, Vol.26, No.1, pp.49-51, (January 1998), ISSN 0091-2751

Muttarak M(2006) & Peh WC. Case 91: Tuberculous Epididymo-orchitis. *Radiology*, Vol.238, No.2, (February 2006), pp.748-751, ISSN 0033-8419

Rosenberg R (1989) & Williamson MR. Lipomas of the Spermatic cord and Testis: Report of Two Cases. *Journal of Clinical Ultrasound*, Vol.17, No.9, (November-December 1989), pp.670-674, ISSN 0091-2751

Wang MT (2005), Mak CW, Tzeng WS, Chen JC, Chang JM & Lin CN. Malignant Mesothelioma of the Tunica Vaginalis Testis: Unusual Sonographic Appearance. *Journal of Clinical Ultrasound*, Vol.33, No.8, (October, 2005), pp.418–420, ISSN 0091-2751

Woodward PJ (2002), Sohaey, R, O'Donoghue MJ & Green DE. Tumors and Tumorlike Lesions of the Testis: Radiologic-Pathologic Correlation. *RadioGraphics*, Vol.22, No.1, (January-February 2002), pp.189–216, ISSN 0271-5333.

Woodward PJ (2003), Schwab CM & Sesterhenn IA. Extratesticular scrotal masses: Radiologic-pathologic correlation. *Radiographics*, Vol.23, No.1, (January-February 2003), pp. 215-40, ISSN 0271-5333.

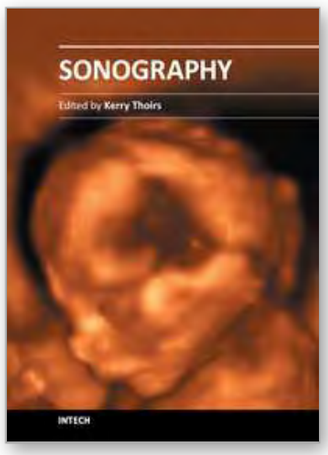

Sonography

Edited by Dr. Kerry Thoirs

ISBN 978-953-307-947-9
Hard cover, 346 pages
Publisher InTech
Published online 03, February, 2012
Published in print edition February, 2012

Medical sonography is a medical imaging modality used across many medical disciplines. Its use is growing, probably due to its relative low cost and easy accessibility. There are now many high quality ultrasound imaging systems available that are easily transportable, making it a diagnostic tool amenable for bedside and office scanning. This book includes applications of sonography that can be used across a number of medical disciplines including radiology, thoracic medicine, urology, rheumatology, obstetrics and fetal medicine and neurology. The book revisits established applications in medical sonography such as biliary, testicular and breast sonography and sonography in early pregnancy, and also outlines some interesting new and advanced applications of sonography.

How to reference

In order to correctly reference this scholarly work, feel free to copy and paste the following:

Chee-Wai Mak and Wen-Sheng Tzeng (2012). Sonography of the Scrotum, Sonography, Dr. Kerry Thoirs (Ed.), ISBN: 978-953-307-947-9, InTech, Available from: http://www.intechopen.com/books/sonography/sonography-of-the-scrotum

INTECH
open science | open minds

InTech Europe
University Campus STeP Ri
Slavka Krautzeka 83/A
51000 Rijeka, Croatia
Phone: +385 (51) 770 447
Fax: +385 (51) 686 166
www.intechopen.com

InTech China
Unit 405, Office Block, Hotel Equatorial Shanghai
No.65, Yan An Road (West), Shanghai, 200040, China
中国上海市延安西路65号上海国际贵都大饭店办公楼405单元
Phone: +86-21-62489820
Fax: +86-21-62489821

IntechOpen

2

Clinical Perspectives of Scrotal Ultrasound in Urology

Shou-Hung Tang, Tai-Lung Cha and Guang-Huan Sun
Tri-Service General Hospital, National Defense Medical Center, Taiwan, R.O.C.

1. Introduction

Scrotal ultrasound is widely used in modern hospitals as the first-line evaluation of almost all scrotal abnormalities. It provides useful and timely information for physicians to make management decisions without delay. This chapter is written in accordance with the clinical perspectives of urologists, as opposed to the technical interpretation of radiologists, in order to provide practical assistance to practicing physicians. An assessment of the commonest scrotal disorders will be discussed in this chapter.

Quick guide to ultrasound equipment and common imaging techniques
Normal ultrasound anatomy of the testis and epididymus
Identify scrotal and testicular emergencies that require surgical attention Testicular torsion Acute epididymitis, orchitis, and epididymo-orchitis Testicular trauma Fournier's gangrene
Neoplasm of the testis Malignant neoplasms of the testis Benign neoplasms of the testis
Non-neoplastic disease of the scrotum and testis Varicocele Hydrocele Spermatocele Testicular microlithiasis Scrotal wall abscess

Table 1. Chapter highlights

2. Quick guide to ultrasound equipment and common imaging techniques

It is generally recommended that a high frequency (7 to 12 MHz) ultrasound transducer should be used whenever possible, set to the "small parts" setting, in order to examine

scrotal contents (Bluth et al., 2001). Transducers with higher frequencies (e.g., >17 MHz) may help to obtain greater resolutions of fine anatomical details and are therefore particularly useful in pediatric patients. A machine that has the ability to perform color Doppler scans is always included as a standard setting. Color Doppler scans are required to diagnose vascular abnormalities, such as varicoceles, or more importantly, testicular torsion. Combined high-frequency scans and color Doppler images are sufficient for the diagnosis of most cases (Sandor et al., 2011). Advanced ultrasound techniques include contrast-enhanced studies, power Doppler scanning, and down-shifted Doppler frequencies in specific clinical situations. However, we do not recommend their use in routine daily practice.

Prior to the ultrasound examination, it is crucial that the patient should be calmed and that the procedure has been fully explained to them. The examiner should obtain a clear clinical history of the patient and any major past medical history should be known about before the study begins. It is recommended that the patient should be placed in the supine position with their thighs slightly abducted, described as the "frog-legs" posture. We have found that putting a rolled towel underneath the scrotum is helpful, but this maneuver should be individualized and only performed when the findings will not be affected by any compressive force.

Routine scanning procedures include the following scans as a minimum: long-axis (longitudinal), short-axis (transverse), and color-Doppler scans of both testicles, the epididymis and the spermatic cords. Care must be taken not to overlook lesions underneath or within the scrotal wall. In most cases, the content of the contralateral scrotum is a good reference guide to assessing the side with the lesion, and it is convenient to use the split-screen function for a contemporaneous comparison of both sides.

3. Normal ultrasound anatomy of the testis and epididymis

Normal testes are responsible for both reproductive and endocrine functions. In the adult human, the testes are ovoid in shape, with a size of approximately 4 x 3 x 2.5 cm (30 ml volume). Each testis is composed of approximately 250-300 lobules that contain seminiferous tubules. The lobules are separated by septa that cannot be visualized under sonography. These septa attach to the inner side of the tunica albuginea and connect to the mediastinum of the testis. At the mediastinum, the convoluted seminiferous tubules become straightened (the so-called "rete testis") and form 10-15 ductules that drain into the epididymis (Campbell et al., 2007).

The epididymis tightly attaches to the posterior lateral aspect of each testis. Grossly, this organ resembles an earthworm with an overall length of 4 to 5 cm. The epididymis contains a head (upper pole), body (mid-part), and a tail which connects to the vas deferens.

4. Identify scrotal and testicular emergencies that require surgical attention

4.1 Testicular torsion

Testicular torsion, or more precisely, torsion of the spermatic cord, is a true urological emergency. It affects approximately 1 in 4,000 young males before the age of 25 years (Datta et al., 2011). Almost all patients with testicular torsion present with excruciating pain, which usually wakes them up during sleep. The pain occurs as a result of testicular ischemia, and in some cases, the pain might have resolved as a result of spontaneous detorsion.

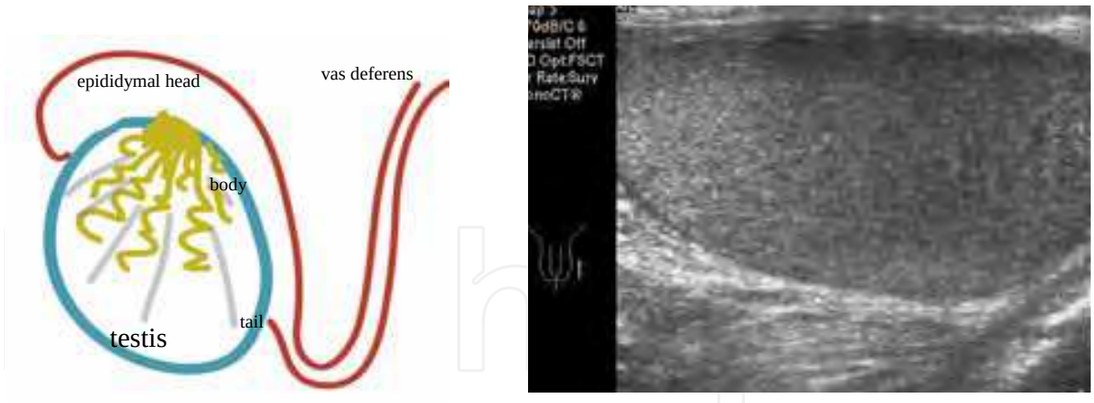

(a) (b)

Fig. 1. (a) Simplified anatomy of the testis and epididymis; (b) normal appearance of the left-sided testis on a longitudinal scan

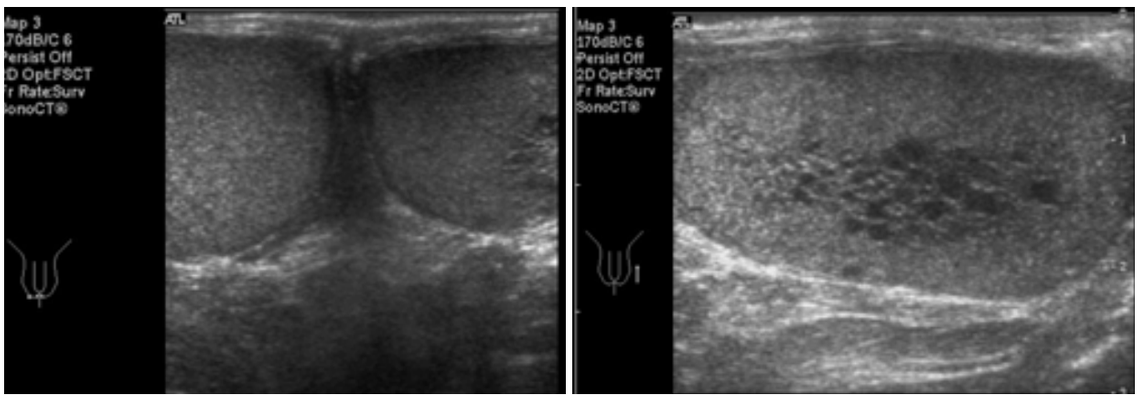

(a) (b)

Fig. 2. The rete testis: (a) hypoechoic foci in the left testis were found on a transverse midline scan; (b) multiple tubule-like hypoechoic areas in the area of testicular mediastinum

The etiology of this condition is attributed to an abnormally high or thin attachment of the tunica vaginalis to the spermatic cord, which makes twisting of the cord more likely. This is known as a bell-clapper deformity. Testicular torsion can be intravaginal, which is seen in all age groups, or extravaginal, which is seen exclusively in neonates.

Torsion of the epididymal appendix should also be included in the differential diagnosis of testicular pain, but is seldom treated as a surgical emergency. Physical examination of the affected testis may reveal that its long axis is altered, and it lies more horizontally. Mildly swelling of the scrotum can be expected, and the testis moves in a cephalad direction towards the external inguinal ring. In up to 99% of patients, there is no cremasteric reflex on the affected side (Schmitz, 2009).

Although manual detorsion has been suggested by some authors, this is not considered to be the definite treatment. All patients in which testicular torsion is suspected should undergo surgical detorsion within 6 hours of the symptoms developing, and a concurrent prophylactic orchiopexy should be performed on the contralateral testis.

Ultrasound with color Doppler flow imaging provides the most useful information to urologists within a very short time. Typically, lower or no vascular flow to the affected testis is compatible with the diagnosis, and a detectable blood flow to the peripheral tunica albuginea may be seen. The echogenicity of the testis may vary from normal to hypoechoic, or even heterogeneous, which reflects the severity of injury.

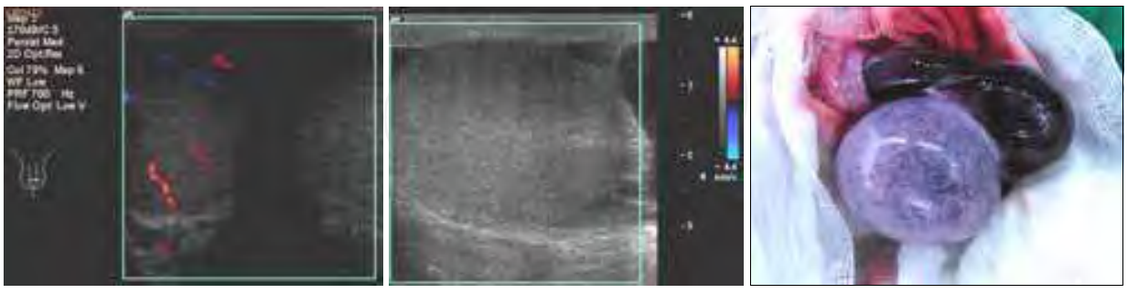

(a) (b) (c)

Fig. 3. Testicular torsion. A 50-year-old male presented to the ER and complained of a sudden painful enlargement of his left testis over 1 day: (a, b) ultrasonography showed absent vascularity with a cystic lesion in the left testis. Testicular echogenicity had not changes; (c) emergent exploration confirmed a 360º torsion and necrotic change of the affected organ. A left-sided orchiectomy was performed

4.2 Acute epididymitis, orchitis, and epididymo-orchitis

Acute epididymitis or epididymo-orchitis is one of the most common urological disorders in males. It primarily occurs in men aged between 18 and 60 years old, but can affect males of any age. This type of inflammatory change is often caused by bacteria (e.g., *E. coli* and *Pseudomonas* species), sexually-transmitted pathogens (e.g., *Neisseria gonorrhea*), or *Mycobacterium tuberculosis*. Ascending infections of pathogens from the urethra is the most common etiology; however, the hematogenous spread of pathogens to the epididymus can occur.

Patients tend to present with unilateral scrotal swelling and pain. Fever and leukocytosis may accompany the pain. If the inflammatory process cannot be controlled during its early phase, the affected epididymis/ testis may undergo infarction and necrotic change, which eventually lead to abscess formation. It is not uncommon to see those abscesses ruptured through the scrotal skin.

Scrotal ultrasound with color Doppler imaging offers a clue to making this diagnosis, if present in conjunction with relevant clinical symptoms. During the early phase of inflammation, focal swelling (most commonly, the epididymal tail is the first to become enlarged) and increased focal blood flow can be detected. Later, the testis becomes tense and enlarged, and its blood flow is therefore compromised in certain areas, which results in a heterogeneous sonographic appearance (de Cassio Saito et al., 2004). The formation of a large abscess is usually an indication for surgery.

Chronic inflammatory changes of the epididymis and testes are not uncommon. Diagnosing chronic epididymitis requires the combination of a relevant clinical history for over 3 months, positive urine cultures, and an inflammatory process that observed with sonography.

(a) (b) (c)

Fig. 4. Bilateral epididymitis. A 21-year-old with a gonococcal urethritis later developed fever and bilateral painful swelling of testicles. The sonography showed (a, b) swelling and hypervascularity of the left epididymal tail. (c) A short-axis scan at the level of the lower scrotum demonstrated bilateral involvement of the inflammatory process

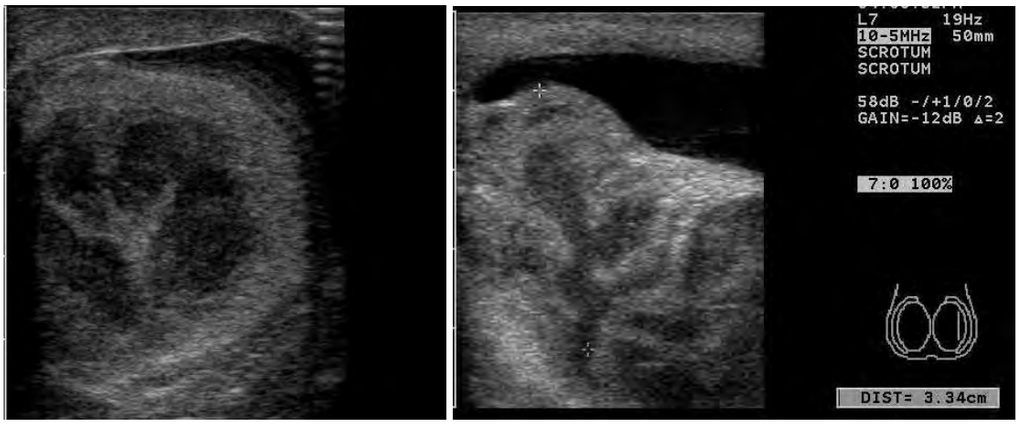

(a) (b)

Fig. 5. A case of chronic epididymo-orchitis with an abscess. An 86-year-old male presented with a low grade fever and painful swelling of his left testicle. (a) A short-axis scan and (b) long-axis scan both revealed a heterogeneous irregularly enlarged epididymis and testis. A hydrocele was also noted. The patient underwent a left-sided orchiectomy and the histopathological findings confirmed a chronic inflammation. It was not sonographically evident to differentiate a neoplasm from the inflammatory changes in this case

4.3 Testicular trauma

4.3.1 Testicular rupture

Testicular trauma is a common presentation to the emergency department. Blunt trauma to the genitalia accounts for more than 80% of these patients, and testicular injury should be considered in any patient with a pelvic fracture.

Patients universally present with a definite mechanism and with pain. At physical examination, the affected testicle is usually enlarged and tender. As only a ruptured tunica albuginea should be surgically corrected, this should be diagnosed as quickly as possible.

Diagnosing testicular rupture with ultrasound has a specificity of over 80% (Cokkinos et al., 2011). The sonography should be focused on the presence of hematocele (fluid between the

layers of the tunica vaginalis), a discontinued line of the tunica albuginea, and unequal testicular sizes. It is important to consider that testicular torsion can occur after a minor trauma, and this should not be overlooked.

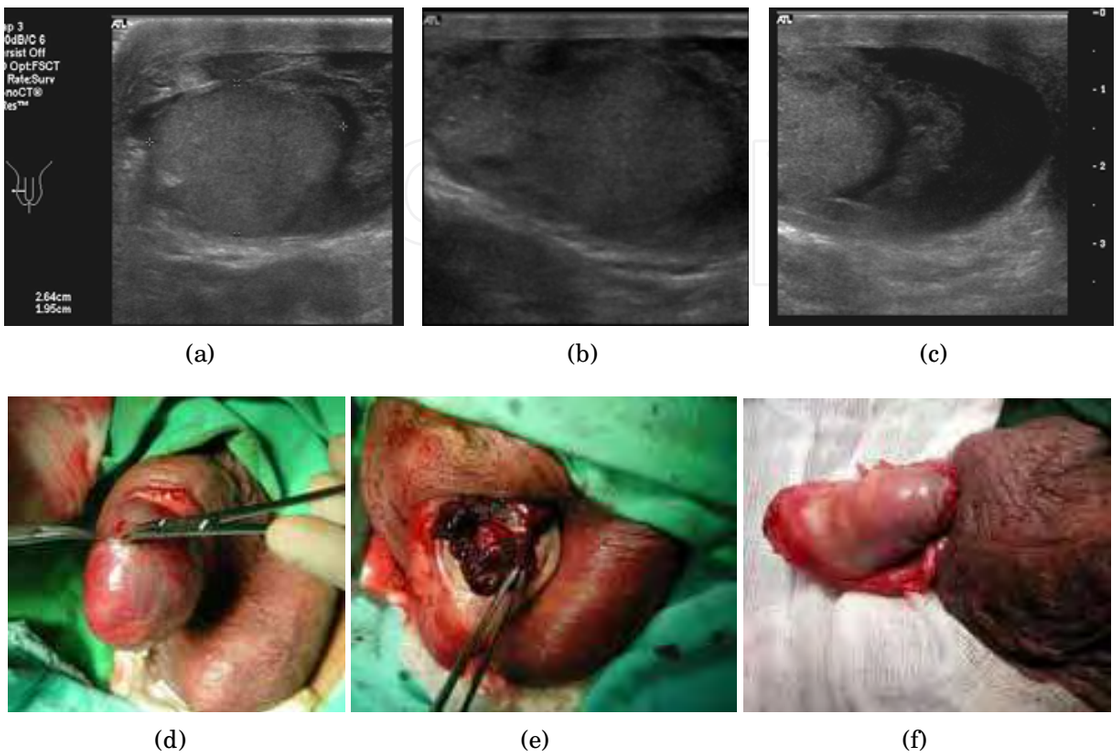

(a) (b) (c)

(d) (e) (f)

Fig. 6. Testicular rupture. A 46-year-old male sustained a blunt force to the genitalia and scrotal painful swelling developed. (a-c) Ultrasonography showed an ill-defined testicular margin, deformity, heterogeneous echogenicity and swelling of the right testis. A hydrocele or hematocele was also noted. (d) On surgical exploration, the tunica vaginalis was intact and a hematocele was found inside. (e) Testicular rupture through the disrupted tunica albuginea. (f) The tunica albuginea was repaired, and swollen testicular tissues were trimmed away

4.3.2 Intratesticular hematoma

After blunt contusion of the testis, testicular hematoma may occur, rather than a true rupture. The patient may complain of a gradually enlarging testis if he is seen few weeks after the injury. The typical sonographic findings reveal various degrees of heterogeneous echogenicity with a focally decreased pattern of blood flow. It is difficult to diagnose an intratesticular hematoma purely based on image findings.

4.3.3 Testicular contusion

Testicular contusion occurs frequently in active males. Contusion can be accidental, related to sports or as a result of violence. It is therefore important to obtain a clear history in order to estimate the force of injury accurately. Scrotal ultrasound is helpful in diagnosing testicular rupture, but making the diagnosis of a contusion by ultrasound is sometimes difficult.

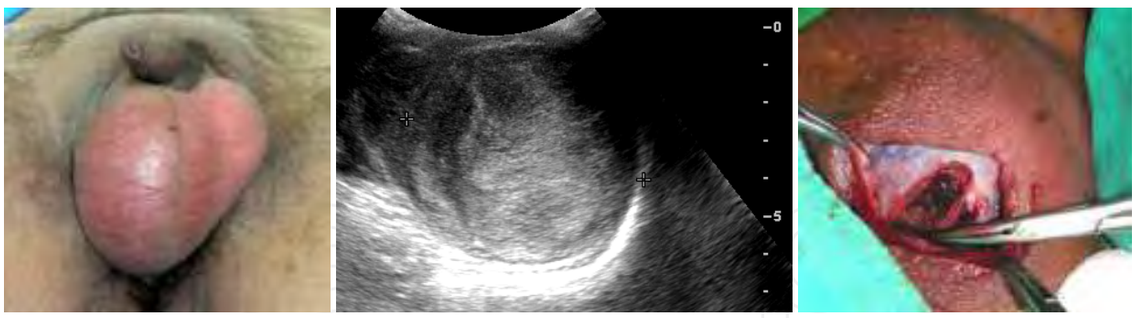

(a) (b) (c)

Fig. 7. Intratesticular hematoma. A 25-year-old male suffered a contused right hemiscrotum while lifting a box 2 weeks before. (a) Gross appearances showed an enlarged right testicle but no scrotal ecchymosis. (b) The right testis was enlarged with a heterogeneous echopattern, diminished blood flow, and an irregular contour that was suspicious of a testicular rupture. (c) Surgical exploration found a tense intratesticular hematoma; decompression was performed

The sonographic pictures may change over the first 72 hours from injury.After a blunt force to the testis, the testis may undergo inflammatory changes and become swollen. Since the tunica albuginea itself is strong and maintains the shape and volume of the testis, blood flow to a tense testis decreases as a result of swelling. Such a mechanism therefore makes the pattern seen on sonography very similar to that of a testicular torsion.

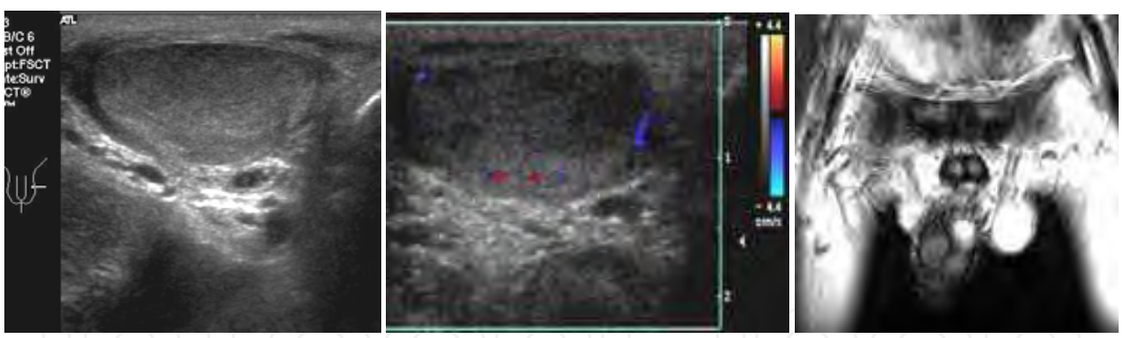

(a) (b) (c)

Fig. 8. A 26-year-old male sustained blunt scrotal injury and presented with left scrotal pain. (a) A transverse sonographic scan showed mild heterogeneous change of the left-sided testis. (b) There was a marked decrease in blood flow to the affected testis. (c) Magnetic resonance imaging: normal testicular perfusion and shape 1 day after the initial sonographic study

4.4 Fournier's gangrene

Fournier's gangrene is the most lethal necrotizing fasciitis that involves the genital and the perianal region. Most of the cases occur in patients between the ages of 20 and 50 years, with a male predominance. The mortality rate remains high at approximately 50% of cases even after aggressive debridement and other modern interventions.

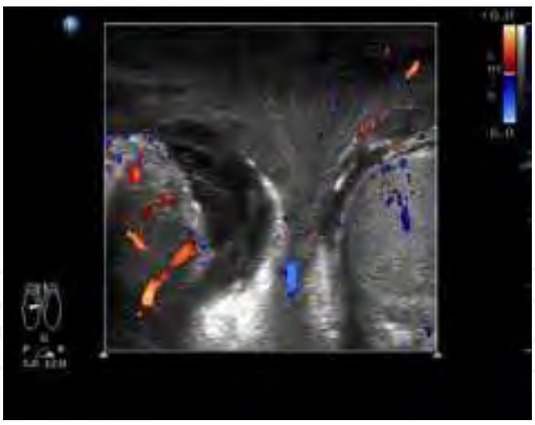

(a)

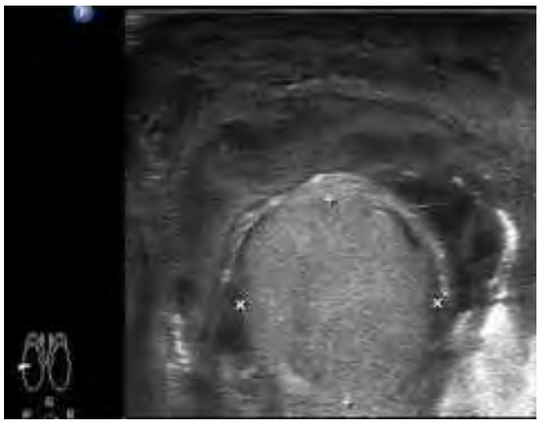

(b)

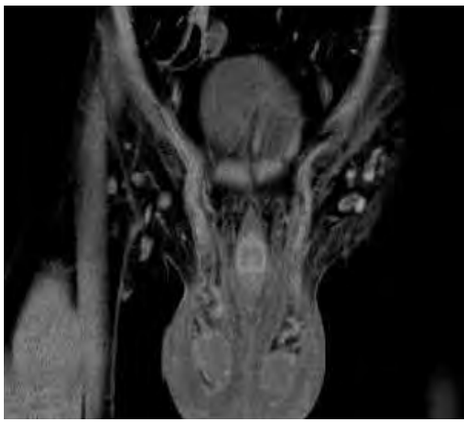

(c)

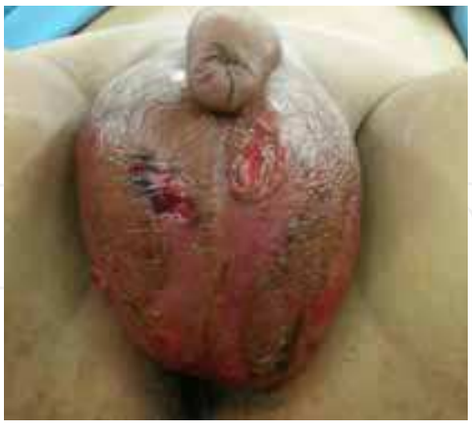

(d)

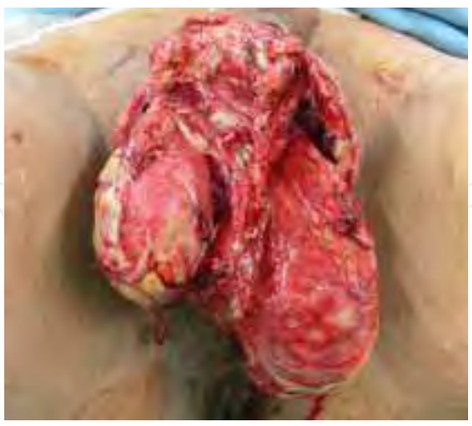

(e)

Fig. 9. A 27-year-old male presented with scrotal pain. (a,b) Enlargement, heterogeneous echogenicity, and increased vascularity of the bilateral epididymis with bilateral scrotal wall thickening on sonography. (c) Edematous scrotal wall on CT scanning. (d) Gross appearance of the scrotum. (e) Intraoperative view, showing that large amount of necrotic tissue should be removed

Urinary tract infection is recognized as the most common etiology, and it is commonly seen in cases that have undergone urethral catheterization; colorectal disease may also progress to Fournier's gangrene. Cases of Fournier's gangrene are associated with mixed flora on bacterial culture and some gas-forming organisms. The diagnosis depends on careful physical examinations, and with the aid of imaging studies to access the extent of the infection. During physical examination, any abnormally red or black skin coloration of the affected area should be observed to indicate ischemia; all examinations should include a test for skin crepitus to assess the presence of subcutaneous air.

Additional imaging study should never delay the timing of surgical intervention, since the infection is characterized by its rapid progression. Scrotal ultrasonography and CT scans of the lower abdomen to pelvic area are usually indicated.

Ultrasound imaging reveals heterogeneous echogenicity and increased vascularity in the affected testis. Thickening of the scrotal wall and areas of fluid-gas accumulation may be observed (Bartolotta et al., 2000). Without additional clear clinical information, a Fournier's gangrene can be mistaken ultrasonographically for acute epididymitis.

5. Neoplasm of the testis

5.1 Malignant neoplasms of the testis

The incidence of malignant neoplasms of the testis is rare compared with the aforementioned disorders. Overall, 90-95% of primary testicular cancers are germ cell tumors. Germ cell tumors can be divided into two major groups: seminomas (35%) and non-seminomatous germ cell tumors (65%). Subgroups that include embryonal cell carcinoma, teratoma, choriocarcinoma, and mixed type tumors are termed as non-seminomatous germ cell tumors (NSGCTs). A small portion of testicular cancers are metastatic lesions of leukemias and lymphomas (Tanagho et al., 2008).

Testicular cancers are more common on the right side, but this is not always the rule. Thirty to fifty percent of primary testicular cancers are seen in patients with a history of cryptorchidism. Approximately 90% of patients have painless enlargement of the testis, while others may present with pain or without symptoms at all. The combination of a sonographic diagnosis and serum tumor markers play an important role in the diagnosis of testicular cancers.

The major role of ultrasonography is to differentiate between malignant and benign testicular enlargement. In difficult cases, testicular cancers may mimic the signs of an infection; both of these share a pattern of increased blood flow of the affected region. However, characteristic sonographic features of malignancy are associated with specific cancer types.

Seminomas are intratesticular lesions, where the size of the lesion ranges from small nodules to the replacement of a whole testis. Seminomas typically appear as homogeneously hypoechoic on ultrasonography. NSGCTs are more aggressive tumors that can distort the contour of the ovoid tunica albuginea. They appear as heterogeneous lesions with irregular margins on ultrasonography. Teratomas consist of all three layers of embryonic tissues; they appear as mixed cysts, heterogeneous masses, and foci of calcification.

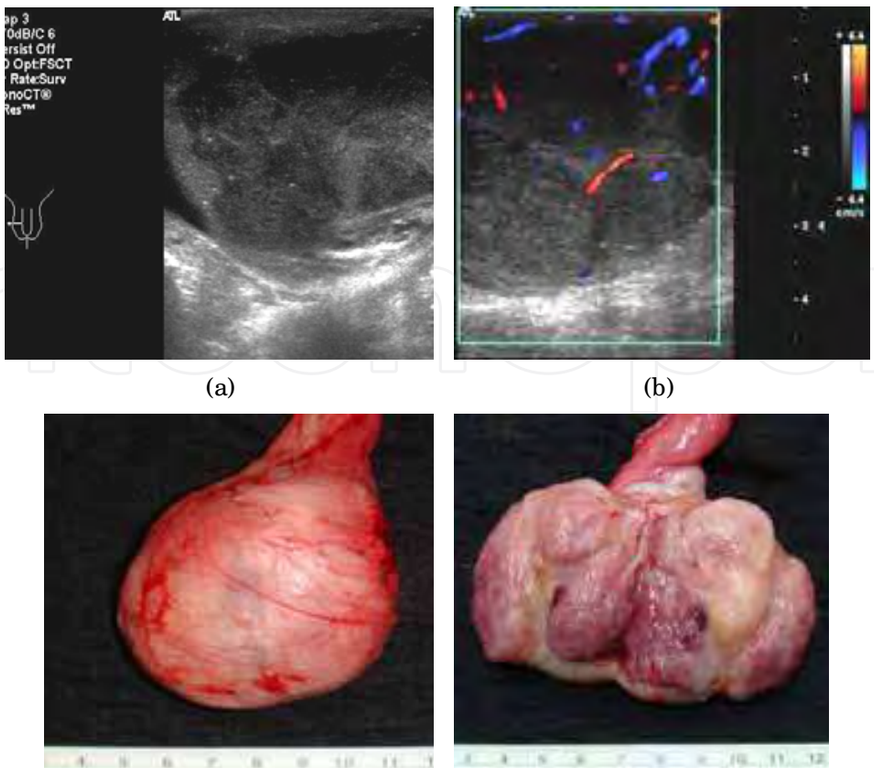

(a) (b)

(c) (d)

Fig. 10. Seminoma of the testis. A 31-year-old male presented with a gradual enlargement of the right testicle over several months. Vague pain was also mentioned. (a,b) Transverse ultrasound images showed multiple well-defined homogeneously hypoechoic lesions (the largest one was approximately 2.1 cm in size) in the right testis with increased vascularity in the peripheral region. (c) Radical orchiectomy was performed: the tumor was grossly confined within the tunica vaginalis. (d) The bivalve specimen showed the typical histological pattern of a seminoma

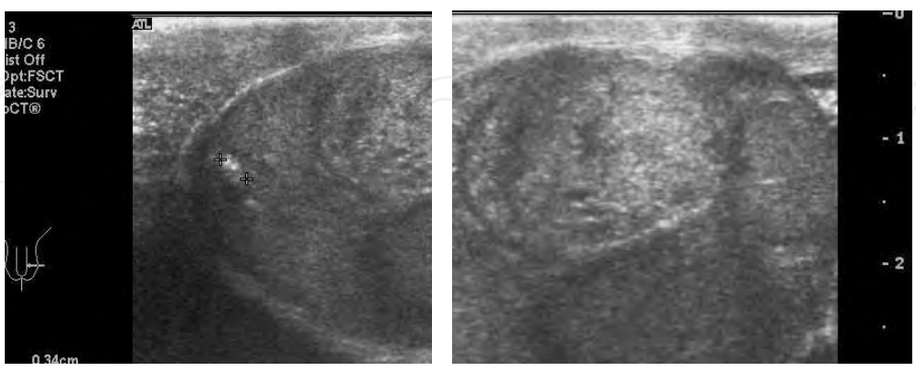

(a) (b)

Fig. 11. A non-seminomatous germ cell tumor of the testis. A 25-year-old male presented with pain over his lower abdomen. (a,b) A heterogenous mass (size: 3.2 x 2.9 cm) was shown to be located in the left testis with a few peripheral calcified spots. Pathology later confirmed that the lesion was a mixed germ cell tumor with embryonal carcinoma and yolk sac tumor components

If a primary testicular cancer is suspected, a biopsy should not be performed before definitive surgery (radical orchiectomy), in order to avoid iatrogenic seeding.

Testicular involvements from leukemia/ lymphoma are usually seen in elderly patients. They appear as homogeneous, hypoechoic lesions within the testes, and are usually bilateral. A biopsy is required to make a definite diagnosis. Lung cancer and prostatic cancer can rarely metastasize to the testes, and sonographic findings may vary according to the nature of the cell of origin.

5.2 Benign neoplasms of the testis

Benign tumors of the testis are rare. Among these, epidermoid cysts are the most common disorder. Epidermoid cysts can be diagnosed with ultrasonography, which avoids an orchiectomy. They occur in men aged between 20 and 40 years and are often found during a routine physical check-up or self-examination. Epidermoid cysts usually grow slowly and seldom cause pain. The characteristics of ultrasonography of an epidermoid cyst are a well-circumscribed lesion with a solid central core surrounded by an echogenic rim(s), which sometimes resemble a hollow target or layers of an onion (Meng et al., 2004). Recently magnetic resonance imaging has also played a role in this diagnosis of epidermoid cysts.

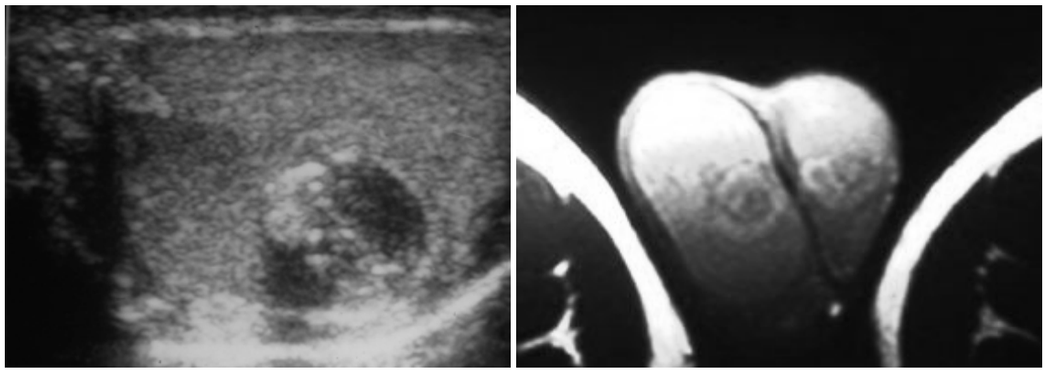

(a) (b)

Fig. 12. Testicular epidermoid cysts. (a) Typical sonographic pattern showing cystic lesion with an echogenic ring and some internal echogenic spots. (b) Magnetic resonance imaging was compatible with the diagnosis. This patient then underwent conservative surgery

6. Non-neoplastic disease of the scrotum and testis

6.1 Varicocele (scrotal varices)

Varicocele is a common cause of scrotal mass, and is estimated to affect 15% of males. It frequently causes symptoms in young males. Symptoms of varicoceles may include dull ache of the affected testis especially after prolonged standing or exercise. Varicoceles have also frequently been diagnosed during studies for male infertility (Tsao et al., 2009).

Varicoceles are more common in left-sided testicles (90%), and can occur bilaterally. By definition, a varicocele is the dilatation of the pampiniform plexus, which are the veins that

drain the testis. The testicular vein (internal spermatic vein) drains to the renal vein on the left side and to the inferior vena cava on the right side. The anatomical characteristics of these drainage routes means that there is a steeper insertion of the internal spermatic vein on the left side, which makes it prone to vascular reflux as a result of gravity. It is also believed that incompetent venous valves will cause reflux within the spermatic veins, which can be responsible for venous reflux back into the testis.

Diagnosing varicoceles is straightforward with physical examination. Varicoceles can be classified as mild, moderate or severe. With severe varicocele, one can easily observe "a bag-of-worms" appearance while the patient is standing. When in doubt, or there is a need to evaluate the underlying testes, ultrasonography with color flow imaging can offer clear information. Most authors agree that dilated veins greater than 2-3 mm in diameter with a change in the direction of flow during the Valsalva maneuver are compatible with the diagnosis of a varicocele.

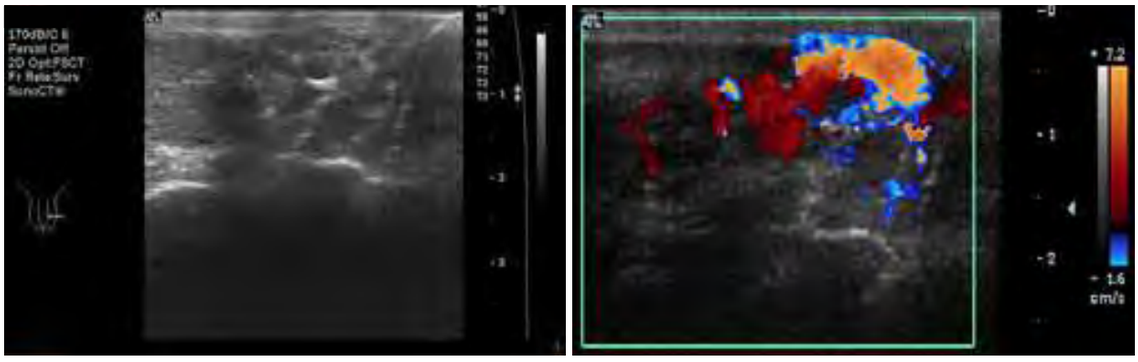

(a) (b)

Fig. 13. Scrotal varices. A 15-year-old male presented with dull ache and a left upper scrotal mass. (a) Upper scrotal transverse scan showed multiple hypoechoic vascular channels. (b) The Valsalva maneuver confirmed the reversed venous flow within the varicocele

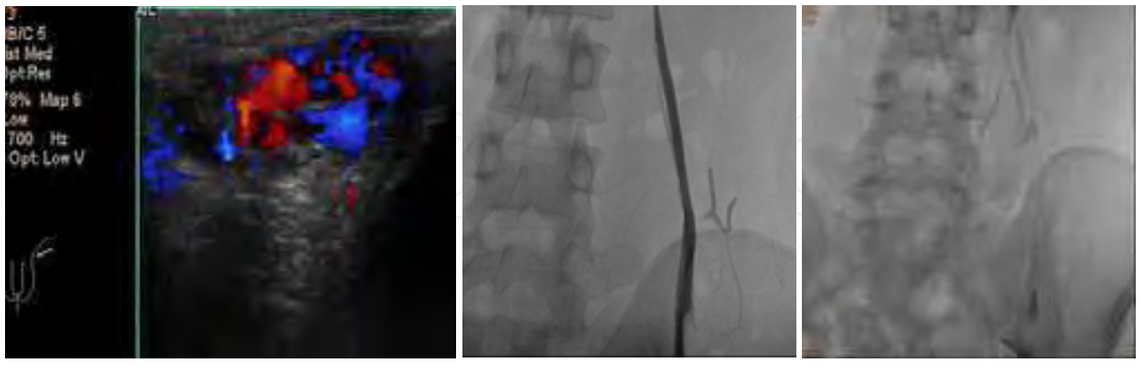

(a) (b) (c)

Fig. 14. Recurrent varicoceles. A 21-year-old male presented with a recurrent scrotal mass after a high ligation of internal spermatic vein (ISV) 2 years previously. (a) Sonographic diagnosis of reflux flow in the dilated left pampiniform plexus; (b) trans-jugular venography demonstrated patency of the left ISV; (c) embolization with coils successfully treated the recurrence

6.2 Hydrocele (hydrocele of the tunica vaginalis)

A hydrocele of the testis indicated fluid accumulation between the two layers of the tunica vaginalis. The tunica vaginalis is a remnant of peritoneum, which should close before birth. In children, a hydrocele is usually congenital and can present with an inguinal hernia. In the adult population, the hydrocele is usually secondary to infections (e.g., epididymitis), renal transplantation, peritoneal dialysis, testicular cancers, or torsion. Hydrocele affects 1% of adult men and is bilateral in 10% of all cases. Bilateral hydroceles should raise the suspicion of other underlying systemic diseases.

A hydrocele typically presents as a gradually enlarged testicle with no obvious pain. Severe and abrupt pain can indicate that the underlying condition should be investigated. During physical examination, good transillumination indicates a fluid content within the scrotum. Definite diagnosis can be made by ultrasonography. Scrotal ultrasound plays an important role not only for the diagnosis of hydrocele, but also to seek other possible etiologies, such as torsion, inflammation or malignancy.

Ultrasonographic findings of hydrocele are of typically pure anechoic fluid collection outside the tunica albuginea (Akin et al., 2004), but the fluid can be mixed with internal echoes in chronic cases. Some complex cases may demonstrate septations and loculations.

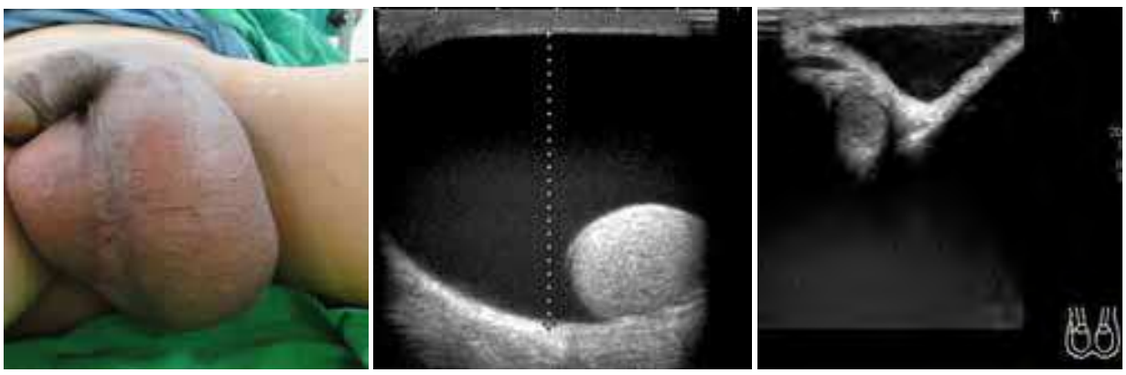

(a) (b) (c)

Fig. 15. A 58-year-old male presented with a feeling of heaviness and a gradually enlarged left scrotum. (a) A grossly enlarged left scrotum that was not tender; (b) transverse scan showed a marked accumulation of anechoic fluid and the testis was pushed aside; and (c) the hydrocele extends to the level of the external inguinal ring

6.3 Spermatocele

A spermatocele is a benign cystic lesion that contains sperm. It is commonly found in the epididymal head. Many spermatoceles are incidental, and are found during ultrasound screening in middle- to old-aged patients. The size of a spermatocele may vary from a few millimeters to several centimeters. Most spermatoceles do not cause symptoms, and the patient may present with a soft palpable mass inside the scrotum. In some cases, discomfort secondary to the mass effect may be present.

The etiology of spermatocele remains unclear. Most authors suggest that an obstruction in the efferent ductules is the origin of the disease. It is expected to grow slowly. Therefore,

aspiration of the cystic lesion will not solve the problem, and surgical excision offers the only curative approach for this disorder.

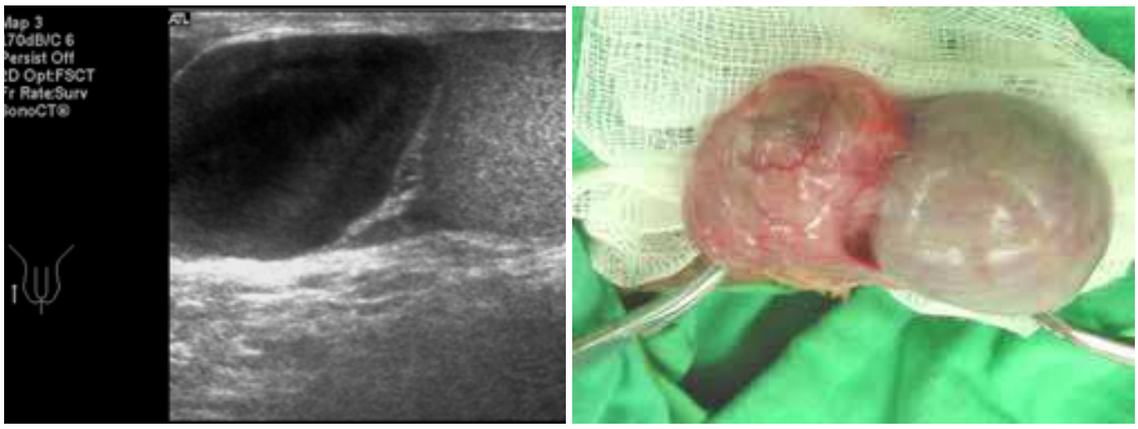

(a) (b)

Fig. 16. Epididymal spermatocele. A 56-year-old male presented with a slow-growing right scrotal mass that developed over several years. (a) Longitudinal scan showed a well-defined, 3-cm cystic lesion at right epididymal head with faint internal echogenicity; (b) scrotal exploration revealed findings that were compatible with the diagnosis of spermatocele

6.4 Testicular microlithiasis

Testicular microlithiasis (TM) is usually incidentally diagnosed by ultrasonography. TM may be correlated with testicular cancer and carcinoma in situ, although this issue remains controversial. In addition, TM is reported to be associated with various conditions, including male infertility, testicular atrophy, cryptorchidism, gonadal dysgenesis, Klinefelter syndrome, male pseudohermaphroditism, testicular torsion and varicocele. By definition, TM consists of small hyperechoic spots that less than 3 mm in size in the testis; the spots are usually multiple. A classic TM was defined as five or more microliths found on an

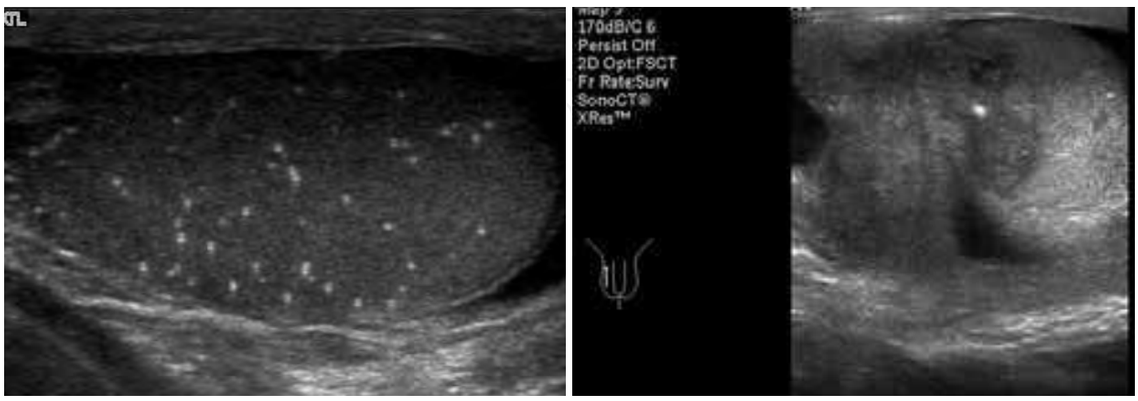

(a) (b)

Fig. 17. Two cases of TM associated with germ cell neoplasms. (a) Classic TM associated with a testicular cancer in the contralateral testis; (b) limited TM associated with an ipsilateral testicular germ cell tumor

ultrasound scan, and fewer the five microliths would be recognized as a form of limited TM. Hyperechoic spots on sonography are usually found without acoustic shadows. The incidence of TM ranges from 0.6%-9% in various retrospective studies (Chen et al., 2010). We also noted that patients with a malignant testicular neoplasm have a higher prevalence of TM (Ou et al., 2007).

6.5 Scrotal wall abscess

Abnormal scrotal conditions can be missed on routine ultrasonography if the clinical information is ignored. Detecting common scrotal disorders, such as an abscess, sebaceous cysts, lipomas, and edematous skin, should be the final step of the sonographic evaluation. The examiner is suggested to ask relevant questions to the patient in order to locate scrotal abnormalities accurately.

The sonographic patterns of scrotal abscesses range from anechoic to irregularly hyperechoic, with areas of internal echoes, septae, or even gas. Manually compressing with the ultrasound probe upon the abscess may induce motion within the abscess material.

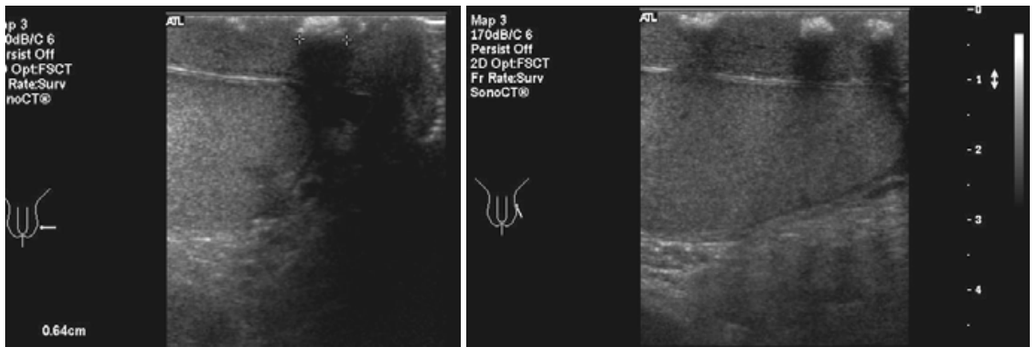

(a) (b)

Fig. 18. A 52-year-old suffered a perineal contusion 3 months previously. He presented with pain and induration over the left lower scrotum. (a) Transverse scan showed scrotal wall edematous changes, with hypoechoic areas and calcified lesions within the skin; (b) a longitudinal scan revealed similar findings that were compatible with chronic inflammatory changes

7. Conclusion

Ultrasound is convenient and important for the diagnosis of various scrotal abnormalities in clinical practice. Most notably, it is a time-saving procedure that requires only a very short time to train personnel to recognize urological emergencies. Nonetheless, a detailed medical history and physical examination should always precede the ultrasound study. Scrotal ultrasound offers clear information on whether a mass is intra- or extra-testicular, is cystic or solid, has increased or decreased focal flow, and whether the normal testicular ovoid shape is intact after a direct trauma.

A physician that performs scrotal ultrasound studies should be able to identify testicular torsion and testicular rupture in the emergency room setting, as both of these conditions require immediate surgical intervention. Lastly, although ultrasonography offers many

important diagnostic clues, it is not a perfect diagnostic tool. Adjunctive diagnostic tools, such as CT or MRI scanning or surgical exploration, may be needed to make a definitive diagnosis in difficult cases.

8. Acknowledgment

We thank Dr. Sheng-Tang Wu, Dr. Feng-Ping Chuang, Dr. Chi-Wei Tsao and Dr. En-Meng (TSGH-urology) for contributing cases to this chapter. We also thank Dr. Dah-Shyong Yu (urology), Dr. Sun-Yran Chang (urology) and Dr. Ching-Jiunn Wu (radiology) for their long-term education and support with our imaging studies.

9. References

Akin, EA., Khati, NJ, Hill, MC., et al. (2004). Ultrasound of the scrotum. *Ultrasound Q*, Vol. 20, No.4, (December 2004), pp.181-200, ISSN 0894-8771

Bartolotta, TV., Midiri, M., Caruso, G. et al. (2000). Necrotizing fasciitis of the scrotum (Fournier's gangrene): ultrasound findings. *Radiol Med,* Vol. 100, No.6, (April 2001), pp. 510-512,ISSN 0033-8362

Bluth, EI., Arger, PH., Benson, CB., et al. (2001). *Ultrasonography in urology* (1st edition), Thieme, ISBN 1588900517, New York

Campbell, MF., Wein, AJ, Kavoussi, LR. (2007). *Campbell-Walsh urology* (9th edition), W.B. Saunders, ISBN 1416029664, Philadelphia

Chen, JL., Chou, YH., Tiu, CM., et al. (2010). Testicular microlithiasis: analysis of prevalence and associated testicular cancer in Taiwanese men. *JClin Ultrasound,* Vol. 38, No.6, (July 2010), pp. 309-313.ISSN 1097-0096

Cokkinos, DD., Antypa, E., Tserotas, P., et al. (2011). Emergency ultrasound of the scrotum: a review of the commonest pathologic conditions. *Curr Probl Diagn Radiol,* Vol. 40, No.1,(January 2011),pp. 1-14, ISSN 1535-6302

Datta, V., Dhillon, G., Voci, S. (2011). Testicular torsion/ detorsion. *Ultrasound Q,* Vol. 27, No.2, (June 2011), pp. 127-128, ISSN 1536-0253

de Cassio Saito, O., de Barros, N., Chammas, MC. et al. (2004). Ultrasound of tropical and infectious diseases that affect the scrotum. *Ultrasound Q,* Vol. 20, No.1, (March 2004), pp. 12-18, ISSN 0894-8771

Meng, E., Sun, GH., Wu, CJ, et al. (2004). Epidermoid cysts of the testes in Taiwanese men. *Arch Androl,* Vol. 50, No.3, (May 2004), pp. 201-205, ISSN 0148-5016

Ou, SM., Lee, SS., Tang, SH., et al. (2007). Testicular microlithiasis in Taiwanese men. *Arch Androl,* Vol. 53, No.6, (November 2007), pp. 339-344, ISSN 0148-5016

Schmitz, D., Safranek, S.(2009). Clinical inquiries. How useful is a physical exam in diagnosing testicular torsion? *JFam Pract,* Vol. 58, No.8, (August 2009), pp.433-434, ISSN 1533-7294

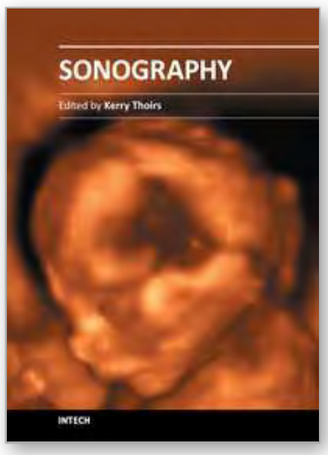

Sonography

Edited by Dr. Kerry Thoirs

ISBN 978-953-307-947-9
Hard cover, 346 pages
Publisher InTech
Published online 03, February, 2012
Published in print edition February, 2012

Medical sonography is a medical imaging modality used across many medical disciplines. Its use is growing, probably due to its relative low cost and easy accessibility. There are now many high quality ultrasound imaging systems available that are easily transportable, making it a diagnostic tool amenable for bedside and office scanning. This book includes applications of sonography that can be used across a number of medical disciplines including radiology, thoracic medicine, urology, rheumatology, obstetrics and fetal medicine and neurology. The book revisits established applications in medical sonography such as biliary, testicular and breast sonography and sonography in early pregnancy, and also outlines some interesting new and advanced applications of sonography.

How to reference

In order to correctly reference this scholarly work, feel free to copy and paste the following:

Shou-Hung Tang, Tai-Lung Cha and Guang-Huan Sun (2012). Clinical Perspectives of Scrotal Ultrasound in Urology, Sonography, Dr. Kerry Thoirs (Ed.), ISBN: 978-953-307-947-9, InTech, Available from: http://www.intechopen.com/books/sonography/clinical-perspectives-of-scrotal-ultrasound-in-urology

INTECH
open science | open minds

InTech Europe
University Campus STeP Ri
Slavka Krautzeka 83/A
51000 Rijeka, Croatia
Phone: +385 (51) 770 447
Fax: +385 (51) 686 166
www.intechopen.com

InTech China
Unit 405, Office Block, Hotel Equatorial Shanghai
No.65, Yan An Road (West), Shanghai, 200040, China
中国上海市延安西路65号上海国际贵都大饭店办公楼405单元
Phone: +86-21-62489820
Fax: +86-21-62489821

IntechOpen

5

The Accuracy of Ultrasound in the Pre-Operative Localisation of Parathyroid Lesions in Primary Hyperparathyroidism: A Review of the Literature

S. Alford[1], W. Barber[1], G. Cheung[2] and K. Thoirs[1]
[1]*School of Health Sciences, University of South Australia*
[2]*Flinders Medical Centre, Bedford Park, South Australia*
Australia

1. Introduction

Primary hyperparathyroidism (PHPT) is caused by excessive autonomous secretion of parathormone (PTH), usually as a result of a parathyroid adenoma (80-85%), and less frequently due to parathyroid gland hyperplasia (15%-20%) or carcinoma (1%) (Kaplan et al.1991). Patients often suffer from mild subjective symptoms such as weakness and tiredness, but if untreated, symptoms progess to include dementia, depression, peptic ulcer disease, pancreatitis, constipation, renal calculi, and diffuse bone and joint pain (Clark 2003).

PHPT can be diagnosed by detecting elevated PTH and blood calcium levels (Carlier et al. 2008). The most effective treatment or cure for PHPT is parathyroidectomy, the surgical removal of the affected parathyroid glands. Surgery has traditionally been performed using a traditional bilateral neck exploration (BNE), but in recent times, minimally invasive parathyroidectomy (MIP) has replaced this approach as a first line surgical choice in the United States, Australia, and mainland Europe (Palazzo 2004). MIP compared to BNE neck exploration has comparable clinical outcomes and complications, but can reduce length of hospital stays and operating times by 50% (Udelsman 1999). Successful cure for PHPT using MIP depends on consistently reliable methods for localizing parathyroid lesions, so the surgeon can direct the dissection to the site of the abnormal parathyroid gland (Johnson et al. 2007). The success of the resection can be assessed by means of intraoperative intact parathyroid hormone (IOPTH) assay (Quiros et al. 2004). Surgeons experienced in MIP can explore both the upper and lower glands on the same side of the neck from a slightly enlarged incision if the localization study has not identified the lesion correctly, and in cases where preoperative localization has failed to identify a gland on the contralateral side, the surgeon may proceed to BNE.

The Nuclear Medicine (NM) Technetium 99m (Tc^{99m}) sestamibi examination is a common imaging choice to preoperatively localize diseased parathyroid glands (Levy et al. 2011). The Tc^{99m} sestamibi examination involves the injection of a radiopharmaceutical, made up of a radioisotope (Tc^{99m}) and a pharmaceutical tracing agent (sestamibi). A dual phased technique is used, where a gamma camera detects the radiation emitted from within the

patient in an early phase at 15–30 minutes (Figure 1) and in a late phase at 2–4 hours (Figure 2) after intravenous administration of the radioisotope. Diseased parathyroid glands are detected based on the time-related differential washout of radioactivity between the thyroid gland and a parathyroid lesion. In diseased parathyroids there is a retention of Tc-99m sestamibi within the parathyroid in the second phase (Nguyen 1999). The disadvantages of NM localization examinations include that they use ionizing radiation, require an injection to the patient of a radiopharmaceutical (Levy et al. 2011) which carries a slight risk of adverse reactions (Mujtaba et al. 2007). NM studies also require a high level of patient cooperation to remain still for extended periods, which may be difficult in elderly, ill or confused patients. This is particularly important when integrated single-photon-emission computed tomography and computed tomography (SPECT/CT) systems (Figure 3), which are prone to misregistration errors due to patient movement (Bybel et al. 2008) are used to improve sensitivity.

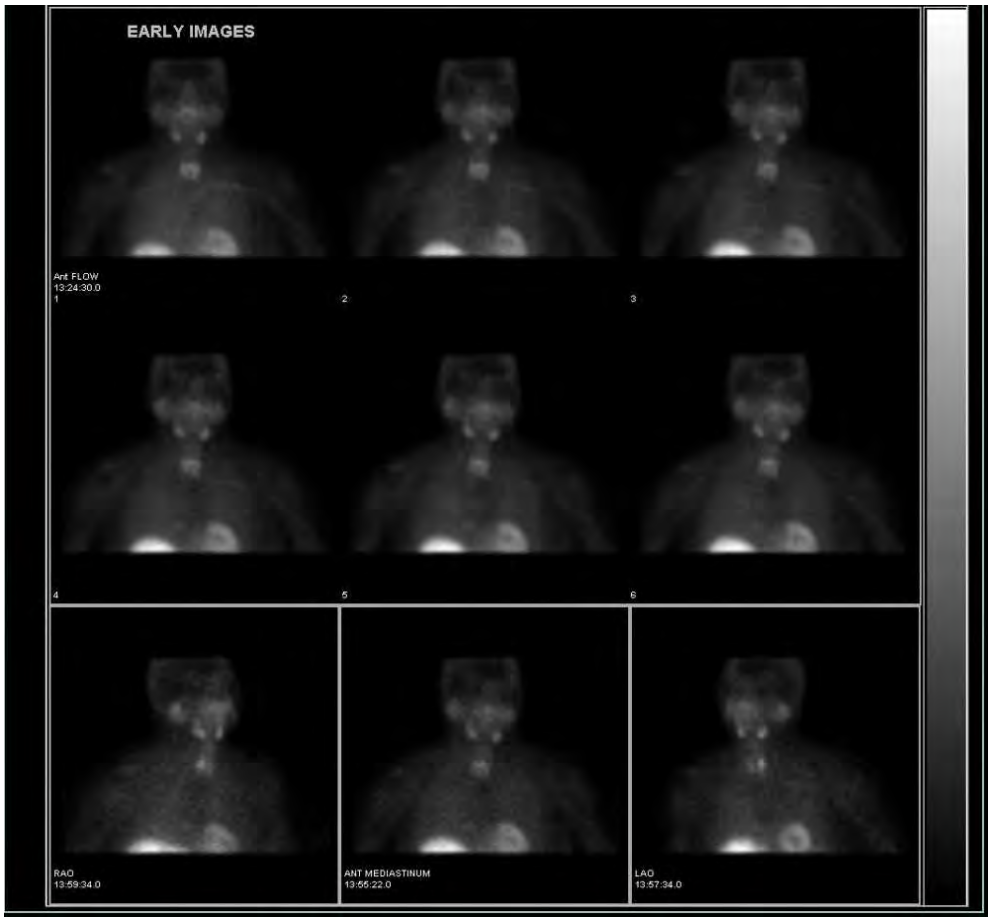

Fig. 1. Early phase parathyroid Nuclear Medicine scan. Image courtesy of Royal Adelaide Hospital, Department of Nuclear Medicine, PET & Bone Densitometry

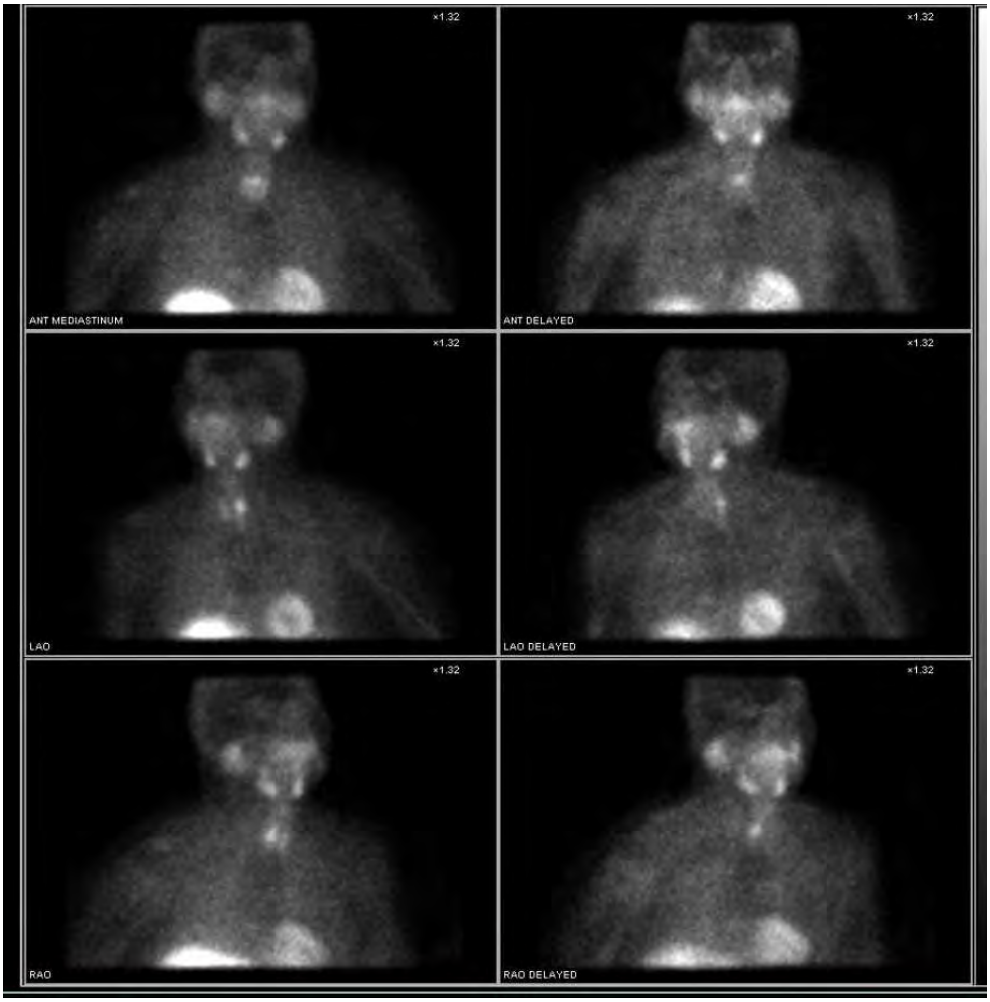

Fig. 2. Late phase parathyroid Nuclear Medicine scan demonstrating parathyroid lesion in superior mediastinum. Image courtesy of Royal Adelaide Hospital, Department of Nuclear Medicine, PET & Bone Densitometry

Parathyroid ultrasound (US) has emerged as an alternative or complementary localization procedure to NM techniques because it does not use ionizing radiation or an injection to the patient (Levy et al. 2011), and has greater tolerance for patient movement. US is considered to be one of the most cost-effective, quick and easy imaging modalities, but it has demonstrated variable performance over time and between varying clinical environments (Whiting et al. 2003; Mihai et al. 2009) when localizing parathyroid lesions. Older studies, such as those by Liou et al. (1996) have shown US to have sensitivities and specificities up to 75 per cent and 95 per cent respectively, compared to Tc^{99m} sestamibi which showed 87.5 per cent sensitivity and 100 per cent specificity.

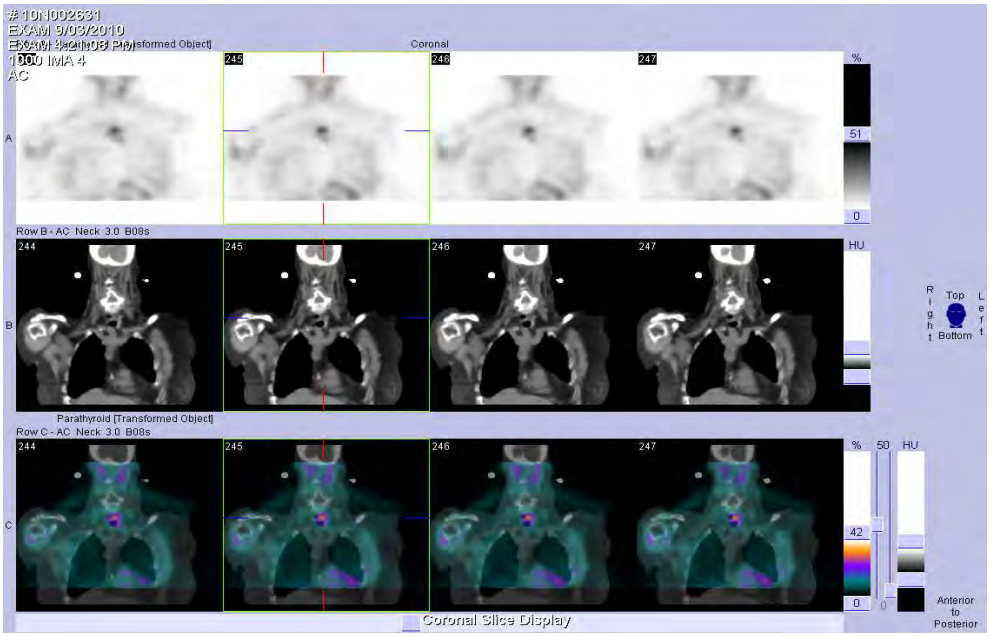

Fig. 3. SPECT/CT parathyroid Nuclear Medicine scan demonstrating parathyroid lesion in superior mediastinum. Image courtesy of Royal Adelaide Hospital, Department of Nuclear Medicine, PET & Bone Densitometry

Variability in the performance of US to localize parathyroid lesion may be due to the variability of the anatomical location of the glands themselves. The possibility of ectopic glands and variation in the number of glands presents challenges for US (Yeh et al. 2006), as the field of view in each image is small and requires a careful and thorough scanning technique. Ectopic glands may be obscured in US examinations by bony and air filled structures that impede US penetration. For example, retro-sternal, retro-oesphageal and retro-tracheal glands are difficult to localize with US. Intra-thyroid lesions (Figure 4), which are rare, may also be difficult to localize because they are difficult to differentiate from thyroid nodules (Kobayashi et al. 1999).

The US equipment and sonographer expertise and protocols also have the potential to influence the accuracy of the ultrasound examination (Mihai et al. 2009). US requires comprehensive and reproducible protocols as it is very operator-dependent, and localization accuracy may vary according to the level of experience of the sonographer (Yeh et al. 2006). The size of diseased glands may be very small and therefore the successful localization of very small structures with US may be constrained by the resolution of the ultrasound system (Lo et al. 2007). Older US units can be compromised by image quality compared to modern equipment, and this may have contributed to the lower rates of accuracy reported in older studies (Levy et al. 2011). The use of colour Doppler (Figure 6) to identify enlarged feeding arteries to parathyroid adenomas has also been reported to increase detection rates (Reeder et al. 2002).

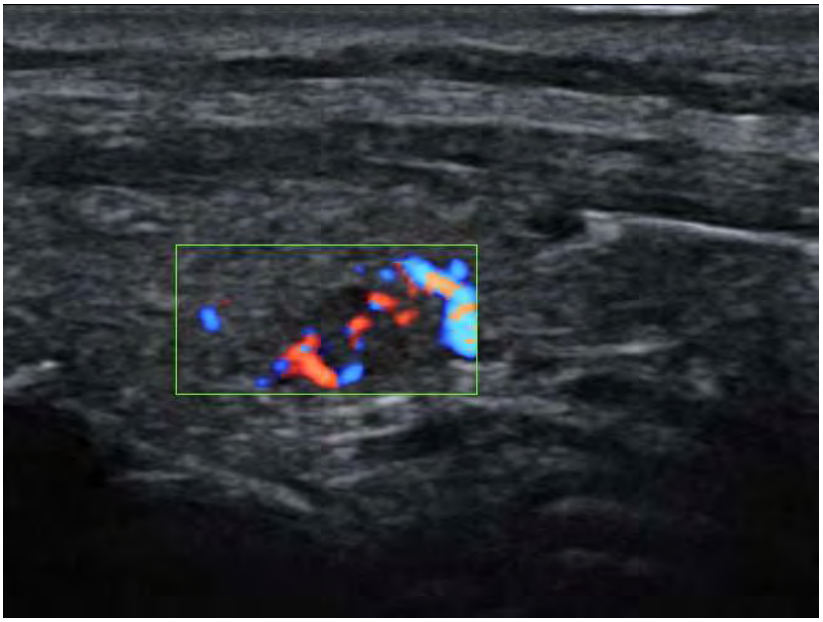

Fig. 4. Intra-thyroid parathyroid adenoma demonstrated on ultrasound image. Image courtesy of Division of Medical Imaging, Flinders Medical Centre

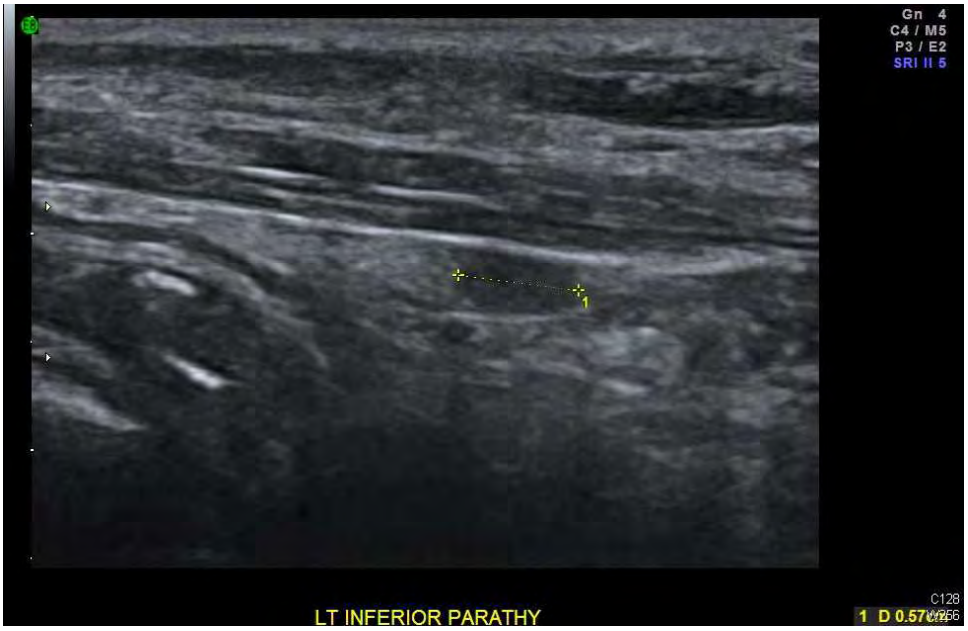

Fig. 5. Small inferior parathyroid adenoma demonstrated on ultrasound image. Image courtesy of Division of Medical Imaging, Flinders Medical Centre

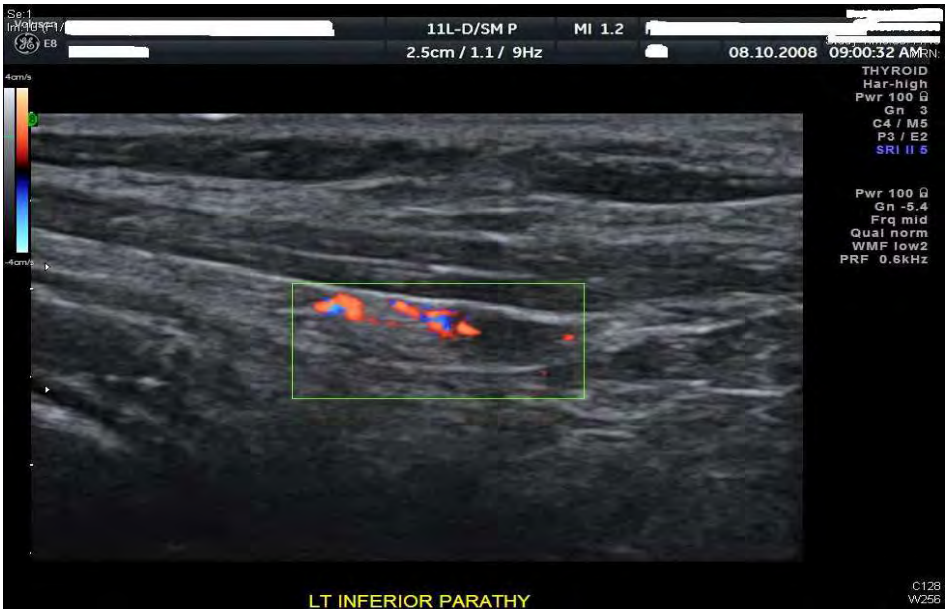

Fig. 6. Small inferior parathyroid adenoma demonstrated on ultrasound image. A feeding artery is demonstrated with the application of Colour Doppler. Image courtesy of Division of Medical Imaging, Flinders Medical Centre

Many medical imaging/radiology departments offer both NM and US studies to localize parathyroid lesions preoperatively. Imaging departments should periodically assess their performance through audits for quality assurance purposes. Benchmark performance levels can be identified through critical review and synthesis of the literature. With this in mind we performed a systematic review of the recent literature to determine the current performance of preoperative parathyroid US localizing parathyroid lesions in PHPT. We included an assessment of NM localization studies as a comparison.

2. Systematic review

2.1 Search strategy

A search of the literature was performed on 25 May, 2011 using Medline via Ovid, EMBASE via Ovid, ScienceDirect and Scopus databases (Table 1). Five groups of terms were searched using the Boolean-phrase methodology.

Category	Search terms
Population	parathyroid* or hyperparathyroid*
Intervention	ultraso* or sonograph*
Intervention	efficacy or effective* or accura* or precis* or sensitiv* or specific*
Outcome	localis* or localis* or locat* or identif*
Population/Assessment	preoperative or pre-operative or pre operative

Table 1. Search strategy

2.2 Inclusion and exclusion criteria

We included prospective studies published after 2003 in English, which focused on the performance of preoperative US and NM localization of parathyroid lesions in PHPT. In order to be included the studies must have described a randomized or consecutive sampling strategy, cases must have been selected based on suspicion or diagnosis of PHPT and all cases must have undergone US, NM and parathyroidectomy. The results of both US and NM must have been compared to surgical findings, with or without postoperative hormone assays. Studies were excluded if they were not available in English. The review excluded all articles reporting on case studies, literature reviews, paediatric focused studies, animals and retrospective study designs. Studies which focused on intra-operative or endoscopic ultrasound were also excluded.

2.3 Search results

The search returned a total of 1205 articles (Table 2), of which 313 duplicates were removed. Twenty-seven articles in languages other than English were excluded. Based on titles alone, 798 studies were excluded after application of the selection criteria. Two authors both reviewed the abstracts of the remaining 67 articles and analyzed them using the inclusion and exclusion criteria. Seven articles were selected to be included in the review (Figure 7).

Database	Limitations applied	Results
Medline via OvidSP	English language, journal article, 2002 to 25 May 2011, human subjects	150
EMBASE via OvidSP	English language, article, 2002 to 25 May 2011, human subjects	155
ScienceDirect	Journal article, 2002 to 25 May 2011	556
Scopus	English language, article, 2002 to 25 May 2011, human or humans	344

Table 2. Search results

All the studies identified from the search were well-designed non-experimental descriptive studies, with no identified randomized clinical trials. The methodological quality of the articles was assessed using an adapted QUADAS checklist (Whiting et al. 2003) (Table 3) by two independent reviewers, with discrepancies between reviewers resolved by consensus. The articles were all of similar methodological quality.

All seven studies examined populations of patients who had a diagnosis of PHPT which was established by elevated PTH and calcium levels in the blood. In all studies, diagnosis was confirmed by successful surgical removal of parathyroid pathology with or without post surgical follow up histology and blood assays. Five studies additionally confirmed surgical success with follow up assays (Bhansali et al. 2006; Carlier et al. 2008; Lo et al. 2007; Prasannan et al. 2007; Shaheen et al. 2008), and three studies confirmed the nature of the excised lesion(s) with histology (Mihai et al. 2006; Lo et al. 2007; Carlier et al. 2008).

The US and NM localization examinations were always performed prior to surgery, therefore bias was minimized due to blinding to the surgical results. All studies, except two,

(Mihai et al. 2009, Prasannan et al. 2007) stated that the US was interpreted without knowledge of the results of the NM scan. While, this approach limits risk of contamination between the two localization studies and provides an independent assessment of the localization study's performance, it does not mirror usual clinical practice. In clinical practice each test is often treated as complementary to the other, and is not interpreted in isolation with the alternate test. The combination of the findings from both US and NM has been proven to increase the overall sensitivity in identifying and localizing parathyroid lesions (Bhansali et al. 2006; Lo et al. 2007; Sugg et al. 2004).

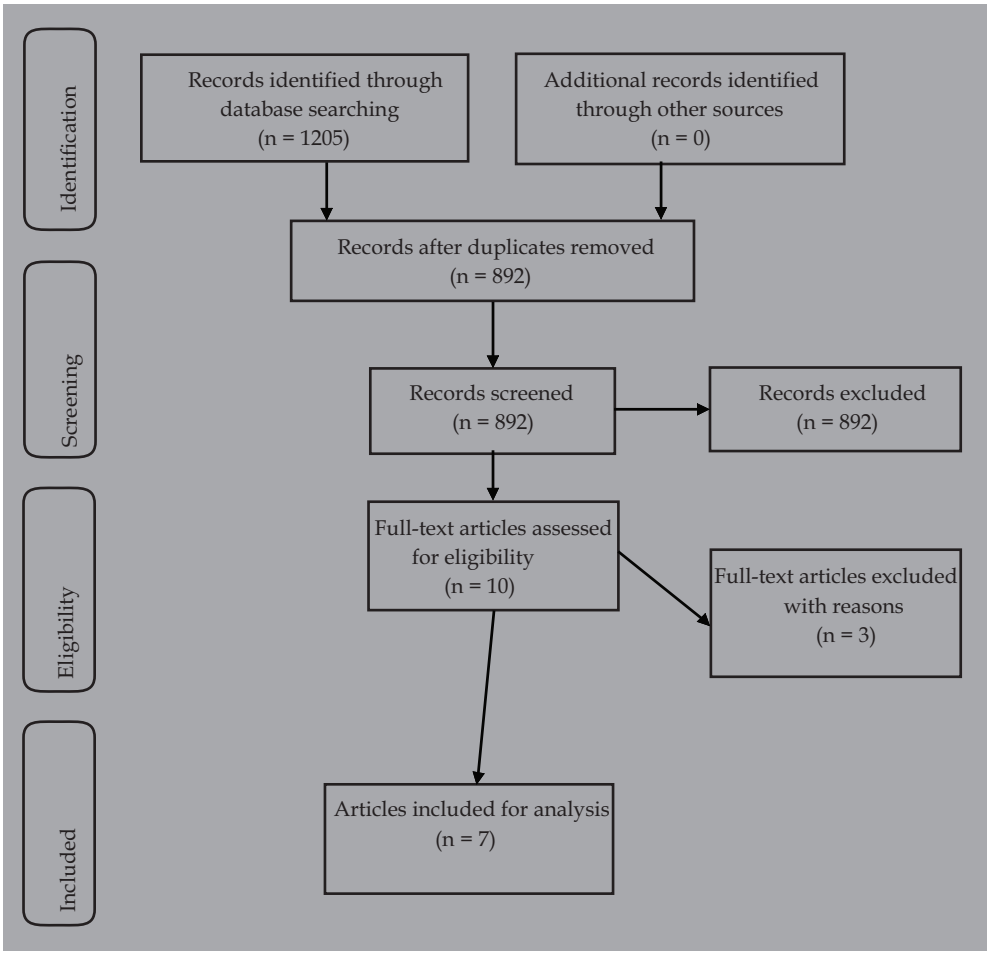

Fig. 7. Flow chart of article selection process

All studies, excepting two, described the ultrasound equipment and the experience or credentials of the operator, the type of NM technique used, the type of surgical technique and cut off values of normal for post- and pre-operative blood assays. This information is important when interpreting and transferring the findings to other settings, especially when

Table 3. Methodologic quality of articles

Item	Bhansali et al. (2006)	Carlier et al. (2008)	Lo et al. (2007)	Mihai et al. (2006)	P et
1 Was the spectrum of patients representative of the patients who will receive the test in practice?					
2 Were selection criteria clearly described?					
3 Is the reference standard likely to correctly classify the target condition?					
4 Is the time period between reference standard and index test short enough to be reasonably sure that the target condition did not change between the two tests?					
5 Did the whole sample or a random selection of the sample, receive verification using a reference standard of diagnosis?					
6 Did patients receive the same reference standard regardless of the index test result?					
7 Was the reference standard independent of the index test (i.e. the index test did not form part of the reference standard?)					
8 Was the execution of the index test described in sufficient detail to permit replication of the test?					
9 Was the execution of the reference standard described in sufficient detail to permit its replication?					
10 Were the index test results interpreted without knowledge of the results of the reference standard?					
11 Were the reference standard results interpreted without knowledge of the results of the index test?					
12 Were the same clinical data available when test results were interpreted as would be available when the test is used in practice?					
13 Were uninterpretable/ intermediate test results reported?					
14 Were withdrawals from the study explained?					

Legend: Cells shaded white = Yes; Cells shaded grey = Unclear; Cells shaded black = No.

tests and procedures are complex and variable. The exceptions were Prasannan et al. (2007) who provided no information on the execution of the Tc^{99m} sestamibi scan, and Shaheen et al. (2008) who provided no information on the experience or credentials of the operator(s). Whilst most studies used pre-operative or post-operative hormone assays, only three studies (Bhansali et al. 2006; Prasannan et al. 2007; Sugg et al. 2004) provided clear cut-off values for normal or abnormal assays.

Only two studies in this review, applied a standardized surgical approach for all patients (Bhansali et al. 2006; Shaheen et al. 2008), with a trend in the studies to mirror current clinical practice, and adjust the surgical approach (MIP or BNE), based on the results of the localization studies (Quiros et al.2004). Common surgical practice is to still to use BNE in cases of suspected multiglandular disease and those with equivocal pre-operative localization (Johnson et al. 2007). The potential bias arising from using more than one approach to confirm the presence and location of lesions is probably minimal because there were few cases reported across the studies where parathyroid lesions were not found at surgery.

All studies appeared to be undertaken under clinical conditions where patients were undergoing diagnosis and treatment in healthcare settings. There was some lack of clarity in areas of reporting which impact on the ability to transfer results to other clinical settings, and also may be sources of bias. For example, there was lack of clarity around the selection criteria used, the time period between the localization studies and the surgery, and no study reported uninterpretable, indeterminate or intermediate results. Only one study (Lo et al. 2007) accounted for withdrawals from the study.

2.4 Study and subject characteristics

A summary of the subject and study characteristics of the articles is demonstrated in Table 4.

Six studies compared US and NM to surgical findings (Bhansali et al. 2006; Carlier et al. 2008, Lo et al. 2007; Prasannan et al. 2007; Shaheen et al. 2008; Sugg et al. 2004). Mihai et al (2006) differed by not directly comparing US to surgical findings, instead comparing it to NM only, then comparing NM to surgical findings.

Across the studies a total of 740 patients were examined, comprising 534 females (72 per cent) and 206 males (28 per cent), a distribution which closely reflects the epidemiology of PHPT (Ljunghall et al. 1991).The 740 patients had 798 pathologic parathyroid glands, comprising mostly of single adenomas (86 per cent), with a lower prevalence of double adenomas (3 per cent), hyperplasia (10 per cent), carcinoma (n=0.5 per cent) and one paraganglioma (n=0.5 per cent).

US was performed by experienced radiologists in two studies (Carlier et al. 200; Lo et al. 2007), experienced sonographers in two studies (Bhansali et al. 2006; Sugg et al. 2004), a parathyroid surgeon in one study (Prasannan et al. 2007) and the operator was not specified by Mihai et al. (2006) or Shaheen et al. (2008). Two studies (Lo et al. 2007; Shaheen et al. 2008) indicated that multiple operators were involved in performing the ultrasound examinations in their studies. US examinations were performed using linear array, small

footprint or unspecified shaped transducers with frequencies of 5-12 MHz, all of which would be found to be used in current clinical practice.

		Bhansali et al. (2006)	**Carlier et al. (2008)**	**Lo et al. (2007)**	**Mihai et al. (2006)**	**Prasannan et al. (2007)**	**Shaheen et al. (2008)**	**Sugg et al. (2004)**
n		46 (33 female, 13 male)	51 (38 female, 13 male)	100 (70 female, 30 male)	155 (115 female, 40 male)	130 (97 female, 33 male)	25 (8 female, 17 male)	233 (173 female, 60 male)
Age	Mean	37.1	56	55.5 MEDIAN	62.1	59.1	18-25 RANGE	56

Table 4. Summary of patients

The most common NM tests were planar Tc^{99m} sestamibi, dual radionuclide subtraction (Tc^{99m}/Tl^{201}), and dual phase Tc^{99m} sestamibi. Patients underwent a range of NM techniques including conventional single photon emission computed tomography (C-SPECT) and pinhole SPECT (P-SPECT).

BNE was performed on 310 patients, and the remaining 430 underwent MIP. Two studies (Bhansali et al. 2006; Shaheen et al. 2008) performed BNE on all subjects. In the other studies the decision to perform MIP rather than BNE was made when the results of the US and NM localization examinations were concordant (Carlier et al. 2008), when suspected lesions were Tc^{99m} sestamibi positive (Lo et al. 2007), or on surgeon's preference (Carlier et al. 2008). It was common procedure in the studies to assess the success of the surgery in removing the parathyroid lesion(s) by performing a post-operative or intra-operative PTH assay, with or without corresponding serum calcium assays. A return of normal assay values was confirmatory for surgical success. Some studies reported that assays were undertaken intra-operatively (Lo et al. 2007; Shaheen et al. 2008; Sugg et al. 2004), and others reported the hormone assays to be taken postoperatively, with follow up which varied between 1 week and 3 years duration (Carlier et al. 2008; Bhansali et al. 2006; Mihai et al. 2006; Prasannan et al. 2007).

2.5 Results

Table 5 provides a summary of the results. Overall, US demonstrated lower sensitivities (51 to 86 per cent), to correctly localize parathyroid lesions compared to NM (64 to 98 per cent). Four studies reported the sensitivities of US to be comparable or slightly less than NM (Bhansali et al. 2006; Lo et al. 2007; Mihai et al. 2006; Shaheen et al. 2008). Two studies reported US to have higher detection rates than NM (Prasannan et al. 2007, Sugg et al. 2004). One study reported US to have significantly lower sensitivity (51 per cent) compared with planar Tc^{99m} sestamibi (75 per cent), conventional SPECT (82 per cent), and planar SPECT (87 per cent) (Carlier et al. 2008). Three studies analyzed data specifically for single gland disease (SGD) and multi-gland disease (MGD) and found US to have higher sensitivity (73-82 per cent) compared to NM (45 to 64 per cent) in identifying MGD (Bhansali et al. 2006; Shaheen et al. 2008; Sugg et al. 2004). There were no apparent trends to suggest that one NM imaging localization technique was better than any other.

2.6 Discussion

Our initial search revealed 892 articles, demonstrating a wide breadth of research into the pre-operative localization of parathyroid lesions. We restricted the review to include only prospective studies with consecutive or randomized sampling. Prospective studies are more easily controlled, and allow more rigorous methodologies including the use of blinding (Euser et al. 2009). The exclusion of retrospective studies significantly reduced the number of studies included in this review, as retrospective studies are more widely reported (Mihai, Simon & Hellman 2009) and prospective studies are less frequently reported due to long data collection periods when this study design is used. Articles prior to 2003 were excluded to capture the most advanced imaging technologies. Older studies using less sensitive equipment have demonstrated lower sensitivities for both US and NM (Ruda et al. 2005). However, the descriptions of US techniques were mostly limited to the operator and basic specifications of the transducer, rather than the make and model of the equipment, and it was not possible to assess if the differences in results were influenced by the capabilities of the technology used in each study.

Despite the limitations of our selection criteria, and resulting narrow range of studies included, we found wide variations in sensitivity rates for both US and NM localization examinations. Sensitivity rates for the detection of parathyroid lesions for preoperative US localization examinations ranged from 51 to 85.7 per cent and ranged from 64 to 98 per cent for NM localization examinations. In most cases successful localization was defined when the lesion(s) was correctly identified on the correct side of the neck. This is an important consideration for surgical planning. The sensitivities rates were similar to what was reported in a similar review (Mihai et al. 2009) which reported ultrasound sensitivity rates of 51 to 96 per cent, and NM sensitivity rates from 34 to 100 per cent. The wider variation reported by Mihai et al. (2009) is likely due to their inclusion of retrospective studies, short case series and older studies which were excluded from our review.

There are a number of factors that may impact on the performance of US in detecting parathyroid lesions including the expertise of the operator, the small size of some lesions, ectopic gland positions, multinodular thyroid goiter and parathyroid hyperplasia (Levy et al. 2011; Mihai et al. 2009; Ruda et al. 2005). Two studies in this review referred to the impact of lesion size on sensitivity rates; Prasannan et al. (2007) stated that US was more sensitive when detecting lesions over 1270 milligrams and Bhansali et al. (2006) stated that sensitivity reached 92.3 per cent sensitivity for glands weighing over five grams. While the sensitivity of US was shown to be lower in smaller glands (Bhansali et al. 2006; Prasannan et al. 2007), US still demonstrates the capability to detect lesions as small as 1.2 grams in weight (Bhansali et al. 2006). Colour Doppler US can be important in the differential diagnosis of a suspected lesion, demonstrating superior feeding vessels in parathyroid glands, as opposed to hilar flow in lymph nodes. However, the use of Doppler US in the differential diagnosis of parathyroid lesions was only reported in one study in this review (Prasannan et al. 2007).

The position of parathyroid lesions also influenced detection rates. The sensitivity of US to detect and localize ectopic parathyroid lesions was notably lower than the sensitivity when localizing those lesions in normal anatomical positions and appeared to be unrelated to the sizes of the ectopic lesions (Bhansali et al. 2006, Carlier et al. 2008). Across the seven studies,

twenty ectopic glands were established at surgery. The overall detection rate of retro-sternal glands was low, regardless of their size. The study with the highest number of ectopic glands gave the lowest sensitivity (51 per cent) (Carlier 2008), and the highest sensitivity was recorded in studies with no or few ectopic glands in their series (Prasannan et al. 2007; Shaheen et al. 2008).

Bhansali et al. (2006) reported that US missed several ectopic glands which were located in retro-oesophageal and mediastinal positions. Both US and NM were more likely to identify ectopic lesions in the neck than those in retro-sternal positions (Carlier et al. 2008). For US, this is likely due to the difficulty in scanning through the narrow sternal notch, to avoid surrounding bony structures. NM is less affected by bone and gas than US, but despite this Bhansali et al. (2006) reported that NM missed the same retro-sternal lesions that were undetected using US.

It is not clear if the expertise of the US operator influences results. In studies which were clear in reporting the expertise of operators, radiologists appeared to be less successful in US localization compared to sonographers. Only one study (Prasannan et al. 2007) reported on surgeon performance of US localization, with good results (sensitivity 82%). Surgeons may have an advantage over other operators by receiving direct feedback on their performance when they perform surgery on the cases they examined with US.

Bhansali et al. (2006), Prasannan et al. (2007) and Sugg et al. (2004) assessed cases with single gland disease (SGD) separately to those with multi gland disease (MGD). US localization studies were better than NM in identifying MGD and also found that US was more effective in detection of MGD than SGD (Bhansali et al. 2006; Sugg et al. 2004), Caution should however be exercised when interpreting this finding due to the low prevalence of MGD compared to SGD.

The presence of thyroid nodules or multinodular goiter was also noted to reduce the sensitivity of US in the detection and localization of parathyroid lesions (Lo et al. 2007).

The variations in the reported performance of US and NM may also be influenced by other factors such as differences in selection criteria, and differences in cut off values of hormone assays both to diagnose PHPT in patients, and to confirm surgical success. These factors may have not had a large effect, but should not be discounted.

Differences in detection rates between US and NM may be due to the nature of the imaging in these techniques. Nuclear medicine scanning relies on a physiological process, and this is reflected in observations by Mihai et al. (2006) that there were lower detection rates for adenomas with predominantly chief cells, and higher detection rates for adenomas with oxyphil cells and mixed cells in NM scanning. Additionally, false positives may occur in NM scanning when non-parathyroid tissue uptakes Tc^{99m} sestamibi (Carlier et al. 2008). US instead relies on structural changes, and false negatives may result when sound reflective tissues such as bone and gas limits the identification of retro-sternal, retro-tracheal and retro-oesophageal lesions (Mihai et al. 2009). False positives may occur in US localization studies, when other structures such as lymph nodes are mistaken for parathyroid glands.

It has been suggested that both US and NM localization examinations should be performed for preoperative localization of parathyroid lesions (Mihai et al. 2009), to determine whether

		Bhansali et al. (2006)	Carlier et al. (2008)	Lo et al. (2007)	Mihai et al. (2006)	
Surgery Type	BNE	46	28	34	63	
	MIP	0	23	66	92	
Ectopic glands		N=1 (retro-oesphageal)	N=11, (6 posterior, 3 thryothymic ligament, 1 mediastinal, 1 intra-thyroid)	N=1 (carotid sheath)	N=7 (retrosternal)	
Conditions	US Operator	Experienced Sonographer	Experienced Radiologist	Radiologist	Single Experienced Operator	
	US Transducer	Linear array 7.5-10 MHz	7-12 MHz	10 MHz	Linear Array Small Footprint 15 MHz	
	NM Scan Type	Dual Phase Tc99m Sestamibi, Dual Radionuclide Subtraction Tc99m/Tl201, C-T SPECT	Dual Phase Subtraction Tc99mO4/Tc99m sestamibi, C-SPECT, P-SPECT	Tc99m sestamibi, C-SPECT	Tc99m sestamibi	
Reference Standard	Surgical Findings	√	√	√	√	
	Histopathology	√	√	√	√	
	Post/intra operative Assay	Post Ca and iPTH	Six Month	Quick PTH		
NM results known		no	no	no	Not stated	
Results	Total number of Lesions	53	55	100	155	
	Lesions detected on US (n)	31/42 SGD 9/11 MGD	28/55	56/100	104/155	
	US Sensitivity	73% (for correct side)	51%	57% (for correct side)	57% (for correct side)	
	Lesions Detected on NM (n)	41/42 SGD 5/11 MGD	Planar Scintigraphy 42/55, C-SPECT 45/55, P-SPECT 48/55	85/100	103/155	
	NM sensitivity	98%	76%, 82%, 87%	89%	93%	

Key: BNE = Bilateral Neck Exploration;Ca=serum calcium level; MIP = Minimally Invasive Parathyroidectomy; n.s. = Not Stated; % = per cent; MHz = megahertz; PTH = Parathyroid Hormone; iPTH = Intact Parathyroid Hormone; IOPTH = Intraoperative Parathyroid Hormone Assay; SGD = Single Gland Disease; MGD = Multi Gland Disease; C-SPECT = Conventional Single Photon Emission Computed Tomography; P-SPECT = Pinhole Single Photon Emission Computed Tomography; SPECT = Single Photon Emission Computed Tomography; Tc99m = Technetium 99m; Tl201 = Thallium 201; O4 = Oxygen 4

Table 5. Key findings

the patient is a viable candidate for MIP. The dependence of NM on physiologic changes, and the dependence of US on anatomic changes supports the argument to use the two techniques as complementary localization techniques. This approach was further supported in our review, with five studies demonstrating improvement in sensitivity when a combination of two localization examinations were employed (Bhansali et al. 2006; Lo et al. 2007; Prasannan et al. 2007; Shaheen et al. 2008; Sugg et al. 2004).

Most studies reported sensitivity (Bhansali et al. 2006, Carlier et al. 2008, Lo et al. 2007, Prasannan et al. 2007, Shaheen et al. 2008) as an outcome measure of the performance of the localization studies. Approximately half of the studies also reported positive predictive value (PPV) (Bhansali et al. 2006; Lo et al. 2007; Prasannan et al. 2007; Shaheen et al. 2008). PPV is influenced by the prevalence of the target condition, with high prevalence rates resulting in artificially elevated PPV rates. The sample populations in this review consisted of patients with recognized and confirmed parathyroid disease (i.e. 100 per cent prevalence), therefore limiting the relevance of the PPV. Other measurements of localization performance included detection rates (Mihai et al 2006; Shaheen et al. 2008; Sugg et al. 2004), accuracy (Lo et al. 2007) and specificity (Carlier et al. 2008). Specificity of US and NM in identifying and localizing parathyroid lesions is not widely reported. Patients are usually conclusively diagnosed using clinical examinations and blood tests prior to undergoing imaging, which is primarily for localization rather than diagnosis. In addition to this, most prospective studies using surgical findings as a reference standard only include patients that have at least one lesion as it is unethical to operate on an unaffected patient, and as such there should be no true-negative results from which to calculate specificity.

2.7 Conclusion

The aim of this review was to investigate the effectiveness of US as a localization technique for pre-operatively detecting and localizing parathyroid lesions. The rationale behind this was to establish benchmark sensitivity rates in order to set best practice goals for departmental audits. Audits are valuable not only as an assessment of performance, but also can be used to improve professional practice (Ridder et al. 2008). The results of the review determined that there was wide variability of US sensitivity in detecting parathyroid lesions, despite the studies being of similar quality and at the same level of evidence. Benchmarking is therefore difficult, without having a clear understanding of the reasons for the wide variability. Patient presentation, including the presence of pathologic ectopic parathyroid glands, are likely to have an impact on the sensitive rates for gland localization. Therefore benchmarking of detection rates will depend on the prevalence of ectopic glands in each setting. This review demonstrates that high detection rates using US can be achieved if there is low prevalence of pathologic ectopic glands.

3. References

Bhansali, A, Masoodi, S, Bhadada, S, Mittal, B, Behra, A & Singh, P (2006). Ultrasonography in detection of single and multiple abnormal parathyroid glands in primary hyperparathyroidism: Comparison with radionuclide scintigraphy and surgery. *Clinical Endocrinology*, vol. 65, no. 3, (September 2006), pp. 340-345, ISSN 1365-2265.

Byel, B, Brunken, R, DiFilippo, F, Neumnn, D, Wu, G, Cerqueira, M. (2008), SPECT /CT Imaging: Clinical Utility of an Emerging Technology, *Radiographics,* vo.28, no.4, (July-August 2008), pp.1097-1113, ISSN 0271-5333.

Carlier, T, Oudoux, A, Mirallie, E, Seret, A, Daumy, I, Leux, C, Bodet-Milin, C, Kraeber-Bodere, F & Ansquer, C (2008), 99mTc-MIBI pinhole SPECT in primary hyperparathyroidism: comparison with conventional SPECT, planar scintigraphy and ultrasonography, *European journal of nuclear medicine and molecular imaging,* vol. 35, no. 3, (March 2008), pp. 637-643, ISSN 1619-7070.

Clark O. (2003), How should patients with primary hyperparathyroidism be treated?[editorial], *Journal of Clinical Endocrinology and Metabolism,* vol.88, no. 7, (July 2003), pp. 3011–3014, ISSN 0021-972X.

Euser, AM, Zoccali, C, Jager, K & Dekker, F (2009), Cohort Studies: Prospective versus Retrospective, *Nephron Clinical Practice,* vol. 113, no. 3, (August 2009), pp. 214-217, ISSN 1660-8151.

Johnson, N, Tublin, M, Ogilvie, J. (2007), Review: Parathyroid Imaging: Technique and Role in the Preoperative Evaluation of Primary Hyperparathyroidism, *American Journal of Roentgenology*, vol. 188, no. 6, (June 2007), pp. 1706-1715, ISSN 1546-3141.

Kaplan, E, Yashiro, T, Salti, G. (1992), Primary hyperparathyroidism in the 1990s: choice of surgical procedures for this disease. *Annals of Surgery*, vol.215, no.215, no.4, (April 1992), pp. 300–316, 1528-1140.

Kobayashi, T, Man-I,M, Shin, E, Kikkawa, N, Kawahara, K, Kurata, A, Fukuda, H, Asakawa, H. (1999), Hyperfunctioning intrathyroid parathyroid adenoma: Report of two cases, *Surgery Today*, vol.29, no.8, (August 1999), pp.766-768, ISSN 0941-1291

Levy, J, Kandil, E, Yau, L, Cuda, J, Sheth, S & Tufano, R. (2011), Can ultrasound be used as the primary screening modality for the localization of parathyroid disease prior to surgery for primary hyperparathyroidism? A review of 440 cases, *Journal for oto-rhino-laryngology and its related specialties,* vol. 73, no. 2, (March 2011) pp. 116-120, ISSN 1423-0275.

Liou M, Huang H, Lin J, Huang BY, Hsueh C, Jeng L, Tzen KY. (1996), The accuracy of ultrasonography and 201Tl-99mTc subtraction scan in localization of parathyroid lesions, *Chang Gung Medical Journal,* vol. 19, no. 2, (June 1996) pp. 121-128.

Ljunghall S, Hellman P, Rastad J, Akerström G. (1991), Primary hyperparathyroidism: epidemiology, diagnosis and clinical picture, *World Journal Surgery*, vol. 15, no.6, (November-December 1991), pp.681-687, ISSN 0364-2313.

Lo, C, Lang, B, Chan, W, Kung, A & Lam, K. (2007), A prospective evaluation of preoperative localization by technetium-99m sestamibi scintigraphy and ultrasonography in primary hyperparathyroidism, *The American Journal of Surgery,* vol. 193, no. 2 February 2007), pp. 155-159, ISSN 0002-9610.

Mihai, R, Gleeson, F, Buley, I, Roskell, D & Sadler, G. (2006), Negative imaging studies for primary hyperparathyroidism are unavoidable: Correlation of sestamibi and high-resolution ultrasound scanning with histological analysis in 150

patients, *World Journal of Surgery,* vol. 30, no. 5, (May 2006) pp. 697-704, ISSN 0364-2313.

Mihai, R, Simon, D & Hellman, P. (2009), Imaging for primary hyperparathyroidism-an evidence-based analysis, *Langenbeck's Archives of Surgery,* vol. 394, no. 5, (September 2009) pp. 765-784, ISSN 1435-2443.

Mujtaba, B, Adenaike, M, Yaganti, V, Mujtaba, N & Jain, D. (2007), Anaphylactic reaction to Tc-99m sestamibi (Cardiolite) during pharmacologic myocardial perfusion imaging, *Journal of Nuclear Cardiology,* vol. 14, no. 2, (April 2007), pp. 256-258, ISSN 1071-3581.

Nguyen B. (1999), Parathyroid imaging with Tc-99m sestamibi, planar and SPECT scintigraphy, *Radiographics,* vol.19, no.3, (May-June 1999), pp. 601-614, ISSN 0271-5333.

Palazzo F. (2004), Minimally invasive parathyroidectomy [editorial], *British Medical Journal*, vol. 328, (April 2004), pp.849-850, ISSN 0959-8138.

Prasannan, S, Davies, G, Bochner, M, Kollias, J & Malycha, P. (2007), Minimally invasive parathyroidectomy using surgeon-performed ultrasound and sestamibi, *ANZ Journal of Surgery,* vol. 77, no. 9, (September 2007), pp. 774-777, ISSN 1445-1433.

Quiros, R, Alioto, J, Wilhelm, A, Prinz, R. (2004) An Algorithm to Maximize Use of Minimally Invasive Parathyroidectomy, *Archives of Surgery*, vol. 139, no. 5, (May 2004), pp. 506-507, ISSN 0272-5533

Reeder, S, Desser, T, Weigel, R, Jeffrey R. (2002), Sonography in Primary Hyperparathyroidism: Review With Emphasis on Scanning Technique, *Journal of Ultrasound in Medicine*, vol.21, no. 5, (May 2002), pp. 539-552, ISSN 0278-4297.

Ruda, J, Hollenbeak, C & Stack, B. (2005), A systematic review of the diagnosis and treatment of primary hyperparathyroidism from 1995 to 2003, *Otolaryngology - Head and Neck Surgery,* vol. 132, no. 3, (March 2005), pp. 359-372, ISSN 0194-5998.

Shaheen, F, Chowdry, N, Gojwari, T, Wani, A & Khan, S. (2008), Role of cervical ultrasonography in primary hyperparathyroidism, *Indian Journal of Radiology and Imaging,* vol. 18, no. 4, (November 2008), pp. 302-305, ISSN 0971-3026.

Sugg, S, Krzywda, E, Demeure, M & Wilson, S. (2004), Detection of multiple gland primary hyperparathyroidism in the era of minimally invasive parathyroidectomy, *Surgery,* vol. 136, no. 6, (December 2004), pp. 1303-1309, ISSN 0039-6060.

Udelsman R. (2002), Six hundred fifty-six consecutive explorations for primary hyperparathyroidism, *Annals of Surgery*, vol. 235, no. 5, (May 2002), pp.665-672, ISSN 0003-4932.

Udelsman, R, Donovan, P & Sokoll, L. (2000), One Hundred Consecutive Minimally Invasive Parathyroid Explorations, *Annals of Surgery,* vol. 232, no. 3, (September 2000), pp. 331-339, ISSN 0003-4932.

Van de Ridder, J, Stokking, K, mCGaghie, W, ten Cate, O. (2008), What is feedback in Medical Education?, Medical Education, vo. 42, no. 2, (February 2008), pp. 189-197, ISSN 0308-0110.

Whiting, P, Rutjes, A, Reitsma, J, Bossuyt, P & Kleijnen, J. (2003), The development of QUADAS: a tool for the quality assessment of studies of diagnostic accuracy included in systematic reviews, *BMC Medical Research Methodology,* vol. 3, no. 25, (November 2003), pp. 25-37, ISSN 1471-2288.

Yeh, M, Barraclough, B, Sidhu, S, Sywak, M, Barraclough, B & Delbridge, L. (2006), Two hundred consecutive parathyroid ultrasound studies by a single clinician: The impact of experience, *Endocrine Practice,* vol. 12, no. 3, (May-June 2006), pp. 257-263, ISSN 1530-891X.

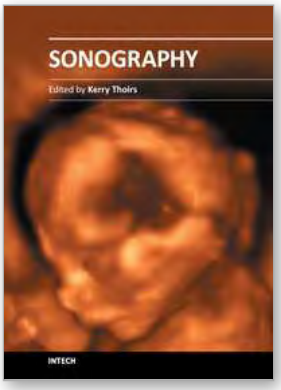

Sonography

Edited by Dr. Kerry Thoirs

ISBN 978-953-307-947-9
Hard cover, 346 pages
Publisher InTech
Published online 03, February, 2012
Published in print edition February, 2012

Medical sonography is a medical imaging modality used across many medical disciplines. Its use is growing, probably due to its relative low cost and easy accessibility. There are now many high quality ultrasound imaging systems available that are easily transportable, making it a diagnostic tool amenable for bedside and office scanning. This book includes applications of sonography that can be used across a number of medical disciplines including radiology, thoracic medicine, urology, rheumatology, obstetrics and fetal medicine and neurology. The book revisits established applications in medical sonography such as biliary, testicular and breast sonography and sonography in early pregnancy, and also outlines some interesting new and advanced applications of sonography.

InTech Europe
University Campus STeP Ri
Slavka Krautzeka 83/A
51000 Rijeka, Croatia
Phone: +385 (51) 770 447
Fax: +385 (51) 686 166
www.intechopen.com

InTech China
Unit 405, Office Block, Hotel Equatorial Shanghai
No.65, Yan An Road (West), Shanghai, 200040, China
中国上海市延安西路65号上海国际贵都大饭店办公楼405单元
Phone: +86-21-62489820
Fax: +86-21-62489821

16

Thyroid Sonography in 3D with Emphasis on Perfusion

Roy Moncayo and Helga Moncayo
WOMED, Innsbruck,
Austria

1. Introduction

Ultrasound examination of the thyroid gland is an essential diagnostic element in daily clinical practice. The aim of this chapter is to describe the advanced clinical value of conducting 3D ultrasound examinations putting emphasis on the quantitative evaluation of perfusion characteristics of the thyroid gland and to relate these results to therapeutic interventions aimed at diminishing inflammation.

2. Historical aspects of ultrasound

The term echo (Greek: Ηχώ, *Ēkhō*; "Sound") refers to the persistence of sound after its source has stopped. Greek mythology tells from an Oread (a mountain nymph) who pined away for love of Narcissus (in Ovid, Metamorphoses). The phenomenon of air being sent back by a wall was described by Aristotles (384-322 BCE). The Greek word echo came into German writings in the 16th century. Athanasius Kircher (1602 – 1680) used the principle of "Echometria" to determine the depth of a well. His book was entitled: "Neue Hall- und Thon-Kunst oder Mechanische Gehaim-Verbindung der Kunst und Natur durch Stimme und Hall" and appeared 1684. At this time he was able to measure the speed of sound propagation.

On May 25th, 1842 Christian Doppler (born in Salzburg, Austria) presented in Prague his talk on "Abhandlung Über das farbige Licht der Doppelsterne und einiger anderer Gestirne des Himmels" (Eng. *On the coloured light of the binary stars and some other stars of the heavens)* at the Prague Polytechnic [1]. The Doppler effect is a main stand of many examinations today.

In 1880 Pierre and Jacques Curie discovered the piezoelectric effect and postulated the generation of ultrasound waves [2]. They found that applying an electric current to a crystal would produce a vibration which could in turn produce sound waves. In turn, sound waves striking a crystal would produce an electric voltage. In 1917 Langevin constructed for the first time a piezoelectric ultrasound transducer based on quartz elements and which was called sandwich-style. This product was oriented towards military use in World War I, i.e. the detection of submarines. The Langevin-type transducers were utilized in depth sounding devices [3]. More details on the work of Langevin is found elsewhere [4]. In 1921 Behm in Vienna described the Echolot which was used to determine the water depth for ships [5].

Source: http://echo.mpiwg-berlin.mpg.de/ECHOdocuView?url=/mpiwg/online/permanent/library/1EZGRF6Y/pageimg&viewMode=images&pn=6&mode=imagepath

Fig. 1. An image from Kircher's book depicting air reflection

Source: http://en.wikipedia.org/wiki/File:Christian_Doppler.jpg

Fig. 2. C. Doppler, born november 29th, 1803 in Salzburg, public domain

Following these fundamental developments, clinical applications began to develop. The first clinical applications of ultrasound are credited to the Austrian neurologist Karl Theo Dussik [6]. In the introduction of his article he mentions that he was motivated to investigate the medical importance of ultrasound in 1937 after having read a review on use of underwater ultrasound techniques (Echolotung) as well as the use of ultrasound for the detection of material flaws in industrial settings by Sokolov [7]. He goes on to discuss the properties of auscultation, which in the end works because changes in tissue density, relative water content, and colloidal structure have occured. Further references on the basic physics of ultrasound can be found in the paper. The initial clinical indications according to Dussik were the ventricle system of the brain and the spinal bones in a procedure called hyperphonography. Further fields of application were liver, kidneys, testicles, and the extremities.

Some of the data mentioned above have been extracted from the publication by Frentzel-Beyme [8]. Additional information has been obtained via Wikipedia.

2.1 Modern history of ultrasound including thyroid examinations

General articles on the historical aspects and developments of ultrasound can be found in recent publications [8-10]. In addition to this some useful clinical publications on thyroid examinations are those of Ruchala and Szczepanek [11] and Sholosh and Borhani [12]. The physics of ultrasound have been presented by Kossoff [13].

In the 1950's Howry and Bliss presented their device which was used for the ultrasonic visualization of body soft tissue structures [14,15]. Some interesting images can be found in their publication [15]: Figure 3 shows the apparatus called "Somascope". Due to its use of a cattle drink tank it was also called the "cattle tank scanner". Figure 4 in shows the anatomical structures of the neck at the C5 level. Figure 5 depicts the findings of a case thyroid carcinoma where liver metastases were present.

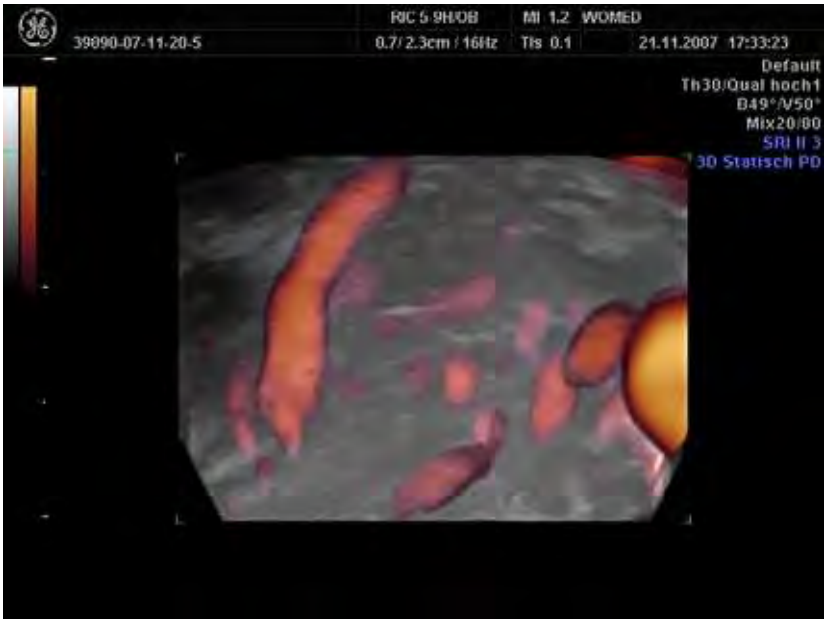

Fig. 3. Case 1. Normal thyroid seen in 3-D power Doppler modus using a vaginal transducer. The thick vessel corresponds to a laryngeal artery

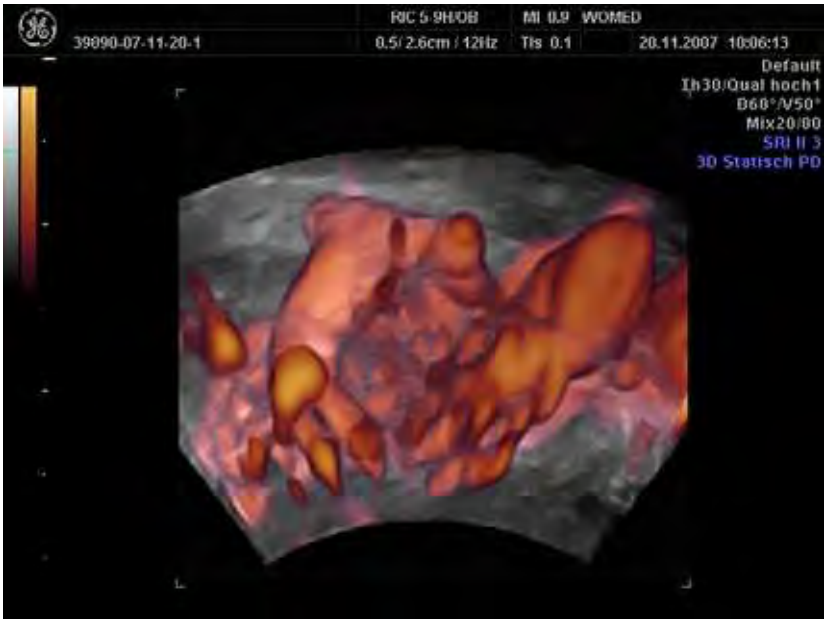

Fig. 4. Case 2. Chronic recurrent thyroiditis in 3-D power Doppler modus using a vaginal transducer. Note the increased vascularity as compared to Figure. 3

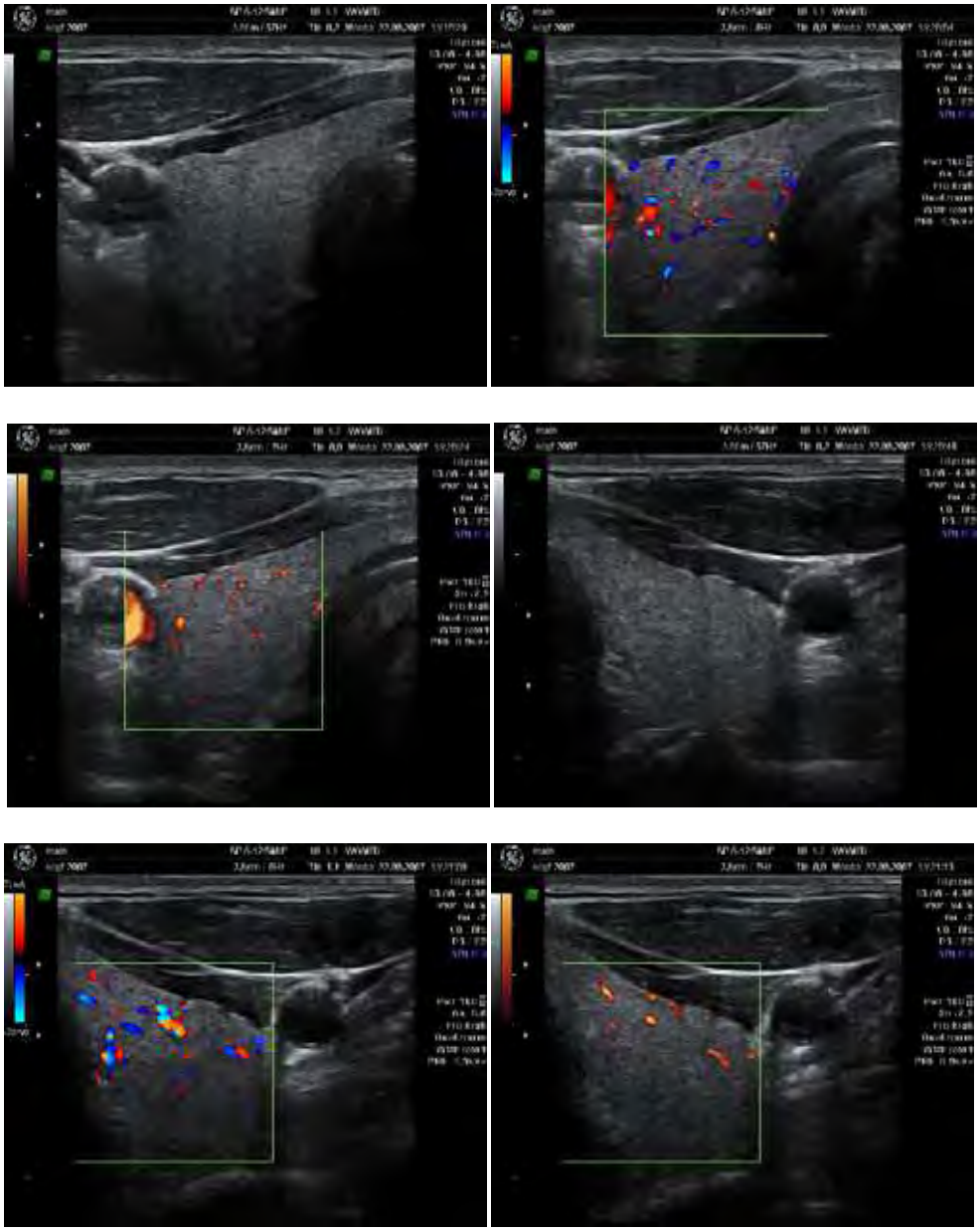

Fig. 5 (a-f). Case 3. Both lobes of a normal thyroid shown in gray, color, and power Doppler modus. The VFI value of 0.09 is reflected by the almost complete absence of perfusion signs. Such cases do not require quantitative evaluation of perfusion

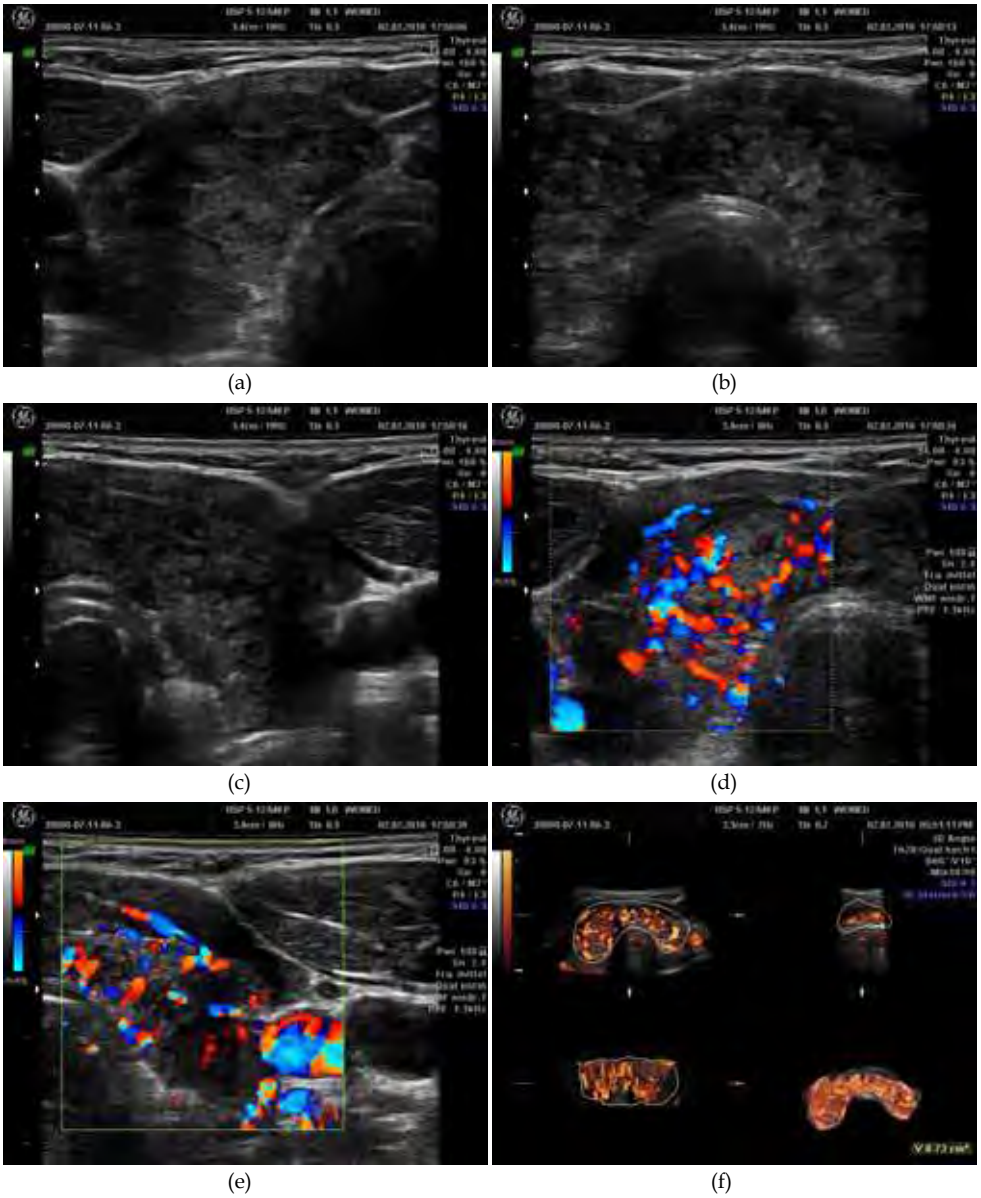

Fig. 6. (continues on next page) Case 4. The same patient shown in Figure. 4 examined with the RSP5-12 transducer. a-c: the hypoechogenic structure of the thyroid. d-e: single slice in color mode showing several vessels. f: the 3D image reconstruction using VOCAL. g: the final 3D image showing total thyroid vascularity. Note the almost total absence of underlying thyroid tissue. h-i: segmented imaging of the thyroid. This procedure is important in order to detect any nodular changes within the gland. j: The parameters obtained after the VOCAL analysis. The gray value is relatively low due to the increased vascular density

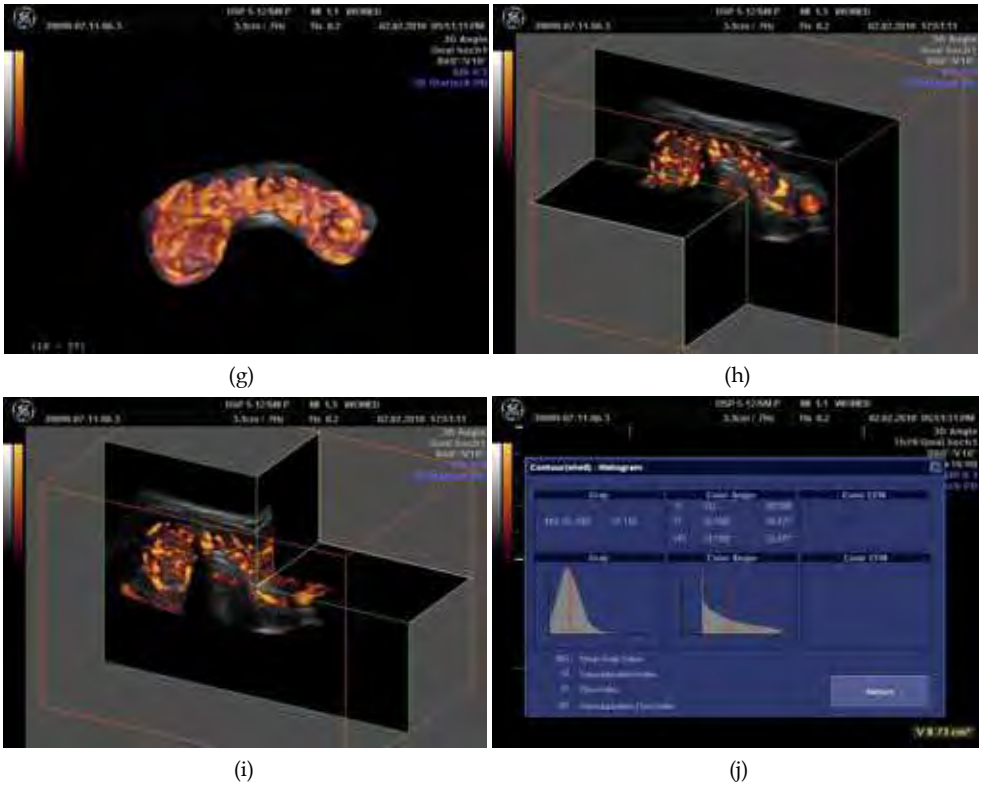

(g) (h)

(i) (j)

Fig. 6. (continued) Case 4. The same patient shown in Figure 4 examined with the RSP5-12 transducer. a-c: the hypoechogenic structure of the thyroid. d-e: single slice in color mode showing several vessels. f: the 3D image reconstruction using VOCAL. g: the final 3D image showing total thyroid vascularity. Note the almost total absence of underlying thyroid tissue. h-i: segmented imaging of the thyroid. This procedure is important in order to detect any nodular changes within the gland. j: The parameters obtained after the VOCAL analysis. The gray value is relatively low due to the increased vascular density

In 1967 Fujimoto et al. published their data on US examination of the thyroid [16]. The authors described 4 basic echo patterns: cystic, sparsely spotted, strong internal echoes, and the lack of internal echoes. In 1971 the first paper by Blum et al. documented the use of A-mode sonography [17]. In 1972 Blum [18] published an article entitled: "Clinical applications of thyroid echography" which described the data on 122 patients who had had thyroid surgery. Both A-mode and B-mode sonography was done with a 5 megahertz apparatus. In the one dimensional A-mode imaging a water-soluble gel was interposed between the transducer and the skin. For 2-dimensional B-mode imaging a mineral oil was used as coupling agent. During the examination the gain was changed in order to detect structures that had a maximal reflection while using low-sensitivity and finally high gain in order to detect lower amplitude echoes. Examples of these examinations can be seen in Figures 2-5 [18]. Acoustic dense structures were described in an adenoma (Fig. 6). Solid masses (benign or malignant) as well as thyroiditis appeared to be sonographically indistinguishable.

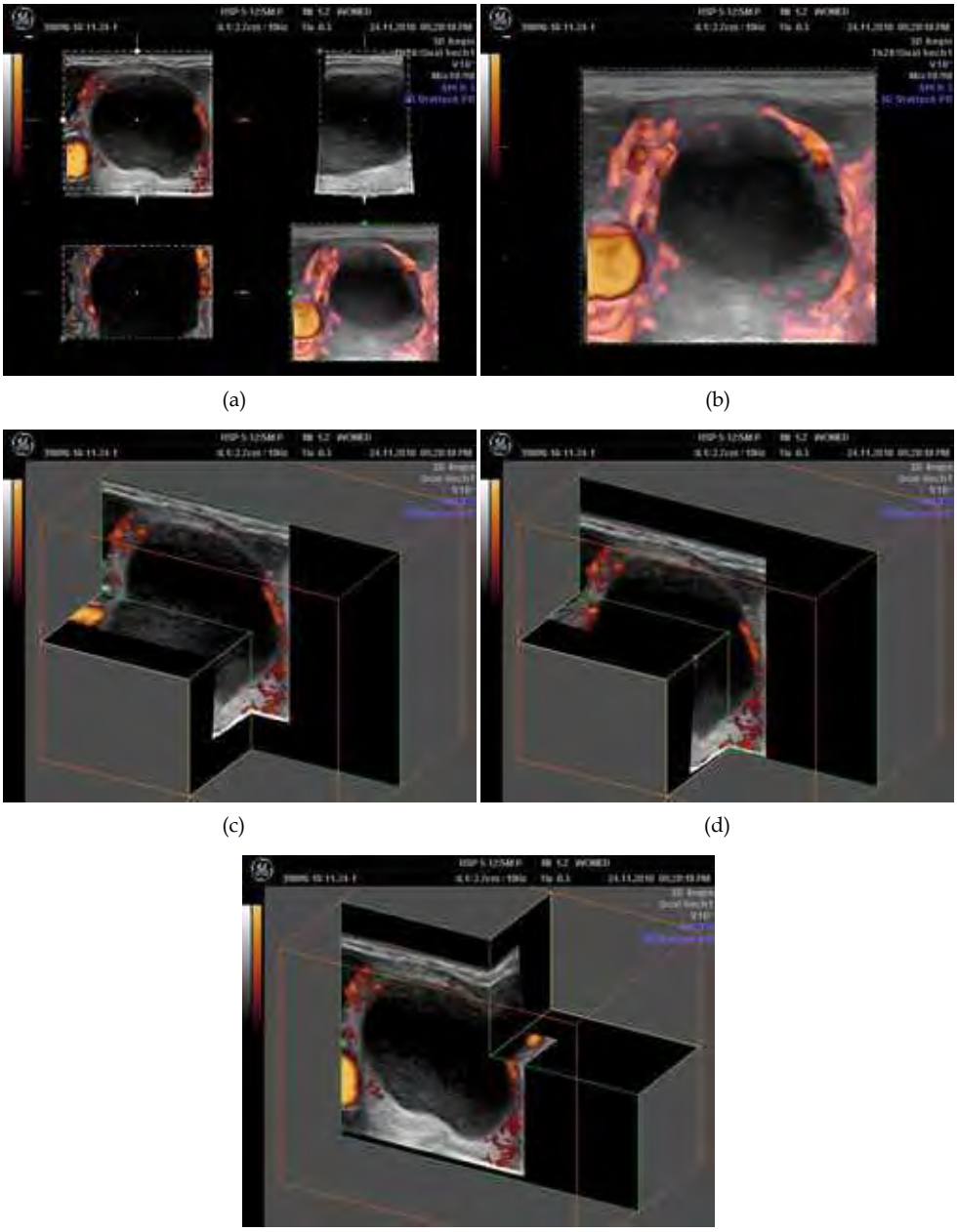

(a) (b)

(c) (d)

(e)

Fig. 7. Case 5. A female patient with a cystic nodule. The cyst has clear limits, no vessels penetrate the cavity. a: the 3D image set. b: enlarged view of the 3D reconstruction. c-e: segmentation of the cyst

In subacute thyroiditis and Graves' disease the authors found very uniform low-amplitude echoes which were only visible at high-gain setting in the A-mode. The image of B-mode was described as having a very fine stippling. According to Blum the basic purposes for conducting thyroid ultrasound examinations were: to determine whether a solitary cold nodule was cystic or solid, to document changes in size of solitary nodules even under suppressive therapy, to evaluate the depth dimension [18]. According to Australian specialists the development of ultrasound techniques for thyroid examinations is based on a breast ultrasound examination apparatus installed at the Royal North Shore Hospital in Sydney. The publication by Crocker and Jellins appeared in 1978 [19].

After the first definitions on the use of ultrasound for thyroid investigations, the notion of adding data on the depth of the nodule was presented by Thijs et al. [20]. The authors combined digital scintigraphy with ultrasound. The classification of nodules into hot, warm, cool, and cold was also advanced. The feature of sonolucent halo of adenomatous nodules was demonstrated by Scheible et al. in 1979 [21]. In 1988 Ralls et al. coined the term "thyroid inferno" to describe the characteristics of color-flow Doppler sonography in patients with Graves' disease [22]. Their study did not include patients with thyroiditis nor with latent hypothyroidism. In 1992 Miyakawa et al. described a pattern of decreased echogenicity in cases of silent thyroiditis. Such patients had a high T3 to T4 ratio [23].

In 1994-1995 Rubin reported the development of Power Doppler technology [24,25]. This development was considered an improvement of color Doppler which can detect fractional moving blood volume. A demonstration of the applicability of this technique for the detection of inflammatory changes in joints was already published 1994 [26]. The authors described increased blood flow as being suggestive of mild inflammation of the tendon examined, and marked hyperemia with vascular blush in severe changes (Fig. 2 in [26]).

The following general considerations on the characteristics of ultrasound investigations are taken from Rose and Nelson [27]. In brightness mode or gray scale US the velocity of US wave propagation in fluids and soft tissues is approximately 1540 meters per second. The time delay between the pulse sent and that of the returned wave is the basis for the determination of the reflector depth. The intensity of the reflected US wave is given as brightness of the image. Spatial resolution is dependent on the wavelength of the US wave. US attenuation increases with increased frequency. Deep structures require low frequencies in the range of 2.5-3.5 MHz, while superficial structures can be investigated within the range of 7-10 MHz. Signals are transmitted by the transducer and at the same time echo reflections are registered. According to the structure of the tissues, some portions of the sound is reflected back to the surface. Dense echoes are reflected from structures with different acoustic densities. Homogeneous liquids transmit sound without reflections. Air-filled structures do not transmit ultrasound. Attenuation of waves can be due to body fat and fascial structures [27]. In thyroid examinations such attenuation can occur due to the cervical fasciae.

2.2 Historical aspects of 3D ultrasound – The Kretz story

The beginnings of Kretz can be traced back to early 1947 when the company started the production of resistance-welded wired goods. The founder of the company was engineer Paul Kretz. Some of the products included glass balloon baskets, milk bottle carriers and potato baskets. The company started in the old rooms of the old brewery in Zipf, Austria. In 1952 the first own building was built.

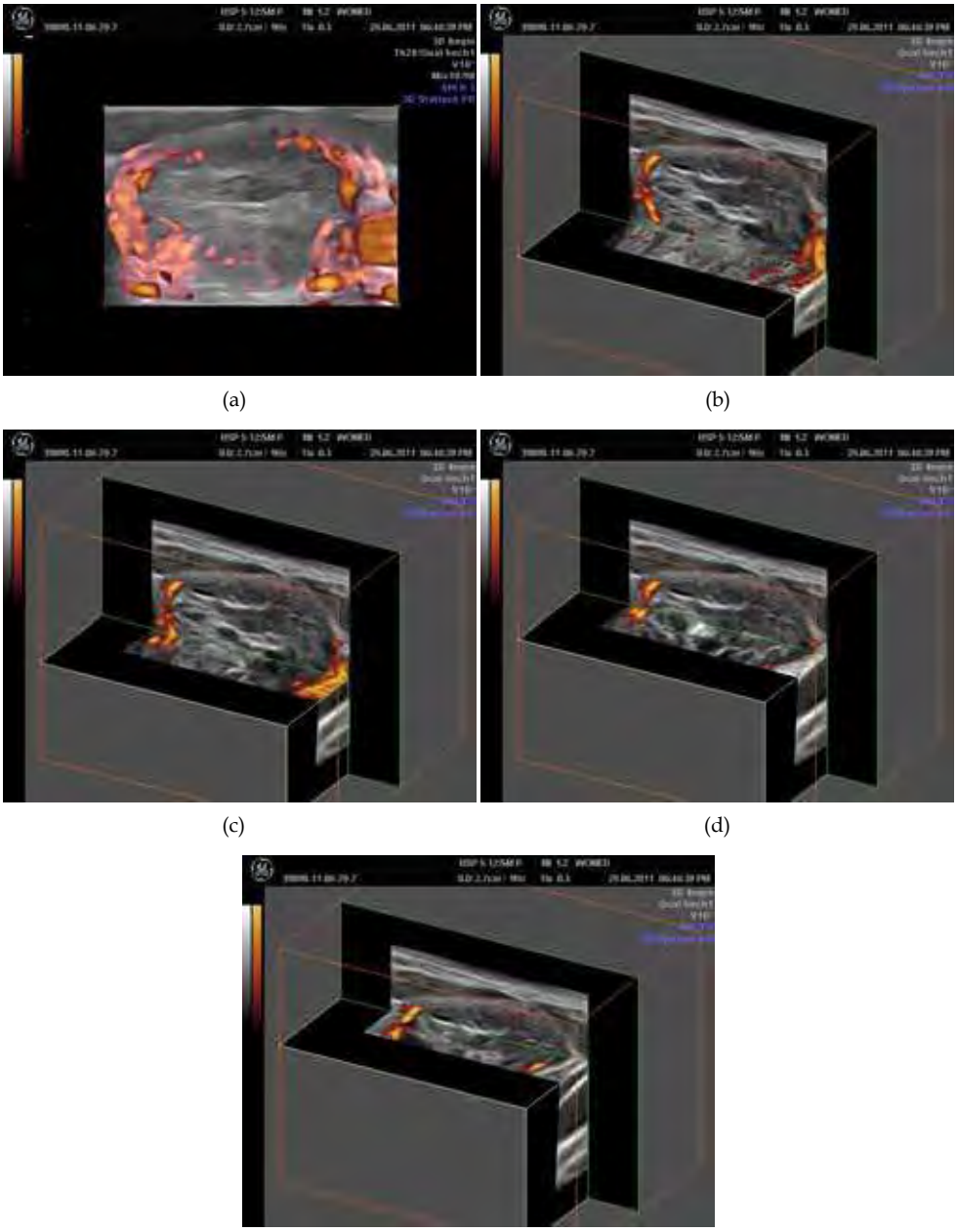

(a) (b)

(c) (d)

(e)

Fig. 8. Case 6. A female patient with a compensated autonomous adenoma. a: demonstration of the vessels surrounding the adenoma. In gray modus these vessels appear as a halo. b-e: segmentation of the nodule that shows lack of vascularity within the nodule

In 1950 the company started to develop Echolot (echo sounding) machines for the purpose of material testing. By 1957 the material testing machines became the main stand of the company.

In 1962 medical professionals start tests on the clinical use of the available material test apparatus. One of the first users was Prof. Kratochwil who used the technology for gynecological examinations, i.e. "ultrasonic placentography" (1962) [28]. In the time between 1967 and 1977 the ultrasound machines were used in gynecology, ophthalmology, neurology, and radiology based on A-mode, B-mode, time-motion and Doppler techniques. Some of the early models which were developed were: Combison 200 (1975-1978), and the improved Combison 202/R, the Minifason (1973-1977) – a hand-held Doppler for fetal heart investigations. The Combison 100 (1977) was the first real-time sector scanner of the world equipped with the first single element rotating transducer. The Combison 310 released in 1987 was a compact ultrasound machine. The following Combison 320 included computer technology.

In 1987 the first images of 3D scanning began. This technology was included in the first generation of 3D machines, having the Combison 330 in 1989. In 1992 the Combison 520 appeared. This was the 2nd generation of 3D machines to be produced in series. Between 1996 and 2001 Kretztechnik and Medison (Korea) fused and brought out the Voluson 530D in 1997. In 2001 Kretztechnik was taken over by G.E. The Austrian press reported: "Medical Systems, a subsidiary of US group General Electric (GE), acquired a 65.4% majority in Austrian Kretztechnik from Korean Medison. GE paid EUR 97.5mn, or EUR 12 per share, for Medison's stake. GE offers to buy widespread shares for EUR 17 per share in the coming two weeks. Zipf-based Kretztechnik is the world market leader for modern ultrasound systems, i.e. three-dimensional real-time imaging systems". The following models were those of the Voluson 730 series. In 2011 the Voluson S8 and S6 were released.

The accomplishments of Carl Kretz were honored in 1999 when he received the Ian Donald Gold Medal for Technical Development by the International Society of Ultrasound in Obstetrics and Gynecology [29]. The publication by Chiou et al. on 3D thyroid investigations provides some additional information as to the development of 3D imaging in general [30].

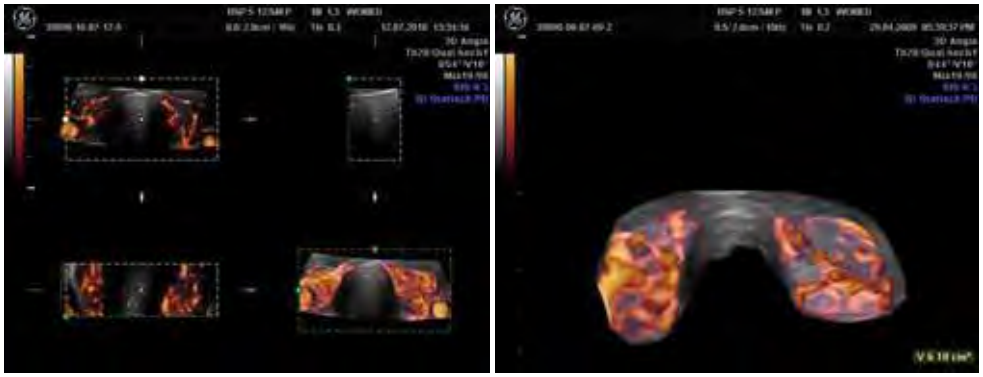

(a) (b)

Fig. 9. Case 7. A female patient with Graves' disease presenting bilateral thyroid associated ophthalmopathy. a: 3D reconstruction. b: detail of the 3D reconstruction. VFI 14.8

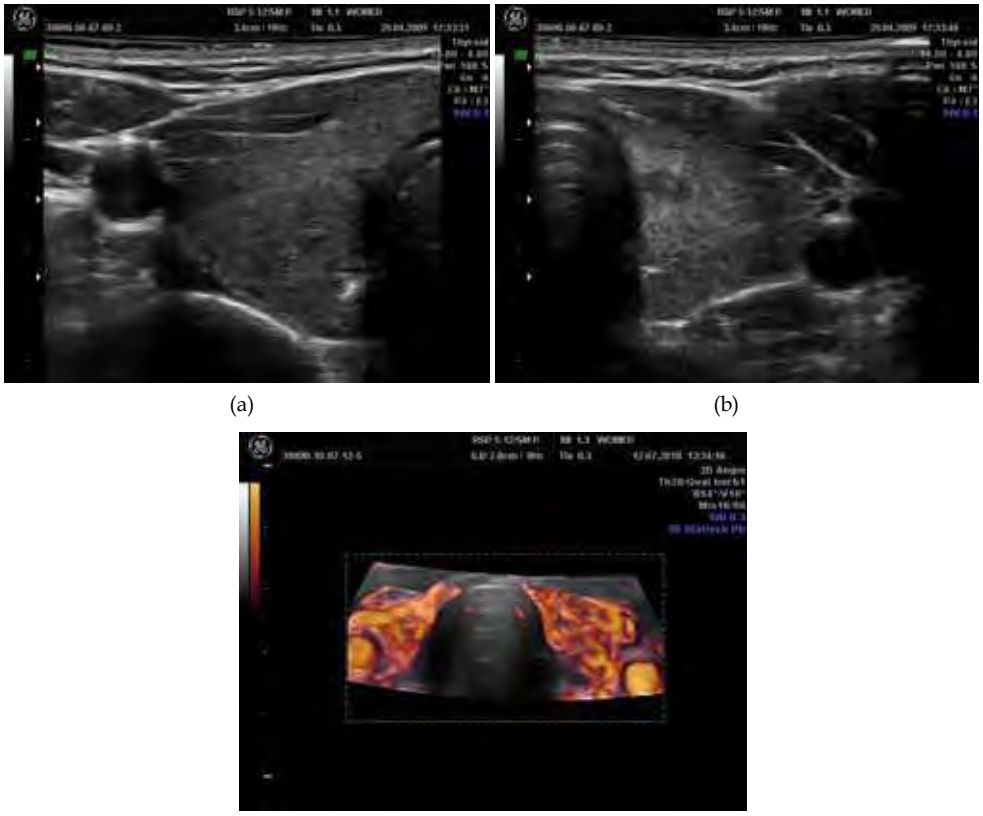

(a) (b)

(c)

Fig. 10. Case 8. A female patient with Graves' disease prior to treatment with selenomethionine and Mg. a-b: low echogenic signal of the thyroid. c: demonstration of increased total vascularity, VOCAL reconstruction, VFI 10.91

The paper describing the characteristics of quantified blood flow analysis using these machines was published by Pairleitner in 1999 [31]. The original definition of the indices states: "VI measures the number of color voxels in the cube, representing the vessels in the tissue (Figure 3). FI, a mean color value of all blood flow or induced flow intensities, represents the intensity of flow at the time of the three dimensional sweep. FI is not an indicator of perfusion, so it cannot give information on the volume of blood pumped through the vessels during a certain period of time. VFI is a combination of vascularization and flow information relating the weighted color values (weighted by their amplitudes) to the cube. Therefore, VFI represents both blood flow and vascularization". The automatic procedure for the quantification of vascularization indices was called VOCAL™. VOCAL stands for the 3D virtual organ computer-aided analysis program developed by Kretz. Data on the reliability of the VOCAL analysis as well as on the parametric setting for the examinations in gynecological applications have been presented by Bordes and Raine-Fenning [32,33].

3. 3D-Ultrasound thyroid examination

3D-Ultrasound examinations in this paper were done using a General Electrics Voluson 730 Pro ultrasound machine equipped with a RealTime 4D linear transducer (RSP5-12, GE Healthcare, Waukesha, WI 53188, USA). Data analysis was done using the VOCAL™ software (4DView Version 5.x, GE Medical Systems - Kretztechnik GmbH & Co OHG) installed on the ultrasound machine. Both the gray-scale values and the color values were normalized from 0 to 100, 100 being the highest intensity. The analysis of the 3D Doppler data sets provided the following indexes: VI, FI, and VFI [31]. The examination was done with the patients lying supine and with a light hyperextension of the neck. The transducer was placed on the midline of the neck having the whole gland inside the field of view. The mean time of data acquisition for the thyroid studies was approximately 20 seconds. The study had to be repeated only when movement artifacts arising from the patients (coughing or swallowing) had occurred. The drawing of the area of the thyroid gland was carried out using manual trace at 15° steps [34]. During drawing care was taken not to include laryngeal vessels which are typically seen on the medial border of the thyroid.

(a) (b)

(c)

Fig. 11. Case 8. A female patient with Graves' disease after treatment with selenomethionine and Mg. a-b: normal echogenic signal of the thyroid. c: demonstration of less total vascularity, VOCAL reconstruction, VFI 3.49

4. Clinical cases: Normal thyroid, nodular disease, cystic disease, latent hypothyroidism, hypothyroidism, hyperthyroidism

The ultrasound data presented here have been obtained during examinations carried out at our Institution WOMED in Innsbruck, Austria. A total of 140 examinations were carried out. The procedures were carried in accordance with the Declaration of Helsinki [35]. The list of representative demonstration cases presented in this chapter is shown in the Table. The initial ultrasound examinations (cases 1 and 2) were done by both authors based on the previous experience of HM in the field of reproductive medicine. These first 2 studies were carried out using a vaginal transducer. Two cases with nodular disease are presented in order to demonstrate the capability of 3-volume visualization of the thyroid. The most relevant perfusion parameter for hypo- and hyperthyroidism, i.e. VFI, is shown.

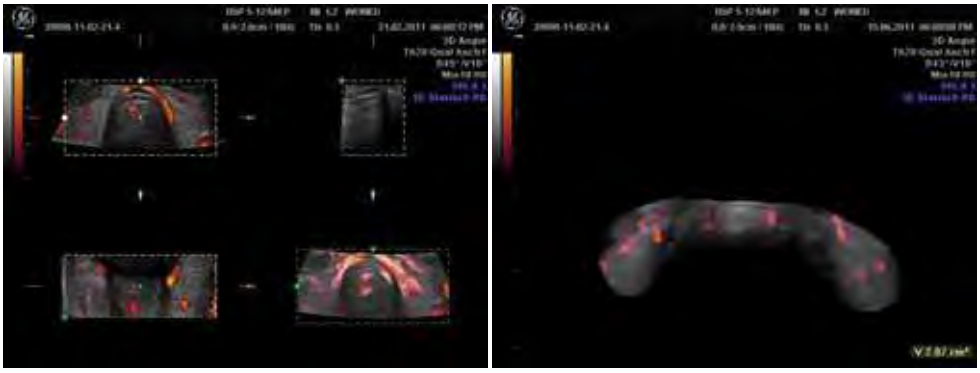

(a) (b)

Fig. 12. Case 9. A female patient with latent hypothyroidism prior to treatment with selenomethionine and Mg. a: 3D reconstruction. b: 3D VOCAL reconstruction, VFI 4.22. Compare with Figure 13 (post-treatment images)

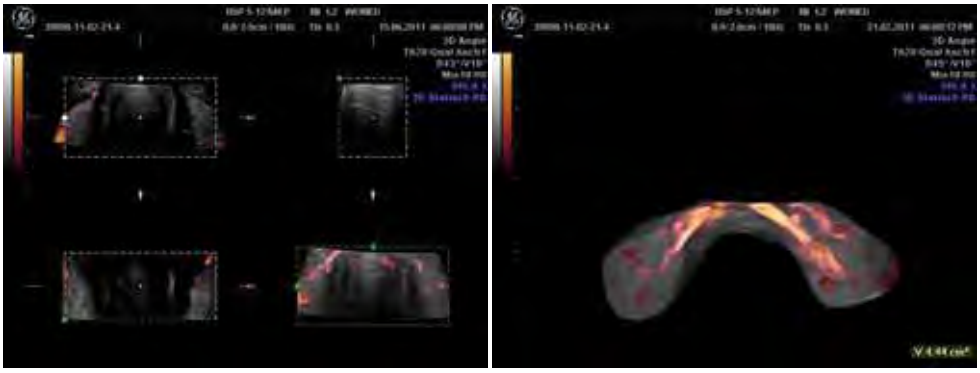

(a) (b)

Fig. 13. Case 9. A female patient with latent hypothyroidism after treatment with selenomethionine and Mg. a: 3D reconstruction. b: 3D VOCAL reconstruction, VFI 1.21. Compare with Figure 12 (pre-treatment images)

Case	Sex	Diagnosis	VFI
1	m	Normal thyroid – (study done with a vaginal transducer)	n.d.
2	f	Chronic recurrent thyroiditis – (study done with a vaginal transducer)	n.d.
3	m	Normal thyroid	0.09
4	f	Chronic recurring thyroiditis	23.97
5	f	Cystic adenoma	n.d.
6	f	Autonomous adenoma	n.d.
7	f	Graves' disease and thyroid associated orbitopathy	14.8
8	f	Graves' disease pre-treatment	10.91
9	f	Graves' disease after treatment	3.49
10	f	Latent hypothyroidism pre-treatment	4.22
11	f	Latent hypothyroidism post-treatment	1.21

Table 1.

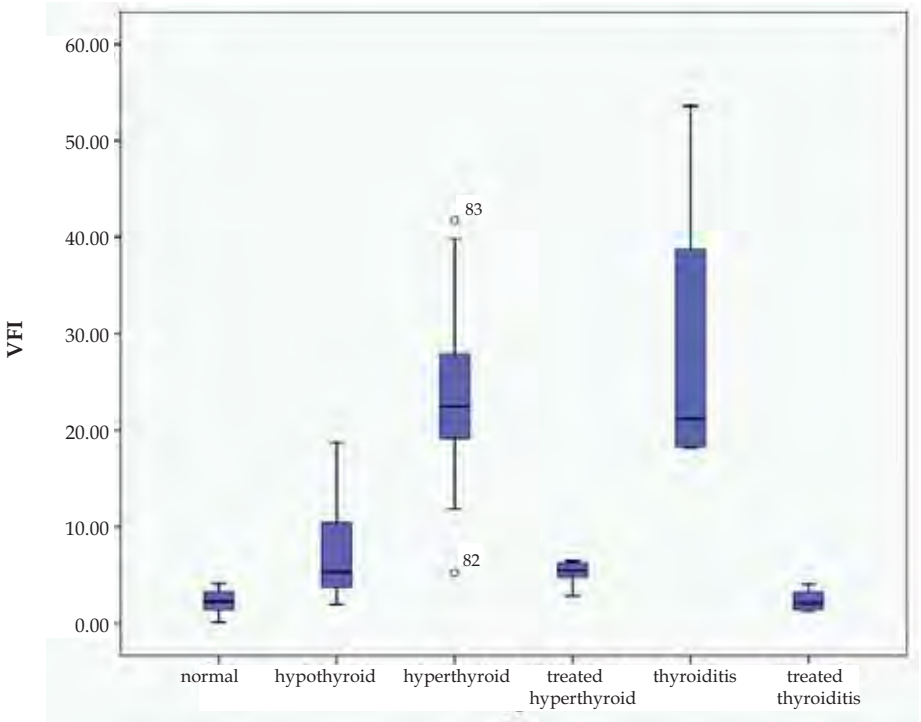

Fig. 14. The VFI value in different thyroid conditions. The first two bars correspond to single observations. The following groups of 2-bars each demonstrate the VFI changes following therapy with selenomethionine and Mg citrate ($p<0.01$)

Based on the results of previous investigations [36-40] supportive treatment included selenomethionine and Mg-citrate. Supplementation with selenomethionine (200 µg/d, Pure

Encapsulations ©, pro medico HandelsGmbH, Graz Austria) was prescribed if the serum levels were less than 80µg/l. Magnesium substitution was prescribed if the serum level was lower than 0.8 mmol/l (Magnesium Verla©, 60mg of Mg-citrate/Mg-L-glutamate, Kwizda Pharma GmbH, Vienna) at a dose of 360mg/day. This treatment was given over a period of 3 months in cases 8 and 10. The changes in thyroid morphology and VFI are given as cases 9 and 11. Statistical analysis of the 140 observations revealed that VFI was the most relevant parameter showing significant changes after our therapy approach (Figure 14).

5. Discussion

Studies with 3D technology concerning thyroid function are scarce. Only 2 publications have addressed this issue [30,41]. The paper by Chiou et al. is the first one in the literature to deal with the same technology as us [30]. This study included patients with Hashimoto's disease as well as Graves' disease. In Figure 1 the authors present the VFI value of a patient with Graves' disease (VFI = 30.7). This value is similar that the ones we have obtained. Unfortunately further individual data are not presented. The authors present exhaustive data on correlation analyses. The second publication on 3D ultrasound of the thyroid by Slapa et al. is centered on nodular thyroid disease [41]. This publication has no comparable data to our results. All together it can be said that 3D perfusion studies of the thyroid are rare.

3D perfusion studies, however, has found much wider application in the field of reproductive medicine since the original publication of the qualitative analysis method by Pairleitner et al. [31]. Data on the reliability of the VOCAL analysis as well as on the parametric setting for the examinations have been presented by Bordes and Raine-Fenning [32,33]. Concerns regarding power Doppler signal attenuation as discussed by Raine-Fenning [33] should not be relevant in thyroid examinations since the distance between the transducer and the organ is relatively constant (app. 1 to 1.5 cm).

Since more data is available from the gynecological field we will mention some data related to ovarian perfusion studies. Examination of the ovaries as reported by in Rainne-Fenning [33] revealed mean VFI values for the ovary of 2.076 and 2.074 (2 observers). Changes in ovarian vascularization during the menstrual cycle has been reported by Järvelä et al. [42]. In Table 2 of [42] a comparison of vascularization parameters between the right and left ovaries is shown. The mean values for VI, FI, VFI, and mean grayness were: 6.2/7.4, 43.4/46.5, 2.8/3.7, and 45.8/46.0, respectively. In 2002 Pan et al. compared the vascularization characteristics between patients with polycystic ovarian syndrome and controls [43]. The mean values for VI, FI, and VFI for normals and PCO patients were: 0.8/2.1, 44.44/50.26, and 1.44/3.99, respectively. In 2003 Pan et al. [44] described a stimulatory effect of HRT on the ovarian vascularization parameters in postmenopausal women (!). The mean values for VI, FI, and VFI before and after HRT were: 0.31/1.12, 30.47/38.41, and 0.13/0.59, respectively. This finding implies a stimulatory effect of conjugated equine estrogen on these parameters. The same group of investigators described increased vascularization parameters in women that showed a hyper-response to stimulation protocols for IVF [45]. Hyperresponders had higher levels of estradiol (>3000 pg/ml) or had more than 15 oocytes retrieved. The mean values for VI, FI, and VFI for patients with a "normal" and patients with an increased response to stimulation were: 1.25/2.27, 43.19/50.23, and 0.63/1.18, respectively.

Comparing the image material presented in the above mentioned citations with our images, it can be clearly recognized that the thyroid gland has a wider range of variation in the

degree of vascularization. The VFI values seen in thyroiditis and Graves' disease are generally higher than in different conditions of ovarian function. These differences cannot be taken as absolute ones. Data variability between different publications has 2 main sources of error. The first one is the use of different Kretz machines (Combison, Voluson). The second one is the fact that each investigator or each machine has different examination settings for carrying out the studies. We recommend the continuous use of the same settings in order to produce comparable results. These facts have been mentioned by de Ziegler [46]. De Ziegler points out the weakness of early studies which were arbitrary and subjective in interpretation [46]. Some of the open expectations mentioned by de Ziegler included the "desire for an understanding of the mechanisms at play" as well as whether ovarian function had a relation to perfusion values. As we show in Figure 12, the relevant parameter VFI decreases significantly following the combined treatment with selenomethionine and magnesium. We postulate that the VFI represents an inflammatory process that is present in several thyroid entities. Initially we had described this as a "low grade connective tissue inflammation" in patients with thyroid associated ophthalmopathy [39]. In this publication we discussed amply the role of Se in inflammation. Data concerning Mg and inflammation can be found in the literature [47-60]. The initial invitation of the Editors of this book was indeed to elaborate on these pathophysiological connections.

6. Conclusions

Increased perfusion characteristics in 3D modus provide an exact picture of the underlying inflammatory changes in the thyroid. This description is better than that of indirect signs said to be associated with such changes (simple Doppler imaging, pulsed Doppler). This technical enhancement will allow the clinician to gain immediate access to the basic underlying processes of thyroid disease, i.e. inflammation. This process of inflammation is directly related to the available body resources of substances that regulate inflammatory processes. Effectiveness of treatment can be uniquely evaluated by the quantitative 3D power Doppler perfusion study of the thyroid.

7. Acknowledgements

Historical data on the development of GE Kretztechnik was kindly provided by GE Austria.

8. References

[1] Doppler C: Abhandlung Über das farbige Licht der Doppelsterne und einiger anderer Gestirne des Himmels. *Abh K Bohm Ges Wissen Prag* 1842, 465-482.
[2] Curie J, Curie P: Development par pression de l'electricite polaire dans les cristaus hemidres a faces inclinees. *C R Acad Sci Paris* 1880, 91: 294-295.
[3] Mason WP: Piezoelectricity, its history and applications. *J Acoust Soc Am* 1981, 70: 1561-1566.
[4] Paty P: Paul Langevin (1872-1946), la relativité et les quanta. *Bull Soc Fr Phys* 1999, 119: 15-20.
[5] Behm A: Das Behm-Echolot. *Ann Hydrogr* 1921, 49: 241-247.
[6] Dussik KT: Über die Möglichkeit, hochfrequente mechanische Schwingungen als diagnostisches Hilfsmittel zu verwerten. *Z Gesamte Neurol Psychatr* 1941, 174: 153-168.
[7] Sokolov SY: On the problem of the propagation of ultrasonic oscillations in various bodies. *Elek Nachr Tech* 1929, 6: 454-460.

[8] Frentzel-Beyme B: [From echo-sounding to color doppler sonography. The history of diagnostic ultrasonic diagnosis.]. *Radiologe* 2005, 45: 363-370.
[9] Jecker P, Frentzel-Beyme B: [The history of head and neck sonography]. *Laryngorhinootologie* 2002, 81: 900-905.
[10] Levine RA: Something old and something new: a brief history of thyroid ultrasound technology. *Endocr Pract* 2004, 10: 227-233.
[11] Ruchala M, Szczepanek E: Thyroid ultrasound - a piece of cake? *Endokrynol Pol* 2010, 61: 330-344.
[12] Sholosh B, Borhani AA: Thyroid ultrasound part 1: technique and diffuse disease. *Radiol Clin North Am* 2011, 49: 391-416.
[13] Kossoff G: Basic physics and imaging characteristics of ultrasound. *World J Surg* 2000, 24: 134-142.
[14] Howry DH, Bliss WR: Ultrasonic visualization of soft tissue structures of the body. *J Lab Clin Med* 1952, 40: 579-592.
[15] Holmes JH, Howry DH, Posakony GJ, Cushman CR: The ultrasonic visualization of soft tissue structures in the human body. *Trans Am Clin Climatol Assoc* 1954, 66: 208-225.
[16] Fujimoto Y, Oka A, Omoto R, Hirose M: Ultrasound scanning of the thyroid gland as a new diagnostic approach. *Ultrasonics* 1967, 5: 177-180.
[17] Blum M, Weiss B, Hernberg J: Evaluation of thyroid nodules by A-mode echography. *Radiology* 1971, 101: 651-656.
[18] Blum M, Goldman AB, Herskovic A, Hernberg J: Clinical applications of thyroid echography. *N Engl J Med* 1972, 287: 1164-1169.
[19] Crocker EF, Jellins J: Grey scale ultrasonic examination of the thyroid gland. *Med J Aust* 1978, 9: 244-248.
[20] Thijs LG, Roos P, Wiener JD: Use of ultrasound and digital scintiphoto analysis in the evaluation of solitary thyroid nodules. *J Nucl Med* 1972, 13: 504-509.
[21] Scheible W, Leopold GR, Woo VL, Gosink BB: High-resolution real-time ultrasonography of thyroid nodules. *Radiology* 1979, 133: 413-417.
[22] Ralls PW, Mayekawa DS, Lee KP, Colletti PM, Radin DR, Boswell WD *et al*.: Color-flow Doppler sonography in Graves disease: "thyroid inferno". *Am J Roentgenol* 1988, 150: 781-784.
[23] Miyakawa M, Tsushima T, Onoda N, Etoh M, Isozaki O, Arai M *et al*.: Thyroid ultrasonography related to clinical and laboratory findings in patients with silent thyroiditis. *J Endocrinol Invest* 1992, 15: 289-295.
[24] Rubin JM, Bude RO, Carson PL, Bree RL, Adler RS: Power Doppler US: a potentially useful alternative to mean frequency-based color Doppler US. *Radiology* 1994, 190: 853-856.
[25] Rubin JM, Adler RS, Fowlkes JB, Spratt S, Pallister JE, Chen JF *et al*.: Fractional moving blood volume: estimation with power Doppler US. *Radiology* 1995, 197: 183-190.
[26] Newman JS, Adler RS, Bude RO, Rubin JM: Detection of soft-tissue hyperemia: value of power Doppler sonography. *AJR Am J Roentgenol* 1994, 163: 385-389.
[27] Rose SC, Nelson TR: Ultrasonographic modalities to assess vascular anatomy and disease. *J Vasc Interv Radiol* 2004, 15: 25-38.
[28] Kratochwil A: [Possibilities of ultrasonic diagnosis in labor gynecology]. *Wien Klin Wochenschr* 1966, 78: 190-191.
[29] Kratochwil A: Presentation of the Ian Donald Gold Medal for Technical Development to Carl Kretz. *Ultrasound Obstet Gynecol* 2000, 16: 107-108.

[30] Chiou SC, Hsieh MH, Chen HY, Lin JD, Chen CC, Hsu WH *et al*.: The reproducibility of the virtual organ computer-aided analysis program for evaluating 3-dimensional power Doppler ultrasonography of diffuse thyroid disorders. *J Endocrinol Invest* 2009, 32: 139-146.

[31] Pairleitner H, Steiner H, Hasenoehrl G, Staudach A: Three-dimensional power Doppler sonography: imaging and quantifying blood flow and vascularization. *Ultrasound Obstet Gynecol* 1999, 14: 139-143.

[32] Bordes A, Bory AM, Benchaïb M, Rudigoz RC, Salle B: Reproducibility of transvaginal three-dimensional endometrial volume measurements with virtual organ computer-aided analysis (VOCAL) during ovarian stimulation. *Ultrasound Obstet Gynecol* 2002, 19: 76-80.

[33] Raine-Fenning NJ, Campbell BK, Clewes JS, Kendall NR, Johnson IR: The reliability of virtual organ computer-aided analysis (VOCAL) for the semiquantification of ovarian, endometrial and subendometrial perfusion. *Ultrasound Obstet Gynecol* 2003, 22: 633-639.

[34] Mercé LT, Gómez B, Engels V, Bau S, Bajo JM: Intraobserver and interobserver reproducibility of ovarian volume, antral follicle count, and vascularity indices obtained with transvaginal 3-dimensional ultrasonography, power Doppler angiography, and the virtual organ computer-aided analysis imaging program. *J Ultrasound Med* 2005, 24: 1279-1287.

[35] World Medical Association Declaration of Helsinki: ethical principles for medical research involving human subjects. *JAMA* 2000, 284: 3043-3045.

[36] Moncayo R, Moncayo H, Kapelari K: Nutritional treatment of incipient thyroid autoimmune disease. Influence of selenium supplementation on thyroid function and morphology in children and young adults. *Clin Nutr* 2005, 24: 530-531.

[37] Moncayo R, Rudisch A, Kremser C, Moncayo H: 3D-MRI rendering of the anatomical structures related to acupuncture points of the Dai mai, Yin qiao mai and Yang qiao mai meridians within the context of the WOMED concept of lateral tension: Implications for musculoskeletal disease. *BMC Musculoskelet Disord* 2007, 8: 33.

[38] Moncayo R, Rudisch A, Diemling M, Kremser C: In-vivo visualisation of the anatomical structures related to the acupuncture points Dai mai and Shen mai by MRI: A single-case pilot study. *BMC Med Imaging* 2007, 7: 4.

[39] Moncayo R, Moncayo H: A musculoskeletal model of low grade connective tissue inflammation in patients with thyroid associated ophthalmopathy (TAO): The WOMED concept of lateral tension and its general implications in disease. *BMC Musculoskelet Disord* 2007, 8: 17.

[40] Moncayo R, Kroiss A, Oberwinkler M, Karakolcu F, Starzinger M, Kapelari K *et al*.: The role of selenium, vitamin C, and zinc in benign thyroid diseases and of Se in malignant thyroid diseases: low selenium levels are found in subacute and silent thyroiditis and in papillary and follicular carcinoma. *BMC Endocrine Disorders* 2008, 8: 2.

[41] Slapa RZ, Jakubowski WS, Slowinska-Srzednicka J, Szopinski KT: Advantages and disadvantages of 3D ultrasound of thyroid nodules including thin slice volume rendering. *Thyroid Res* 2011, 4: 1.

[42] Järvelä IY, Sladkevicius P, Kelly S, Ojha K, Nargund G, Campbell S: Three-dimensional sonographic and power Doppler characterization of ovaries in late follicular phase. *Ultrasound Obstet Gynecol* 2002, 20: 281-285.

[43] Pan HA, Wu MH, Cheng YC, Li CH, Chang FM: Quantification of Doppler signal in polycystic ovary syndrome using three-dimensional power Doppler ultrasonography: a possible new marker for diagnosis. *Hum Reprod* 2002, 17: 201-206.
[44] Pan HA, Li CH, Cheng YC, Wu MH, Chang FM: Quantification of ovarian stromal Doppler signals in postmenopausal women receiving hormone replacement therapy. *Menopause* 2003, 10: 366-372.
[45] Pan HA, Wu MH, Cheng YC, Wu LH, Chang FM: Quantification of ovarian Doppler signal in hyperresponders during in vitro fertilization treatment using three-dimensional power Doppler ultrasonography. *Ultrasound Med Biol* 2003, 29: 921-927.
[46] de Ziegler D: Uterine Doppler studies: technology driven data, or answers to our pathophysiological queries? *Hum Reprod* 2004, 19: 2615-2618.
[47] Brautbar N, Carpenter C: Skeletal myopathy and magnesium depletion: cellular mechanisms. *Magnesium* 1984, 3: 57-62.
[48] Weglicki WB, Phillips TM: Pathobiology of magnesium deficiency: A cytokine/neurogenic inflammation hypothesis. *Am J Physiol* 1992, 263: R734-R737.
[49] Garcia LA, Dejong SC, Martin SM, Smith RS, Buettner GR, Kerber RE: Magnesium reduces free radicals in an in vivo coronary occlusion-reperfusion model. *J Am Coll Cardiol* 1998, 32: 536-539.
[50] Tejero-Taldo MI, Chmielinska JJ, Gonzalez G, Mak IT, Weglicki WB: N-methyl-D-aspartate receptor blockade inhibits cardiac inflammation in the Mg2+-deficient rat. *J Pharmacol Exp Ther* 2004, 311: 8-13.
[51] Bo S, Durazzo M, Guidi S, Carello M, Sacerdote C, Silli B *et al*.: Dietary magnesium and fiber intakes and inflammatory and metabolic indicators in middle-aged subjects from a population-based cohort. *Am J Clin Nutr* 2006, 84: 1062-1069.
[52] Guerrero-Romero F, Rodríguez-Morán M: Hypomagnesemia, oxidative stress, inflammation, and metabolic syndrome. *Diabetes Metab Res Rev* 2006, 22: 471-476.
[53] Almoznino-Sarafian D, Berman S, Mor A, Shteinshnaider M, Gorelik O, Tzur I *et al*.: Magnesium and C-reactive protein in heart failure: an anti-inflammatory effect of magnesium administration? *Eur J Nutr* 2007, 46: 230-237.
[54] Mazur A, Maier JA, Rock E, Gueux E, Nowacki W, Rayssiguier Y: Magnesium and the inflammatory response: potential physiopathological implications. *Arch Biochem Biophys* 2007, 458: 48-56.
[55] Evangelopoulos AA, Vallianou NG, Panagiotakos DB, Georgiou A, Zacharias GA, Alevra AN *et al*.: An inverse relationship between cumulating components of the metabolic syndrome and serum magnesium levels. *Nutr Res* 2008, 28: 659-663.
[56] Balage M, Averous J, Rémond D, Bos C, Pujos-Guillot E, Papet I *et al*.: Presence of low-grade inflammation impaired postprandial stimulation of muscle protein synthesis in old rats. *J Nutr Biochem* 2010, 21: 325-331.
[57] Nielsen FH: Magnesium, inflammation, and obesity in chronic disease. *Nutr Rev* 2010, 68: 333-340.
[58] Weglicki WB, Mak IT, Chmielinska JJ, Tejero-Taldo MI, Komarov AM, Kramer JH: The role of magnesium deficiency in cardiovascular and intestinal inflammation. *Magnes Res* 2010, 23: 199-206.
[59] Bo S, Milanesio N, Schiavone C, Villois P, Durazzo M, Gentile L *et al*.: Magnesium and trace element intake after a lifestyle intervention. *Nutrition* 2011, 27: 108-110.
[60] Nielsen FH, Johnson LK, Zeng H: Magnesium supplementation improves indicators of low magnesium status and inflammatory stress in adults older than 51 years with poor quality sleep *. *Magnes Res* 2011, 23: 158-168.

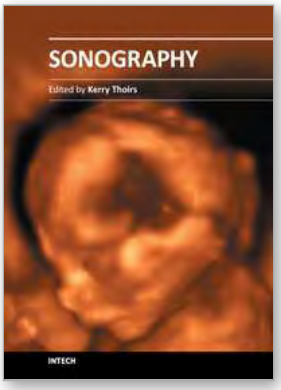

Sonography

Edited by Dr. Kerry Thoirs

ISBN 978-953-307-947-9
Hard cover, 346 pages
Publisher InTech
Published online 03, February, 2012
Published in print edition February, 2012

Medical sonography is a medical imaging modality used across many medical disciplines. Its use is growing, probably due to its relative low cost and easy accessibility. There are now many high quality ultrasound imaging systems available that are easily transportable, making it a diagnostic tool amenable for bedside and office scanning. This book includes applications of sonography that can be used across a number of medical disciplines including radiology, thoracic medicine, urology, rheumatology, obstetrics and fetal medicine and neurology. The book revisits established applications in medical sonography such as biliary, testicular and breast sonography and sonography in early pregnancy, and also outlines some interesting new and advanced applications of sonography.

INTECH
open science | open minds

InTech Europe
University Campus STeP Ri
Slavka Krautzeka 83/A
51000 Rijeka, Croatia
Phone: +385 (51) 770 447
Fax: +385 (51) 686 166
www.intechopen.com

InTech China
Unit 405, Office Block, Hotel Equatorial Shanghai
No.65, Yan An Road (West), Shanghai, 200040, China
中国上海市延安西路65号上海国际贵都大饭店办公楼405单元
Phone: +86-21-62489820
Fax: +86-21-62489821